Development of high-throughput mass spectrometry modalities to enhance drug discovery in immunology

PhD Thesis

Leonie Mueller

Thesis submitted for the qualification of Doctor of Philosophy (Biosciences)

Newcastle University Biosciences Institute

Submission date: September 2024

Engineering and Physical Sciences Research Council

Abstract

Mass spectrometry (MS) is a powerful analytical technique, enabling unbiased and comprehensive analysis of analytes without requiring potentially disadvantageous chemical modifications that are used in label-based methods traditionally relied on for instance in high-throughput (HT) screening. In this thesis, I will showcase the advantages of different MS approaches which provide increased throughput suitable for early drug discovery. I will apply these approaches to the immunology field and establish workflow performance by comparison to established techniques.

First, I developed a matrix-assisted laser desorption/ionisation time-of-flight (MALDI-TOF) MS-based biochemical drug discovery assay to identify inhibitors of ERAP1, an antigen modulator and therapeutic target for immuno-oncology and auto-immune diseases. With equal performance, this workflow increased throughput, enabled miniaturisation, and reduced costs compared to an established MS workflow. I addressed the demand to improve the translation of early drug candidates into the clinic by developing an innovative MALDI-TOF MS-based phenotypic screening assay, utilising human induced pluripotent stem cell-derived macrophages to study cell activation. The assay consistently distinguished between resting and pro-inflammatory macrophages, and successfully identified polarisation-specific “biomarkers”. A screen of 87 broad mechanism of action compounds demonstrated assay robustness. Screening of 86 inflammation-focused compounds identified 21 hits which correlated with an established label-based cytokine secretion assay. Complementary proteomics analysis provided insights into hit compounds mechanism of action and determined undesirable off-target effects.

In summary, I established two novel HT capable screening applications that leverage MALDI-TOF MS. For both, biochemical and cellular applications, I demonstrated their power to support early drug discovery in immunology. Additionally, I showed the utility of proteomics for early drug discovery by functionally grouping compounds at the molecular level based on on-target and off-target pathway engagement. Further adoption of these MS techniques promises to enhance hit compound selection efficacy in early drug discovery.

Keywords: MALDI-TOF MS, proteomics, drug discovery, immunology, high-throughput screening

Declaration

(i) I declare that this thesis is my own work and that I have correctly acknowledged the work of others. This submission is in accordance with University and School guidance on good academic conduct.

(ii) I certify that no part of the material offered has been previously submitted by me for a degree or other qualification in this or any other University.

(iii) I confirm that the word length is within the prescribed range as advised by my school and faculty.

Leonie Mueller
Newcastle University Biosciences Institute (NUBI)
Newcastle University
Newcastle upon Tyne

Acknowledgements

I would like to thank Professor Matthias Trost for his expertise and guidance in shaping this project and the trust in me. In addition, I would like to thank Dr Maria Emilia Dueñas and Dr Rachel Peltier-Heap for their day-to-day support, technical expertise, and mentorship which was invaluable for the project progression.

I want to express appreciation for the input from my annual review panel (Akane Kawamura, Ian Hardcastle). I would like to thank the MosMed CDT for encouraging my professional development and for creating a supportive network. I would like to acknowledge the UKRI EPSRC and GSK for funding this project.

I want to thank Roland Annan, Melanie Leveridge, and Julie Quayle for giving me the opportunity to conduct a secondment at GSK which changed my views as a scientist. The support of various GSK teams was invaluable to complete this project, including the former discovery analytical, screening profiling and mechanistic biology, sample management and lab automation groups. I was supported in the assay development (SPMB: Tim Ashlin, Jonathan Hutchinson, Richard Kasprowicz), cell culture (Perkin Elmer: Margarida Almeida, Serena Bateman, Thomas Dawson, Charlie Haslam), compound selection (Chemical biology: Karen Menezes, Amelie Joffrin), data analysis (Data Sciences: Denise Vlachou, Abdullah Athar, Evan Rosa-Roseberry) and model evaluation (Immunology RU: Lee Booty). I thoroughly enjoyed my time and would like to extend a special thanks to Ben Allsop, Amy Burton, Chloe Tayler, and Eleanor Dickinson for all the help and making my secondment a truly great experience.

Many thanks to past, current and associated members of the Trost laboratory, including Ritika Chatterjee, Abeer Dannoura, Andrew Frey, Akshada Gajbhiye, Amy George, Jack Gudgeon, Joe Inns, Atakan Nalbant, Andrew Porter, Benjamin Raymond, Frances Sidgwick, and Ruth Walker, from whom I was able to learn a lot, for the maintenance of lab equipment and for becoming friends.

Lastly, I want to thank my family and friends that were by my side throughout my journey's highs and lows.

Contents

List of figures

List of tables

Chapter 2

Chapter 5

Abbreviations

9-AA	9-aminoacridine
ADE	Acoustic droplet ejection
ASMS	Affinity selection mass spectrometry
a.u.	Arbitrary unit
BMDM	Bone marrow-derived macrophage
CHAPS	3-((3-cholamidopropyl) dimethylammonio)-1-propanesulfonate
CHCA	α-cyano-4-hydroxycinnamic acid
CV	Coefficient of variation
DABP	3,4-diaminoparabenzophenone
DAN	1,5-diaminonaphthalene
DDA	Data-dependent acquisition
DESI	Desorption electrospray ionisation
DHAP	2,5-dihydroxyacetophenone
DHB	2,5-dihydroxybenzoic acid
DIA	Data-independent acquisition
DMSO	Dimethyl sulfoxide
ERAP1	Endoplasmic reticulum aminopeptidase 1
ESI	Electrospray ionisation
FA	Formic acid
GO	Gene ontology
HEPES	4-(2- hydroxyethyl)-1-piperazineethanesulfonic acid
HLA	Human leukocyte antigen
HPLC	High-performance liquid chromatography
HT	High-throughput
HTS	High-throughput screening
IAA	Iodoacetamide
IC_{50}	Half-maximal inhibitory compound concentration
IFN	Interferon
IFN-γR	Interferon-γ receptor
IL	Interleukin

IM	Ion mobility
iPSC	Induced pluripotent stem cell
IR-MALDESI	Infrared matrix-assisted laser desorption electrospray ionisation
JUMP	Joint undertaking of morphological profiling
KEGG	Kyoto encyclopaedia of genes and genomes
K_M	Substrate concentration at half maximum velocity
LAP	Liquid atmospheric pressure
LC	Liquid chromatography
Leu-SH	Leucinethiol
LOD	Limit of detection
LPS	Lipopolysaccharide
m/z	Mass-to-charge-ratio
M0	Resting macrophage
M1	Classically activated macrophage
M2	Alternatively activated macrophage
MALDI	Matrix-assisted laser desorption/ionisation
M-CSF	Macrophage colony-stimulating factor
MeCN	Acetonitrile
MeOH	Methanol
MoA	Mechanism of action
MS	Mass spectrometry
MS/MS	Tandem mass spectrometry
MSI	Mass spectrometry imaging
NA	Not available value
NaCl	Sodium chloride
OPI	Open port interface
PAINS	Pan-assay interference compounds
PASEF	Parallel accumulation serial fragmentation
PBMC	Peripheral blood mononuclear cell
PCA	Principal component analysis
PTM	Post-translational modification

RT	Room temperature
SA	Sinapinic acid
SAMDI	Self-assembled monolayers coupled with laser desorption/ionisation
SDS	Sodium dodecyl sulphate
TAM	Tumour-associated macrophage
TCEP	Tris(2-carboxyethyl)phosphine hydrochloride solution
TEAB	Triethylammonium bicarbonate buffer
TFA	Trifluoroacetic acid
THAP	2,4,6-trihydroxy acetophenone
TIMS	Trapped ion mobility spectrometry
TLR	Toll-like receptor
TNF	Tumour necrosis factor
TOF	Time-of-flight
Tris-HCl	Tris(hydroxymethyl)aminomethane hydrochloride

Chapter 1. Introduction

1.1 The drug discovery pipeline

Continuous development of novel drugs and drug repurposing is essential to address conditions with no existing treatments, particularly as new diseases emerge and our understanding of disease biology is growing.[1] Additionally, improving current treatment options is a key aspect of drug discovery, especially when potent drugs lose efficiency due to resistance. Reducing adverse effects, enhancing therapeutic efficacy, improving patient compliance, and reducing drug-drug interactions are further vital goals.[2]

Traditionally in drug discovery, enzyme activity is modulated via small molecules but expanding the drug toolbox unfolds exciting opportunities. This includes strategies like targeted protein degradation via proteolysis targeting chimeras[3], modulating RNA expression with oligonucleotides[4] and targeted protein recognition through monoclonal antibodies[5]. These modalities hold great promise for treating challenging areas, such as immune-mediated diseases, for which drug adverse effects are frequently reported.[6]

However, the drug discovery process remains arduous, often taking 10 to 15 years to bring a drug to market.[7] Traditionally, the drug discovery and development pipeline entails multiple phases, starting with target identification, which is then followed by lead generation, lead optimisation, pre-clinical and clinical trials, and finished with drug approval (Figure 1.1).

1. **Target identification**: Protein or gene targets are identified through diverse methodologies, such as bioinformatics, genomics and biochemistry, guided by insights into disease mechanisms or cellular experiments.[8]
2. **Lead generation**: Conducting high-throughput screening (HTS), either computationally or chemically (*in vitro)* against large compound libraries (often exceeding 1 million compounds) to identify potential hits.[9] Secondary *ex/in vivo* assays are performed with identified hit compounds to refine lead selection.
3. **Lead optimisation**: Rational drug design is applied to selected hits for chemical library expansion with lead-like structures that include chemical modifications to achieve structural simplification, optimised potency, reduced cytotoxicity, increased efficacy, beneficial pharmacokinetics, and simplified synthesis and isolation. Beneficial structures are identified by *in vitro* assays and in animal models.[10]

4. **Pre-clinical trials**: Drug safety and selectivity are assessed in cellular disease and animal models.[11]
5. **Clinical trials:** Within three different phases, drug safety, effectiveness, and dosage is established in humans.[8]
6. **Drug approval**: Approval is sought from regulating bodies like the Food and Drug Administration and European Medicines Agency before a drug is released into the market.[8]

In addition to the lengthy timeline, the drug discovery process is costly and inefficient, with recent studies indicating a 90% failure rate in clinical drug development.[7] A key challenge in drug discovery is to increase the speed, robustness, efficiency, and translational success of methodologies across the pipeline, thereby reducing development times and costs. This task is further exacerbated by the introduction of novel drug modalities which require different design and validation approaches, hence requiring integration of specialised and advanced technologies into the drug discovery pipeline.

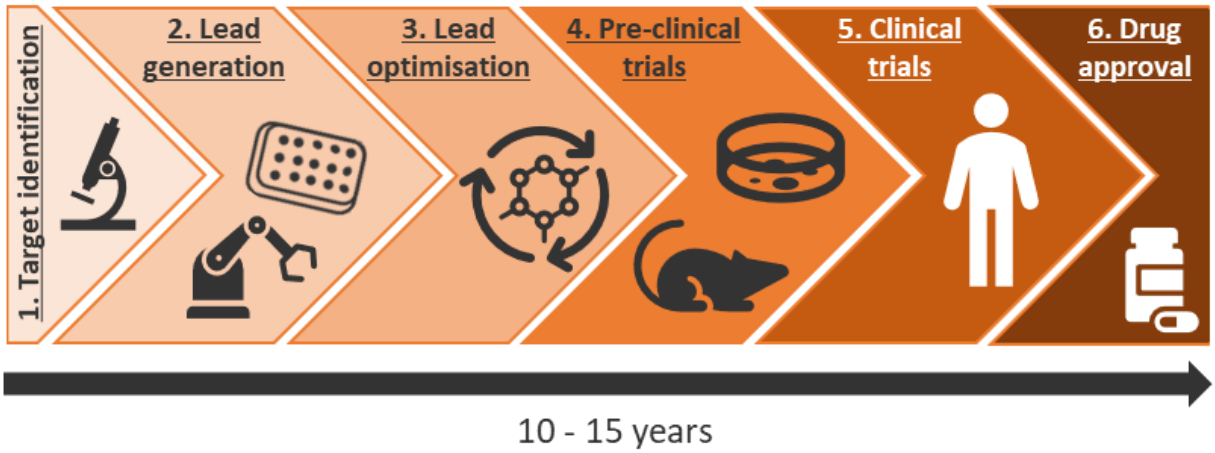

Figure 1.1. Drug discovery and development pipeline.
The pipeline entails six different steps and takes on average 10-15 years; (1) Target identification: Identification of gene or protein target, (2) Lead generation: High-throughput screening to allow hit compound selection, (3) Lead optimisation: Iterative rational drug design to improve lead compound properties, (4) Pre-clinical trials: Assessment of drug efficacy and safety in cellular and animal models, (5) Clinical trials: Drug safety, effectiveness, and dosage establishment in humans, and (6) Drug approval: Approval is sought from regulating bodies.

1.2 Mass spectrometry as a tool in drug discovery

Mass spectrometry (MS) is a well-established analytical technique used for the analysis of small and large biomolecules. It measures the mass-to-charge-ratio (*m/z*) and abundance of

analyte ions, allowing precise empirical mass determination and structural elucidation.[12] A basic mass spectrometer consists of three main components: an ionisation source, a mass analyser, and a detector.[12] In the ionisation source, sample analytes are converted into gas-phase ions, which are then separated in the mass analyser based on their *m/z* and finally detected while the ion count is recorded.[12] Mass spectrometers are often coupled to a chromatography system, allowing for sample separation prior to analysis.[12] This integration is particularly valuable in the drug discovery pipeline, where MS technologies are prized for their high sensitivity, reproducibility, and versatility.

Liquid chromatography-tandem mass spectrometry (LC-MS/MS) is widely employed in proteomics and metabolomics to gain insights into disease biology[13], and to elucidate drug mechanism of action (MoA) and ligand-protein interactions[14,15]. LC-MS techniques are used in lead optimisation to assess compound structure and purity.[16] Furthermore, they play a pivotal role in drug metabolism and pharmacokinetic studies, which are performed throughout the drug discovery process to evaluate drug safety by tracking the drug and selected biomarkers.[17]

Chromatography-free methods, such as matrix-assisted laser desorption/ionisation (MALDI) time-of-flight (TOF) MS and MALDI Fourier-transform ion cyclotron resonance MS, are also valuable. These techniques allow for image-based examination of disease state by tracking metabolites and identifying disease biomarkers during target validation. Additionally, they can be used in lead optimisation to assess drug absorption, distribution, and metabolism at the sub-cellular organelle level.[18,19]

Despite the widespread application of MS strategies throughout the drug discovery pipeline, they are currently underrepresented in the lead generation stage, primarily due to limitations in throughput and automation. Overcoming these challenges could further enhance the role of MS in this early drug discovery stage.

1.3 Screening approaches in lead discovery stage of the drug discovery pipeline

Screening approaches used to identify hit compounds from chemical libraries in the lead discovery phase are broadly categorised into computational- and experimental-based methods. Computational-based approaches predict ligand-target binding by surveying structural similarities within existing libraries. These methods are both fast and cost-

effective.[20] However, they are limited by their reliance on existing libraries, making them less suitable for exploring novel chemistry and biology. Moreover, even when potential binders are identified, experimental validation is required.[20] Experimental-based approaches are categorised into target-based and phenotypic screens, each focusing on different aspects of drug discovery. Target-based approaches use workflows that are centred around a key disease protein target. In affinity binding assays, the biomolecular target is incubated with library compounds, followed by removal of unbound ligands.[21] The detection of binding events typically requires labelling the target molecule or ligand, using various techniques such as radioligand assays, affinity chromatography, surface plasmon resonance, isothermal titration calorimetry, or light-based methods (e.g., absorbance, fluorescence, or luminescence).[22] Recently, DNA-encoded libraries have gained popularity. These libraries involve barcoding compounds with DNA, allowing for binder identification through high-throughput (HT) DNA sequencing.[23]

Affinity binding assays are useful tools when the identified biomolecular target serves an unknown function, hampering development of biochemical assays. While these methods involve screening extensive small molecule compound libraries (>1 million compounds), a novel fragment-based screening approach has emerged. This technique uses smaller libraries of molecular fragments, offering improved coverage of the chemical space and better targeting of previously undruggable proteins.[24,25] For instance, cysteine reactive fragments can be used to evaluate fragment engagement at the active protein site.[26,27] However, fragment-based screening can encounter challenges, such as the need to couple warheads to fragments to ensure covalent binding, which may lead to side reactions.[28] A further aspect that needs to be considered is the weak binding affinity of fragments to their targets.[25]

Both traditional and fragment-based binding methods are adept at identifying molecule binders but fall short in assessing biological activity directly. To address this, enzymatic assays are employed to evaluate how compounds modulate protein function by measuring product generation and substrate depletion, providing greater biological relevance for hits.[29] These biochemical or cellular assays mostly track product and substrate via absorbance or fluorescence[29], but fluorescence and chemiluminescence-based method can suffer from high false-positive rates and reduced dynamic range[30-33]. Offering a different approach to assessing

biological activity and compound effects, electrophysiological measurements are used to evaluate ion channel activity in the presence of compounds.[34]

Phenotypic screens on the other hand, focus on observable characteristics such as gene expression or cell morphology. These screens assess compound activity in a complex biological system, observing efficacy not only against the proposed target but also potentially involving unknown pathways, revealing additional information such as compound toxicity.[35] Phenotypic screens are thought to improve the translation of early-stage hits, which is crucial for accelerating the drug discovery pipeline.[36]

However, phenotypic screens are typically more challenging to implement. Ensuring physiological relevance requires careful selection of the model, stimulus, and assay endpoint.[37] Phenotypic assays range from highly specific models, such as mucus clearance cell model for evaluating cystic fibrosis treatments[38], to tracking of disease specific biomarkers like cytokines via ELISA[39] or monocyte cell surface markers via flow cytometry[40], to broader approaches like Cell Painting and DrugSeq. Cell Painting uses fluorescence dyes to assess features such as signal area, intensity and shape of different cell components and compartments to compare morphological phenotypes against a large reference database.[41] DrugSeq involves bulk RNA sequencing of disease-relevant or directed mutation cell models to evaluate gene signatures, revealing compound activity such as resistance or sensitivity.[42,43] Despite their utility, these approaches often leave the protein target unknown, necessitating further downstream target deconvolution.[36]

Overall, whether a target-based or phenotypic screening approach is chosen, depends on the biology being probed and the readout technology used. Across all strategies, there is a clear potential for novel fast and versatile HTS technologies that could enhance the efficacy of the lead discovery phase.

1.4 Mass spectrometry in high-throughput screening

A main advantage of MS is that it does not require labelling, thus eliminating the use of non-native substrates, reducing cost, and increasing the dynamic range, hence, addressing limitations of traditional HTS approaches. However, affinity selection MS and fragment-based screening have primarily relied on LC-MS setups which take several minutes per sample,

making them unsuitable for HTS.[44] With technological advancements, newer systems have emerged that offer higher throughput. I categorised these systems broadly based on the ionisation technique used: electrospray ionisation (ESI) or laser ionisation.[45] These ion sources can be coupled to diverse mass analysers to achieve different mass resolution, dynamic ranges, and analysis times.

1.4.1 Electrospray ionisation in high-throughput screening compatible mass spectrometers

ESI is a soft ionisation technique. In this method, liquid-phase analytes are sprayed through a fine metal or glass needle near the sampling entry cone of the mass spectrometer (Figure 1.2).[46] A high voltage is applied to the needle, dispersing the sample into highly charged droplets.[46] These droplets are exposed to heat and a flow of nitrogen gas to speed up the evaporation of the liquid within the droplets. Coulombic explosion or fission takes place when the decreasing droplets reach their Rayleigh limit, leading to ion expulsion.[47] This process yields multiply charged ions.[48] HT MS setups using ESI include RapidFire MS, and modified versions such as Echo MS, and DESI MS.

The RapidFire MS (Agilent) automates the analysis of 96- and 384-well plates. It consists of a microfluidic sample collection system that aspirates the sample and loads it onto a cartridge to remove interfering components, such as salts and detergents, via solid-phase extraction, and from there injects the sample into an ESI-MS.[49] This setup allows for sample processing speeds of four to eight seconds, although this is still slower than typical HTS speeds of less than one second per sample.[49] Processing speeds of the setup can be improved by multiplexing samples[50,51] or using the BLAZE-mode which bypasses the sample cleanup stage, reducing sample cycle times to 2.5 seconds[49]. The use of RapidFire MS has been reported for fragment screens[52,53], enzymatic biochemical assays[30-33,54-60], and cellular assays[61-64]. Furthermore, RapidFire MS has been used to measure intracellular compound concentrations.[63]

Echo MS (Sciex), introduced in 2020, uses acoustic droplet ejection (ADE) to deliver nanolitre sample droplets to the mass spectrometer. This method reduces sample processing time, and consumables compared to the RapidFire MS setup and allows for repeat measurements.[65] An acoustic ejection pulse pings nanolitre sample droplets into an open port interface (OPI) which delivers the sample to the mass spectrometer (Figure 1.2).[66] The setup has been used to track

analytes in enzymatic assays[67-70] and to identify covalent binders in intact protein analysis[71]. However, Echo MS can suffer from well-to-well variability as nanolitre volumes are difficult to control and ionisation interference from the sample matrix due to the lack of a purification step might be observed.[66,72]

Desorption electrospray ionisation (DESI) MS is another ESI-based technique where electrospray droplets are directed onto a surface-based sample, resulting in desorption of analyte ions (Figure 1.2).[73] This technique offers high-speed atmospheric pressure sampling and is more tolerant to matrix interference.[73] While primarily marketed as a platform used for imaging, providing spatial resolution, DESI-MS has also been employed for enzyme activity monitoring[74-76], and bacterial phenotyping[77].

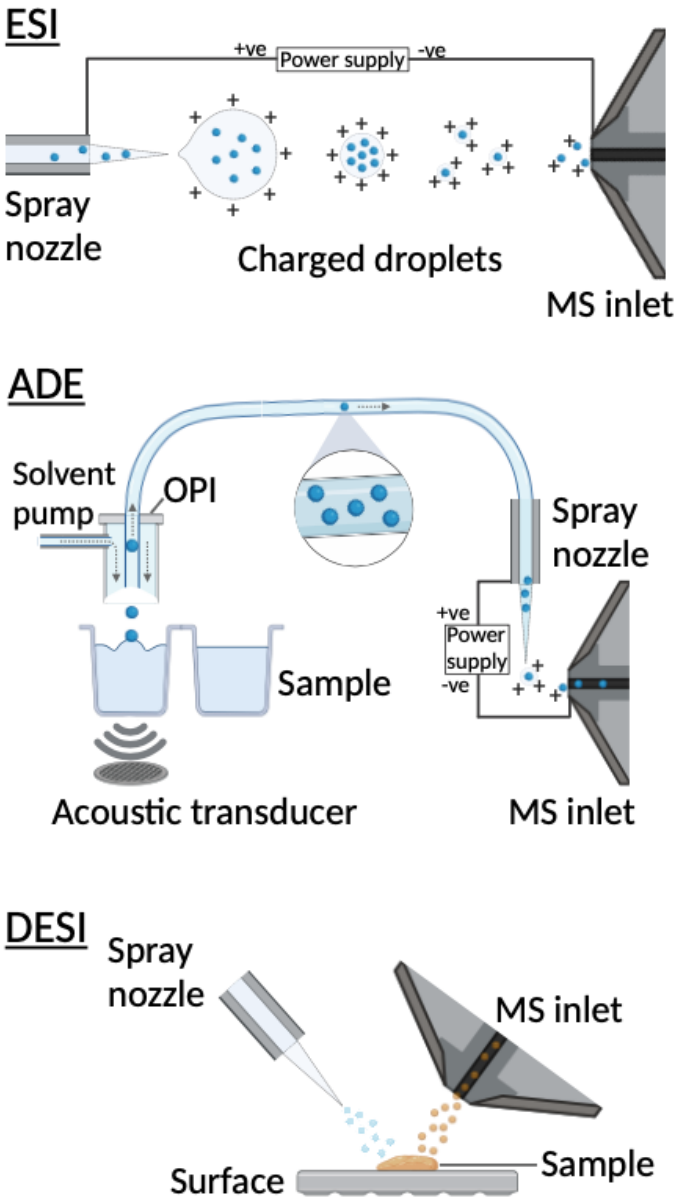

Figure 1.2. Electrospray ionisation (ESI) and accompanying sample delivery techniques.

ESI: charged analyte droplets are generated by the spray nozzle and the liquid in the droplets reduced, leading to ion expulsion and subsequent delivery to the MS inlet. ADE: nanolitre sample droplets are ejected from the sample by an acoustic impulse and transported through an open port interface (OPI) to the mass spectrometer. DESI: electrospray droplets are directed onto a surface-based sample, resulting in desorption of analyte ions which are directed into the MS inlet.

1.4.2 Laser ionisation in high-throughput screening compatible mass spectrometers

Laser ionisation techniques include self-assembled monolayers coupled with laser desorption/ionisation (SAMDI) and MALDI. SAMDI involves immobilising analytes on a thiolate-gold coated surface, and laser irradiation to cleave the thiolate-gold bond, resulting in analyte desorption and ionisation.[78] While SAMDI has been used for affinity binding studies[79,80] as well as biochemical assays[81-88], its broad applicability is limited by the need to design surface chemistry suitable for analyte immobilisation.

MALDI-TOF MS has been successfully used in binding assays[89], and various biochemical assays. It is a gold standard in clinical settings for bacterial phenotyping, indicating its potential for phenotypic screens.

1.5 MALDI-TOF MS

MALDI was first described by Hillenkamp and Karas.[90] It is a soft ionisation technique capable of ionising oligonucleotides, metabolites, lipids, peptides, and proteins with a mass of up to 100 kDa.[91-93] MALDI has become amenable to HTS due to advancements in instrumentation, such as the integration of a 10kHz laser, enabling analysis times of less than one second per sample. Unlike other techniques, MALDI has a higher tolerance for contaminants (e.g. salts, buffers, detergents) and hence can be conducted without sample cleanup. Instead, samples are co-crystallised with a low molecular weight organic matrix on a metal target plate.[94] The laser is then fired at the sample, and the energy absorbed by the matrix which facilitates desorption into the gas phase and proton transfer for analyte ionisation.[95] MALDI is a soft ionisation technique and produces primarily singly charged ions.[96]

The ion acceleration into the TOF mass analyser is delayed for a short time after the laser pulse to compensate for ion energy spreads (delayed extraction).[97,98] The TOF mass analyser a field-free high vacuum tube where lighter ions travel faster and reach the detector earlier than

heavier ions, under the premise that all ions receive the same kinetic energy.[46] This mass analyser can operate in two modes: linear mode for larger biomolecules, where ions reach the detector immediately at the end of the flight path, and reflector mode, which extends the flight path for improved ion separation (Figure 1.3A). The latter is achieved by placing an ion mirror with a gradual electric field at the end of the linear path, allowing higher energy ions to penetrate deeper into the mirror before being repelled back. Finally, the detector measures both the ion arrival time and ion count, generating a spectrum that plots *m/z* against the signal intensity (Figure 1.3B). With this setup, MALDI-TOF MS can achieve attomolar sensitivity, making it a powerful tool for HTS in drug discovery.[99]

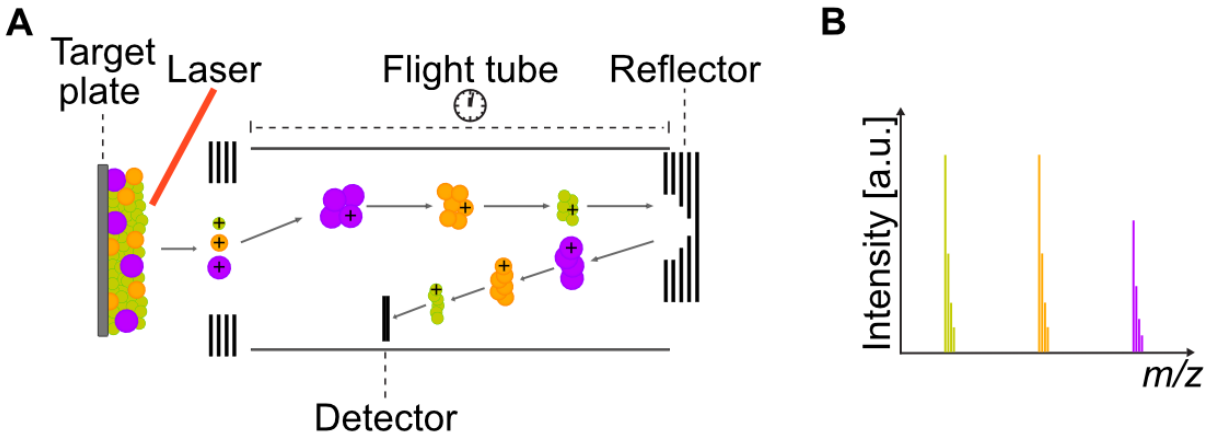

Figure 1.3. Principles of MALDI-TOF MS.
(A) Analyte (purple and orange) desorption and ionisation in the ion source by the aid of a laser and matrix (yellow), which is followed by ion separation and detection in the mass analyser which is equipped with a reflector to extend the flight path. (B) An exemplary mass spectrum obtained by MALDI-TOF MS.

Several enhancements and modifications to the standard MALDI-TOF MS setup have emerged over the years, demonstrating potential for implementation in HTS. For instance, MALDI-2 is an advanced technique where a second laser pulse is applied post-ionisation to boost ion yields.[100] Another notable development is atmospheric pressure MALDI MS, introduced by Laiko *et al.* in 2022. This method aims to generate multiple ion charge states similar to ESI, while using MALDI sample preparation techniques.[101] This was further developed into liquid atmospheric pressure MALDI (LAP-MALDI) MS, where the analyte, MALDI matrix, and a viscous support matrix are co-deposited on the sample carrier. This allows prolonged laser excitation under atmospheric pressure[102-104], improving workflow efficiency with acquisition speeds of up to 40 samples per second[105,106]. LAP-MALDI MS can be applied to detect lipids, peptides and proteins[107], with uses ranging from distinguishing milk origins[108] to rapid disease

diagnostics for bovine mastitis[109-111], enzyme activity screening[105], and bacterial phenotyping[112].

Infrared matrix-assisted laser desorption electrospray ionisation (IR-MALDESI) MS is another innovative approach, combining ESI with laser ablation to ionise neutrals.[113] Originally used for imaging[114-116], recent advancements have made it compatible with HTS and ultra HTS workflows, enabling measurements up to 22.7 samples per second[117-119]. This technology has been demonstrated in various applications[120], including kinetic studies of isocitrate dehydrogenase 1[118], analysis of monoclonal antibodies[121], and a compound screen of tris(2-carboxyethyl)phosphine oxidation[119].

MALDI-TOF MS, being more widely available, can be integrated with nanolitre liquid handling robots to automate and miniaturise workflows, making it suitable for industrial HTS and facilitating the move into the ultra HTS environment.[122-125] To achieve optimal analyte detection with MALDI-TOF MS, several parameters must be optimised for each analyte. Without sample cleanup, ionisation can be affected by interfering solvent additives[126], and adducts of common contaminant ions such as Na^+ and K^+ should be monitored[127].

Matrix choice, concentration, and sample ratio are crucial for efficient ionisation and minimised interference effects.[128] Different matrices can be chosen based on the analyte's ionisation properties, including organic matrices possessing an aromatic ring to absorb the laser energy, and acidic functional groups to facilitate ionisation. Proteins and peptides are often analysed in positive ion mode with sinapinic acid (SA) or α-cyano-4-hydroxycinnamic acid (CHCA) matrix.[129,130] Lipids, due to their chemistry, can be detected in positive and negative ion mode, with matrices such as 9-aminoacridine (9-AA) in negative ion mode, and 2,5-dihydroxybenzoic acid (DHB) in positive ion mode.[94,131] For metabolites, matrix selection is crucial to avoid interference from matrix peaks. Metabolites are therefore frequently detected with 9-AA in negative ion mode.[132] Oligonucleotides are analysed in negative ion mode with 2,4,6-trihydroxy acetophenone (THAP) or 3,4-diaminoparabenzophenone (DABP).[133] Different matrix additives can be used to improve analyte ionisation efficiency and sensitivity, as well as to reduce matrix clusters.[134,135] Further, there are many inorganic matrices, including carbon-, silicon-, and metal-based (e.g. gold nanoparticles) materials which are distinguished by the absence of matrix associated peaks, hence showing reduced interference with low mass analytes.[136] For organic matrices, the shape of the formed matrix crystals which is influenced

by solvent, matrix-sample deposition technique, and the drying method[137] can affect spot-to-spot reproducibility and analyte detection efficacy, especially for matrices that frequently form heterogeneous crystals[138-140]; vacuum drying can for instance be used to reduce matrix heterogeneity[141].

1.6 MALDI-TOF MS-based enzymatic *in vitro* screens

MALDI-TOF MS is a versatile technology capable of detecting a wide range of analytes, making it an ideal readout technology for biochemical reactions that result in a mass shift. In a standard enzymatic assay, at the initial time point (t_0), only the substrate is present. As the reaction progresses over time (Δt_1, Δt_2), the substrate is converted into the product, altering the substrate-to-product ratio. This change can be measured by MS, providing valuable insights into the reaction dynamics (Figure 1.4).

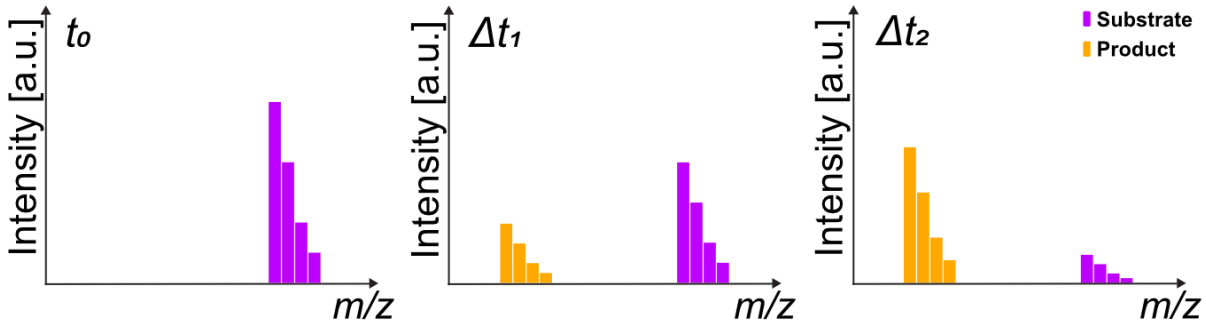

Figure 1.4. Schematic of a MS readout from an enzymatic reaction.
At the initial time point (t_0), only the substrate (purple) is detected but over time the substrate is converted into the product, leading to detection of the substrate and product (orange) in different ratios at different time points (Δt_1, Δt_2).

MALDI-TOF MS can be used to determine important enzyme kinetic parameters, such as K_M and the reaction velocity. In HT screening, substrate concentrations are typically set around the substrate concentration at half maximum velocity (K_M) to ensure the identification of all inhibitor classes.[142] Furthermore, enzyme concentration, incubation time, and assay temperature are optimised to maintain low substrate turnover at the assay endpoint, enabling reaction monitoring under conditions close to the initial velocity.[143] Dose-response curves have also been successfully measured by MALDI-TOF MS, allowing reliable determination of compound activity and calculation of half-maximal inhibitory compound concentrations (IC_{50}s).[144] To minimise errors caused by spot-to-spot variability, normalisation can be achieved using the substrate-product-ratio or by adding an internal standard, such as a heavy labelled

product.[145] For large-scale HT screens, establishing platform quality and reproducibility is essential. The coefficient of variation (CV) is used to assess robustness of individual *m/z* features, while the Z' factor provides a measure of overall assay robustness.[146] This factor, which accounts for the mean and standard deviation of both positive (no compound) and negative (no enzyme) controls can be used with the median and robust standard deviations to mitigate the impact of outliers.[147,148]

MALDI-TOF MS has proven effective in HT enzymatic screens, successfully identifying inhibitors of kinases[122,149], phosphatases[123], methylases[125,150], deubiquitylases, and ubiquitin E3-ligases[124,151,152]. It was also used in cellular assays to measure substrate-product concentrations in the presence of compounds, such as studies of histone acetylation[153] and transporter activity[154,155]. Moreover, the technology has been exploited to track various metabolites, including trimethylamine[156], acetylcholine[126], cyclic GMP-AMP[157] and 3-methoxytyramine[158]. Despite its powerful capabilities for monitoring enzymatic reaction *in vitro* and in cellular assays, MALDI-TOF MS remains underutilised in the screening of high-profile immunology targets.

1.6.1 Use case: Endoplasmic reticulum aminopeptidase 1 as drug target

The primary function of the immune system is defence of the host from harmful threats.[159] The immune system can be divided into two branches: the innate immune system, which provides rapid but non-specific responses, and the adaptive immune system, which offers slower but highly specific responses.[159] Mammals have evolved a complex network of diverse cell types, chemical messengers, signalling pathways and physiological structures to achieve effective immune responses.[159] In innate immunity, cellular responses are mediated by pattern recognition receptors, such as toll-like receptors (TLRs), which recognise harmful threats like microbial pathogens.[160] In adaptive immunity, the immune system monitors peptides displayed on the host cell surface, allowing adaptive immune cells to identify diseased and aberrant cells.[161] Alterations in the host cell state, in response to infection or cancer, leads to the presentation of "unusual" peptides, activating adaptive immune cells.[162] These peptides, collectively known as the immunopeptidome, are presented on the host cell surface by human leukocyte antigen (HLA) molecules, where they can be recognised by CD8+ T cells.[163] The presented peptides are generated through the antigen processing pathway (Figure 1.5A). In

this process, ubiquitylated proteins are degraded in the cytosol by the proteasome or immunoproteasome, resulting in peptide fragments of 2-25 amino acids.[164,165] These fragments may be further cleaved by cytosolic aminopeptidases or transported directly into the endoplasmic reticulum.[166,167] Within the ER, the peptide fragments are trimmed to lengths of eight to ten amino acids by the endoplasmic reticulum aminopeptidase 1 (ERAP1) to ensure the correct length for loading onto HLA molecules. The peptide-HLA complex is then transported to the cell surface via the secretory pathway where it plays a critical role in immune surveillance.[166,167]

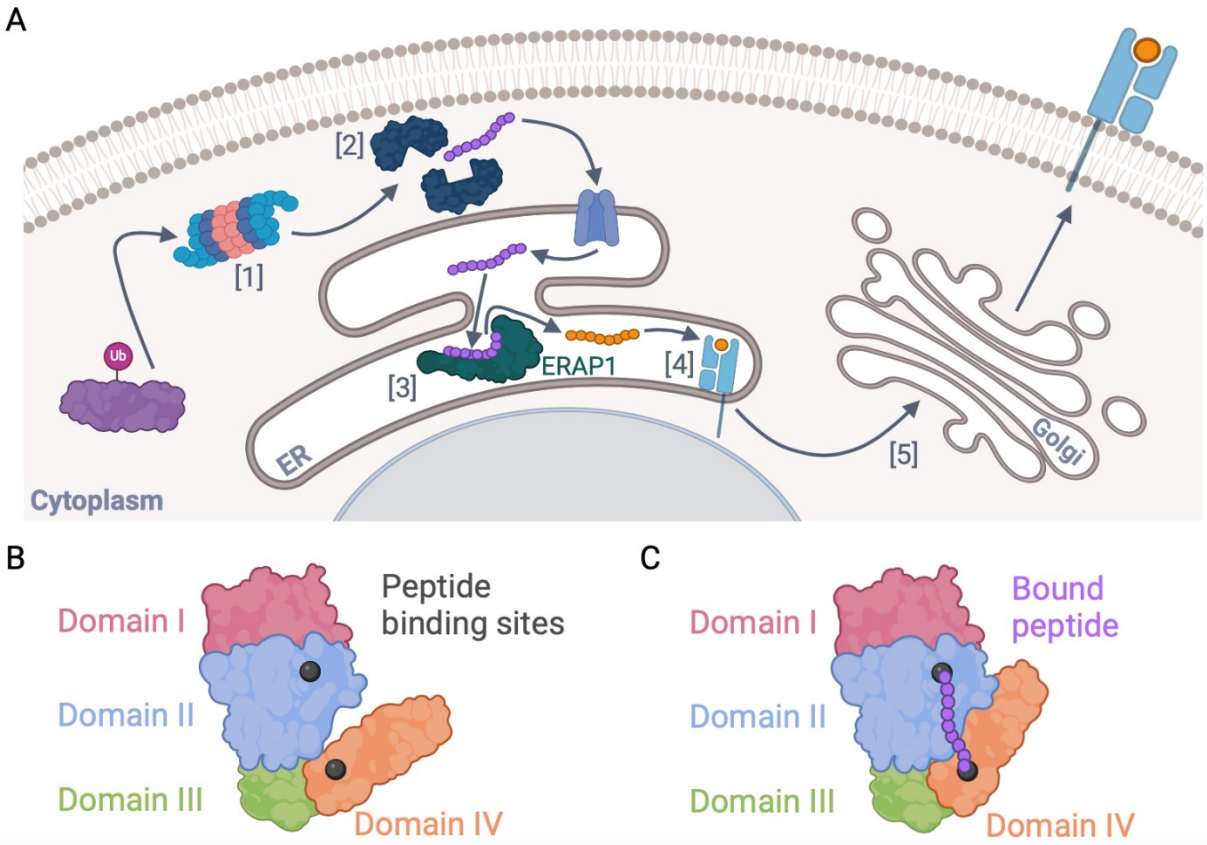

Figure 1.5. Simplified representation of the antigen processing machinery and the ERAP1 structure.
(A) Antigen presentation machinery. [1] Proteasomal degradation of ubiquitylated proteins, [2] Elongated antigenic peptide precursor degradation by cytosolic aminopeptidases with transport into the endoplasmic reticulum (ER), [3] Precursor peptide trimming to mature antigenic epitopes by ERAP1, [4] Mature antigenic peptide loading onto HLA, [5] HLA-peptide transport to the cell membrane via the secretory pathway. (B) ERAP1 structure in an open state. (C) ERAP1 structure in the closed state with a peptide bound to the active and regulatory binding sites.

ERAP1 is a member of the M1 subfamily of zinc metalloaminopeptidases, characterised by a highly conserved catalytic sequence and zinc-binding motive, which is crucial for a variety of

cellular functions.[168,169] For instance, endoplasmic reticulum aminopeptidase 2 complements ERAP1 by further trimming peptides that ERAP1 does not fully process.[170] Structurally, EARP1 consists of four domains, with three key features critical to its biological function. The active site and catalytic zinc ion, located in domain two, serve as the binding site for the peptide N-terminus (Figure 1.5B).[171] Domain four harbours a regulatory site where the peptide C-terminus binds[172], and it is hypothesised that this interaction triggers conformational changes that shift the enzyme into its active state, mediating the trimming of peptides to their mature length (Figure 1.5C)[173,174]. Additionally, the large cavity between the active and regulatory sites exhibits strong electrostatic potential, which likely contributes to ERAP's preference for trimming peptides with positively charged or hydrophobic residues.[175,176] Contrary to the current understanding, recent reports suggest that ERAP1 may also trim peptides while the peptides N-terminus is bound to the HLA molecule.[177,178]

The role of ERAP1 in shaping the immunopeptidome is still not fully understood. However, certain ERAP1 allotypes, in conjunction with specific HLA mutations, have been identified as risk factors for auto-immune and auto-inflammatory diseases, including ankylosing spondylitis, Behcet's disease, inflammatory bowel disease, insulin-dependent diabetes mellitus, multiple sclerosis, and psoriasis.[179-181] Furthermore, ERAP1 has been proposed as a target in viral infections[182], and its expression levels fluctuate in cancers of different histological origin[183,184]. Notably, ERAP1 upregulation is suspected to facilitate immune evasion by promoting the destruction of immunogenic tumour antigens.[162,185] In 2023, Grey Wolf Therapeutics started a Phase I clinical trial with their lead immuno-oncology candidate, GRWD5769, an ERAP1 inhibitor tested for use alone and in combination with immune checkpoint inhibitors to treat different solid tumours.[186] The development of ERAP1-targeting compounds has been challenging due to the enzyme's structural homology with other M1 aminopeptidase family members. Previously described inhibitors such as leucinethol and DG013A target ERAP1's active site, but this approach has limited selectivity and therapeutic utility.[187,188] However, in 2020, Liddle *et al.* discovered an ERAP1 inhibitor that targets the enzyme's regulatory site, promoting selectivity.[55]

Several HTS assays have been developed to measure ERAP1 activity. A fluorescence-based assay was initially used but found to have a limited dynamic range, leading to its replacement by a chemiluminescence-based assay.[55] Both assays required peptide labelling at the C-

terminus, which interfered with peptide binding to the enzymes' regulatory site. This interference led to substrate hydrolysis upon simultaneous binding of the substrate to the N-terminus and compound to the C-terminus, necessitating further analysis to confirm the activity of hit compounds in the presence of biologically relevant peptide precursors.[55] To address this limitation, a RapidFire MS-based assay was introduced, enabling the evaluation of compound activity under conditions that preserve biological relevance. This platform also allowed for both single-concentration and dose-response screening.[55] However, with analysis speeds of 7 seconds per sample, this setup proved incompatible with ultra HT screening efforts. A MALDI-TOF MS-based ERAP1 assay would be able to improve the screening throughput.

1.7 MALDI-TOF MS-based cell phenotyping

MALDI-TOF MS use was also reported in phenotypic screening and it is a standard technique for microorganism phenotyping in the clinical setting.[189-192] Bacterial species are distinguished through differential expression of ribosomal proteins, a process known as biotyping.[193,194] Species identification based on the mass spectrum is achieved by either comparison against an annotated spectral library or by harnessing trained machine learning algorithms.[195-197] The introduction of MALDI glycotyping, a workflow enabling the analysis of glycan patterns, has improved subtyping within bacterial species.[198,199] As MALDI-TOF MS can provide rapid, reliable, and cost-effective microorganism identification in the clinic[200,201], this technology is now also applied in other settings, including food and environmental testing[202-205].

1.7.1 Eukaryotic cell phenotyping by MALDI-TOF MS

MALDI-TOF MS-based cell phenotyping approaches for whole mammalian cells have not yet reached the level of success seen in microorganism phenotyping. However, initial applications have emerged, primarily using specific *m/z* features ("biomarkers") to distinguish between cell phenotypes, indicating broad applicability in phenotypic drug discovery screening.

For eukaryotic cell phenotyping, most assays to date have focussed on the high molecular range (2,000 – 20,000 Da) which contains peptides and small proteins.[44] These signatures have been used to differentiate between different cell types.[206-208] For instance, Karger *et al.* 2010 observed the clustering of 66 cell lines from 34 different species.[209] Similarly, clustering has

been reported for different neuroblastoma[210] and glioblastoma[211] cell lines. In primary cell mixtures, different glial cell types[212] or non-cancerous versus cancerous cells[213] have been distinguished by MALDI-TOF MS. Beyond cell type differentiation, MALDI-TOF MS approaches have successfully identified different cell stages, such as stress, apoptosis, and necroptosis[214,215], and have been used to detect neutrophil differentiation in whole blood samples[216].

In contrast to earlier workflows, most cellular MALDI-TOF MS drug discovery screening efforts have focussed on the low molecular mass range (100 – 1,000 Da) which is populated by metabolites and lipids.[44] Lipid profiles are highly dynamic and often indicative of cell phenotype or disease state.[217-219] Metabolite and lipid *m/z* features are commonly used in MS imaging (MSI), e.g. MALDI-TOF MS imaging[220], for instance to classify astrocytes, neurons or tumours.[221-224] In 2018, Weigt *et al.* identified lipid biomarkers in a phenotypic MALDI-TOF MS screen that enabled inference of kinase inhibitor activity.[138] In another study, Weigt *et al.* 2019 described a HTS-compatible MALDI-TOF MS assay that evaluated fatty acid synthase activity via the substrate malonyl-coenzyme A while also profiling additional metabolic pathways.[225] Recently, metabolite markers have also been used to infer complement-dependent cytotoxicity from different batches of antibodies.[140] While these approaches focus on selected biomarkers, it has been suggested that analysing multiple features using unsupervised clustering approaches or machine learning strategies could additionally allow for MoA elucidation when performing large scale screens of unknown compounds in conjunction with well-annotated control compounds.[44]

1.7.2 Immune cell phenotyping by MALDI-TOF MS

In 2022, Blank *et al.* investigated lipopolysaccharide (LPS)-induced lipid alterations in microglia using MALDI-TOF MS, identifying 21 potential inflammation biomarkers, six of which were significantly reduced in a proof-of-concept treatment with the histone deacetylase inhibitor SAHA.[139] Other studies aiming to conduct immune cell phenotyping by MALDI-TOF MS have focussed on the high mass range (2,000 – 20,000 Da).

In 2010, Ouedrago *et al*. pioneered the field by phenotyping immune cells from the blood. At that time, flow cytometry was a standard technique for immune cell phenotyping, classifying cells based on labelled membrane proteins. Using the MALDI-TOF MS workflow, they

successfully distinguished between human macrophages, T cells, neutrophils and red blood cells.[226] They improved clustering between different cell types by using a spectral reference library, similar to the bacterial phenotyping approach. An automated workflow was soon published, enabling phenotyping of differentiating neutrophils and monocytes from whole blood.[216] Further publications have focussed on human macrophages, distinguishing between polarised pro- and anti-inflammatory cell states, and identifying a macrophage signature with a polarisation-independent mass peak at *m/z* 4964.[227,228]

To address the challenge of translating these protocols into an industrial setting, Heap *et al.* 2019 systematically evaluated the effect of various parameters, including cell lysis protocol, cell number, MALDI-TOF MS matrix choice, matrix concentration, and laser power on mass feature numbers and robustness, using different cell lines.[208] Consistent with previous literature, they identified the macrophage-specific mass peak at *m/z* 4964 in monocyte cells, and they used this mass feature for intensity normalisation. This allowed them to conduct a compound screen with THP1 monocyte cells and evaluate compound activity in primary monocytes and acute myeloid leukaemia samples.[229] Unlike other assays, they also employed multiple mass features to achieve separation between mouse embryonic stem cells with and without kinase inhibitor treatment. They distinguished between resting macrophages and different pro-inflammatory stimuli and further identified inflammation inhibitors as well as compound cytotoxicity by using unsupervised clustering.[208,229]

1.7.3 Use case: macrophages as drug target

During an inflammation response, immune cells such as monocytes, macrophages, dendritic cells, eosinophils, basophils, mast cells, and neutrophils are quickly recruited within hours following pathogen infection or tissue damage.[159] Most of these cells originate from hematopoietic stem cells, which reside in the bone marrow and spleen. Tissue-resident macrophage pools originate from the yolk sack and are established during embryogenesis.[230] They can be found in organs like the brain, bones, kidney liver, and lung. The primary functions of these cells include pathogen detection and maintenance of tissue homeostasis, which they achieve through the internalisation of foreign matter and cellular debris.[231-233]

Macrophages exhibit remarkable plasticity, allowing them to polarise into different cell states based on their environment.[234] In the simplified model, macrophages can be categorised into

resting (M0), classical activated (M1), and alternatively activated (M2) macrophages (Figure 1.6). M2 macrophages can for instance promote tissue regeneration and wound healing.[235] Polarisation into the M2 phenotype is induced by exposure to cytokines, such as IL-4, which binds to interleukin membrane receptor, and triggers the janus kinase/signal transducers and activators of transcription (JAK/STAT) signalling cascade.[236,237]

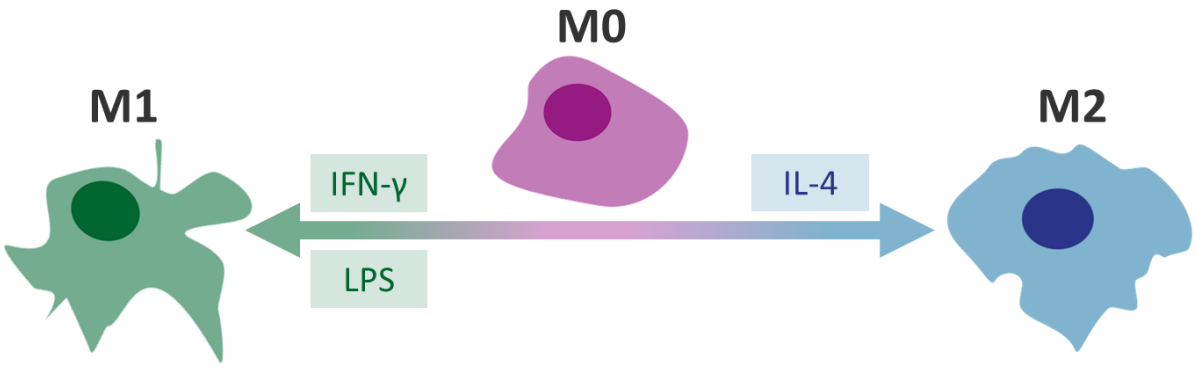

Figure 1.6. Schematic representation of macrophage polarisation.
Unstimulated macrophages are in the resting state (M0) from which they can be polarised into a classical activation (M1) or alternatively activated state (M2) by different stimuli.

The pro-inflammatory M1 phenotype is better understood than the anti-inflammatory M2 phenotype. M1 polarisation is triggered by exposure to pathogen-associated molecular patterns. These are biological molecules which are highly conserved within different pathogens and which the immune system is primed to respond to.[160] They are recognised by pattern recognition receptors of immune cells, including c-type lectin, NOD-like receptors, and TLRs.[160] For instance, LPS, a cell membrane component of gram-negative bacteria, binds to TLR4.[238] LPS binding initiates downstream signalling cascades through both myeloid differentiation primary response protein (MyD88)-dependent and independent pathways (Figure 1.7). Both pathways activate interferon regulatory factors (IRFs, e.g. IRF-5, IRF-3), but only the MyD88-dependent pathway also activates mitogen-activated protein kinases (MAPKs, e.g. p38), as well as nuclear factor-kappa B (NF-κB) and its modulators (e.g. IKK).[239,240] This pathway activation leads to the expression of pro-inflammatory genes and the secretion of pro-inflammatory cytokines.[241]

Macrophages also respond to a variety of chemo- and cytokines, including interferons (IFNs), interleukins (ILs), and tumour necrosis factors (TNFs), which are secreted by host cells additionally in response to infection or cellular stress.[242] For instance, IFN-γ, the only type II IFN, can enhance both innate and adaptive immune responses.[243] IFN-γ signalling is mediated

through heterodimeric receptors (IFN-γR) and the JAK/STAT signalling cascade (Figure 1.7). Upon IFN-γ binding, the receptors dimerise and associate with another receptor pair, triggering a phosphorylation cascade from JAK2 via JAK1 to STAT1.[244-246] The phosphorylated STAT1 dimer then translocates to the nucleus, where it induces the expression of IFN-regulated genes.[247]

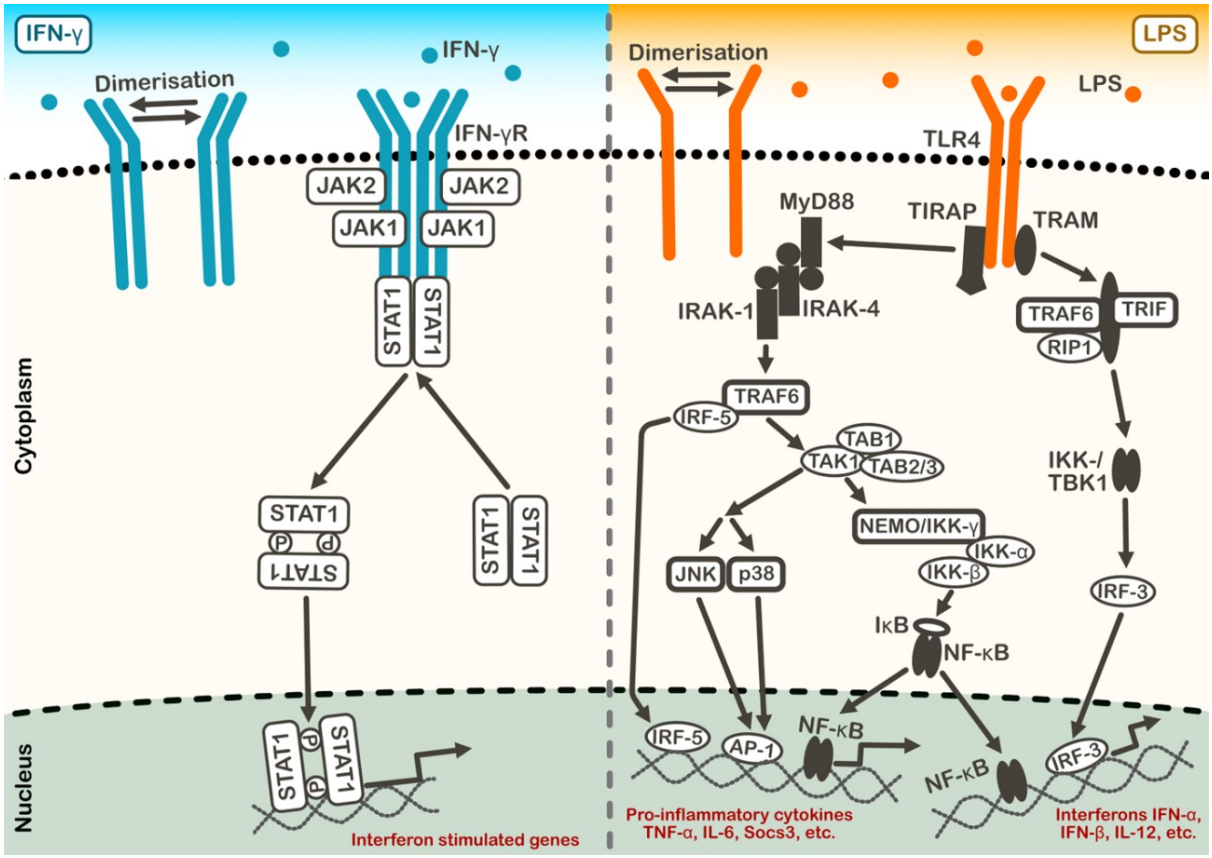

Figure 1.7. IFN-γ and LPS signalling pathways.
(Left) IFN-γ signalling is mediated by receptor dimerization, and a JAK/STAT phosphorylation cascade that leads to transcription of interferon stimulated genes. (Right) LPS binding elicits downstream signalling cascades though MyD88-dependent and independent pathways. Both pathways result in activation of interferon regulatory factors (e.g. IRF-5, IRF-3), but only the MyD88-dependent pathway also activates MAPKs (e.g. p38), and NF-κB. LPS binding elicits for instance transcription of pro-inflammatory cytokines and interferons.

The acute inflammation response mediated by macrophages is tightly regulated, but when over-activated or prolonged, it can lead to tissue damage and various diseases. Macrophage dysregulation is implicated in a broad range of conditions, including several auto-immune diseases such as diabetes[248] and inflammatory bowel disease[249]. In the brain, macrophages play a crucial role in synapse formation, plasticity, and elimination; dysregulation in this context can contribute to neurodegenerative disorders such as Parkinson's and Alzheimer's.[250]

In cardiac tissue, macrophages are involved in immune defence, electrical conduction, and arterial tone regulation.[251] Dysregulation in these cells is linked to heart failure, obesity (a risk factor for heart failure), and hypertension.[251] Kupffer cells in the liver, which normally protect against drug-induced liver injury and toxin-induced fibrosis, can cause liver tissue damage when dysregulated.[252] In oncology, tumour-associated macrophages (TAMs) are of significant interest because they promote tumour growth and metastasis development through different functions.[253] TAMs promote angiogenesis by producing angiogenesis-promoting factors, and they remodel the extracellular matrix to facilitate tumour progression and to weaken the matrix around blood vessels.[253] They enhance the invasive and migratory properties of cancer cells through the secretion of TNF-α and TGF-β, which can then migrate into the circulation (intravasation), subsequently forming metastasis in distal organs.[253] TAMs also block the activity of cytotoxic T cells targeting tumour cells, making TAM modulation a potential strategy for cancer treatment, with many current drug discovery efforts focused on restoring cytotoxic T cell function.[253]

1.7.4 Tools to study macrophages

Consequently, macrophages are crucial targets for drug development. Studying macrophages and performing macrophage targeted drug discovery is challenging due to their complexity, plasticity and variability across species and individuals.[254,255]

Selecting the appropriate model for macrophage research is critical as responses can vary significantly between enzymatic *in vitro* assays, cellular assays, and *in vivo* models. Cellular assays often use various cell models, including immortalised monocyte cell lines (e.g. THP1), induced pluripotent stem cell (iPSC)-derived macrophages, and primary macrophages from either murine (bone marrow derived, BMDMs), or human (peripheral blood derived, PBMCs) sources. Differences between species and cell models have been reported. For instance, Reynolds *et al.* 2015 observed increased inducible nitric oxide synthase in mouse models following LPS stimulation, while human responses included upregulation of CCL20, CXCL13, IL-7R, and STAT4.[256] Additionally, murine BMDMs and human PBMCs exhibit distinct metabolic responses in inflammation, highlighting the need to carefully select the model species.[257] Gudgeon *et al.* 2024 found significant variability in responses to inflammatory stimuli among murine cell lines, immortalised cells, and BMDMs.[258] Likewise, human THP1 cells with genetic

mutations have displayed different immune responses compared to PBMCs.[259] A limitation of primary cells is their constrained availability, leading to increased interest in iPSC-derived macrophages for disease modelling and drug discovery due to their higher biological relevance and scalability.[260]

When evaluating macrophage polarisation, the choice of stimulus is also crucial. Current studies use isolated bacterial membrane proteins, such as LPS, or heat-killed and live bacteria to induce polarisation.[261] Moore *et al.* 2000 demonstrated that pro-inflammatory cytokine release in response to *Escherichia coli* and LPS is mediated through different cell surface receptors.[262] Further, external stimulants can be combined with host-derived chemokines and cytokines such as IFNs that are frequently released in inflammation responses.

Macrophage polarisation is commonly determined using image-based or label-based methods. T cell activation can serve as a redout method for macrophage polarisation.[263] Fluorescence-based techniques can measure real-time phagocytosis activity[264]. Flow cytometry detects pro-inflammatory (CD40, CD80, and CD25) and anti-inflammatory (CD206 and CD163) cell surface markers[40,265,266]. Compounds that increase M1 marker expression are typically explored in infection and immuno-oncology, while those that decrease M1 markers may be promising for auto-immune disease treatment. Another HTS approach to determine macrophage polarisation involves label-based analysis of pro-inflammatory and anti-inflammatory cytokine secretion.[39] However, while used for hit triaging in large scale screens, these techniques do not elucidate the MoA or intracellular targets of identified compounds.

1.8 Proteomics

Omics approaches, including genomics and transcriptomics provide a holistic view of the molecular landscape within a biological system.[267] Insights into biological processes, such as the molecular basis of diseases, can be gained through understanding protein structure, function, and abundance, which are studied via proteomics.[268] Beyond target identification and validation in the drug discovery and development pipeline, proteomics is also used in lead optimisation, pre-clinical trials, and clinical trials.[269] The incorporation of proteomics into early drug discovery stages has gained increasing interest, as understanding drug MoA and drug targets in a physiologically relevant context can enhance the understanding of compound safety and efficacy.[15] Techniques such as MS are frequently used to analyse protein expression,

modification, and interaction.[268] "Top-down" and "bottom-up" MS-based proteomic approaches are distinguished by their analysis of intact proteins or peptides from proteolytic digestion of the protein, respectively.[270] The four steps in a "bottom-up" proteomics workflow that enable the detection of thousands of proteins in a single sample are sample preparation, peptide separation, MS acquisition, and data analysis (Figure 1.8).[271]

1. **Sample preparation:** Proteins are extracted from the biological sample and digested into peptides.
2. **Peptide separation:** Chromatography, usually C18-based liquid chromatography (LC), is used to reduce the complexity of the peptide mixture before samples enter the mass spectrometer.
3. **Mass spectrometry acquisition:** Peptides are ionised, precursor ions selected, selected ions fragmented, and *m/z* and abundance of fragment ions measured.
4. **Data analysis:** Bioinformatic tools are used to infer peptide sequence from the mass spectrum, allowing for protein identification and quantification.

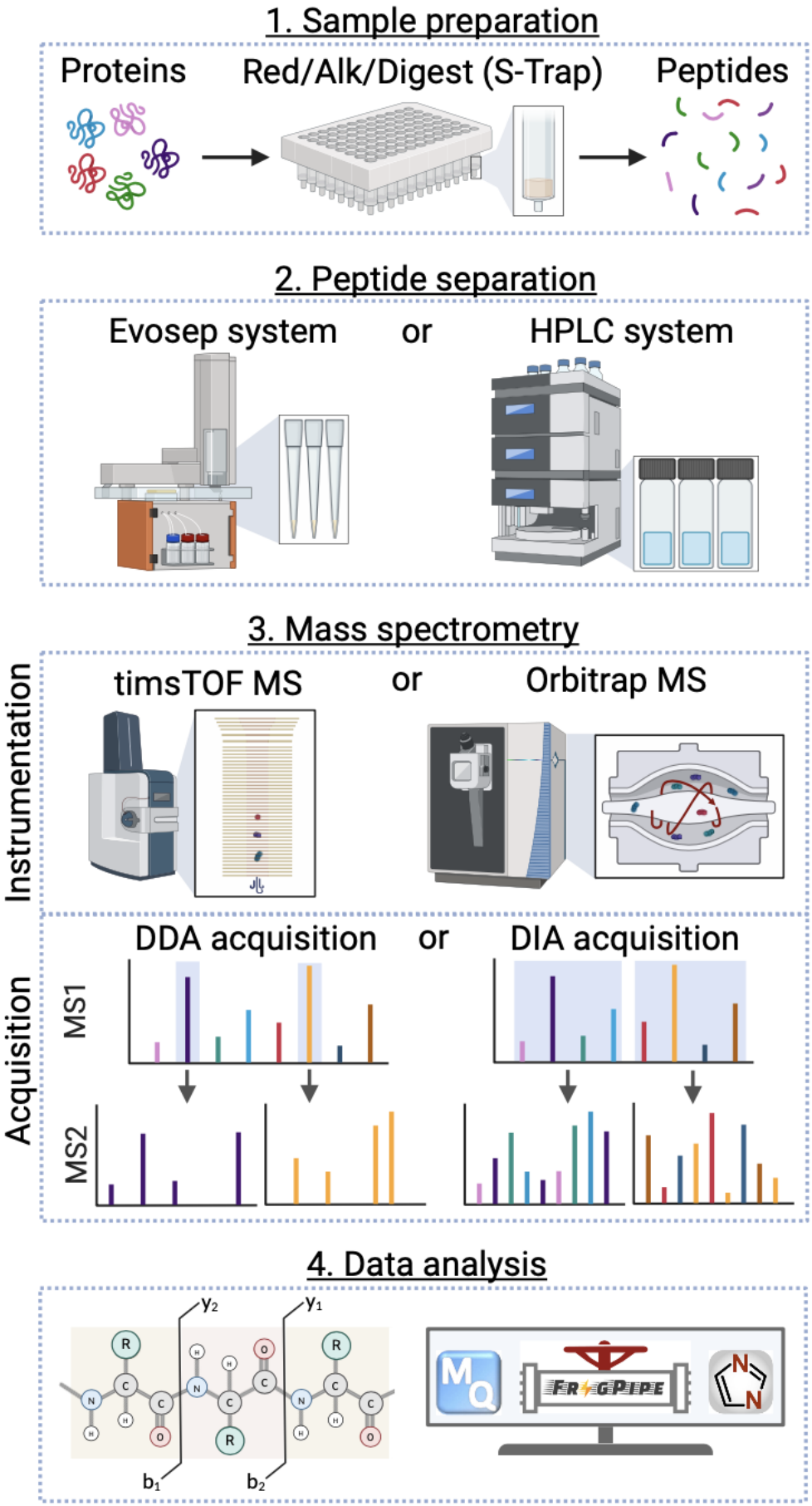

Figure 1.8. Schematic bottom-up proteomics workflow.

The workflow entails four different steps; (1) Sample preparation: Protein extraction, reduction, alkylation, and digestion into peptides (e.g. S-Trap method), (2) Peptide separation: Sample complexity reduction by liquid chromatography (e.g. Evosep or HPLC system), (3) Mass spectrometry: ESI is used for analyte ionisation in different MS instruments (e.g. timsTOF or Orbitrap MS) where peptide precursor ions are detected (MS1), ions which are selected either by an intensity (DDA) or window (DIA) dependent fashion fragmented, and fragment ion features such as *m/z* and abundance measured (MS2), (4) Data analysis: Bioinformatic tools infer peptide sequence, protein identification, and quantification.

1.8.1 Sample preparation in proteomics

The aim of the sample preparation step is to produce peptides with known cleavage motifs through enzymatic digestion that can be later analysed by MS.[271] Sample preparation methods are numerous and can be mostly categorised into in-solution, in-gel, on-bead, and matrix-aided digestion techniques.[271] Varnavides *et al.* 2022 compared 16 widely used sample preparation methods and found that most showed high reproducibility and significant overlap between identified proteins. They noted differences in recovery for specific protein features, which should be considered alongside sample nature, processing time, and cost when selecting a sample processing technique.[272]

A versatile and robust matrix-aided digestion method commonly used in proteomics workflows is the S-Trap method (Figure 1.8). Although it is associated with higher costs, it requires minimal hands-on time and improves the detection of low-abundant proteins.[272] In this workflow, sample lysis and protein solubility are achieved by adding sodium dodecyl sulphate (SDS) to the sample.[273,274] A reducing agent is then used to reduce disulfide bonds between cysteine residues, leading to protein denaturation, which is crucial for efficient enzymatic digestion.[273,274] An alkylation agent is added to prevent the reformation of cysteine bonds.[273,274] The samples are acidified and loaded onto a solid phase that non-specifically immobilises the denatured proteins.[273,274] Interfering solvents are removed from the sample before endoproteinases such as trypsin (Lys-Arg cleavage, missed cleavage in proline proximity), Lys-C (C-terminal Lys cleavage) or Lys-N (N-terminal Lys cleavage) are used for protein digestion.[275] The peptides are then eluted, dried, and resuspended in a MS-suitable buffer for analysis.

1.8.2 Peptide separation and mass spectrometry setups in proteomics

LC is coupled to mass spectrometers to separate the resulting complex peptide mixtures before sample injection to improve MS sensitivity and resolution.[276] Different LC systems have emerged (Figure 1.9); high-performance liquid chromatography (HPLC) and the Evosep One system (Evosep) are commonly used in proteomics analysis. In a conventional HPLC setup for proteomics analysis, the peptides are present in solution and picked up in the sample loop. They are then concentrated and purified on the trap column and eluted onto the analytical column where they are separated prior to MS injection. These HPLC systems are customisable, compatible with a range of flow rates, gradients, and column types, allowing for optimised resolution.[277] A stationary phase, such as octyldecylsilane (C18), is frequently used in these columns for proteomics. Analyte elution from the column is controlled by the mobile phase, which often includes varying concentrations of an organic solvent.[278]

In contrast, the Evosep system emphasises speed and reproducibility, using pre-defined, standardised gradients and providing compatibility with automation.[279] Key features of the Evosep system are its unique sample delivery and loading strategies. For sample delivery, the peptides are bound to a C18 resin within the Evosep tip rather than using in-solution delivery as in HPLC.[279] This resin acts as the trap column, concentrating and purifying the peptides while minimising sample carryover by using a new tip for each sample.[279] Further, an organic gradient is formed in the sample loop, aiding pre-separation of analytes before they are eluted onto the analytical column where they are further separated before MS injection.[279]

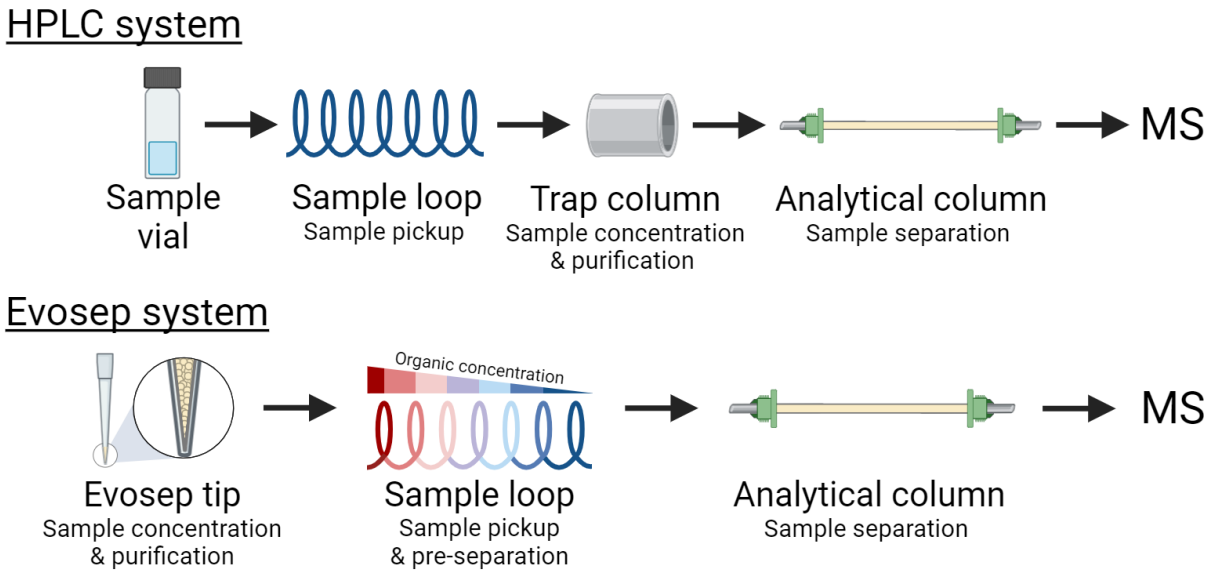

Figure 1.9. Schematic representation of different LC systems.

In conventional HPLC, samples are placed in vials and taken up in the sample loop, followed by sample concentration and purification on the trap column before samples are separated on the analytical column prior to MS. In the Evosep system, samples are first concentrated and purified in the Evosep tips before they are taken up and pre-separated in the sample loop, followed by more extensive sample separation on the analytical column prior to MS.

Ionisation of the peptides is typically achieved by ESI, which is usually operated in positive ion mode.[280,281] Within the mass spectrometer, the ESI ion source is traditionally coupled to a series of mass analysers which together form tandem/hybrid configurations. In the first mass analyser (MS1), a complex mixture of precursor ions is detected, and ion subsets selected for fragmentation.[282] Fragmentation occurs in a collision cell where molecular bonds, often peptide bonds, are dissociated by collision with an inert gas.[282] This process enables peptide sequence identification based on the *m/z* and abundance of fragment ions measured in the second mass analyser (MS2).[282]

Two types of mass spectrometry instruments are commonly used within the proteomics field. The first type are hybrid Orbitrap instruments, such as the Q Exactive or Orbitrap Exploris 480 from Thermo Fisher Scientific (Figure 1.10). After analyte ionisation, the ions are guided into the quadrupole which is composed of four metal rods that create an electric field to guide and eject ions based on their *m/z*, serving as a mass filter. The selected ions are passed through the C-Trap trap into the HCD cell where they are fragmented by collisional dissociation before being transported back into the C-Trap.[283] The C-Trap consists of electrodes to which voltages are applied to initially trap, and stabilise ions, before ejecting them into the Orbitrap mass analyser.[283] The Orbitrap, with its spindle-like central electrode and two cup shaped outer electrodes, traps ions in an orbital motion around the inner electrode. The frequency of rotation correlates with the ion *m/z* and the amplitude of the rotation correlates to the ion intensity; the mass spectrum is derived by Fourier-transformation.[284] While Orbitrap mass analyser offer high mass resolution and accuracy, they have longer acquisition times compared to lower resolution mass analysers such as TOF, limiting throughput.[284] When coupled with HPLC systems, cycle times of 60 to 120 minutes per sample are typically achieved. The recently released Orbitrap Astral by Thermo Fisher Scientific is a different type of instrument that combines the Orbitrap technology with the novel Astral mass analyser to offer enhanced acquisition speeds.[285]

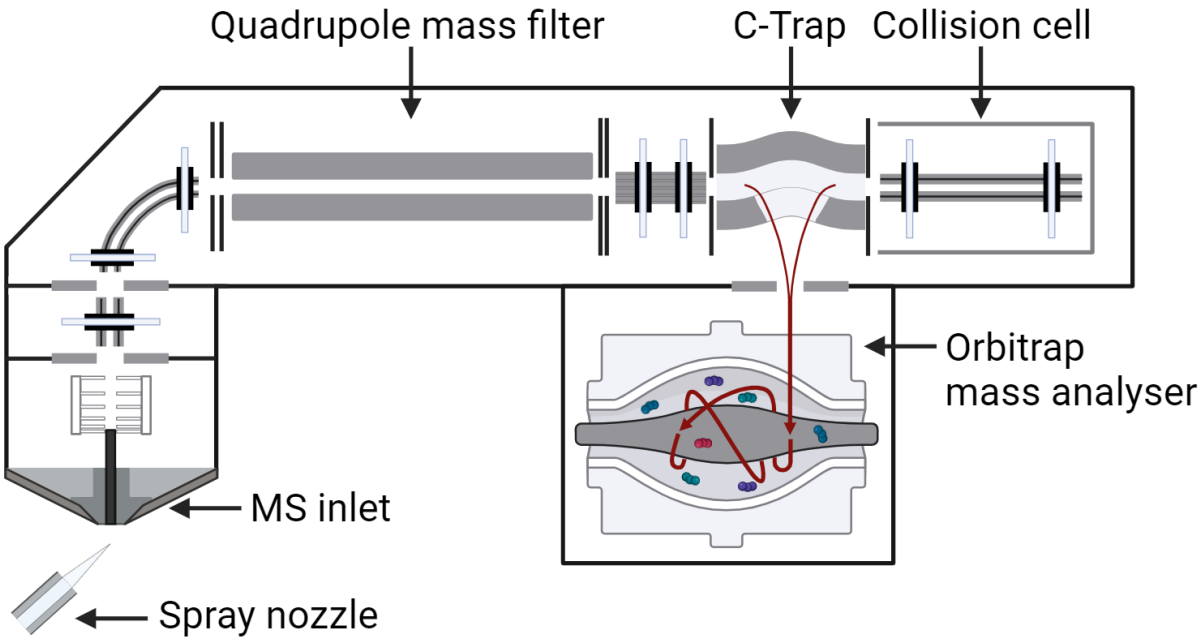

Figure 1.10. Schematic representation of a hybrid Orbitrap instrument.
Sample ionisation occurs in an ESI source and the generated ions are filtered in the quadrupole, fragmented in the collision cell and guided into the C-Trap from which they are injected into the Orbitrap mass analyser.

The second type of mass spectrometry instruments that are frequently used in proteomics are featuring the TIMS technology to further reduce sample complexity and a different mass analyser, a TOF (chapter 1.5) in comparison to the hybrid Orbitrap instruments. Successful coupling of the TIMS technology with the TOF has resulted in instruments such as the timsTOF Pro or timsTOF HT from Bruker which achieve increased acquisition speeds, resolution and sensitivity. After analyte ionisation, the ions are delivered to the TIMS cell where they are initially bundled in the TIMS tunnel. Then they are subsequently separated according to their ion mobility (IM).[286] The separation is achieved through a gas flow that pushes ions forward with a force that is proportional to their collisional cross-section (i.e. size). At the same time, an electric field is applied to the TIMS tunnel to additionally separate the ions according to their charge. A pulsed release is performed to transfer the ions from the TIMS cell into the quadrupole mass filter from which they get transported into the collision cell and subsequently into the TOF mass analyser.[286] The timsTOF instruments offer higher speed and sensitivity but have reduced mass resolution and accuracy compared to Orbitrap instruments.[287] They are invaluable for large-scale proteomics, as coupling with the Evosep One system allows whole proteome analysis in as little as 6 min per sample (200 samples per day method).[288]

Two acquisition modes, data-dependent acquisition (DDA) and data-independent acquisition (DIA) can be used with either hybrid Orbitrap or timsTOF instruments (Figure 1.8). DDA, the more established technique, selects the most abundant ions within MS1 for fragmentation.[289] This method provides high accuracy of peptide sequence identifications but may miss lower intensity precursor ions, reducing sample coverage and resulting in higher missing values (NAs) between samples.[289] DIA, developed to increase sample coverage, selects all ions within a specified *m/z* and/or IM window of an MS1 scan for fragmentation, reducing NAs significantly in an exemplary study from 51% with DDA to 1.6% with DIA.[290] However, DIA generates more complex fragment patterns, hampering peptide identification. Reference spectral libraries created in DDA mode are often used to increase accuracy of peptide identification, but their generation requires additional sample and instrument time.[291]

1.8.3 Data analysis in proteomics

The amino acid sequence of the peptide can be derived from the MS2 scan. Collision induced dissociation preferentially cleaves the amide bond in the peptide back bone, resulting in various fragment ions that differ by a single amino acid (Figure 1.8).[292] The mass difference between these fragment ions, derived from the *m/z*, allows for the inference of the amino acid sequence of the precursor peptide. The only limitation of this technique is the inability to distinguish between leucine and isoleucine, which share the same monoisotopic mass.[293]

Peptide identification and subsequent peptide-to-protein matching can be conducted in an automated fashion using various bioinformatic tools, known as search engines, such as MaxQuant and DIA-NN.[294,295] In the software, the process begins with uploading and processing the raw spectrum data files.[296] Peptide identification is then performed by comparing the obtained mass spectra to a peptide library, which can be either theoretically or experimentally derived. In a theoretical approach, an *in silico* digest of a species-specific FASTA file is performed with the chosen endopeptidase to generate peptides that can be theoretically observed within the analysis.[296] Alternatively, experimental libraries are created by analysing samples with MS to generate a spectral library that is then used to match the acquired data.[288] After peptide matching, scoring and filtering steps are applied to minimise incorrect identifications.[296] Finally, proteotypic peptides can be used to infer protein identity.[297]

1.8.4 Proteomics applications

Applications of proteomics are diverse due to the customisable nature of sample preparation, peptide separation, MS, and data analysis techniques. For instance, in plasma proteomics, highly abundant proteins such as albumin and immunoglobulins can obscure the analysis of low-abundant proteins without specific enrichment or depletion strategies.[298] Enrichment strategies are also used to study post-translational modifications (PTMs)[299], such as phosphorylation[300,301], ubiquitination[302-304], and glycosylation[305]. A rapidly evolving field is single-cell proteomics, which demands minimal sample loss during preparation and high sensitivity in MS analysis.[306]

Workflow modifications are also significant in chemoproteomics, a field which combines chemical biology and MS to identify drug-target interactions.[307] Target enrichment is employed in workflows for affinity- or activity-based profiling.[308] Additionally, methods inducing thermal, chemical, or enzymatic denaturation can be used to assess drug binding stability.[15,309] While these methods provide valuable insights, they historically have low throughput, require a large sample amount, and are costly.[15] Recent developments are improving workflow throughput, but further integration with unmodified standard proteomics workflow could enhance compatibility with early drug discovery stages. This approach's feasibility was exemplified by studies such as Saei *et al.* 2019, which employed full proteome expression atlases to deduce MoAs and off-target effects through a fingerprinting approach.[310] Furthermore, Mitchel *et al.* 2023 conducted a comprehensive study documenting proteome-level changes induced by 875 compounds in HCT116 cells, linking compound structure with MoA.[311]

1.9 Aims

This thesis aims to demonstrate the advantages of MS in early drug discovery stages, where it is currently underutilised. I will exemplify this on research questions within the immunology field, a key drug discovery area due to its links to various diseases. Several MS systems exist that are compatible with HTS workflows. This thesis will highlight the potential of MALDI-TOF MS, a promising technology for target-based and phenotypic screens. I will further illustrate how leveraging a new wave of proteomics technologies that allow increased throughout can aid lead compound candidate selection by identifying desired and undesired compound effects.

<u>The key aims of my thesis are as follows:</u>

- Develop a biochemical MALDI-TOF MS drug discovery assay for the high-profile immunology target ERAP1.
- Introduce automation for the developed MALDI-TOF MS-based ERAP1 workflow to enable robust screening against large compound libraries.
- Compare the results from the MALDI-TOF MS ERAP1 screen to those from an established RapidFire MS assay to validate hit calling.
- Optimise cell culture and stimulation conditions for iPSC-derived macrophages from human donors.
- Develop a robust proteomics workflow to characterise pro-inflammatory human iPSC-derived macrophage polarisation.
- Develop a MALDI-TOF MS assay to phenotype resting and pro-inflammatory iPSC-derived macrophages.
- Introduce automation for the MALDI-TOF MS macrophage phenotyping workflow to screen compound libraries that cover broad and inflammation-specific mechanisms of action.
- Compare the MALDI-TOF MS phenotypic screen of inflammation-specific compounds to an established pro-inflammatory cytokine screen.
- Compare inflammation-specific compound hits determined by proteomics to the MALDI-TOF MS and cytokine screens.
- Determine proteomics capability to identify on- and off-target pathway engagement for identified inflammation-specific hit compounds.

Chapter 2. Materials and methods

Table 2.1. List of general chemicals and reagents. Indicated are also their supplier.

Chemical/ reagent	Supplier
3-((3-cholamidopropyl) dimethylammonio)-1-propanesulfonate (CHAPS) hydrate	Sigma-Aldrich
4-(2- hydroxyethyl)-1-piperazineethanesulfonic acid (HEPES)	Sigma-Aldrich
Acetonitrile (MeCN) MS grade	Thermo Fisher Scientific / VWR Chemicals
Ammonium dihydrogen phosphate ($NH_4H_2PO_4$)	Sigma-Aldrich
Ammonium formate HPLC grade	Thermo Fisher Scientific
Ammonium hydroxide	Sigma-Aldrich
Benzonase® Nuclease HC, Purity > 99%	Merck
Bovine serum albumin (BSA)	Sigma-Aldrich / Thermo Fisher Scientific
Diammonium hydrogen citrate	Sigma-Aldrich
Dimethyl sulfoxide (DMSO)	Sigma-Aldrich
Dulbecco's phosphate buffered saline (DPBS)	Sigma-Aldrich
Ethanol MS grade	Thermo Fisher Scientific
Fetal Bovine Serum, qualified, heat inactivated, Australia	Thermo Fisher Scientific
Formic acid (FA) LC-MS grade, 98-100%	Sigma-Aldrich, Thermo Fisher Scientific
Glycerol	Thermo Fisher Scientific
Hela protein standard	Pierce
Iodoacetamide (IAA)	Merck
Isopropanol MS grade	Thermo Fisher Scientific
Macrophage colony-stimulating factor (M-CSF)	Peprotech
Methanol (MeOH) MS grade	Thermo Fisher Scientific
Phosphoric acid, 85%	Merck
Pierce™ BCA protein assay kit	Thermo Fisher Scientific
Roswell park memorial institute (RPMI) 1640 Medium	Gibco
Sodium chloride (NaCl)	Sigma-Aldrich
Sodium dodecyl sulphate (SDS)	Merck
Triethylammonium bicarbonate buffer (TEAB), 1 M	Merck
Trifluoroacetic acid (TFA)	Sigma-Aldrich / Thermo Fisher Scientific / Merck
Tris(2-carboxyethyl)phosphine hydrochloride solution (TCEP), 0.5 M	Sigma-Aldrich / Thermo Fisher Scientific
Tris(hydroxymethyl)aminomethane hydrochloride (Tris-HCl), 1M, pH 7.5	Invitrogen
Trypsin	Worthington Biochemical
Trypsin/Lys-C Protease Mix MS grade	Thermo Fisher Scientific / Pierce
Tween-20	Sigma-Aldrich
Water (H_2O) MS grade	Sigma-Aldrich / Thermo Fisher Scientific

2.1 ERAP1 assay peptide detection and *in vitro* assay conduction

2.1.1 ERAP1 biochemical assay specific materials

Table 2.2. List of assay peptides utilised in the ERAP1 biochemical assay. Indicated are also their peptide sequence, monoisotopic mass, DMSO stock concentration, and corresponding assay buffer.

Peptide description	Peptide sequence†	Monoisotopic mass	DMSO stock	Assay buffer supplement
Non-basic substrate	YTAFTIPSI	1011.5	10 mM	0.1 M CHAPS or 0.002% Tween-20‡
Non-basic standard	Ac-YTAFTIPSI	1053.5	10 mM	0.1 M CHAPS or 0.002% Tween-20‡
Non-basic product	TAFTIPSI	848.5	10 mM	0.1 M CHAPS or 0.002% Tween-20‡
Basic substrate	YTAFRIRSI	1125.6	10 mM	0.1 M CHAPS
Basic product	TAFRIRSI	962.6	10 mM	0.1 M CHAPS
Basic standard	TAFRIRSI($^{13}C^{15}N$)	969.6	10 mM	0.1 M CHAPS

† All peptides were obtained from Cambridge Research Biochemicals
‡ 0.002% Tween-20 was only utilised in biochemical assays analysed by RapidFire MS

Gistas *et al.* 2019 and Hutchinson *et al.* 2021 described how the C-terminal 6-His tagged ERAP1 full-length protein (allotype 2) was produced.[174,312] It was stored in a buffer with 50 mM HEPES, 100 mM NaCl pH 7.0, 10% glycerol and 0.5 mM TCEP. While the Leucinethiol (Leu-SH) compound was purchased from Sigma-Aldrich, all remaining compounds were provided by GSK from their internal compound library. They utilised an Echo acoustic dispenser (Labcyte) to dispense the compounds into assay plates to final concentrations of 0.1 – 1% DMSO, 10 µM compound for single concentration screens, and from 1.7 nM to 1×10^5 nM compound for ERAP1 binder dose-response curves. The compound concentrations for the dose-response curves of known ERAP1 inhibitors (Leu-SH and DG013A) were manually pipetted and ranged from 3×10^{-3} nM to 1×10^4 nM with up to 1mM final TCEP concentration for Leu-SH.

2.1.2 Detection of ERAP1 assay peptides

Equimolar concentrations (1 µM) of the non-basic and basic peptides listed in chapter 2.1.1 were prepared in a 1:1 mixture of the assay buffer (5 mM HEPES, 100 mM NaCl pH 7.0, 0.01% BSA, 0.1 M CHAPS) and 2x quench solution (0.75% TFA) and acquired by MALDI-TOF MS to

determine ionisation efficiency. To determine the limit of detection (LOD) with MALDI-TOF MS, serial dilutions of the assay peptides were prepared in a 1:1 assay buffer quench mixture. The LOD was reached when the analyte signal was detected in less than three out of five replicates when applying a signal to noise cut-off ≤ 3. Lastly, the linearity of signal detection by MALDI-TOF MS was determined at a constant peptide concentration of 2 µM in a 1:1 assay buffer quench mixture. The peptide concentrations were stepwise increased or decreased in increments of 0.2 µM to mimic the enzymatic reaction progression (product: start concentration = 0 µM, end concentration = 2 µM; substrate: start concentration = 2 µM, end concentration = 0 µM). For both, limit and linearity of detection experiments, 1 µM internal standard final concentration was supplemented.

2.1.3 ERAP1 biochemical in vitro assay

Detailed information about the original RapidFire MS-based ERAP1 enzymatic assay can be retrieved from Liddle *et al*. 2020.[55] Briefly, the assay was conducted in 25 µL 50 mM HEPES, 100 mM NaCl pH 7.0, 0.01% BSA, 0.002% Tween-20 buffer and 5 µM non-basic substrate incubated with 1 nM ERAP1 for 1 h at RT. The reaction was stopped by addition of 25 µL quench solution (0.38% TFA final concentration) which contained 5 µM of the non-basic internal standard (2.5 µM final standard concentration).

The initial MALDI-TOF MS workflow was based on the RapidFire MS method, utiling 5 µM non-basic substrate, 3 nM ERAP1 and 2.5 µM non-basic internal standard. However, the assay was optimised and hence the workflow described in the following used for most experiments. ERAP1 (0.25 nM) was pre-incubated with compounds for 30 min at RT in the assay buffer (5 mM HEPES, 100 mM NaCl pH 7.0, 0.01% BSA, 0.1 M CHAPS). The reaction was started by addition of 2 µM basic substrate and incubated for 60 min at RT (total volume = 4 µL). The reaction was stopped by addition of 4 µL quench solution (0.38% final TFA) which contained the basic internal standard (1 µM final concentration). The assay was conducted at two different locations which provided different automation capabilities. The previously outlined workflow was developed at Newcastle University where the Xrd- 384 reagent dispenser (fluidX) and Mosquito LV (SPT Labtech) were used. The full automation workflow at GSK was based around the Multidrop Combi dispenser which required adjustment to 5 µL dispense volumes while maintaining final assay concentrations and incubation times.

2.2 Cell culture of iPSC-derived macrophages

The initial steps for the culture of the iPSC-derived macrophages cover the thawing and culture of the iPSCs, formation and cultivation of the embryoid bodies, as well as the harvest of the monocytes from the embryoid body factories. Detailed protocols for these steps have been previously published by van Wilgenburg *et al.* 2013 and Bernard *et al.* 2021.[313,314] All monocytes were sourced from a GSK proprietary production pipeline which featured iPSC lines from three different human biological donors; UKBi006-A (Censo Biotechnologies), WTSIi018-A (Sanger Institute (EBiSC)), and S02315_C5 (UC San Diego, Frazer Lab). I received the monocyte precursors in suspension and then counted them with a NucleoCounter® NC-200 (Via1-Casette™, ChemoMetec). Cells were centrifuged for 5 min at 300 xg, RT and resuspended in macrophage differentiation media (RPMI + 10% FBS + M-CSF (10 ng/mL or 100 ng/mL)) to a concentration of $1x10^5$ cells/mL. Cells were either seeded manually or with a Multidrop Combi reagent dispenser (Thermo Fisher Scientific) (6 well = 4.8 mL cell suspension/well, 96 well = 160 µL cell suspension/well). The cells were incubated at 37°C, 5% CO_2 for 6 days. Only for the 6 well plates, a media change was performed on day 4. On day 6, the compound incubation (optional) and stimulation were conducted. First, the media was replaced by fresh macrophage differentiation media. DMSO (final concentration 1%) or the compounds which originated from two different compound sets which will be referred to as Joint Undertaking of Morphological Profiling (JUMP), and inflammatory compound sets (Tables 2.3, and 2.4 respectively) were added to a final concentration of 1 µM (JUMP set) and 10 µM (inflammation set) respectively. The different stimulants (Table 2.5) were added after 3 h compound incubation at 37°C, 5% CO_2. The cells were harvested after another 24 h incubation at 37°C, 5% CO_2. The media was collected, and the cell pellets washed twice with DPBS. Cells and supernatants were stored at -80°C until further use. Brightfield microscopy images were captured throughout the cell cultivation, compound treatment and stimulation periods with an EVOS M5000 (Thermo Fisher Scientific).

The outlined steps were automated when handling 96 well plates. The utilised platform featured a liquid dispenser (dragonfly® discovery; SPT Labtech) and a liquid handler robot (Bravo; Agilent) that conducted media change, compound, and stimulation addition, as well as media harvest and cell pellet washing.

Table 2.3. List of JUMP set compounds. Indicated are also their mechanism of action (MoA), and target annotation.

Compound name†	Mechanism of action (MoA)	Target annotation
A-366	Histone lysine methyltransferase inhibitor	EHMT1, EHMT2
ABT-737	BCL inhibitor	BCL2, BCL2L1, BCL2L2
Acriflavine	Hypoxia inducible factor inhibitor	HIF1A
Aloxistatin	Protease inhibitor	CTSG
AMG900	Aurora kinase inhibitor	AURKA, AURKB, AURKC
Andarine	Androgen receptor modulator	AR
Apratastat	Matrix metalloprotease inhibitor, tumor necrosis factor production inhibitor	ADAM17, MMP1, MMP13, MMP9
APY0201	Phosphoinositide dependent kinase inhibitor	IL12A, IL12B, PIKFYVE
AZ191	DYRK inhibitor	DYRK1B
AZD2014	mTOR inhibitor	MTOR
AZD7545	Pyruvate dehydrogenase kinase inhibitor	PDK1
BI-78D3	JNK inhibitor	MAPK8
BIX-02188	MEK inhibitor	MAP2K5
BLU9931	FGFR inhibitor	FGFR4
BMS-566419	Inosine monophosphate dehydrogenase inhibitor	IMPDH1, IMPDH2
BMS-863233	CDC inhibitor	CDC7, PIM1
BX-912	Pyruvate dehydrogenase kinase inhibitor	CDK2, CHEK1, GSK3B, KDR, PDK1, PDPK1
Carmustine	DNA alkylating agent, DNA inhibitor	GSR
CHIR-99021	Glycogen synthase kinase inhibitor	CDK1, GSK3A, GSK3B, MAPK1
Cilostamide	Phosphodiesterase inhibitor	PDE3A, PDE3B
CP-724714	EGFR inhibitor, protein tyrosine kinase inhibitor	ERBB2
CPI-0610	Bromodomain inhibitor	BRD4
Dexamethazone	Glucocorticoid receptor agonist	ANXA1
Dimethindene-(S)-(+)	Acetylcholine receptor antagonist	CHRM2
Dosulepin	Norepinephrine reuptake inhibitor, serotonin-norepinephrine reuptake inhibitor (SNRI)	CHRM1, CHRM2, CHRM3, CHRM4, CHRM5, HRH1, SLC6A2, SLC6A4
Filanesib	Kinesin inhibitor, kinesin-like spindle protein inhibitor	KIF11
Filgotinib	JAK inhibitor	JAK1, JAK2, JAK3, TYK2

FK-866	Niacinamide phosphoribosyltransferase inhibitor	NAMPT
FR-180204	MAP kinase inhibitor	MAPK1, MAPK3
GDC-0879	RAF inhibitor	BRAF
GNF-5	Bcr-Abl kinase inhibitor	ABL1, BCR
GSK2334470	Phosphoinositide dependent kinase inhibitor	AURKA, AURKB, PDPK1
GSK-3-inhibitor-IX	Glycogen synthase kinase inhibitor, lipoxygenase inhibitor	GSK3A, GSK3B
GSK-J4	Histone lysine demethylase inhibitor	KDM6A, KDM6B
GW-3965	LXR agonist	NR1H2, NR1H3
GW-5074	RAF inhibitor, leucine rich repeat kinase inhibitor	NTRK1, RAF1
Halopemide	Phospholipase inhibitor	PLD1, PLD2
Homochlorcyclizine	Antihistamine	HRH1
ICG-001	Beta-catenin inhibitor	CTNNB1
IOX2	Hypoxia inducible factor inhibitor	EGLN1, KDM2A, KDM5C
KH-CB19	CDC inhibitor	CLK1, CLK3, DYRK1A
LLY-283	Protein arginine N-methyltransferase inhibitor	PRMT-5
LY2109761	TGF beta receptor inhibitor	TGFBR1, TGFBR2
Mepyramine	Antihistamine	HRH1
Mizoribine	Immunosuppressant, inosine monophosphate dehydrogenase inhibitor	IMPDH1
MK-5108	Aurora kinase inhibitor	AURKA, AURKB, AURKC
ML-298	Phospholipase inhibitor	PLD2
ML-323	Ubiquitin specific protease inhibitor	USP1
ML324	Histone lysine demethylase inhibitor	KDM4A
Neratinib	EGFR inhibitor	EGFR, ERBB2, KDR
NVP-AEW541	IGF-1 inhibitor	IGF1R, INSR
NVS-PAK1-1	p21 activated kinase inhibitor	PAK1
Olaparib	PARP inhibitor	PARP1, PARP2
P5091	Ubiquitin specific protease inhibitor	USP7
Palbociclib	CDK inhibitor	CDK4, CDK6
PD-198306	MAP kinase inhibitor, MEK inhibitor	MAP2K1, MAP2K2
PF-477736	CHK inhibitor	CHEK1, CHEK2
PFI-1	Bromodomain inhibitor	BRD4
Pitavastatin	HMGCR inhibitor	HMGCR

PNU-74654	Beta-catenin inhibitor	CTNNB1, TCF4
Pomalidomide	Angiogenesis inhibitor, tumor necrosis factor production inhibitor	CRBN, PTGS2, TNF
Ponatinib	Bcr-Abl kinase inhibitor, FLT3 inhibitor, PDGFR tyrosine kinase receptor inhibitor	ABL1, BCR, FGFR1, FGFR2, FGFR3, FGFR4, FLT3, KDR, KIT, LCK, LYN, PDGFRA, RET, SRC, TEK
PS178990	Androgen receptor modulator	AR
Purmorphamine	Smoothened receptor agonist	SMO
Quazinone	Phosphodiesterase inhibitor	PDE3A, PDE3B
RGFP966	HDAC inhibitor	HDAC3
Rheochrysidin	Protein tyrosine kinase inhibitor	PTPN1
Romidepsin	HDAC inhibitor	HDAC1, HDAC2, HDAC3, HDAC4, HDAC5, HDAC6, HDAC7, HDAC8, HDAC9
Ruxolitinib phosphate	JAK inhibitor	JAK1, JAK2, JAK3, TYK2
SAG	Smoothened receptor agonist	SMO, TRPC6
SCH-900776	CHK inhibitor	CDK2, CHEK1
Selumetinib	MEK inhibitor	MAP2K1
SGC-707	Protein arginine N-methyltransferase inhibitor	PRMT3
SGX523	Hepatocyte growth factor receptor inhibitor	MET
SHP099	Protein tyrosine kinase inhibitor	PTPN11
Sirolimus	mTOR inhibitor	FGF2, FKBP1A, MTOR
Skepinone-l	p38 MAPK inhibitor	MAPK14
SU-11274	Hepatocyte growth factor receptor inhibitor, tyrosine kinase inhibitor	MET
SU3327	JNK inhibitor	MAPK8
T-0901317	LXR agonist	NCOA1, NCOA2, NR1H2, NR1H3, NR1I2, RXRB
TC-S-7004	DYRK inhibitor	DYRK1A, DYRK1B
THZ1	CDK inhibitor	CDK7
UNC0642	Histone lysine methyltransferase inhibitor	EHMT1, EHMT2
Valrubicin	DNA inhibitor, topoisomerase inhibitor	TOP2A
Veliparib	PARP inhibitor	PARP1, PARP2
VX-475	p38 MAPK inhibitor	MAPK11, MAPK12, MAPK14
WZ4003	AMPK inhibitor	NUAK1, NUAK2

† All compounds were provided by GSK

Table 2.4. List of inflammatory set compounds.

Compound name†		
\N GSK2680029B	GIT 27	PROTAC RIPK degrader-2
\N GSK2941404A	GSK 0660	RAC-MODIPAFANT
A-485	GSK 2837808A	Resiquimod
ALLM	GSK2580335	RP 52770
AP-III-a4 (hydrochloride)	GV109188	Ruxolitinib phosphate
Apremilast (CC-10004)	GW296115X	S4
ARN-3236	I-CBP 112	SAHA
Astragalin	Isoetharine mesylate	SB219994
AZD-5153	JNJ 27141491	Selinexor (KPT-330)
AZD8055	KML 29	SH-4-54
Bafetinib (INNO-406)	L 748415	Spermidine trihydrochloride
Batimastat	LG 100754	Spermine tetrahydrochloride
BMS 509744	Lonidamine	ST 2825
BMS-911543	LY294002 hydrochloride	Staurosporine
C188-9	M62812	T6167923
Canertinib dihydrochloride	MSDC-0602	TAK-242
CGP 3466B maleate	Neratinib (HKI-272)	TCMDC-125545
CGP 57380	Nilotinib	Temsirolimus
CHMFL-FLT3-122	NKH 477	TLR1
Compound 41	OTAVA-BB 7119983925	TMI 1
Corticosterone	P005091	TPCA-1
CP 690550 citrate	Parthenolide	Tulobuterol
Dactolisib	PD 166285	Ulixertinib (BVD-523, VRT752271)
EGCG	PF 543 hydrochloride	Vistusertib (AZD2014)
Emixustat	PF-06447475	VU 0155069
ERBSTATIN	Pifithrin-mu	WYE-125132
Febuxostat	Ponesimod (ACT-128800)	Z433927330
FLLL32	Prednisolone acetate (Omnipred)	Z-Phe-CH2Cl
Flupenthixol dihydrochloride	Prostaglandin E2	

† All compounds were provided by GSK

Table 2.5. List of different stimuli applied to iPSC-derived macrophages. Indicated are also treatment concentrations and supplier information.

Stimulant	Treatment concentration	Supplier
Interleukin-4 (IL-4)	20 ng/mL	Thermo Fisher Scientific
Interferon gamma (IFN-γ)*	20 ng/mL	R&D systems
Lipopolysaccharide (LPS)*	100 ng/mL	Sigma-Aldrich

* IFN-γ and LPS were also combined for cell treatment

2.3 Cytokine measurement

2.3.1 Cytometric bead array on Mirrorball®

The cell supernatant from the iPSC-derived macrophages containing secreted chemo- and cytokines was defrosted at RT and dilutions in PBS + 1% BSA prepared. 10 µL sample was placed in the wells of a black, µClear® bottom assay plate (#781091, Greiner). The BD™ Cytometric Bead Array (CBA) human IL-6 and TNFα flex sets (BD) were used. First, the included lyophilised standards were pooled and dissolved in a total volume of 1 mL (PBS + 1% BSA). For the calibration curve, at least ten 1:2 dilutions of the standard were prepared and transferred into the assay plate (10 µL/well). The bead mixture was prepared as a 1:175 dilution of the IL-6 and TNFα beads in PBS + 1% BSA buffer. After addition of 5 µL bead mixture to each well, the assay plate was shaken for 2h in the dark at RT. The antibody mixture was prepared as a 1:175 dilution of the IL-6 and TNFα antibodies in PBS + 1% BSA buffer. After addition of 5 µL antibody mixture to each well, the assay plate was shaken for 2h in the dark at RT. The assay plate was centrifuged for 15 sec at 100 xg before data acquisition with the mirrorball® fluorescence cytometer (SPT Labtech) using the Cellista software. The following general settings were used: threshold type shot, feature length 1 - 100 µM, meniscus smoothing length 301 µM, object identification 0.5 µM (for x and y separation), and 5 µM minimum object depth. The 488 nm and 640 nm laser were enabled, and both operated at 6 mW. Three channels were enabled (FL-3: 565 - 605 nm, 400 V; FL-4: 667 - 685 nm, 450 V; FL-5: 717 - 800 nm, 680 V) and their sensitivity set to two. The FL-4 channel was selected as trigger. The IL-6 population was defined by FL-4 peak intensity 1376.119 - 5426.866, FL-5 peak intensity 5079.505 - 10275.62 and FL-4 perimeter range 40 - 150. The TNFα population was defined by FL-4 peak intensity 7317.054 - 12317.05, FL-5 peak intensity 3695.97 - 8195.971 and FL-4 perimeter range 40 - 150. The cytokine concentration in the samples was derived from the standard calibration curve fits (linear regression), taking prior sample dilutions into account.

2.3.2 Multiplexed panels on Luminex®

The cell supernatant from the iPSC-derived macrophages containing secreted chemo- and cytokines was thawed over night at 4°C and diluted in PBS. The cytokine 10-plex human panel kit (GM-CSF, IFN-γ, IL-1β, IL-2, IL-4, IL-5, IL-6, IL-8, IL-10, TNF-α) and the ProcartaPlex™ human cytokine & chemokine convenience panel 1A 34plex kit (CCL11, GM-CSF, CXCL1, IFN-α, IFN-γ, IL-1α, IL-1β, IL-1RA, IL-2, IL-4, IL-5, IL-6, IL-7, IL-8, IL-9, IL-10, IL-12p70, IL-13, IL-15, IL-17A, IL-

18, IL-21, IL-22, IL-23, IL-27, IL-31, CXCL10, CCL2, CCL3, CCL4, CCL5, SDF-1α, TNF-α, TNF-β) (both Thermo Fisher Scientific) were used. Bead activation was conducted by bead addition to the Luminex plate (50 µL/well), 2 min plate incubation on magnet, liquid removal on magnet, two times wash with 150 µL 1X wash buffer. The standards were prepared by adding 50 µL RPMI medium to the standard tube, 10 min incubation on ice and preparation of seven 1:4 dilutions. The standards and samples were added to the assay plate containing the activated beads at 50 µL per well. Only for the 10-plex kit, another 50 µL incubation buffer and 50 µL assay diluent were added to the plate. The assay plate was shaken for 30 min at 450 rpm, RT and incubated over night at 4°C. The plate was shaken again at RT for 15 min before being washed twice with 1X wash buffer. The antibody was made up according to the manufacturer's instructions and added to the assay plate. The assay plate was shaken for 1h at 450 rpm, RT and then washed. The Streptavidin-PE was added to the assay plate (25 µL/well). The plate was shaken for 30 min at 450 rpm, RT and then washed. Finally, wash (10-plex) or read buffer (34-plex) was added to the plate before it was measured by the Luminex FLEXMAP 3D® (R&D systems). A protocol with MagPlex™ bead type and 7,500 – 15,000 bead region was used for acquisition of the calibration-validation and sample plate in the Bioplex software. The cytokine concentration in the samples was derived from the calibration curves (4/5PL curve fit in Bioplex software), taking prior sample dilutions into account. For the IL-6 and IL-8 cytokines, the intensity values for the high concentration standards were extrapolated from the rest of the standard curve and a new 4/5PL curve fit performed in GraphPad Prism for cytokine concentration calculations. A standard curve was placed on each assay plate for larger batches. Positive and negative controls were used for batch effect corrections.

2.4 RapidFire MS setup for the ERAP1 biochemical assay

The RapidFire MS system that was used to acquire ERAP1 biochemical assay samples was a Rapidfire365 autosampler (Agilent Technologies) coupled to an API4000 triple quadrupole mass spectrometer (SCIEX) operated with a spray voltage of 5000V and a source temperature of 600°C. Samples were aspirated for 250 ms under vacuum. Solvent A (0.1% (v/v) FA) was used at a flowrate of 1.5 mL/min for 2000 ms to load samples onto the C18 cartridge. Sample elution was conducted for 2500 ms with solvent B (80% LC-MS grade MeCN, 0.1% (v/v) FA) at a flow rate of 1 mL/min. Re-equilibration of the cartridge followed for 500 ms with solvent A

at a flow rate of 1.5 mL/min. This resulted in a total cycle time of ~7 seconds per sample. The following transitions (Q1/Q3) were monitored for each analyte in positive electrospray multiple reaction monitoring mode with a dwell time of 50 ms: YTAFTIPSI 1012.6/697.4; TAFTIPSI 849.4/534.3; and Ac-YTAFTIPSI 1054.6/739.5. The RapidFire peak integration software (version 4.0.1) was utilised for peak integration and processing. The substrate-product ratio was calculated and utilised for subsequent data analysis in a GSK proprietary software.

2.5 MALDI-TOF MS

2.5.1 MALDI-TOF MS setup for the ERAP1 biochemical assay

Two different workflows were used for MALDI-TOF MS target plate spotting and acquisition of the ERAP1 biochemical assay samples. At Newcastle University, equal sample and matrix (5.6 mg/ml CHCA in 85% MeCN, 0.1% TFA, 1 mM $NH_4H_2PO_4$) volumes were mixed (3x 1000 nL) and then 0.5 µL deposited onto a stainless steel MTP384 MALDI-TOF MS target plate (Bruker Daltonics) with the Mosquito liquid handling robot (SPT Labtech). The plates were air dried and manually loaded into the rapifleX PharmaPulse MALDI TOF/TOF mass spectrometer (Bruker Daltonics). In contrast, at GSK, this process was fully automated. A robotic arm (Analytic Jena) moved ERAP1 assay and MALDI-TOF MS target plates from their storage locations onto a rotating disk where all pipetting steps were executed with a pipetting robot that was equipped with a 384 format pipetting head (CyBio Well vario, Analytic Jena). Equal volumes of the assay sample and matrix (6.25 mg/mL CHCA dissolved in 70% MeCN, 0.1% TFA) were mixed and 1 µL deposited onto HTS MALDI-TOF MS target plates (Bruker Daltonics). The plates were loaded into a heated vacuum dryer and then moved into the mass spectrometer. In parallel to the plate acquisition, the next target plate was prepared.

The following MS instrument settings were utilised at Newcastle University for data acquisition in flexControl (version 4.0): positive ion reflector mode, *m/z* 920 – 1220, mass suppression up to *m/z* 635, 5000 shots at a 10 kHz frequency per spot, random walk pattern (complete sample), M5 Thin-layer laser, 50 µm x 50 µm scan range, 2000 µm spot diameter, and 200 shots per raster position. At GSK, these parameters were adjusted to 10000 shots at a 5 kHz frequency per spot, custom M5 flat laser, 50 shots per raster position, and mass suppression up to *m/z* 736. For each experiment, the laser power was individually adjusted to ensure an

overall spectrum intensity in the range of ~10^5 arbitrary units (a.u.) and the method was calibrated with peptide calibration standard II (Bruker Daltonics). Data acquisition and processing was performed with the MALDI PharmaPulse software (version 2.2). A centroid peak detection algorithm was utilised for basic assay peptide detection and the SNAP2 algorithm was used for the non-basic peptides. A signal to noise threshold of three was used for initial exploratory experiments and later increased to five to improve signal reproducibility. The report.csv file from the MALDI PharmaPulse software contained the following information: *m/z* and summed area of all adducts for the product, substrate and internal standard peptide. The further data analysis is outlined in chapter 2.7.1.

2.5.2 MALDI-TOF MS setup for the iPSC-derived macrophage assay

Table 2.6. List of MALDI-TOF matrices used during the workflow development. Indicated are also solvent and supplier information.

Matrix	Matrix solvent	Supplier
1,5-diaminonaphthalene (DAN)	70% MeCN, 0.1% TFA (or 0.1% FA)	Sigma-Aldrich
2,5-dihydroxyacetophenone (DHAP)	750 µL ethanol + 250 µL 12mg/mL diammonium hydrogen citrate + 0.1% FA	Bruker Daltonics
2,5-dihydroxybenzoic acid (DHB)	70% MeCN, 0.1% TFA (or 0.1% FA)	Bruker Daltonics
9-aminoacridine (9-AA)	50% EtOH	Sigma-Aldrich
α-cyano-4-hydroxycinnamic acid (CHCA)	70% MeCN, 0.1% TFA (or 0.1% FA)	Sigma-Aldrich
Sinapinic acid (SA)	70% MeCN, 0.1% TFA (or 0.1% FA)	Bruker Daltonics

The HTS compatible MALDI-TOF MS workflow that was used to phenotypically profile compound treated iPSC-derived macrophages was as follows: First, the cells previously frozen in 96 well cell culture plates were lysed by thawing for 20 min at RT, followed by 10 min shaking at RT, 1000 rpm in 6 µL/well extraction buffer (100 mM Tris-HCl, 0.1% FA). The cell suspension was transferred into a small volume, high base 384 well plate which was shaken again for 3 min, 400 rpm. Three 1000 nL mix cycles were executed in the cell sample before 1 µL was spotted onto a plain steel HTS MALDI target plate with the Mosquito pipetting robot (SPT LabTech). The plate was dried at ambient temperature before 900 nL matrix (22.22 mg/mL DHB in 70% MeCN, 0.1% FA, 30 min sonicated) was deposited onto the target plate with the Mosquito. The plate was dried at ambient temperature and then loaded into the rapifleX

PharmaPulse MALDI TOF/TOF mass spectrometer. The following AutoExecute method settings were used for data acquisition in flexControl (version 4.0): positive ion reflector mode, *m/z* 400 – 1000, mass suppression up to *m/z* 320, 10000 shots at a 10 kHz frequency per spot, random walk pattern (complete sample), M5 custom laser, 50 µm x 50 µm scan range, 2000 µm spot diameter, and 500 shots per raster position. For each experiment, the laser power was individually adjusted to ensure an overall spectrum intensity between high 10^5 arbitrary units (a.u.) to low 10^6 a.u. and the instrument was calibrated with peptide calibration standard II (Bruker Daltonics). The data processing and peak list extraction is described in section 2.7.2.

2.6 Proteomics of the iPSC-derived macrophages

2.6.1 Proteomics sample preparation

Table 2.7. List of buffers for the proteomics sample preparation. Indicated are also the final buffer composition and buffer components.

Buffer name	Final buffer composition	Buffer components
2x S-Trap lysis buffer	10% SDS, 100 mM TEAB pH 8.5	SDS (20%), HPLC grade water, 1M TEAB
S-Trap binding buffer	100 mM TEAB pH 7.55 in 90% MeOH	Phosphoric acid (to pH), HPLC grade water, 1M TEAB
S-Trap digestion buffer	50 mM TEAB pH 8.5	HPLC grade water, 1M TEAB
Acidification buffer	12% phosphoric acid	HPLC grade water, phosphoric acid (85%)
Elution buffer 1	0.1% FA	HPLC grade water, FA (98 - 100%)
Elution buffer 2	50% MeCN, 0.1% FA	HPLC grade water, MeCN HPLC grade, FA (98 - 100%)

For the proteomics sample preparation, cell culture plates containing the iPSC-derived macrophages were defrosted at RT for 20 min. 1x S-Trap lysis buffer was supplemented with Benzonase® 5000:1 and added onto the wells (6 well plate = 200 µL, 96 well plate = 50 µL). The solution was transferred into fresh reaction tubes or plates, mixed for 15 min at RT, 800 rpm (ThermoMixer C, Eppendorf) and then centrifuged at 1500 xg, RT for 2 min.

The protein concentration in the lysate was quantified with the Pierce™ BCA protein assay kit (Thermo Fisher Scientific); 6 well plates only. 1x S-Trap binding buffer, supplemented with Benzonase®, was used to prepare the BSA standard curve according to the manufacturer's

instructions and to dilute the samples. The standards and samples were placed in an assay plate (20 µL/sample) and 200 µL of a 50:1 mixture of the Pierce™ BCA solutions A&B added. The plate was incubated at 37°C for 30 min and then the absorbance at 562 nm measured with the SpectraMax iD3 microplate reader (Molecular Devices). The protein concentration in the samples was calculated from the BSA calibration curve (linear regression), taking prior sample dilutions into account.

Sample preparation was continued with 10 µg protein from 6 well plates or the full lysate from the 96 well plates. TCEP was added (10 mM final concentration) and incubated for 20 min at 60°C. IAA was added (10 mM final concentration) and incubated in the dark for 30 min at RT. Acidification buffer was added to a final concentration of 1.2%. The S-Trap binding buffer volume added was determined by the sample volume (7x sample volume = S-Trap binding buffer volume). The samples were loaded onto a 96-well S-Trap™ plate (ProtiFi) and centrifuged for 2 min at 1500 xg. The columns were washed three times with 200 µL S-Trap binding buffer per well, intercepted by 2 min centrifugations at 1500 xg. The digestion buffer was supplemented with Trypsin (1:10 ratio µg Trypsin to µg protein on column). A minimum of 1 µg Trypsin was used even when less than 10 µg protein were bound to the column. A total of 125 µL trypsin digestion buffer was placed in each well. The plate was loosely covered and incubated for 2 h at 47°C. The peptides were eluted from the column by sequential addition of 80 µL 50 mM TEAB, 80 µL elution buffer 1 and 80 µL elution buffer 2, with 2 min centrifugations at 1500 xg between each elution step. The samples were frozen and dried in a vacuum concentrator (Savant SPD1010 SpeedVac, Thermo Fisher Scientific).

2.6.2 Proteomics sample acquisition with the timsTOF HT

The lysed and digested iPSC-derived macrophage samples from a time course and an inflammation compound set treatment were acquired with a timsTOF HT MS (Bruker Daltonics) that was coupled to an Evosep One LC system (Evosep). The LC system specific C18 Evosep tips were conditioned and equilibrated with the following steps: buffer B (100% MeCN, 0.1% FA) wash, isopropanol incubation (5 min), buffer A (0.1% FA) wash. The dried down peptide samples were resuspended in buffer A and centrifuged for 1 h at 4000 xg. The equivalent of 0.5 - 2 µg protein sample load was placed onto the tip (standard load 0.5 µg). The tips were centrifuged, washed once with buffer A and then stored covered with buffer A.

The Evosep system was operated with an 8 cm x 100 µm reverse-phase column packed with 3 µM C18 beads (Evosep, EV1094) at 23°C and the pre-defined 60 SPD (sample per day) protocol (21 min linear gradient from 0 to 35 % buffer B, 1 µL/min flow rate).

The timsTOF HT was equipped with a 20 µm nano-electrospray ion source (CaptiveSpray, Bruker Daltonics) which was operated at 1600 V capillary voltage, 3.0 L/min dry gas and 50°C dry temperature. The DDA MS1 acquisition was performed with mass and IM ranges of *m/z* 100 - 1700 and 0.6 - 1.45 1/K_0 respectively. MS2 was performed using 10 parallel accumulation serial fragmentation (PASEF) MS/MS scans, target intensity and threshold of 20000 and 2500 respectively, active exclusion for 0.4 min (with precursor reconsideration for MS2 if current/previous intensity was ≥4), ~1.17 sec total cycle time and 0.6 - 1.6 1/K_0 IM. For all dia-PASEF methods, the TIMS ramp and accumulation times were 100 ms, total cycle time ~1.8 sec, and collision energy (applied in linear fashion) between 20 - 59 eV, auto-calibration enabled. The IM and mass ranges of the iPSC time course 16 variable width IM - *m/z* window dia-PASEF method with two quadrupole positions per window were 0.6 - 1.4 1/K_0 and *m/z* 300 - 1200 respectively. The pooled sample from all time course conditions was also acquired with 5 different dia-PASEF methods optimised by Andrew Frey (Trost laboratory) that each covered a subset mass and IM range between IM 0.6 - 1.4 and *m/z* 350 - 1250 with overlaps (Range 1: m/z = 350 - 550, IM = 0.6 - 0.95; range2: m/z = 450 - 600, IM = 0.7 - 1; range 3: m/z = 550 - 750, IM = 0.75 - 1.1; range 4: m/z = 650 - 950, IM = 0.8 - 1.25; range 5: m/z = 850 - 1250, IM = 0.9 - 1.4) to assemble a gas fractionated spectral library.[315] With exception of IM and *m/z*, PASEF parameters of this method, including number of windows, were the same as previously described. For the acquisition of the inflammatory compound set treatment samples, a custom dia-PASEF method was generated with the py_diAID software from a 500 ng pool sample that was subjected to dda-PASEF.[288] The IM and mass ranges of the resulting 16 variable width IM - *m/z* window pyDIA-PASEF method with two quadrupole positions per window were 0.6 - 1.4 1/K_0 and *m/z* 300 – 1400, respectively (Table 2.8).

Table 2.8. Customised dia-PASEF method for the acquisition of iPSC-derived macrophages.

#MS Type	Cycle Id	Start IM [1/K0]	End IM [1/K0]	Start Mass [m/z]	End Mass [m/z]	CE [eV]
MS1	0	-	-	-	-	-
PASEF	1	0.89	1.4	717.86	741.38	-
PASEF	1	0.6	0.89	300.17	387.53	-
PASEF	2	0.91	1.4	741.38	764.9	-

PASEF	2	0.6	0.91	387.53	422.58	-
PASEF	3	0.92	1.4	764.9	787.78	-
PASEF	3	0.6	0.92	422.58	448.24	-
PASEF	4	0.94	1.4	787.78	812.09	-
PASEF	4	0.6	0.94	448.24	472.52	-
PASEF	5	0.95	1.4	812.09	836.92	-
PASEF	5	0.6	0.95	472.52	494.76	-
PASEF	6	0.96	1.4	836.92	862.47	-
PASEF	6	0.6	0.96	494.76	515.95	-
PASEF	7	0.97	1.4	862.47	888.92	-
PASEF	7	0.6	0.97	515.95	535.28	-
PASEF	8	0.99	1.4	888.92	918.9	-
PASEF	8	0.6	0.99	535.28	554.3	-
PASEF	9	1	1.4	918.9	950.94	-
PASEF	9	0.6	1	554.3	572.64	-
PASEF	10	1.01	1.4	950.94	982.26	-
PASEF	10	0.6	1.01	572.64	592.35	-
PASEF	11	1.03	1.4	982.26	1018.53	-
PASEF	11	0.6	1.03	592.35	611.32	-
PASEF	12	1.04	1.4	1018.53	1056.51	-
PASEF	12	0.6	1.04	611.32	631.55	-
PASEF	13	1.06	1.4	1056.51	1101.58	-
PASEF	13	0.6	1.06	631.55	651.67	-
PASEF	14	1.08	1.4	1101.58	1154.57	-
PASEF	14	0.6	1.08	651.67	673.36	-
PASEF	15	1.11	1.4	1154.57	1232.11	-
PASEF	15	0.6	1.11	673.36	694.88	-
PASEF	16	1.17	1.4	1232.11	1399.68	-
PASEF	16	0.6	1.17	694.88	717.86	-

2.6.3 Offline high-pH liquid chromatography fractionation of proteomics samples

A pooled peptide sample composed of equal amounts from all macrophages treated with the inflammatory compound set was solubilised in 20 mM ammonium formate (pH 8.0) and separated on an UltiMate 3000 RSLCnano System (Thermo Fisher Scientific). The setup was operated with a Gemini C18 column (250 × 3 mm, 3 µm C18 110 Å pore size; Phenomenex) and a 72 min gradient from 1.0% to 37.5% MeCN, final wash 5 min 90% MeCN (flow rate 0.25 ml/min) to generate 72 fractions. Those fractions were concatenated into 24 fractions so that the first sample was pooled with the 25th and the 49th sample up to the 24th sample that was pooled with the 48th and 72nd sample before all fractions were dried in a vacuum concentrator (Savant SPD1010 SpeedVac, Thermo Fisher Scientific) and resolubilised in 0.1% (v/v) TFA.

The samples (volume equivalent to ~125 ng protein) were acquired with a timsTOF HT (Bruker Daltonics) that was coupled to a nanoElute II HPLC system (Bruker Daltonics). The HPLC system was operated with a Bruker10 C18 column, 300 nL/min flowrate and a 60 min linear gradient (2 - 35% buffer B), followed by a 5 min elution at 95% buffer B. The timsTOF HT MS was equipped with the 20 µm CaptiveSpray source, as well as a pre-column 5 mM PepMap™ C18 trap (Thermo Fisher Scientific) and operated in dda-PASEF mode as described in section 2.6.2.

2.7 Data analysis and software

2.7.1 MALDI-TOF MS-based ERAP1 assay data analysis

The summed area of the protonated $[M+H]^+$ and sodiated $[M+Na]^+$adduct peaks which were measured by MALDI-TOF MS for the product and internal standard peptides of the ERAP1 assay were used in the following. The product signal was normalised to the internal standard according to equation 1 to obtain the normalised product area.

$$Normalised\ product\ area = \frac{\sum Area\ adducts_{product}}{\sum Area\ adducts_{internal\ standard}} \quad (1)$$

The absolute product concentration was then calculated from this normalised product area (equation 2). The utilised scaling factor was obtained from a calibration curve where the normalised product area was plotted against the known product concentration (Figure 3.3, linear regression fit).

$$[Product] = Normalised\ product\ area/1.27 \quad (2)$$

The normalised product area of the positive and negative controls was also utilised to determine the % enzyme activity and the Z' of the assay based on a plate-by-plate analysis. The enzyme activity for each well was calculated according to equation 3:

$$\%\ enzyme\ activity = \frac{sample_{norm} - mean\ negative\ control_{norm}}{mean\ positive\ control_{norm} - \text{mean}\ negative\ control_{norm}} \times 100 \quad (3)$$

The standard deviation of positive (σ_p) and negative (σ_n) controls, as well as their mean values (μ_p , μ_n) were utilised to determine assay quality; Z' (equation 4).

$$Z' = 1 - \frac{3 * \sigma_p + 3 * \sigma_n}{|\mu_p - \mu_n|} \quad (4)$$

GraphPad Prism (version 5.0.4 and 9.0.0) and a GSK in house software were utilised for all subsequent statistical analysis, including linear regression, column statistics, correlation analysis, Michaelis-Menten curve, robust cut-off value determination and four-parameter logistic curve fits.

2.7.2 MALDI-TOF MS-based iPSC-derived macrophages assay data analysis

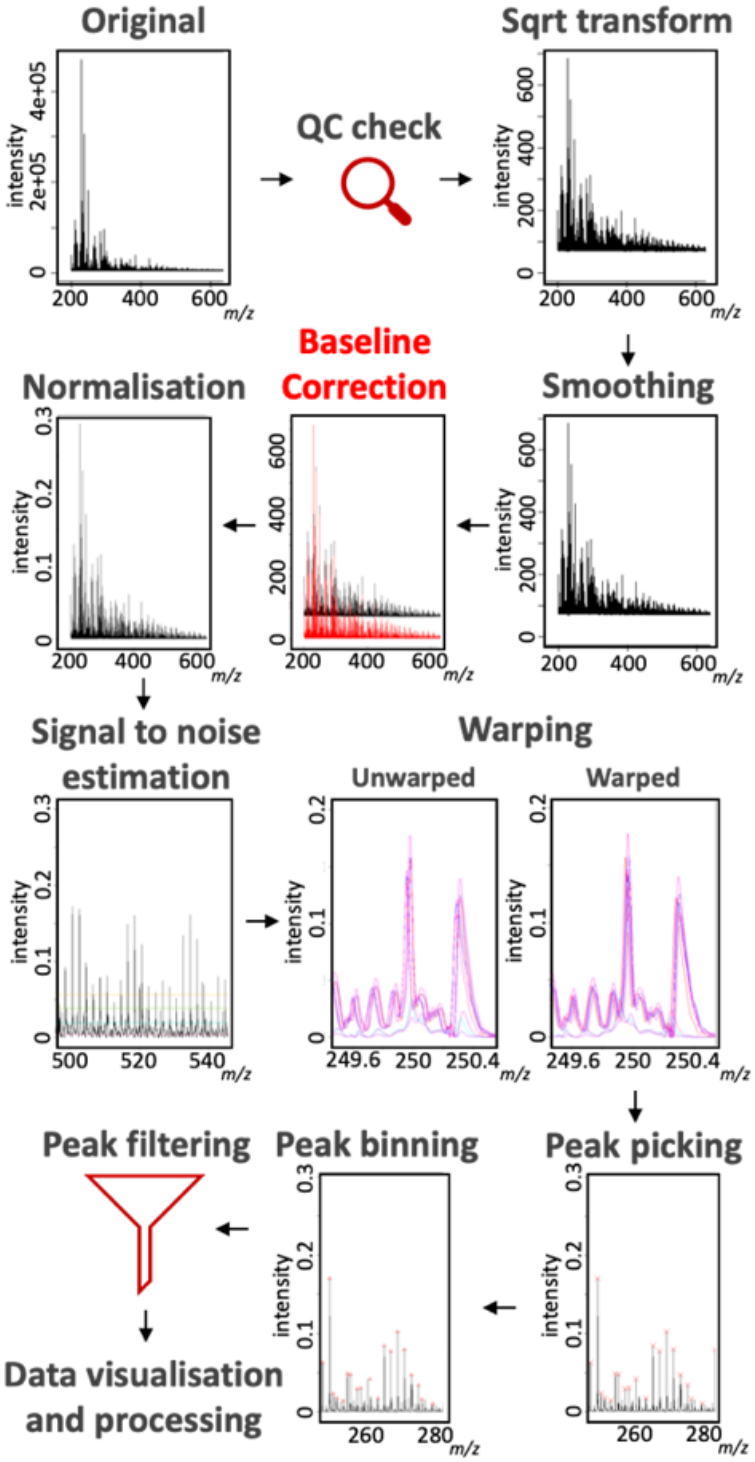

Figure 2.1. Schematic workflow of MALDI-TOF MS spectrum processing for cellular screens.

The original spectra were loaded into R where QC check, square root transformation, smoothing, baseline correction, normalisation, signal to noise estimation, warping, peak picking, peak binning, peak filtering and finally data visualisation and statistical testing were carried out.

The raw data obtained from the MALDI-TOF MS acquisition of the iPSC-derived macrophages were converted into the open .mzxml file format with the CompassXport software (Bruker Daltonics). The peak list extraction from the MALDI-TOF MS data was performed in R (R version 4.3.0, RStudio version 2021.09.2) with a customised workflow that was based on the MALDIquant package.[316] The following R packages were required: MALDIquant, readMzXmlData, MALDIquantForeign, readBrukerFlexData, dplyr, MALDIrppa, rmarkdown, lmtest, usethis, devtools, tinytex, broom, tidyverse, RColorBrewer, corrplot, pvclust, sda, crossval, ggplot2, plyr, ggrepel, stats, ellipse, ggforce, plotly, rgl, IMIFA, umap, plot3D. The customised workflow will be briefly outlined and is depicted in Figure 2.1. The data was imported, and different quality controls (empty check, irregular check and *m/z* check) conducted. The spectrum intensity was square root transformed, peak smoothing conducted (default settings, threshold = 1), baseline corrected (TopHat, half window size = 200) and normalised (TIC method). Spectra were aligned with halfWindowSize = 200, noiseMethod = MAD, signal-to-noise ratio = 7, tolerance = 0.005, warpingMethod = lowess. Finally, the peaks were detected and binned (strict, tolerance = 0.001). Batch correction was performed with the limma package. Additional filtering was applied to the generated output file based on the positive and negative control columns. Mass features that showed a CV > 75% or a log2 fold change between 0.2 and -0.2 were excluded from further analysis. The filtered data was utilised in R to perform principal component analysis (PCA) and uniform manifold approximation and projection (UMAP). Statistical testing was carried out in GraphPad Prism (version 5.0.4 and 9.0.0) and heatmaps were generated in Perseus (version 2.0.3.1), as well as R.

2.7.3 Proteomics data analysis

Two different types of timsTOF MS raw data files were obtained from the iPSC-derived macrophages: DDA and DIA data. Both data types were matched against the SwissProt *Homo*

sapiens (UP000005640, with reviewed (DIA search) and unreviewed isoforms (DDA search) both downloaded in May 2023) and Hao Lab protein contaminants reference databases.[317]

Protein identification and library construction from DDA data was performed using FragPipe (version 21.1) with MSFragger and Percolator for PSM, and EasyPQP for library construction.[318] Next to the default settings, the following parameters were used: mass tolerance for precursor and fragment ions 20 ppm, peptide length 7-50 residues, 1% FDR for peptide- and protein-identification, trypsin specific digestion with 2 missed cleavages, fixed modification: IAA alkylation of cysteine, and variable modifications: oxidation of methionine, acetylation of protein N-termini. The resulting library.tsv file produced by easyPQP was further utilised in py_diAID to generate a custom-made dia-PASEF method as outlined in section 2.6.2 or for the search of DIA data in DIA-NN.

DIA data was searched in DIA-NN software (version 1.8)[295] with the following settings: protease trypsin, missed cleavages 1, maximum number variable modifications 2, modifications (N-term M excision, carbamidomethylation, oxidation, N-term acetylation), peptide length 7 - 30, precursor charge 2 - 4, mass and MS1 accuracy 15, MBR, single-pass mode, QuantUMS. The mass range and library-free/spectral library settings were individually selected for each experiment.

The protein and peptide group files that were obtained from the DIA-NN software were imported into a custom R script (R version 4.3.0, RStudio version 1.4.1717) to merge, filter (remove contaminants, unique peptides per protein ≥2), transform (log2), normalise and batch correct (limma package) the data. General QC plots, including boxplots, density plots and PCA plots, as well as heatmaps and volcano plots were generated with R. In addition, a GSK proprietary R script was used to perform scalar projection analysis. The processed protein lists were imported into Perseus (version 2.0.3.1) to conduct statistical testing, including t-tests (Benjamin-Hochberg correction) and hierarchical clustering. The protein lists were also imported into STRING (https://string-db.org/, version 12.0) and ShinyGO (http://bioinformatics.sdstate.edu/go/, version 0.77) to perform network and GO Term analysis respectively. STRING network analysis was performed with medium confidence score (0.4) and experiments and databases as active interaction resources.

2.7.4 Data visualisation

FlexAnalysis (version 4.0) was utilised for mass spectrum visualisation. Affinity designer (version 1.7.2.471), BioRender, ChemDraw 20.0, GraphPad Prism, R and Perseus were used for illustration.

Chapter 3. Application of MALDI-TOF MS high-throughput biochemical assays: A case study of ERAP1

Chemiluminescence and fluorescence label-based enzymatic assays are traditionally used formats in drug discovery high-throughput screening (HTS) as they are fast, sensitive and robust. However, they are susceptible to artefacts and labelling might perturb the observed biology. Therefore, label-free MS methods are increasingly used alongside them.[319] Specifically MALDI-TOF MS is ideally positioned for the use in HTS due to the analysis speed, which can facilitate large compound screens.[125,320]

This chapter is based on my first author publication "A high-throughput MALDI-TOF MS biochemical screen for small molecule inhibitors of the antigen aminopeptidase ERAP1" published in SLAS Discovery in 2023.[321] The RapidFire MS, affinity selection MS and Xevo-TOF MS data generation was carried out by employees of GSK (Amy Burton, Chloe Tayler, James Rowedder). Herein, I present the development of a biochemical MALDI-TOF MS-based drug discovery assay for a high-profile immunology target, ERAP1, and set it in the context of existing workflows to show the value of this method for early drug discovery screens. The M1 aminopeptidase ERAP1 trims precursor peptides in the endoplasmic reticulum to a mature length for display on antigen presenting molecules.[171,172,174,312] These antigens are detected by T cells and can trigger an immune response. Hence, ERAP1 is an important drug target in immuno-oncology and auto-immune diseases. However, the development of ERAP1-targeting compounds has been challenging due to the enzyme's structural homology with other M1 aminopeptidase family members. Building on a previously developed RapidFire MS assay by Liddle *et al.* 2020, I adapted this workflow to develop an automated MALDI-TOF MS screening method and benchmark its performance against the established assay.[55]

3.1 Assay buffer and peptide alterations to ensure compatibility with MALDI-TOF MS

Initially, I had to assess compatibility of the RapidFire MS assay with MALDI-TOF MS. Before outlining buffer and peptide optimisation steps, I will briefly summarise the original RapidFire MS assay, followed by a short description of a standard MALDI-TOF MS workflow.

In the original assay, developed by Liddle *et al.* 2020, N-terminal ERAP1 trimming of the 9mer peptide with the sequence YTAFTIPSI, a 9-amino acid antigenic epitope from Gag-Pol

polyprotein from human immunodeficiency virus 1, into the peptide 8mer TAFTIPSI was observed.[55] First, compounds were pre-incubated with the ERAP1 enzyme for 30 min. The reaction was started by addition of the substrate and stopped after 60 min reaction time by addition of an acidic quench solution. The quench solution contained an internal standard, the N-terminally acetylated version of the substrate (Ac-YTAFTIPSI), which cannot be cleaved by ERAP1. The total assay volume was 50 µL. The RapidFire autosampler, that was used for sample purification and enrichment, was coupled to a triple quad MS instrument. The substrate and product intensities were measured by targeted MS to derive the product concentration and the internal standard was monitored for quality control purposes.

In the MALDI-TOF MS workflow, which is depicted in Figure 3.1, the enzymatic reaction is performed under the same conditions in an assay volume of 15 µL. Initially, I utilised the same buffer components, and peptides but then optimised these components which is described in chapters 3.1.1 and 3.1.2. After addition of the quench solution, samples for MALDI-TOF MS analysis were mixed with an organic matrix and spotted onto a MALDI-TOF MS target plate. In the MALDI ion source, the matrix facilitates analyte desorption and ionisation, before the ions are separated according to their *m/z* ratio in the TOF mass analyser. The substrate and product intensities were measured and normalised against the internal standard before they are further analysed.

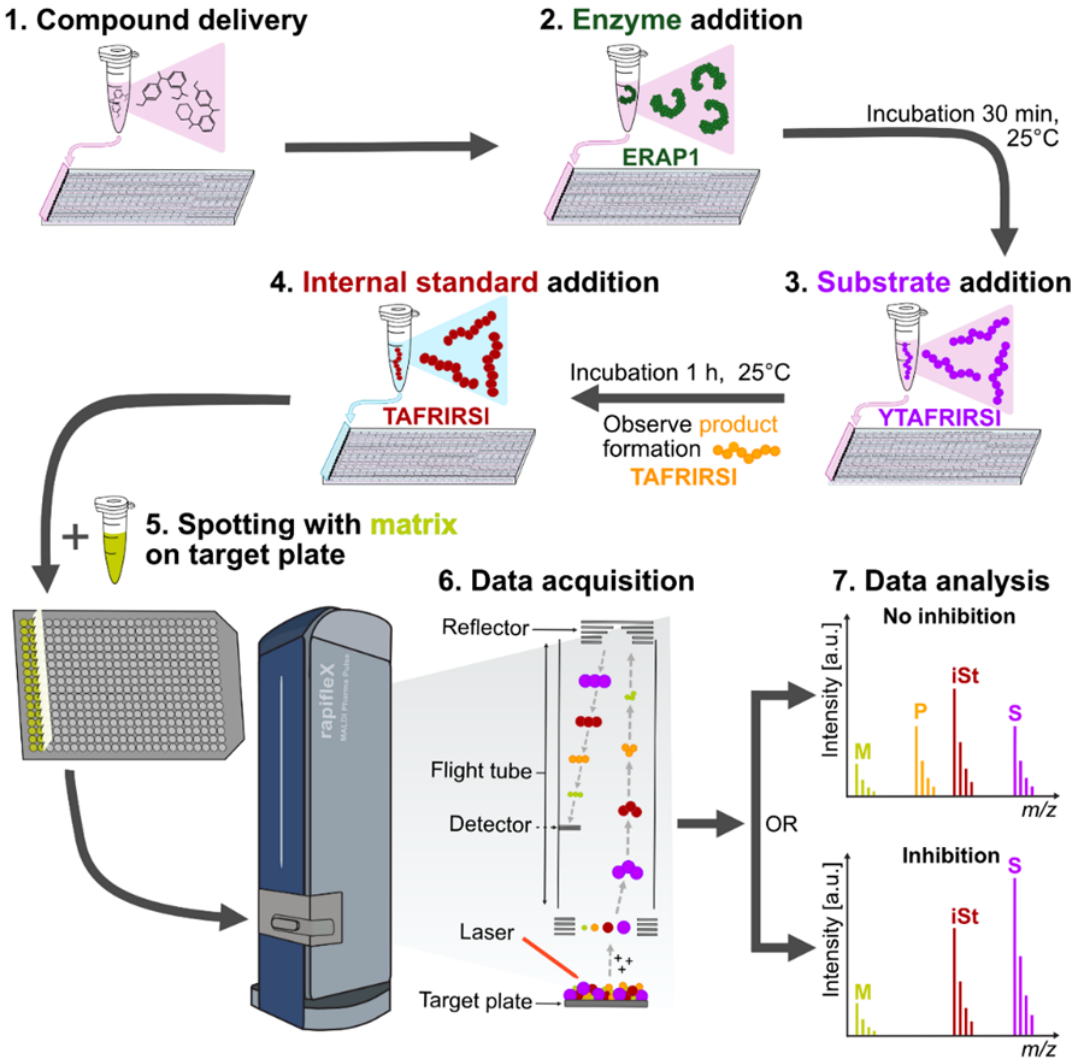

Figure 3.1. Optimised MALDI-TOF MS workflow for ERAP1 screening.
The compound is incubated with the enzyme (ERAP1) and the enzymatic reaction started by addition of the substrate (YTAFRIRSI). After a set time, the reaction is quenched using an acidic solution that contains the internal standard (heavy-labelled TAFRIRSI). The sample is mixed with an organic matrix (CHCA) to aid analyte desorption and ionisation in the MALDI ion source. Ions are separated in the TOF mass analyser according to their *m/z* ratio and then recorded by the detector. The signal intensities are normalised against the internal standard to infer product (TAFRIRSI) and/or substrate concentrations in the presence of compounds.

3.1.1 HEPES reduction and Tween substitution in the assay buffer improved analyte detection by MALDI-TOF MS

Firstly, the assay buffer composition was systematically evaluated. The initial enzymatic reaction was conducted in 50 mM HEPES (pH 7.0), 100 mM NaCl, 0.002% Tween-20 and 0.01% BSA. To ensure compatibility with MALDI-TOF MS, the buffer components were adjusted in accordance with the guidelines for MALDI-TOF MS compatible buffer components published by Chandler *et al.* 2017.[126]

First, the HEPES concentration was lowered from 50 mM to 5 mM to reduce ion suppression. Although, according to the guide, a high sodium chloride (NaCl) concentration (100 mM) is not expected to impact ionisation efficiency, spectra should be thoroughly examined for the presence of both, protonated and sodiated adduct peaks. Lastly, the detergent Tween-20 was assessed. Tween-20 shows multiple peaks in the mass spectrum which arise from the repeating polyethylene glycol units that make up Tween-20.[322] Some of those peaks lay in the mass range of the assay analytes and hence might interfere with signal detection. In addition to signal interference, Chandler *et al.* 2017 reported ion suppression in the presence of this detergent.[126] As a detergent was required in the buffer to facilitate liquid handling and improve protein solubility, Tween-20 was substituted with CHAPS which showed few background peaks and which was not reported to suppress ionisation efficiency.[323] To summarise, the final optimised MALDI-TOF MS compatible assay buffer was composed of 5 mM HEPES (pH 7.0), 100 mM NaCl, 0.01% BSA and 0.1 M CHAPS.

Initial experiments were conducted with this optimised buffer but unfortunately, only sodium adducts of the assay peptides were identified (Figure 3.2) with a relatively poor limit of detection (LOD YTAFTIPSI: 8 fmol, LOD TAFTIPSI: 31 fmol). In a full screen with this buffer, the coefficient of variation (CV) was used to evaluate assay sensitivity while assay robustness was indicated by the Z' which should be Z' >0.5 for large HTS campaigns.[146] I observed an increased data scatter (CV = 16%) and reduced assay quality (Z' = 0.5) in comparison to the established RapidFire MS setup (CV = 3%, Z' = 0.8). Hence, I investigated next if the assay peptides could be altered to improve LOD, assay sensitivity and robustness.

3.1.2 Arginine introduction improved analyte detection by MALDI-TOF MS

It is established that peptides containing arginine have increased ionisation efficiency due to their enhanced gas-phase basicity.[324,325] Therefore, I decided to introduce arginine residues into the peptide sequence, resulting in the creation of the basic peptide pair YTAFRIRSI (substrate) and TAFRIRSI (product). As expected, the basic peptides showed enhanced ionisation compared to the non-basic peptides when tested at equimolar amounts (Figure 3.2). The protonated adduct was prevalent for the basic peptides, resulting in improved detection limits (YTAFRIRSI: 0.5 fmol, TAFRIRSI: 1 fmol).

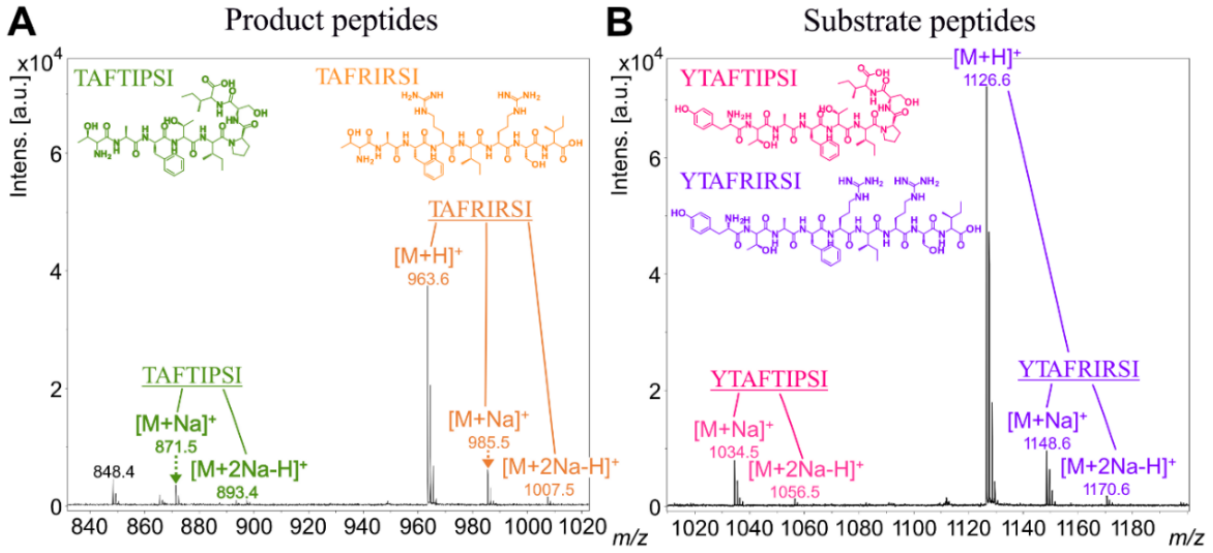

Figure 3.2. Exemplary MALDI-TOF MS spectra displaying improved ionisation efficiency and adduct formation of basic peptides.
(A) Product peptide peaks along their chemical structure (TAFTIPSI: non-basic, green; TAFRIRSI: basic, orange). (B) Substrate peptide peaks along their chemical structure (YTAFTIPSI: non-basic, pink; YTAFRIRSI: basic, purple).

Based on these findings, I decided to change the internal standard to the same arginine-containing peptide wherein the C-terminal isoleucine of the product peptide was heavy labelled. No major differences in ionisation were observed between the product and internal standard when comparing the product concentration to the normalised product MALDI-TOF MS signal (Figure 3.3). This resulted in robust linearity of detection across five technical MALDI spot acquisitions and three experimental repeats indicated by an R^2 of 0.97.

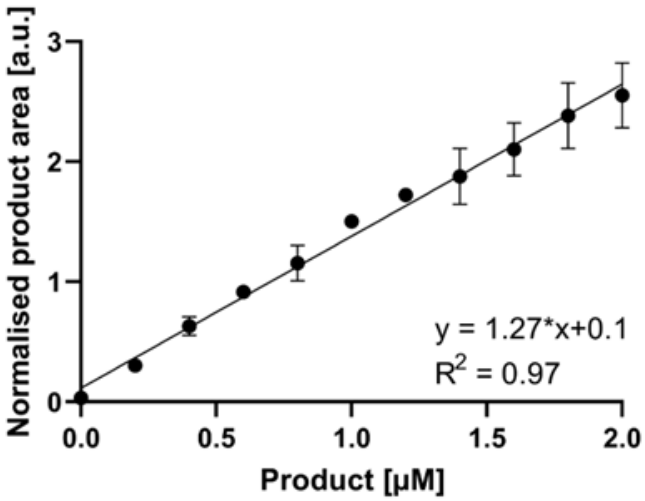

Figure 3.3. Linearity of detection for the basic peptide product by MALDI-TOF MS.
MALDI-TOF MS product signal area after normalisation with the internal standard plotted against the product concentration; linear regression, mean ± standard deviation, $n_{analytical} = 3$, $n_{technical} = 5$.

To summarise, the newly introduced basic peptides were favourable for detection by MALDI-TOF MS and hence they were utilised in combination with the optimised buffer composition (5 mM HEPES (pH 7.0), 100 mM NaCl, 0.01% BSA and 0.1 M CHAPS) for the MALDI-TOF MS-based ERAP1 biochemical assay.

3.2 Testing the optimised MALDI-TOF MS assay with known inhibitors of ERAP1

With the introduction of the optimised assay buffer and peptides, general enzyme activity, as well as new peptide and enzyme concentrations had to be established for the biochemical assay. The enzymatic assay performance was subsequently validated with known ERAP1 inhibitors.

During the enzymatic reaction, successful N-terminal cleavage of the substrate peptide by ERAP1 was observed. I was able to establish two important reagent concentrations: (1) the substrate concentration at which target inhibitors and activators can be equally identified and (2) the enzyme concentration at which the reaction progression was linear. The required substrate concentration is reached when half of the maximum reaction velocity is achieved (K_M). Analysing the substrate turnover across a wide range of concentrations, I identified the K_M as 2 µM which was slightly lower than the non-basic substrate using the RapidFire MS setup ($K_{M\,=}$ 5 µM), indicating increased binding affinity of substrate and enzyme (Figure 3.4A).[55] The selected enzyme concentration for linear reaction progression was 0.25 nM ERAP1 which was again lower than the non-basic peptide assay in the RapidFire MS setup (1 nM), enabling a lower tight-binding limit (Figure 3.4B).[55] To summarise, the use of assay reagents, more specifically the substrate and enzyme concentrations were lowered in the MALDI-TOF MS assay compared to the RapidFire MS assay. It was hypothesised that the decrease in substrate and enzyme concentration was indicative of an increased binding affinity of substrate and enzyme.

The performance of the optimised MALDI-TOF MS-based enzymatic assay was evaluated by determining pIC_{50} values for known ERAP1 inhibitors. I evaluated Leucinethiol (Leu-SH), which targets the zinc ion in the enzyme's active site, and is commonly used in cellular assays[326-328]. Further, DG013A, an inhibitor whose side chains interact with the enzyme's active pocket was probed[188]. The pIC_{50} values for both ERAP1 active site inhibitors were determined to be 7.7 for Leu-SH and 8.0 for DG013A (Figure 3.4C and D). DG013A exhibited a pIC_{50} in a range consistent

with reported literature data (pIC_{50} = 7.3 - 7.5) and the original RapidFire MS assay using non-basic peptides (pIC_{50} = 7.0).[188] These results suggested that minor variations in biological activity could arise from the differing enzymatic assay conditions used to determine the pIC_{50}. Nevertheless, they emphasise the suitability of the MALDI-TOF MS assay for identifying ERAP1 inhibitors.

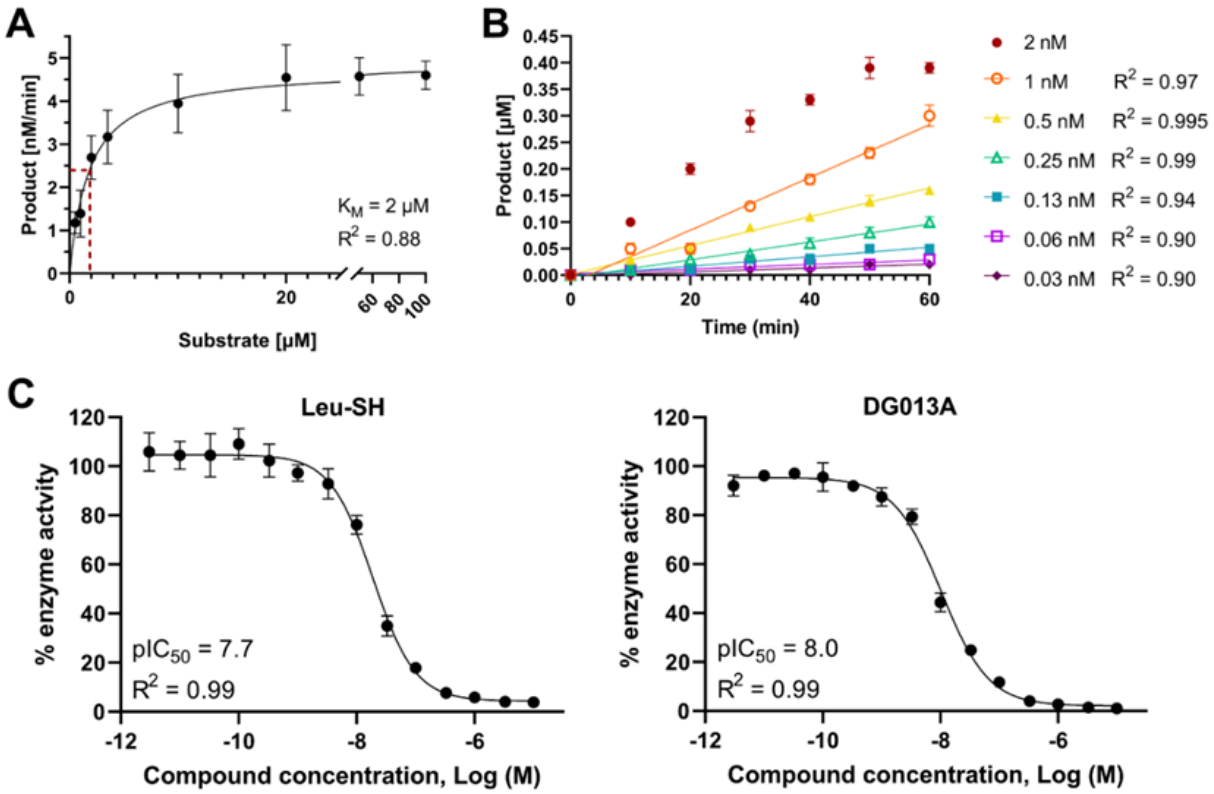

Figure 3.4. Substrate and enzyme concentration optimisation, as well as assay validation with the basic peptides by MALDI-TOF MS.
(A) Enzymatic constant (K_M = 2 µM) determined from the reaction velocity plot; Michaelis-Menten curve, mean ± standard deviation, $n_{analytical}$ = 4, $n_{technical}$ = 5. (B) Reaction progression with enzymatic titration and constant substrate concentration (2 µM); linear regression, mean ± standard deviation, $n_{analytical}$ = 1, $n_{technical}$ = 5. (C&D) Does-response-curves determined for two known ERAP1 inhibitors, Leu-SH (C) and DG013A (D); four-parameter logistical curve fit, mean ± standard deviation, $n_{analytical}$ = 3, $n_{technical}$ = 4.

3.3 The MALDI-TOF MS-based ERAP1 assay shows stability, robustness and reproducibility upon automation

To conduct effective HTS, implementation of automation was required. I was able to utilise automation equipment at GSK, including a Multidrop Combi (Thermo Fisher Scientific) liquid dispenser for addition of reagents in the biochemical assay and access to a fully automated MALDI-TOF MS platform which was capable of MALDI-TOF MS target plate preparation, drying,

injection and measurement for 200 plates at a time. I had to establish assay stability and robustness in this setup, and needed to ensure that there was no reactivity towards common pan-assay interference compounds (PAINS). Those PAINS included compounds such as chelators, redox active, and highly conjugated compounds that can interfere with the enzyme activity.[329]

Intra-plate and inter-day stability was demonstrated by measuring multiple DMSO plates which showed no inner-plate effects (Figure 3.5A), as well as low CV and high Z' across multiple plates and days (CV = 2.67 - 3.04%, Z' = 0.89 - 0.91) (Figure 3.5B). Consequently, assay stability was now comparable to the RapidFire MS assay (CV = 3, Z' = 0.8). Enzyme activity was evaluated with a pilot set of ~1400 compounds containing diverse drug-like structures and PAINS. The assay was stable (Z' = 0.7 – 0.9) and non-reactive to PAINS (Figure 3.5C). Further, two drug-like compounds just below the activity cut-off were identified as hits. Next, a set representative of a HTS collection as it contained ~9,600 compounds with broad chemical diversity, was used to evaluate HTS capacities. The compounds were tested at a single concentration (10 µM). The resulting 58 plates showed an average Z' of 0.8 and by selecting a 75% enzyme activity cut-off, the noise was excluded while 0.9% of compounds were annotated as hits (Figure 3.5D). In HTS efforts, the goal is to identify ~1% hits because this presents a sensible number for follow-up experiments.[125] Further, the screen was highly reproducible as indicated by the correlation between replicate screens (r = 0.90, R^2 = 0.80, Figure 3.5E).

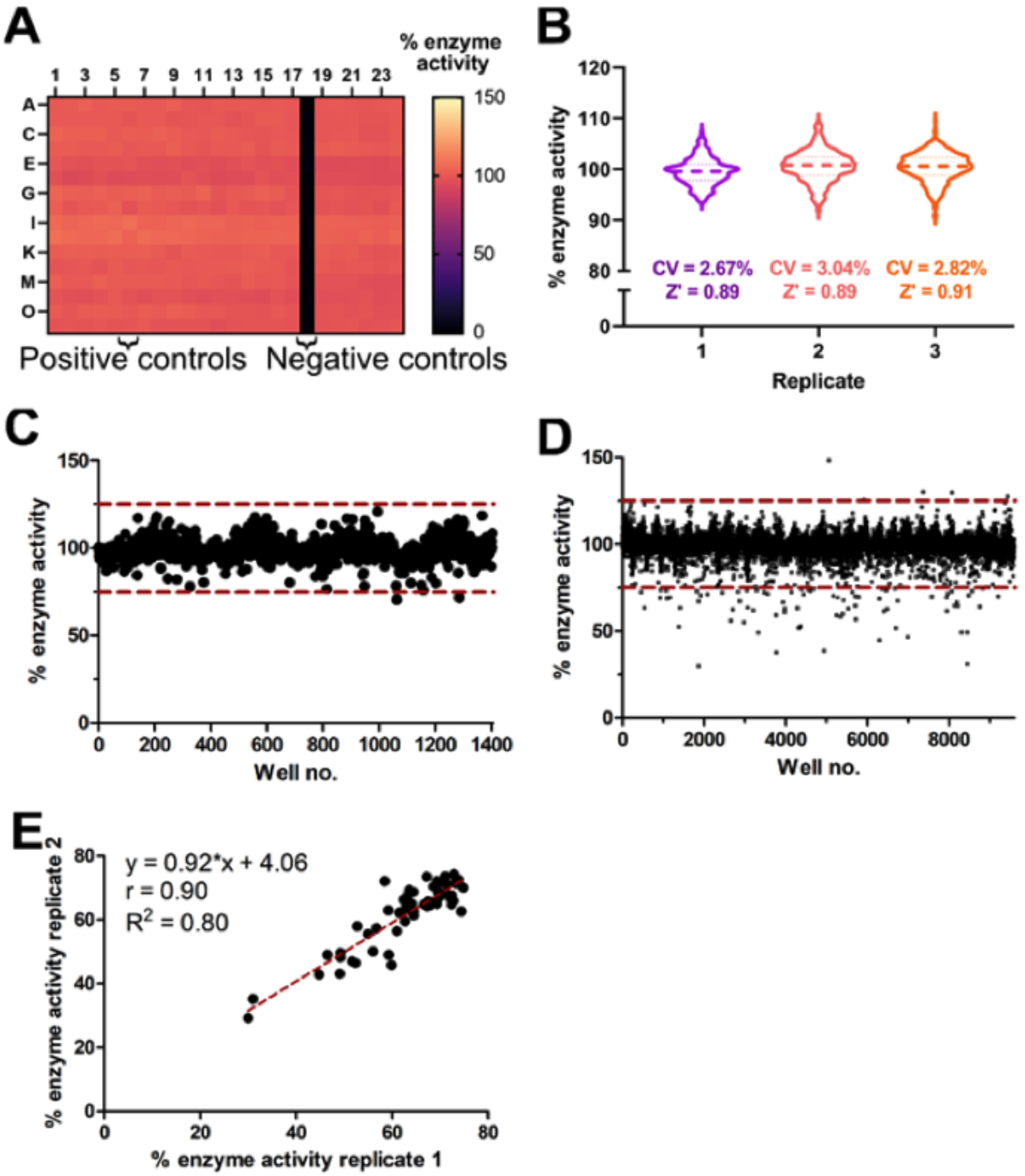

Figure 3.5. Robust MALDI-TOF MS assay performance in automated DMSO, pilot test and ~9,600 compound set screening.

(A&B) Results from the full plate DMSO stability screen (A) Exemplary plate activity plot with single negative control column, (B) Violin plots from well activity (excluding negative controls) across three plates; CV, Z'. (C) Enzyme activity after exposure to compounds from pilot test set (1403 compounds) with 75% and 125% hit cut-off (red dashed line); n = 1. (D) Enzyme activity after exposure to compounds from validation set (~9600 compounds) with 75% and 125% hit cut-off (red dashed line); n = 1. (E) Correlation of enzymatic activity from hit compounds of two replicate screens of the validation set; linear regression.

3.4 The MALDI-TOF MS-based ERAP1 assay showed comparable performance to the established RapidFire MS assay

Following optimisation, validation and automation of the MALDI-TOF MS assay, I assessed its performance in the presence of experimentally confirmed ERAP1 binders identified via affinity selection mass spectrometry (ASMS). Moreover, I compared the assay's performance with that of the established RapidFire MS assay.

The single concentration screen of these binders using MALDI-TOF MS demonstrated a stable Z' (0.8 - 0.9). Notably, a single activator was identified (Figure 3.6A). Most importantly, potent, and weak ERAP1 inhibitors were reproducibly identified (r = 0.96, R^2 = 0.92, Figure 3.6B). The identification reproducibility of ERAP1 inhibitors by MALDI-TOF MS was comparable to that of the RapidFire MS setup (r = 0.98, R^2 = 0.95, Figure 3.6C).

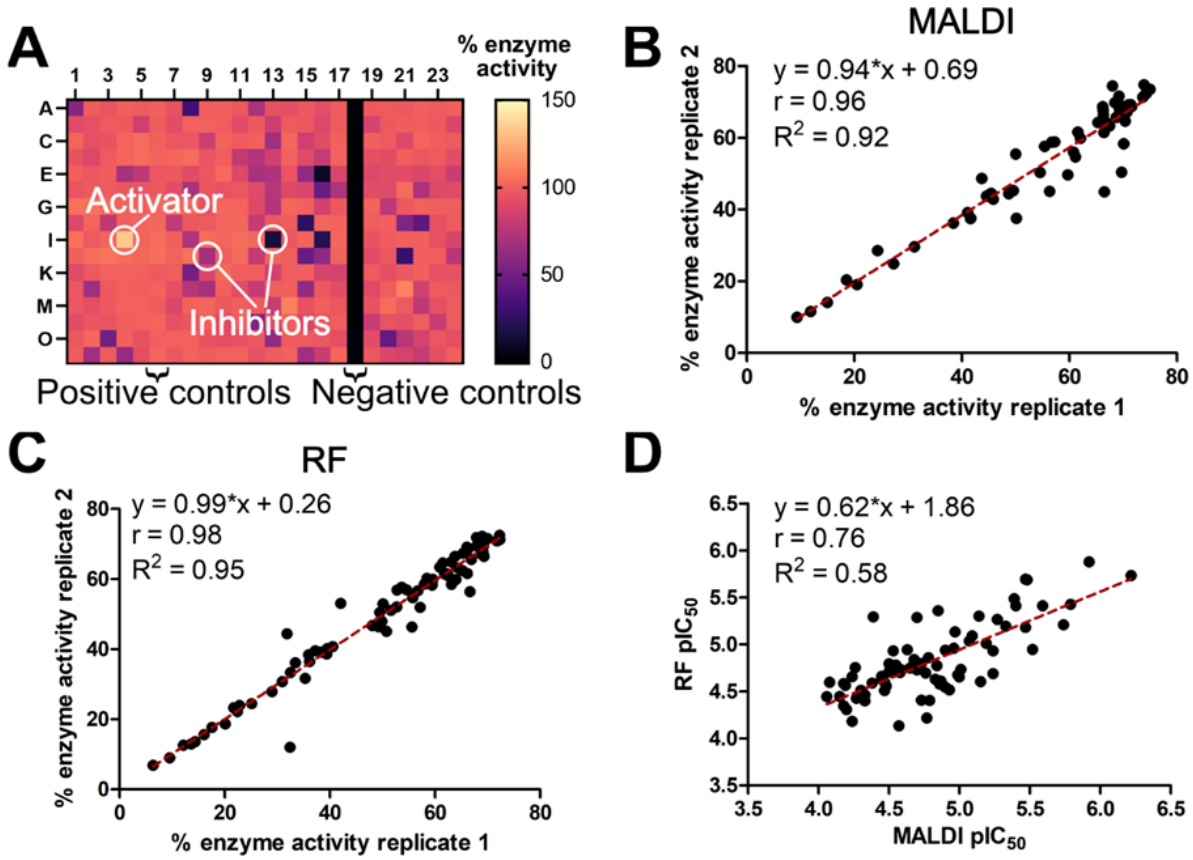

Figure 3.6. Reproducibility of MALDI-TOF MS and RapidFire MS hit calling for 699 ERAP1 binders.

(A) Exemplary plate activity plot from the MALDI-TOF MS screen with positive and negative control columns to identify inhibitors and activators. (B) Correlation of enzymatic activity from hit compounds of two individual MALDI-TOF MS screens; linear regression. (C) Correlation of enzymatic activity from hit compounds of two individual RapidFire MS screens; linear regression. (D) Correlation of averaged pIC_{50} from dose-response screening of single screen hit compounds obtained by MALDI-TOF MS (n = 3) and RapidFire MS (n = 2); linear regression.

Dose-response curves were measured for 100 compound hits from the single concentration screen and pIC_{50} values determined to identify potential false-positives. Five compounds that were also hits in the single concentration screen could not be followed up as they were no longer available in the GSK compound library. As hypothesised previously, a slight shift in the pIC_{50} values between the different MS setups was observed due to differences in the enzymatic assays. To allow for better comparison, the enzymatic assay with the basic peptides should be analysed by RapidFire MS. However, in "substrate only wells", detection of the substrate 9mer, product 8mer and a 7mer was observed (Supplementary Figure 1A and B). Ion chromatograms ruled out substrate contamination as the cause of these findings. In a XEVO-TOF MS experiment with "substrate only wells", elution occurred at a single retention time, which was distinct from the product elution time measured in "product only wells" (Supplementary Figure 1C), suggesting in-source fragmentation in ESI MS.[330] This observation was consistent with the mobile proton theory. This model describes that a mobile proton which is first localised on the most basic site of the molecule (N-terminus or basic peptides) can be transferred to less basic sites like the peptide backbone, allowing charge-directed cleavage at various sites.[331]

Despite differences in the enzymatic assays, one-third of the hit compounds identified in the single concentration screen overlapped between the MALDI-TOF MS and RapidFire MS setups (Figure 3.7A). Between 78% and 84% hit compounds from the single concentration screen were validated as true hits in the dose-response curve screening depending on the platform (Figure 3.7B). Some exemplary stronger hits showed a pIC_{50} of 5.74, 6.23 and 6.54 in dose-response curves obtained by MALDI-TOF MS (Figure 3.7C). Upon closer examination, compounds identified solely as hits in the RapidFire MS screen, clustered near the selected enzyme activity cut-off in the MALDI-TOF MS screen (RapidFire MS cut-off = 72.5%, MALDI-TOF MS cut-off = 75%). This highlights the importance of carefully selecting the enzyme activity cut-off as this may explain discrepancies observed in hit identification (Figure 3.7D).

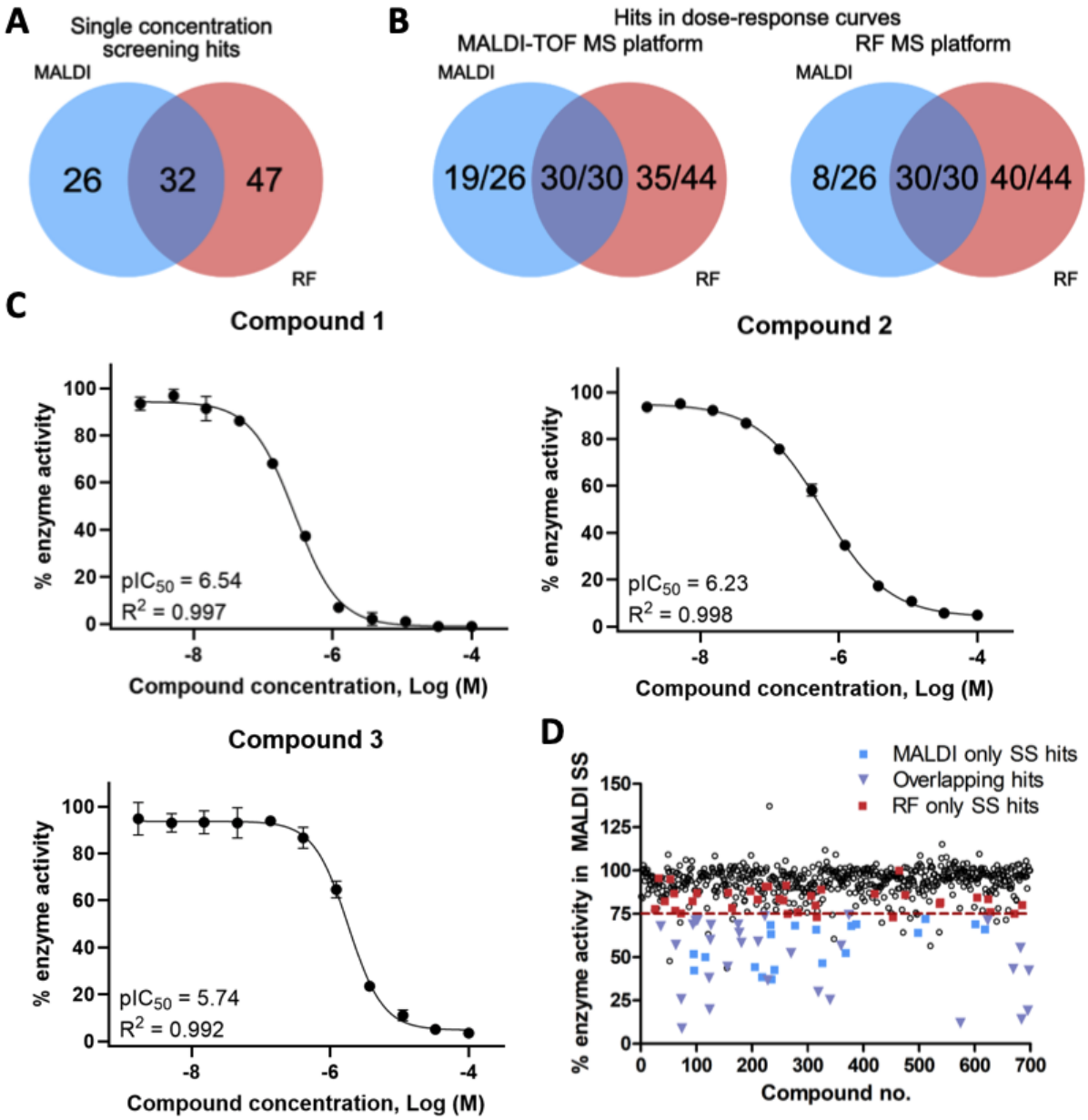

Figure 3.7. Overlap of the MALDI-TOF MS and RapidFire MS hit calling for 699 ERAP1 binders. (A) Venn diagram of hits identified in at least two replicates of the single concentration screens for MALDI-TOF MS or RapidFire MS respectively. (B) Venn diagram indicating the number of real hits based on the pIC_{50} (pIC_{50}>4.0) when evaluated in dose-response curves on the MALDI-TOF MS (left) or RapidFire MS (right) platform respectively along the total number of investigated single hit compounds. (C) Exemplary dose-response curves obtained with the MALDI-TOF MS platform; four-parameter logistical curve fit, mean ± standard deviation, n = 3. (D) Averaged (n = 3) enzyme activity after exposure to 699 ERAP1 binder compounds obtained from MALDI-TOF MS single concentration screening efforts with 75% hit cut-off (red dashed line). Hits that were identified in the single concentration screen on both screening platforms or only on a single one are indicated (Both platforms: purple triangle, MALDI-TOF MS only: blue square, RapidFire MS only: red square).

Nevertheless, a strong correlation was observed between the pIC_{50} values of the hit compounds measured by the two different MS platforms (r = 0.76, R^2 = 0.95) (Figure 3.6D). Similar correlation has been reported in the literature for screens using the same enzymatic assay but different redout methods.[125,157] The slope of the correlation suggests varying potency of the compounds in the newly developed MALDI-TOF MS assay, attributable to differences in enzyme activity. However, the ranking of compounds remained consistent across both MS platforms, highlighting their comparable performance.

3.5 Discussion

In this chapter, I have presented the optimisation of the ERAP1 assay buffer and assay peptides for MALDI-TOF MS detection. The adjustment of the enzyme assay conditions reduced the assay reagents in comparison to the established RapidFire MS setup. I have shown that the novel MALDI-TOF MS assay was stable, robust, free from interference, automatable and suitable for general HTS efforts. Moreover, the setup showed equal performance in evaluating activity of confirmed ERAP1 binders when compared to the RapidFire MS setup.

3.5.1 The benefits and drawbacks of MALDI-TOF MS

Chemiluminescence and fluorescence label-based biochemical assays are still widely used in the early drug discovery stages due to their speed, sensitivity and general robustness also when utilised by inexperienced users.[319] They are however susceptible to artefacts, leading to a larger proportion of initial false positives, hence needing substantial subsequent follow up. In addition, label-based assays might have a limited dynamic range or perturb biology as it was reported for the fluorescence-based ERAP1 screen.[55,171,332] The assay faced difficulties in hit compound identification as it suffered from the inner filter effect where a loss in product fluorescence intensity was observed due to the high substrate concentration that was utilised. Further, substrate labelling influenced ERAP1 enzyme activity. Traditional label-based assays are increasingly used alongside or replaced by label-free MS approaches which can directly quantify analytes and thereby circumvent the described issues of label-based setups.[55] Different MS systems can be used but one must consider the initial cost for a mass spectrometer and the need for trained personnel when comparing the benefits to label-based setups. A popular system used in MS screening is the RapidFire MS which was also used for

ERAP1 screening. Sample purification and enrichment on the cartridge prior to injection into the mass spectrometer eliminates the need to optimise buffer conditions, as required for MALDI-TOF MS.[54,58] However, this clean-up comes at a cost of a cycle time of 7 – 13 seconds per sample as opposed to less than 1 second per sample for MALDI-TOF MS.[54,58] Direct injections without cartridge, also known as BLAZE mode or multiplexing and pooling can increase the speed of RapidFire MS but it cannot match the speed of MALDI-TOF MS.[49-51,125] Further, the MALDI-TOF MS setup requires lower sample volumes, allowing miniaturisation (RapidFire MS: 50 µL assay volume, MALDI-TOF MS: 15 µL assay volume). In the presented ERAP1 example, the substrate and enzyme concentrations were lowered (RapidFire MS: 5 µM substrate, 1 nM enzyme; MALDI-TOF MS: 2 µM substrate, 0.25 nM enzyme), decreasing the enzyme tight-binding limit and also the overall assay cost. This highlighted the benefits that MALDI-TOF MS can provide in HTS drug discovery.

3.5.2 The current application landscape of MALDI-TOF MS

With the development of the novel MALDI-TOF MS-based ERAP1 assay, I was able to add to the growing number of targets that can be assessed by MALDI-TOF MS; targets include kinases[122,149], phosphatases[123], methylases[125,150], trimethylamine-lyase[156], deubiquitylases, and ubiquitin E3-ligases[124,151,152]. However, even with buffer, analyte, and matrix optimisation, not all interfering effects observed in MALDI-TOF MS can be eliminated, hampering analysis of enzymatic screens with products and substrates in the small molecular weight region (<500 Da). To address this, Winter *et al.* 2022 have introduced an automation compatible post-reaction derivatisation workflow to enable determination of catechol-o-methyltransferase activity by MALDI-TOF MS.[158]

Alternatively, the RapidFire MS technology can be utilised to execute compound screens. This platform has been used to evaluate enzyme activity of targets such as kynurenine 3-monooxygenase[333], elongation of very long-chain fatty acids family 6 enzyme[32] and major m17-leucyl aminopeptidase[334]. The field of MS is constantly evolving, recognising an increasing interest in the development of label-free biochemical HT assays which led to the launch of the EchoMS system (SCIEX). This system has been used to screen activity of several enzyme targets, including diacylglycerol acyltransferase 2, and isocitrate dehydrogenase 1.[67-70]

These MS-based technologies are mainly applied in the field of biochemical screens. However, awareness for limited transferability of biochemical screen hits increases in the HTS community. There is an increasing demand to work with more biologically complex systems in the early stages of drug discovery to improve the translation of findings into the clinic. Hence, I want to evaluate if label-free MS approaches can provide benefits for screening more biologically complex models.

Chapter 4. Characterisation of induced pluripotent stem cell-derived macrophage phenotypes

There is an increasing demand for screening cell-based models in the HT stage of the drug discovery pipeline to improve the translation of early drug candidates into the clinic. Unlike biochemical assays that track only a substrate and its product, cellular assays offer a more comprehensive evaluation of compound characteristics, including uptake, target engagement, and potency within a physiological context.[35] This increased biological complexity allows for a deeper understanding of cytotoxicity, mechanisms of action, and off-target interactions.[35] Various cell models with different complexity, ranging from 2D models with a single cell type to 3D models with multiple cell types, can be used.[335] Within these models, established cell lines, induced pluripotent stem cell (iPSC)-derived cells, or primary cells from different genetic backgrounds can be utilised.[37]

I opted to work with iPSC-derived macrophages because they can be scaled up for culture and are genetically closer to primary cells than conventional cell lines.[336] I polarised these cells into classically activated (M1) and alternatively activated (M2) macrophages. In this chapter, the aim was to optimise cell culture and stimulation conditions for iPSC-derived macrophages from human donors to facilitate subsequent phenotypic screening. I assessed the immune cell phenotypes by investigating their morphology, secreted cytokine profile, and proteomics profile. I developed a robust proteomics workflow to measure macrophage phenotype biomarkers and to validate them for subsequent use.

4.1 Pro- and anti-inflammatory macrophage phenotypes were identified based on cell morphology

The cell culture workflow for iPSC-derived macrophages involved thawing and culturing iPSCs obtained from three different human donors over a period of 14 days (Figure 4.1). Subsequently, from day 15 to 21, embryoid bodies were formed. Upon reaching full establishment, these embryoid bodies released monocytes into the cell suspension. The iPSC-derived monocytes used throughout this thesis were generously provided by my industrial collaborator, GSK (Charlie Haslam, Thomas Dawson).

Following the isolation of monocytes, I proceeded with monocyte differentiation and macrophage polarisation (supported by Serena Bateman, GSK). Monocytes were seeded into well plates and induced to differentiate into macrophages through the addition of macrophage colony-stimulating factor (M-CSF) to the culture medium.[337] Differentiation was complete after 6 days, when the initially floating monocytes developed into adherent macrophages on the culture plates.[313] These macrophages were then polarised into M1 macrophages with interferon gamma (IFN-γ), and lipopolysaccharide (LPS), and into M2 macrophages with IL-4. IFN-γ and LPS are synergistic stimulants *in vivo* that robustly activate macrophages during infection, and IL-4 is a cytokine commonly involved in tissue repair signalling.[338] Cells were harvested at either 4- or 24-hours post-stimulation. To enhance efficiency and throughput, I implemented automation equipment for tasks such as cell seeding, media changes, addition of stimuli, and cell harvesting, enabling workflow miniaturisation into 96-well plates.

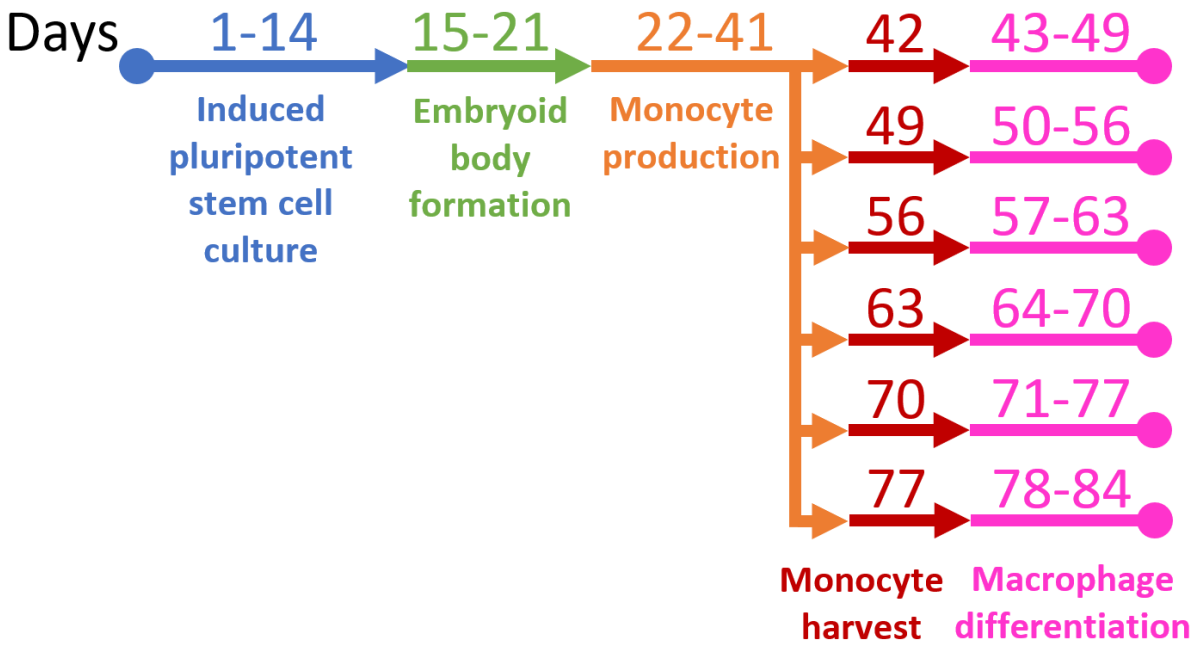

Figure 4.1. Induced pluripotent stem cell (iPSC)-derived macrophage cell culture timeline. Workflow illustrating the culture process of iPSC-derived macrophages, encompassing iPSC culture (days 1-14), embryoid body formation (days 15-21), monocyte production (days 22-41), and six monocyte harvest/macrophage differentiation cycles (days 42-84).

In an initial experiment, I utilised different concentrations of M-CSF (10 ng/mL and 100 ng/mL) for monocyte differentiation. In both conditions, cells attached firmly to the culture dish after six days. Additionally, these unstimulated macrophages (M0) exhibited a spindle-like cell shape (Figure 4.2).[339] When macrophages were polarised with IFN-γ and LPS (IFN-γ+LPS) for 24 hours, they displayed a flatter, rounder cell morphology and they had many cell protrusions compared

to the M0 phenotype; this morphology is characteristic for pro-inflammatory macrophages (M1).[339] Stimulation with IL-4 resulted in a more M0-like phenotype with further elongation of the cell body, a morphology commonly associated with M2 macrophages.[339] These distinct cell morphologies were consistent across both M-CSF concentrations, confirming successful macrophage differentiation and polarisation in all conditions.

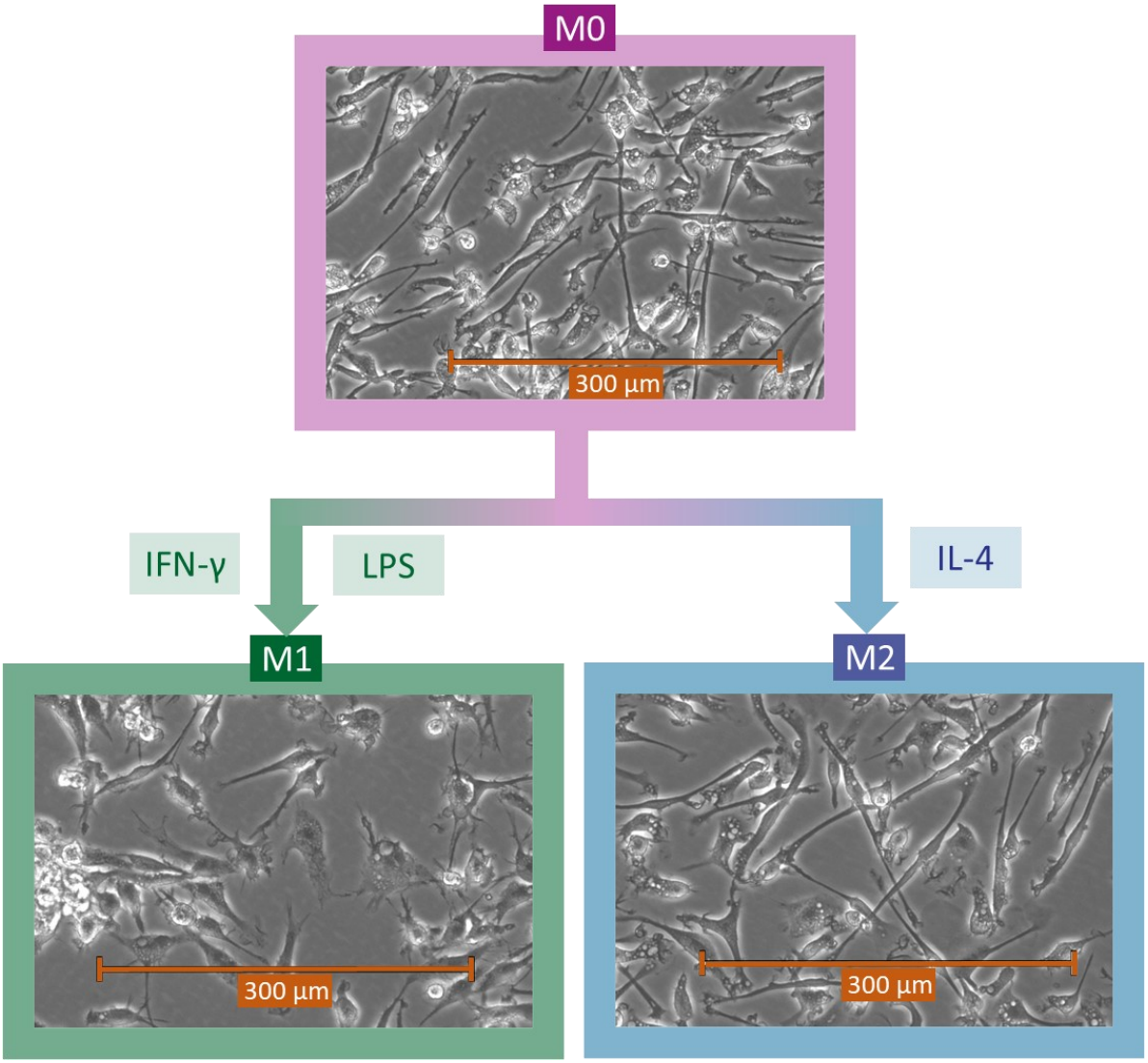

Figure 4.2. Cell morphology of unstimulated and polarised macrophages.
Representative morphology of terminally differentiated M0 resting macrophages, and classically activated (M1) and alternatively activated (M2) macrophages after 24 hours of stimulation with IFN-γ+LPS (dual) or IL-4 respectively.

4.2 Search of LC-MS/MS DIA data with a hybrid spectral library improved search speed and number of protein identifications

To further characterise macrophage phenotypes, a proteomics workflow was established based on time course experiment samples. I investigated iPSC-derived macrophages from

three different human donors that were differentiated with either 10 ng/mL or 100 ng/mL M-CSF and polarised with IFN-γ+LPS (M1 phenotype) or IL-4 (M2 phenotype) for either 4 or 24 hours. This resulted in a total of 42 samples, including resting macrophage (M0) controls at 0, 4 and 24 hours.

Sample preparation involved utilising the 96-well format S-Trap technology from ProtiFi, which integrates seamlessly with the macrophage culture automation workflow. Briefly, S-Trap involves suspension trapping of reduced and alkylated proteins to allow for protein digestion and subsequent peptide elution.[340] The samples were acquired using an Evosep One LC system operated in 60SPD (sample der day) mode and a timsTOF HT. TimsTOF MS has been shown to produce high data quality at these sample run times.[341,342] Finally, data independent acquisition (DIA) was conducted to increase sample coverage.[343] The DIA-NN software was used for peptide and protein identification from the raw data. Three distinct DIA data search methods were evaluated: (1) library-free, (2) gas fractionation library, and (3) hybrid library search. The library-free approach employed theoretical methods to infer peptide identity, while the gas fractionation library method used a spectral library constructed from a pooled experimental sample acquired using five methods targeting different mass and ion mobility (IM) ranges.[315] In the hybrid library approach, the spectral library incorporated both, previous experimental data and current experiment data that were consolidated into a large spectral library.

Post-processing of the obtained peptide and protein lists included two filtering steps. First, known contaminants, including bovine proteins from the cell medium, keratins from the researchers' skin and dust, as well as trypsin from enzymatic digestion were removed.[317] Further, proteins identified by only a single unique peptide match were removed according to standard proteomics practices.[344] To remove unwanted variability that can derive from cell culture (e.g. different donors), storage conditions or sample preparation, normalisation and batch correction are routinely applied.[345] Here, I used median normalisation, as well as batch correction on an iPSC donor level.

First, the data quality was assessed. Overall, even prior to sample normalisation and batch correction, no outlier samples or batch effects were observed (Figure 4.3). All samples showed a similar log2 protein intensity average around 15, and the distribution of intensity values

within each sample was consistent across all samples. This was representatively shown for the hybrid library approach (Figure 4.3) but equally observed for the label-free and gas fractionation library search approaches. Additionally, there was a tight correlation (r = 0.97, R^2 = 0.94) between the log2 protein intensity values obtained from the library-free and hybrid library search approaches on an individual sample level (Figure 4.4, exemplary shown for 21 macrophage samples differentiated with 100 ng/mL M-CSF). Together, this indicated high data quality and workflow robustness across the 42 samples.

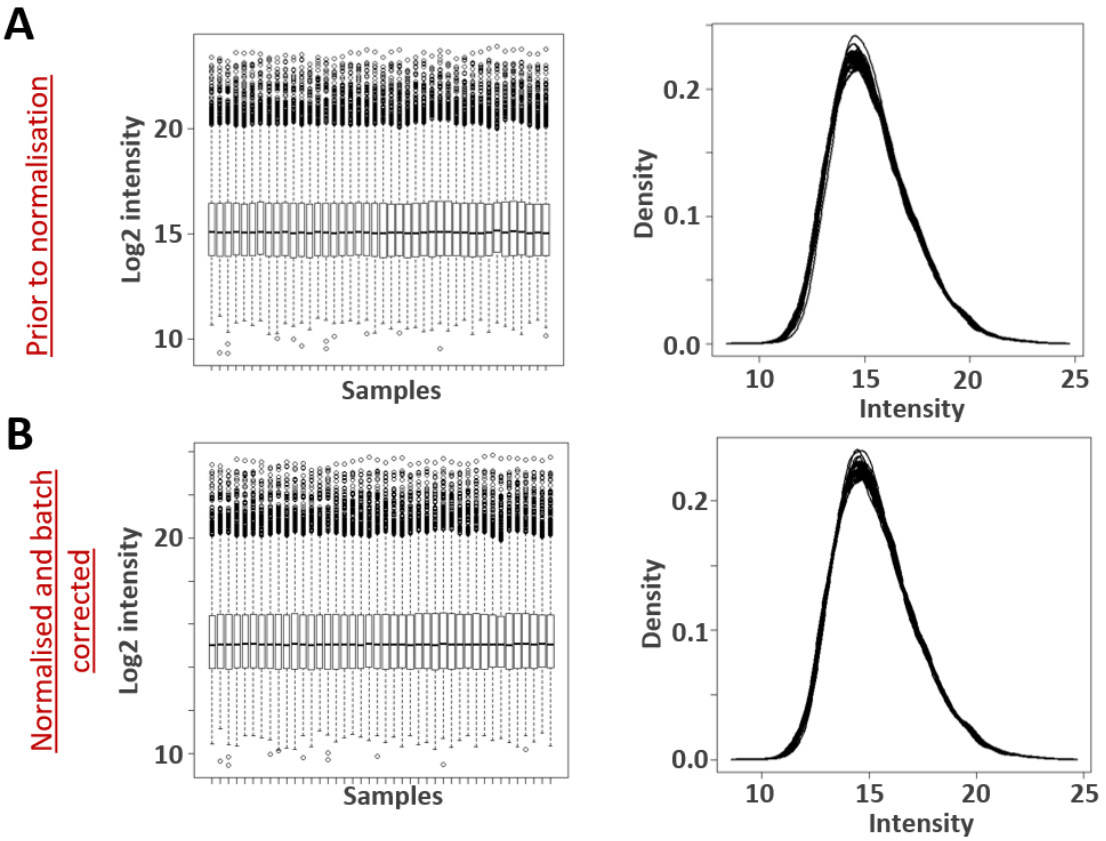

Figure 4.3. Data quality shown after hybrid library search of the cell culture condition optimisation experiment.
Quality control plots for LC-MS/MS data of an iPSC-derived macrophage time course experiment obtained (A) prior and (B) after normalisation (median) and batch correction (donor level). Macrophages from three different human donors were differentiated with either 10 ng/mL or 100 ng/mL M-CSF and polarised with IFN-γ+LPS or IL-4 for either 4 or 24 hours resulting in a total number of 42 samples, including resting macrophage (M0) controls.

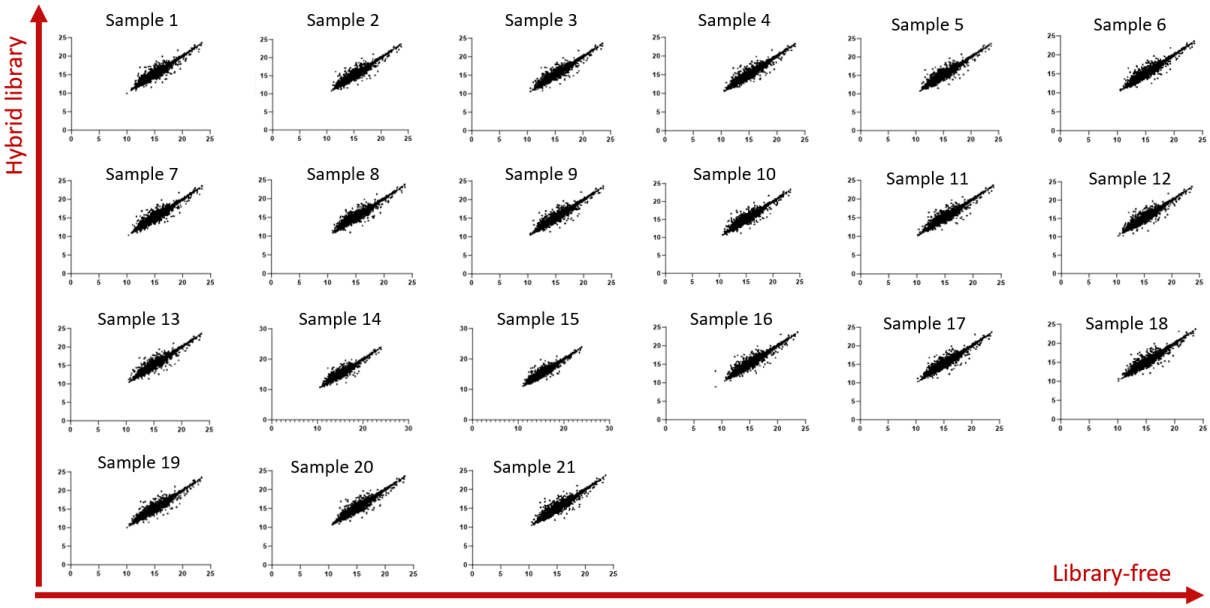

Figure 4.4. Correlation of log2 protein intensity between different library search methods from samples of the cell culture condition optimisation experiment.
Plots of the normalised and batch corrected log2 protein intensity of iPSC-derived macrophages obtained with the library-free and hybrid library search approaches. 21 macrophage samples that were cultured with 100 ng/mL M-CSF and polarised with IFN-γ+LPS or IL-4 for 4 or 24 h, as well as M0 controls at 0, 4 and 24 hours from three different human donors were plotted.

While data quality was comparable, a major difference between the data search approaches was the search speed: ~35 minutes per sample for library-free versus ~3 minutes per sample for library-based approaches on a desktop work station (Intel(R) Core(TM) i9-10900X CPU @ 3.70GHz processor and 128 GB RAM). Pre- and post-filtering, the number of identified peptides and proteins was similar across the different methods (Figure 4.5). The highest number of peptides (average 55,157 per sample) and proteins (average 5,366 per sample) was observed with the hybrid library approach while the lowest was observed with the gas fractionation library approach (average 51,102 peptides and 5,090 proteins per sample), though the differences were marginal.

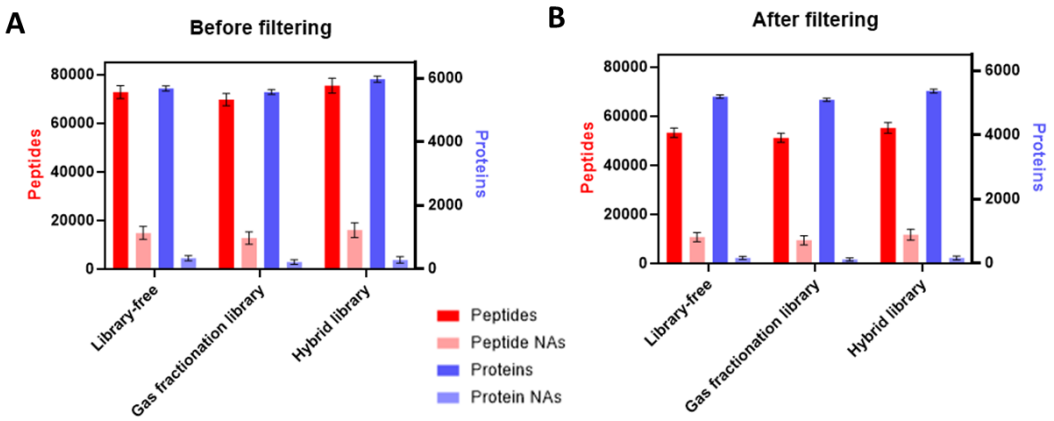

Figure 4.5. Peptide and protein numbers from different library searches of the cell culture condition optimisation experiment.
Peptide (red) and protein (blue) identifications, along with the number of missing values (NAs) identified in the library-free, gas fractionation library and hybrid library searches of iPSC-derived macrophage samples from three different human donors. Cells were differentiated with 10 ng/mL or 100 ng/mL M-CSF and polarised with IFN-γ+LPS or IL-4 for 4 or 24 h. (A) Before filtering. (B) After filtering for contaminants and unique peptides per protein ≥2.

4.3 Macrophage polarisation with an IFN-γ+LPS dual stimulus for 24 h elicited large changes on a proteomics level

Based on the data quality assessment (section 4.2), I decided to analyse the normalised and batch-corrected data from the hybrid library search approach to further characterise macrophage phenotypes. This approach offered the fastest search speed and highest number of protein identifications, enabling potentially the most detailed phenotype characterisation. Unsupervised clustering revealed no donor-specific clustering, indicating robust proteome level changes across donors (Figure 4.6A). Further, distinct clustering of the 10 ng/mL M-CSF (cluster 1 and 2) and 100 ng/mL M-CSF (cluster 3 and 4) cell culture conditions was observed. Within the 10 ng/mL M-CSF cluster one, the 24-hour macrophages clustered away from 0 and 4-hour cell phenotypes, showing instead alignment with the 100 ng/mL M-CSF cluster three. It has been previously reported that higher or more prolonged M-CSF exposure resulted in a more pronounced macrophage phenotype, explaining these observations.[337] The most distinct clustering from all other M-CSF concentration matched cell phenotypes was observed for the 24-h polarisation with IFN-γ+LPS (cluster 2 and 4). Contrary to these findings, Murugesan *et al.* 2022 described distinct clustering for M0, M1 and M2 macrophages.[346] Here, due to the nature of PCA, subtle differences are likely overlooked, whereas major changes, such as variations in M-CSF concentration or 24-hour polarisation with IFN-γ+LPS, dominate the plot space.[347]

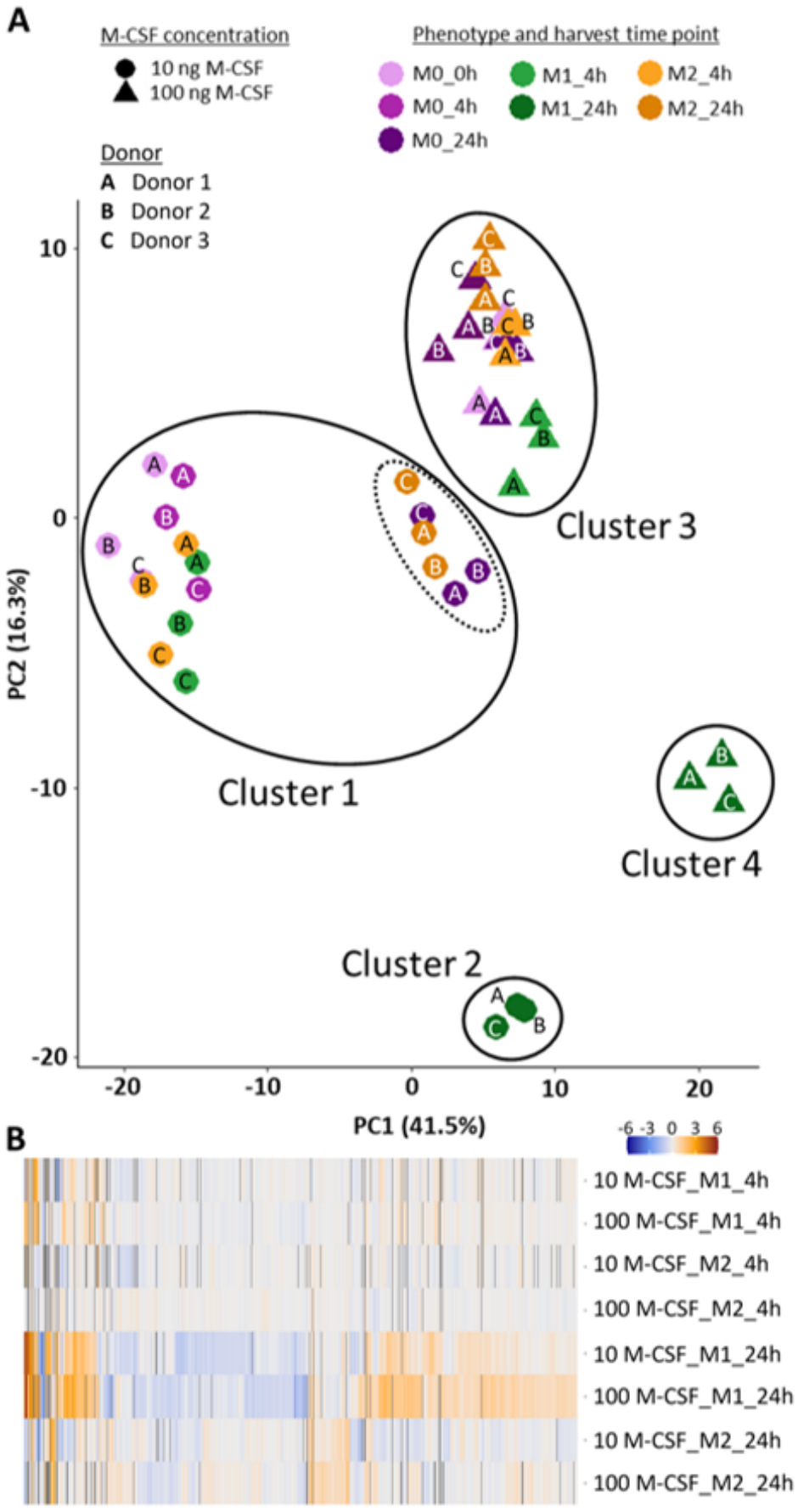

Figure 4.6. Global proteome analysis from the cell culture condition optimisation experiment.

iPSC-derived macrophages from three different human biological donors were differentiated with 10 ng/mL or 100 ng/mL M-CSF and polarised with IFN-γ+LPS (M1) or IL-4 (M2) for 4 or 24 h. (A) PCA plot generated with the normalised and batch corrected hybrid library search data. (B) Heatmap of the protein fold change obtained by t-testing (Benjamin-Hochberg correction) each condition to its time respective M0 control.

Protein fold changes obtained by comparison of the different cell stimulations against their respective M0 control were visualised in a heatmap (Figure 4.6B). Few differentially regulated proteins were identified following 24-hour IL-4 treatment, though the number of proteins that showed a change remained minimal. This aligns with findings by Murugesan *et al.* 2022 who noted modest proteomics shifts induced by M2 polarisation, primarily affecting metabolic shifts.[346] Further, M2 macrophage polarisation is frequently conducted for 48-hours to achieve a full macrophage shift.[348] Consequently, this phenotype was not further examined. The heatmap confirmed most significant alterations in protein expression after 24-hour polarisation with IFN-γ+LPS. The protein expression changes after 24-hours likely included both, novel protein synthesis, as well as responses based on activation of secondary signalling cascades, a change potentially missed after 4-hour stimulation. Thus, I focussed my subsequent analysis efforts on the 24-hour IFN-γ+LPS dual stimulus to explore macrophage phenotypes suitable for MS-based cellular HTS endeavours.

4.3.1 Differentiating macrophages with low levels of M-CSF reduced the magnitude of the inflammation response

The proteins that were significantly changed during the 24-hour IFN-γ+LPS macrophage polarisation in comparison to their untreated controls were further analysed. The number of significantly downregulated proteins was similar for both the 10 ng/mL and 100 ng/mL M-CSF cell differentiation, with 25 and 34 proteins, respectively (log2 protein fold change cut-off = 2, -log10 adjusted p-value cut-off = 0.01) (Figure 4.7A and B). A closer examination of these downregulated proteins revealed minimal overlap between the two conditions: 8 proteins were common for both, while 17 proteins were unique to the 10 ng/mL M-CSF condition and 26 proteins were unique to the 100 ng/mL M-CSF condition (Figure 4.7C). No STRING interactions were identified between more than two proteins (medium confidence and active interaction sources: experiments, databases), indicating that no downregulated signalling cascade was associated with the pro-inflammatory cell polarisation.

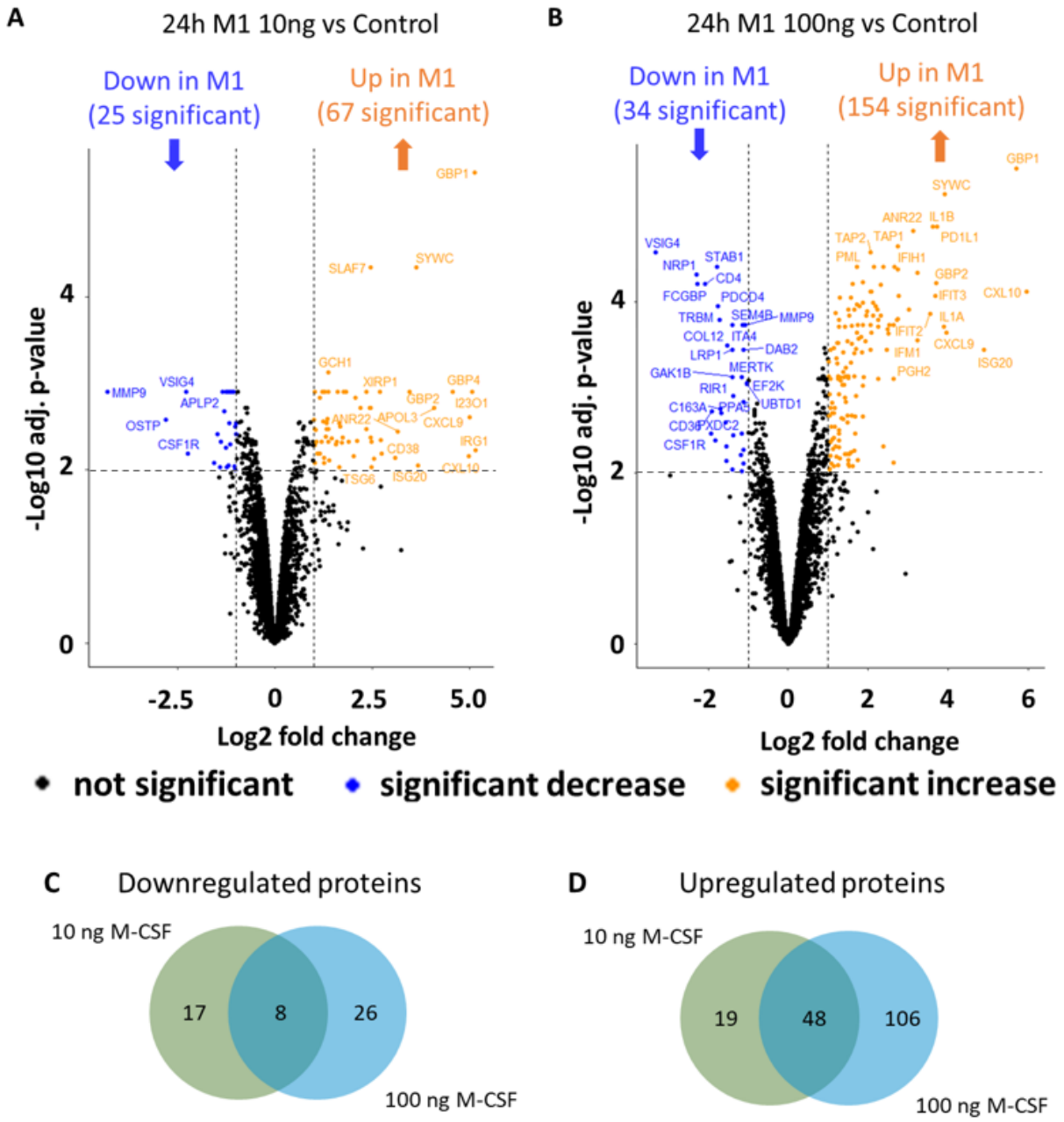

Figure 4.7. Significantly up- and downregulated proteins after 24h macrophage polarisation with IFN-γ+LPS after differentiation with 10 ng/mL or 100 ng/mL M-CSF.
(A&B) Volcano plot showing log2 protein fold change (cut-off = 2) against -log10 adjusted p-value (cut-off = 0.01) after t-testing (Benjamin-Hochberg correction) the polarised macrophages against the untreated controls with highlighted significantly down (blue) and upregulated (orange) proteins; (A) 10 ng/mL M-CSF, (B) 100 ng/mL M-CSF. Venn-Diagram comparing the significantly (C) down- and (D) up-regulated proteins highlighted in the volcano plots between the 10 ng/mL and 100 ng/mL M-CSF conditions.

A larger number of proteins was significantly upregulated in both M-CSF conditions. The number of significantly upregulated proteins nearly doubled in the 100 ng/mL M-CSF condition

from 67 in the 10 ng/mL M-CSF condition to 154 in the 100 ng/mL M-CSF condition (Figure 4.7A and B). A considerable overlap was observed in the upregulated proteins between the treatments: 48 proteins were common to both conditions, 19 were unique to the 10 ng/mL M-CSF condition, and 106 were unique to the 100 ng/mL M-CSF condition (Figure 4.7D). These increased protein levels in the higher M-CSF concentration were in line with previous observation indicating a stronger macrophage phenotype as cells seemed to respond more effectively to pro-inflammatory stimuli.

I performed network analysis for these stronger responding macrophages which revealed that most differentially expressed proteins were associated with the immune system biological GO term. To further investigate the involved signalling pathways, proteins were assigned to different signalling cascades based on well-established GO terms, KEGG pathways, and a publication from Murugesan *et al.* 2022.[346] The observed protein fold changes were then mapped accordingly to identify proteins that can be detected with the presented proteomics workflow and further used as biomarkers for M1 activation.

Initially, cell surface markers were examined to evaluate the M1-like characteristics of the polarised iPSC-derived macrophages. Consistent with Murugesan *et al.* 2022, well-characterised M1 cell surface markers such as PLD1 (CD274), CD38, TNR5 (CD40) and CD48 were upregulated in response to IFN-γ+LPS stimulation (Figure 4.8). These markers are important immune checkpoints, cytokine secretion promoters and costimulatory molecules for T cell activation.[346] Conversely, a decrease in CD36, a M0 marker involved in phagocytosis, was observed following IFN-γ+LPS stimulation.[346] In addition, some novel markers suggested by Murugesan *et al.* 2022 were identified, such as CLM8 (CD300a) and CSF1R, both M0 markers, as well as LILRB2, a M1 marker. This further consolidated the pro-inflammatory phenotype of the iPSC-derived macrophages and informed on biomarkers that can be reliably used for phenotype identification.

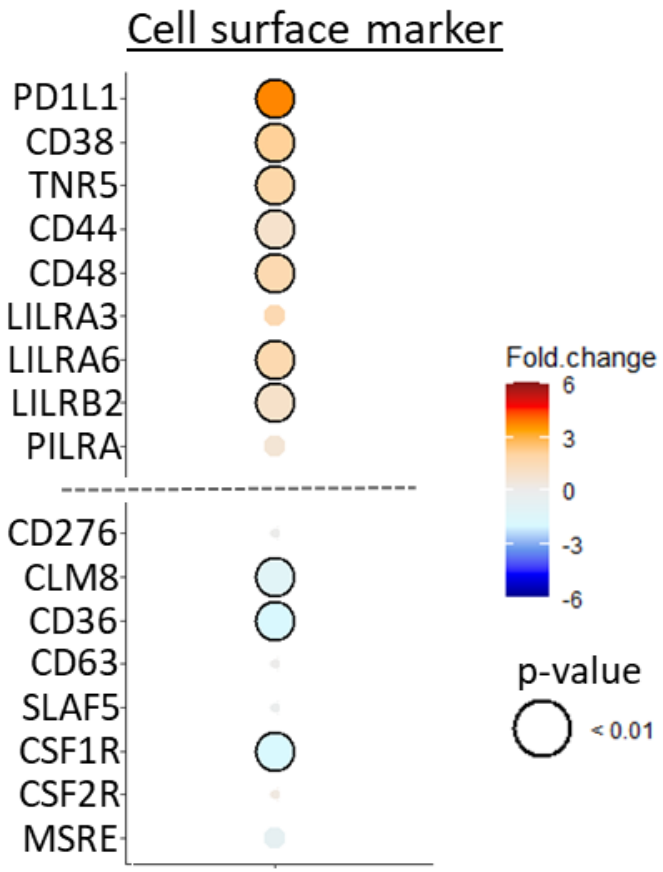

Figure 4.8. Expression of cell surface markers in the 100 ng/mL M-CSF 24 h IFN-γ+LPS dual stimulation.
Shown are the log2 protein fold changes in the pro-inflammatory macrophages in comparison to the resting macrophages (t-testing: Benjamin-Hochberg correction) alongside highlighted circling for significance (adjusted p-value < 0.01).

Next, I assessed the stimulus-specific signalling cascades. Few significantly upregulated proteins were detected in the TLR4 signalling pathway, which is activated by LPS binding (Figure 4.9). This may be because pathway activation is often associated with post-translational modifications (PTMs) rather than changes in protein expression levels.[349] However, NFKB2, which signals downstream of TLR4-MyD88 activation, along with its modulators TANK and TNIP3, were significantly upregulated.[350] Additionally, the transcription factors TF65 (RelA) and RelB, which are downstream of NF-κB signalling, were also upregulated.[350] It was important to note that NF-κB activity is also associated with TNF-α signalling and that TLR4 stimulation leads to the expression of various chemo- and cytokines.[351] Therefore, secondary signalling responses might also be captured in this proteomics analysis.

In contrast, many upregulated proteins were associated with IFN-γ signalling (Figure 4.9). JAK and STAT proteins, which bind to the IFN-γR, were upregulated.[346] STAT also serves as

transcription factor, which explains the high expression of IFN-γ induced genes such as IFIH1, IFIT1, IFIT2, IFIT3, ITIF5, IFM1, ISG15, ISG20, MX1, MX2 and OAS3 in response to the stimulus.[346] Furthermore, IFN-induced GTPases, including GBP1, 2, 4, and 5 were increased.[346]

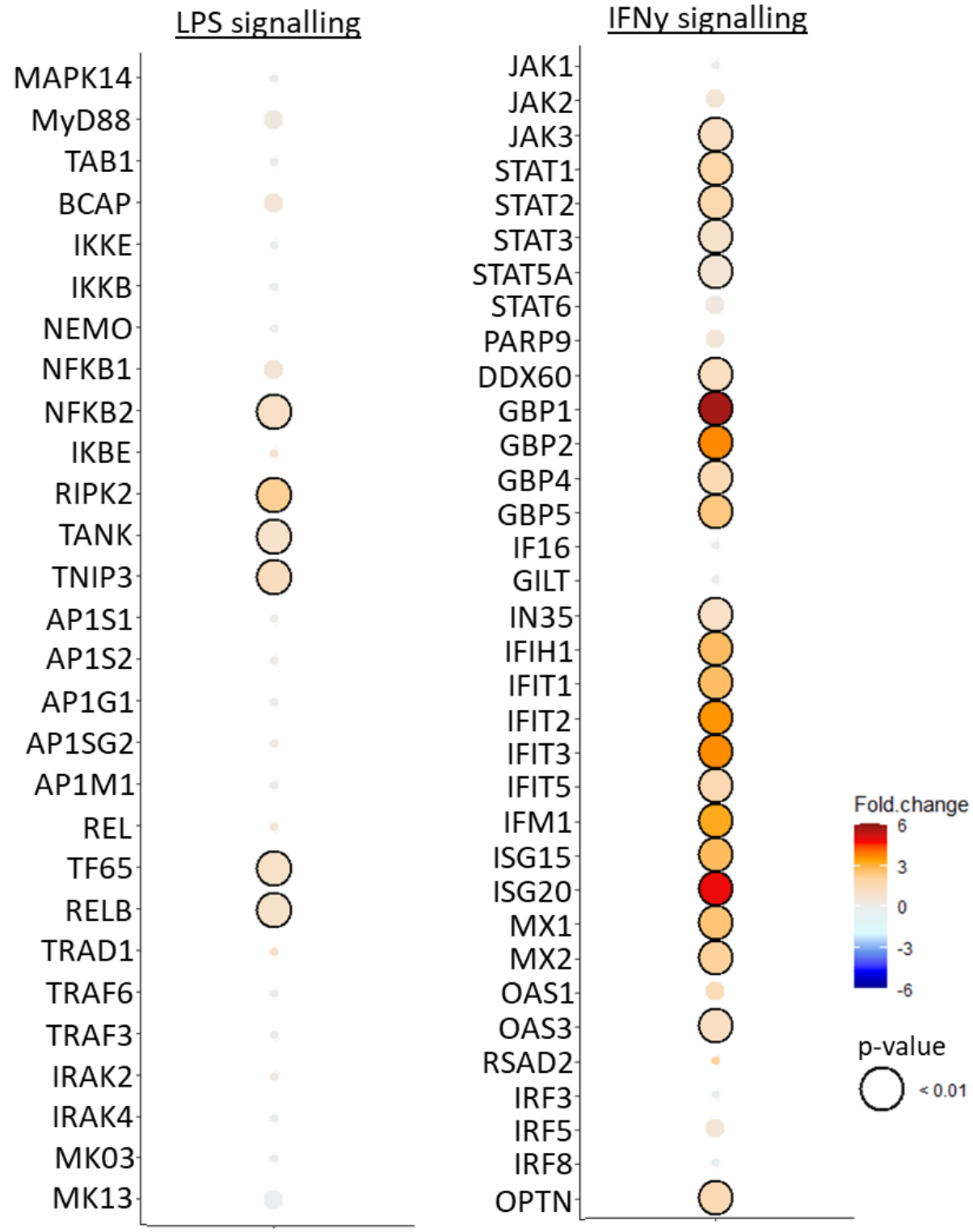

Figure 4.9. Expression of LPS (left) and IFN-γ (right) signalling markers in the 100 ng/mL M-CSF 24 h IFN-γ+LPS dual stimulation.

Shown are the log2 protein fold changes in the pro-inflammatory macrophages in comparison to the resting macrophages (t-testing: Benjamin-Hochberg correction) alongside highlighted circling for significance (adjusted p-value < 0.01).

These results demonstrated that 24-hour IFN-γ+LPS stimulation effectively elicited a pro-inflammatory immune response, M1 macrophage polarisation. Successful identification of biomarkers in both signalling cascades suggested that the MoA for this stimulation can be partially elucidated through proteomics. Additionally, it highlighted that this analysis is slightly biased towards detection of the IFN-γ signalling pathway, as this was associated with more significant protein expression changes compared to the LPS signalling cascade.

Murugesan *et al.* 2022 reported changes in cell processes closely associated with the immune system, including antigen presentation and metabolism. Consistent with these findings, nearly all major proteins involved in antigen presentation, such as various HLA and TAP proteins, were upregulated (Figure 4.10). Additionally, Murugesan *et al.* 2022 described a metabolic shift towards tryptophan metabolism and aerobic glycolysis in response to pro-inflammatory stimuli. I observed upregulation of KYNU, SYWC (WARS), and I23O1 (IDO1), which are involved in tryptophan catabolism (Figure 4.10). Markers of aerobic glycolysis, such as F263 (PFKB3) and CMPK2, were also upregulated. However, several other glycolysis and ROS signalling markers, like F16P1, KCY and SODM, remained unchanged. In line with published literature, I also observed upregulation of apolipoproteins (APOL2 and APOL3), which regulate cholesterol levels.[346]

I investigated the differential expression of proteins associated with secondary signalling pathways including responders to chemo- and cytokines (Figure 4.10). Proteins involved in TNF-α signalling, such as TNAP, TFIP, and TRADD, were upregulated.[352] Other pattern recognition receptors and their modulators, like TLR8 and UN93B, were also upregulated, supporting the hypothesis that secondary signalling responses were captured by this proteomics analysis.[353]

Furthermore, intracellular levels of various chemo- and cytokines were altered, including CXCL10, IL8, CXCL9, IL27B, IL1A, IL1B and OXLA (Figure 4.10). The secreted cytokine profile can be assessed via secretomics, however in HTS efforts, assessment is typically undertaken with label-based assays.[39]

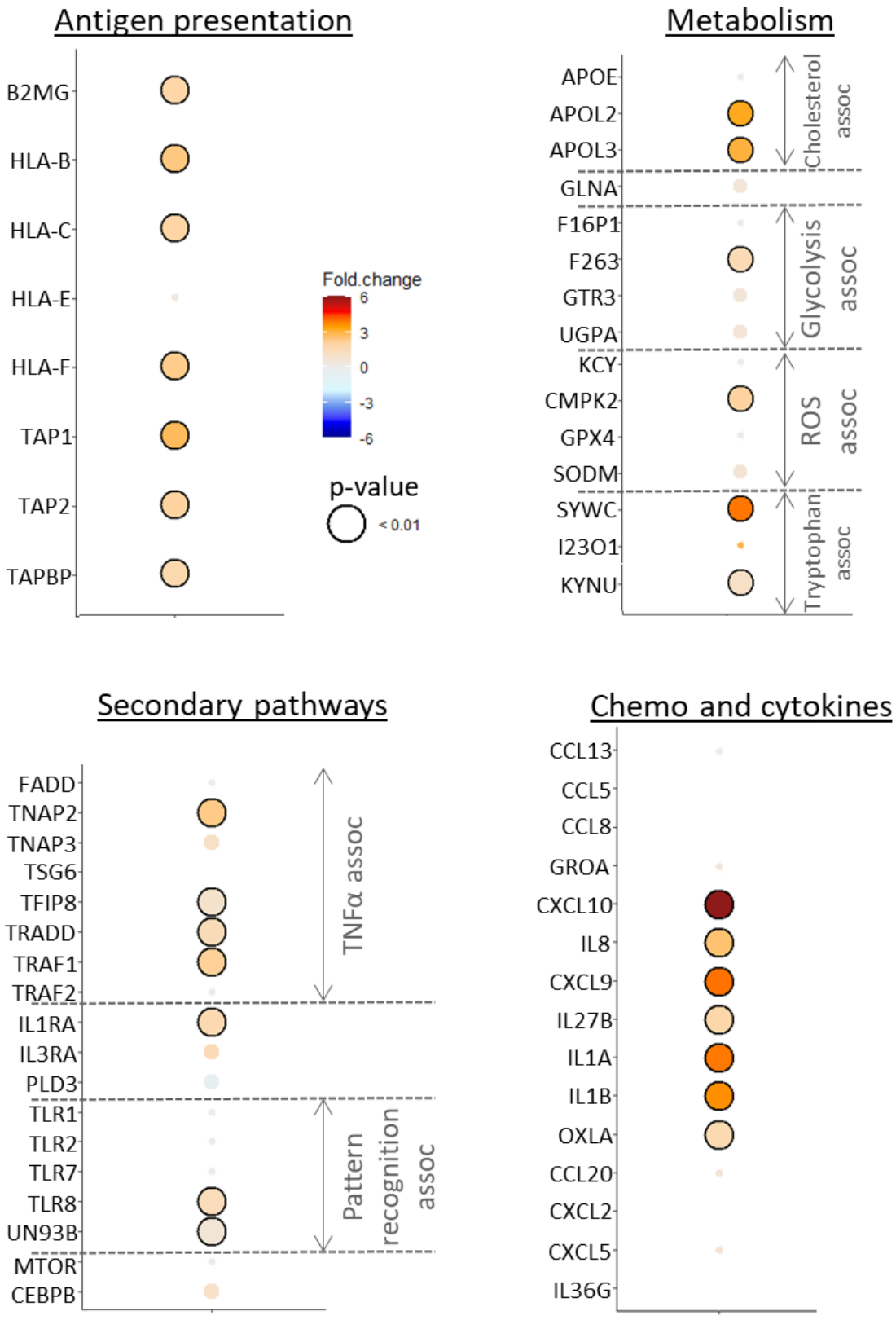

Figure 4.10. Expression of antigen presentation (top left), metabolism (top right), secondary pathway (bottom left), and chemo and cytokine (bottom right) markers in the 100 ng/mL M-CSF 24 h IFN-γ+LPS dual stimulation.

Shown are the log2 protein fold changes in the pro-inflammatory macrophages in comparison to the resting macrophages (t-testing: Benjamin-Hochberg correction) alongside highlighted circling for significance (adjusted p-value < 0.01).

4.4 Pro-inflammatory macrophage polarisation for 24 h with LPS+IFN-γ was linked to pro-inflammatory cytokine secretion

A bead-antibody based assay was used to determine the levels of pro-inflammatory TNF-α and IL-6 cytokines in the cell media. Control samples at all time points showed low signal for the inflammatory markers (Figure 4.11). TNF-α concentrations remained constant across 4 and 24 hours of stimulation (~10 pg/mL) (Figure 4.11A). The rapid increase in TNF-α levels can be attributed to the presence of a TNF-α precursor stored in the cell membrane.[351] The early detection of TNF-α also suggested that secondary responses were captured at the proteome level after 24-hour stimulation. In contrast, IL-6 levels showed a time-dependent increase, rising from ~20 pg/mL to ~60 pg/mL (Figure 4.11B). This trend exemplified the progression from pathway activation to protein expression and protein excretion over time.[354]

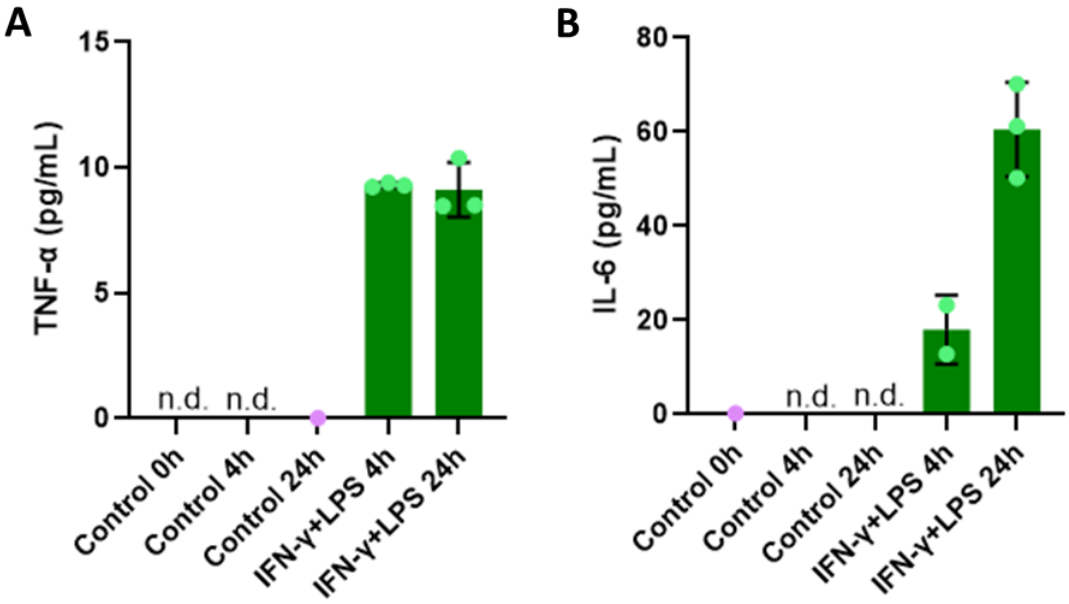

Figure 4.11. Cytokine levels in the media of 100 ng/mL M-CSF cultured macrophages. Macrophages from three different human donors were probed after 4 and 24 h stimulation with IFN-γ+LPS and compared to unstimulated controls at the indicated timepoints. A fluorescence readout (Mirrorball®) was used to determine cytokine levels of (A) TNF-α, and (B) IL-6; n = 3, mean ± standard deviation, n.d. = non-detected.

4.5 Discussion

In this chapter, I first validated successful M1 and M2 macrophage polarisation by morphology. Proteomics analysis showed that macrophage differentiation with 100 ng/mL M-CSF and 24-hour IFN-γ+LPS stimulation produced the most distinct pro-inflammatory macrophage phenotype consistently across three human iPSC donors. Macrophages cultured with higher M-CSF concentrations seemed to exhibit a stronger macrophage phenotype. Further, the

customised proteomics workflow robustly identified pro-inflammatory marker proteins from different cell signalling pathways. Signalling responses that lead to novel protein expression and activity in secondary signalling cascades was captured with the proteomics workflow. Lastly, pro-inflammatory cytokine screening from the cell media was introduced as a HTS compatible technology for rapid pro-inflammatory macrophage polarisation phenotyping.

4.5.1 The proteomics workflow

In the following discussion, I will outline the components of the proteomics workflow that I selected for my customised iPSC-derived macrophage analysis, focussing on two key criteria: (1) workflow speed and (2) data quality.

For sample preparation, I selected the S-Trap method. According to Varnavides *et al.* 2022, who evaluated 16 different sample preparation methods, most exhibited comparable overall performance, although there were variations in the recovery of specific protein features, such as low expression proteins that were enriched with the S-Trap sample preparation method.[272] Despite the potential for testing alternative workflows, I opted for the S-Trap method due to its established robustness. In addition, the 96-well plate format of the S-Trap facilitated efficient handling, allowing sample preparation with reduced hands-on time, and hence allowing preparation of multiple sample plates in parallel.

High-performance liquid chromatography (HPLC) with a 2-hour gradient is a common setup for peptide separation in proteomics workflows.[355] Instead, I chose the Evosep One system to achieve a significant reduction in sample run times to 24 minutes per sample while maintaining high data quality. The system can accommodate even higher throughput with 5.6 minutes per sample, though this significantly reduces protein identifications.[341]

The samples were acquired with a dia-PASEF method on the timsTOF HT, followed by analysis with DIA-NN software. As anticipated, each sample yielded a high number of protein identifications. However, I observed that incorporating a spectral library decreased search speed. In addition, my data indicated that the quality of the library positively influenced protein identifications as the hybrid library approach revealed slightly more identifications than the spectral library search. An alternative, traditional approach would be to use off-line fractionation to reduce sample complexity and then acquire the sample in DDA mode to

improve accuracy of peptide sequence identifications.[356] Reduced sample complexity might also be particularly useful for peptide pools of large sample to improve the generated spectral library. In addition, custom dia-PASEF acquisition methods could be generated with the py_diAID software to improve sample coverage.[288]

Ongoing advances in MS are poised to further enhance workflow speed while preserving data quality. Innovations such as the 500 SPD method for the Evosep system, the Orbitrap Astral MS equipped with novel mass analyser technology[357], as well as artificial intelligence and machine learning-driven real-time data analysis tools are leading the way. Despite these advancements, the speed of proteomics analysis is still significantly slower than the previously outlined HTS compatible MS setups, e.g MALDI-TOF MS and RapidFire MS. However, proteomics offers higher content data.

4.5.2 Cell models in inflammation research

In the subsequent chapters of this thesis, I will explore how different MS technologies can contribute to advancements in the immunology drug discovery space by profiling polarised iPSC-derived macrophages. In this chapter, I have successfully benchmarked the iPSC-derived macrophages through morphology, proteomics, and cytokine profiling, demonstrating a physiologically relevant response, particularly when differentiated with 100 ng/mL M-CSF and polarised for 24 h with IFN-γ+LPS. The consistency of the responses across three different human iPSC donors suggested a high level of biological relevance for this model.

In macrophage research, various cell types are used, including immortalised human THP1 cells, iPSC derived macrophages, primary murine bone marrow-derived macrophages (BMDMs), and primary human peripheral blood mononuclear cells (PBMCs). THP1 cells, derived from monocytes of an acute myeloid leukaemia patient, possesses significant genetic mutations such as partial mono- and triploidy and various chromosomal rearrangements.[259,336] Vincent *et al.* 2020 demonstrated that genetic changes can impact the translation of drug efficacy from cellular assays to animal models and patients.[358] Indeed, differences in immune response between THP1 cells and PBMCs have been documented.[259] Gudgeon *et al*. 2024 reported significant variability in responses to inflammatory stimuli among cell lines, immortalised cells, and primary murine BMDMs.[258] Further, murine BMDMs and human PBMCs exhibit distinct metabolic responses to inflammation, with PBMCs relying on oxidative phosphorylation for

the generation of ATP.[257] Although primary PBMCs and murine BMDMs provide high physiological relevance, they are challenging to maintain in culture. In contrast, iPSC-derived macrophages offer a favourable compromise, as they can be cultured at scale and are genetically closer to primary cells than THP1 cells.

Considering the complexity of the inflammatory response, which involves crosstalk between various cell types, secondary cell responses, and diverse stimuli, a range of *in vitro* models, from simple 2D cultures to complex organoids with multiple cell types, are employed in inflammatory disease research.[335,359] When designing cellular assays for HTS drug discovery efforts in immunology, it is crucial to balance the benefits of biological complexity with factors such as cost, resources, scalability, and the desired readout method. In the next chapter of this thesis, I will explore a MALDI-TOF MS-based readout for macrophage phenotyping.

Chapter 5. Application of cellular MALDI-TOF MS high-throughput assays: A case study of induced pluripotent stem cell-derived macrophages

In the previous chapter, I characterised an inflammation cell model using proteomics and cytokine profiling, label-free medium-throughput, and label-based HT methods, respectively. With MALDI-TOF MS, fast and label-free cell phenotyping can be achieved. It is already the gold-standard tool for bacterial phenotyping in clinical settings, distinguishing microbial species based on unique fingerprints composed of ribosomal proteins and biomolecules.[189,193,360] However, workflows for eukaryotic cell fingerprinting are less developed due to the cells' complex composition and higher spatial and temporal dynamics.[213,361] Mass features in the peptide and small molecular weight protein region have been harnessed to distinguish between different cell types, including different cell lines and complex cell mixtures[206,207,209-213,362], to determine different cell states, including apoptosis and stress[214,363], and to characterise cell differentiation for instance of neutrophils[216]. MALDI-TOF MS has been used to distinguish different immune cell types from blood and to classify monocyte subsets challenged with different bacterial stimuli.[226-228] The lack of standardised protocols and data analysis procedures has limited the use of MALDI-TOF MS in cellular drug discovery efforts. Heap *et al.* 2019 initiated efforts to integrate this technology into HTS by developing an automation-compatible workflow to distinguishing between different cancer cell lines, including THP1 cells based on signals in the high mass region.[208,229] Further, Weigt *et al.* 2019 monitored concentrations of the fatty acid synthase substrate malonyl-coenzyme A in a cellular assay and simultaneously evaluated expression of other lipid biomarkers.[225] This paved the way for some first in line metabolite/lipid signature MALDI-TOF MS phenotypic screens that have been used to evaluate kinase activity[138], microglial activation in response to LPS[139] and complement-dependent cytotoxicity[140] in the presence of a few selected drugs.

In this chapter, I will present the development of a metabolite/lipid signature MALDI-TOF MS-based cell phenotyping workflow for iPSC-derived macrophages, which were differentiated with 100 ng/mL M-CSF and stimulated for 24-hours with IFN-γ+LPS, by building on established methods. I will introduce automation to enable assay validation with a set of 87 well-annotated compounds with known mechanisms of action. Subsequently, I will test a curated inflammation-specific set of 86 compounds and compare the results to cytokine secretion measurements to further asses the performance of the novel screening workflow.

5.1 MALDI-TOF MS cellular assays required optimisation of cell culture, sample preparation, and sample acquisition

In the first 7 days of the customised workflow (Figure 5.1), the iPSC-derived macrophages from three human donors were cultured, compound treated, stimulated, and frozen, as described in chapter 4. The subsequently optimised sample preparation involved two key steps:

1. Cell lysis: Different cell numbers and lysis conditions were tested to ensure analyte abundance.
2. Target plate preparation: The matrix, its concentration and mixing ratio with the sample, as well as the spotting technique itself were optimised to improve analyte desorption and ionisation in the MALDI ion source.

Upon data acquisition by MALDI-TOF MS, various instrument parameters, including mass range, and laser energy were altered. Initially, spectra were visually examined. Subsequently, different data analysis streams were established:

1. Global analysis via unsupervised clustering: This approach provided an overview of the data and helped identify patterns and clustering which can be harnessed to multiplex assays for instance with cytotoxic compounds or known inhibitors to uncover compound MoA.
2. Condition-specific “biomarkers”: This analysis focused on identifying unique “biomarkers” to inform phenotype-specific fingerprints. Selected “biomarkers” can then be used for hit-triaging in HTS efforts.

The optimised workflow should be able to reliably distinguish between resting (M0) and pro-inflammatory (M1) macrophage phenotypes and assess the effects of various compounds on these cells.

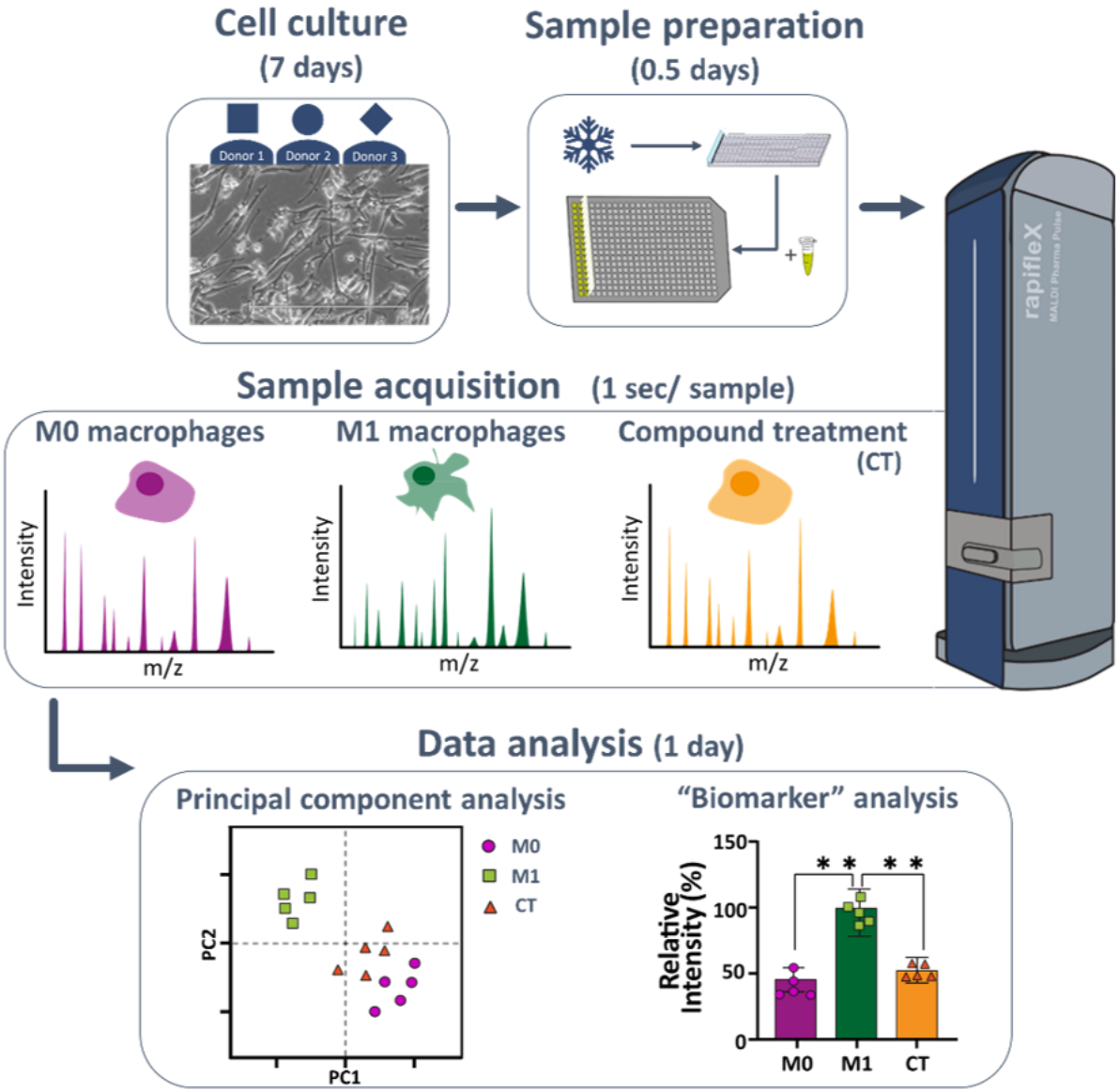

Figure 5.1. Schematic cellular MALDI-TOF MS assay workflow.
iPSC-derived macrophages from three human donors were cultured, treated with compounds, stimulated, and frozen. The preparation for MALDI-TOF MS acquisition involved defrosting the cells, preparing cells in a sample buffer, and spotting cells with the matrix onto the MALDI-TOF MS target plate. Following acquisition, the mass spectra were analysed using unsupervised clustering (e.g. principal component analysis (PCA)) or selected "biomarker" analysis to phenotype the macrophages and evaluate effects of compound treatment.

5.1.1 Macrophage polarisation unique peaks were observed in a mass range of m/z 400 – 1,000 with Tris-HCl extraction buffer and DHB matrix

A list of parameters that were tested and combined to optimise the MALDI-TOF MS-based macrophage phenotyping workflow can be found in Table 5.1.

Table 5.1. List of workflow components tested during the cellular MALDI-TOF MS assay development. The components include different cell numbers, extraction buffers, matrices, matrix concentrations, matrix-sample-ratios, spotting techniques, and acquisition ranges.

Optimisation stage	Tested conditions
Cell number	5000, 4500, 4000, 3500, 3000, 2500, 2000, 1500, 1000, 500
Extraction buffer	MALDI-TOF MS matrix, 100 mM Tris-HCl + 0.1% TFA, 30% MeCN + 0.1% TFA, 50% MeOH + 0.1% TFA, 100 mM Tris-HCl + 0.1% FA, 30% MeCN + 0.1% FA, 50% MeOH + 0.1% FA
Matrix	No matrix, Sinapinic acid (SA), α-cyano-4-hydroxycinnamic acid (CHCA), 2,5-dihydroxybenzoic acid (DHB), 9-aminoacridine (9-AA), 1,5-diaminonaphthalene (DAN), 2,5-dihydroxyacetophenone (DHAP)
Matrix concentration	Saturated, 1:2, 1:3, 1:5, 1:10, 1:20, 1:30, 1:50
Matrix-sample-ratio	1:1, 1:3, 1:5
Spotting technique	Sample matrix mix, Dried droplet
Acquisition range (*m/z*)	120 - 1200, 350 - 2000, 400 - 1000, 2000 - 10000

First, the optimal cell number was titrated as previous studies have highlighted the importance of this step.[216] Unsupervised hierarchical clustering showed separation between M0 and M1 phenotypes when using higher cell numbers (3500 - 5000 cells), but no separation with lower cell numbers (500 - 3000 cells) (Figure 5.2). Previous studies working with peptide and protein mass features of immune cells have suggested ideal cell numbers ranging from 1,000 to as high as 1 million cells per spot.[208,216,227] The variation in optimal cell number is likely explained by differences in the cell size and observed analytes.[208] Previous lipid profile MALDI-TOF MS screens have reported an ideal cell number of 5,000.[138] I decided to work with 4,500 cells to balance ionisation efficiency and ion suppression which was previously observed with larger cell numbers by Heap *et al.* 2019.[208]

Further, it is important to ensure efficient analyte extraction from the cell. Multiple studies have established the necessity of a freeze-thaw cycle for effective analyte extraction.[208,216] Protocols involving cell resuspension in PBS or methanol (MeOH) fixation have emerged[208,216,228], and the use of low acid concentrations in the extraction buffer and mild lysis conditions were recommended[216,226]. Here, I decided to perform a freeze-thaw cycle, followed by a test of different extraction buffers: Tris(hydroxymethyl)aminomethane hydrochloride (Tris-HCl), acetonitrile (MeCN), and methanol (MeOH), supplemented with formic acid (FA) or trifluoroacetic acid (TFA) acid. Consistent high-intensity peaks were observed across the different extraction buffers and cell phenotypes (Figure 5.2), but they were likely associated

with the matrix, due to their ubiquitous detection, and not analyte detection. I observed uncontrollable evaporative loss with the MeCN and MeOH extraction, which affected reproducibility. Therefore, I decided to resuspend the lysed cells in Tris-HCl to investigate the proposed matrix effect.

Various matrices traditionally used in positive (CHCA, DHB, SA) and negative ion (9-AA, DAN) mode were tested to enable ionisation of different classes of analytes.[94,131,364] CHCA and SA are commonly selected for their homogenous matrix crystals, improving signal robustness, while DHB, known for forming heterogeneous crystals, usually results in higher signal variability.[94,208,216] Each matrix showed a different peak pattern in the mass spectrum, dominated by low mass features (< *m/z* 500), mainly matrix-associated features, in both M0 and M1 phenotypes (Figure 5.2). Notably, peaks with stable peak intensity above *m/z* 500 were observed for DHB matrix and these features showed differences between the M0 and M1 phenotypes.

Assay parameters such as matrix concentration and sample-to-matrix ratio were carefully optimised and balanced to increase analyte ionisation efficiency and decrease matrix interference effects, which can lead to analyte suppression.[128] The matrix and sample spotting technique was also optimised. Samples were either pre-mixed with the matrix or individually dried on the target plate in a sandwich fashion. I opted to use the second method as I observed, in line with other developed lipid-based MALDI-TOF MS assays, improved DHB matrix heterogeneity.[138-140] Potentially, different organic solvent concentrations affected matrix drying time, explaining the observed crystallisation effects.[137]

The final optimisation involved the acquired mass range. As eluded to earlier, previous MALDI-TOF MS-based immune cell phenotyping workflows focussed on the *m/z* 2,000-20,000 range, which is mostly populated by peptides and small molecular weight proteins.[208,227,228] I detected only ~20 peaks in this region, with three reproducible peaks, including *m/z* 4964, previously reported in monocytes and macrophages and associated with Thymosin-β4, an actin-regulating protein with anti-inflammatory properties.[216,365] Monitoring the low mass range revealed >300 peaks between *m/z* 400-1,000, which showed differences between the M0 and M1 phenotypes upon visual spectral inspection. Features from this mass range have been successfully used to distinguish cell phenotypes and determine drug efficacy of a few selected compounds in dose-response screening.[138-140,225]

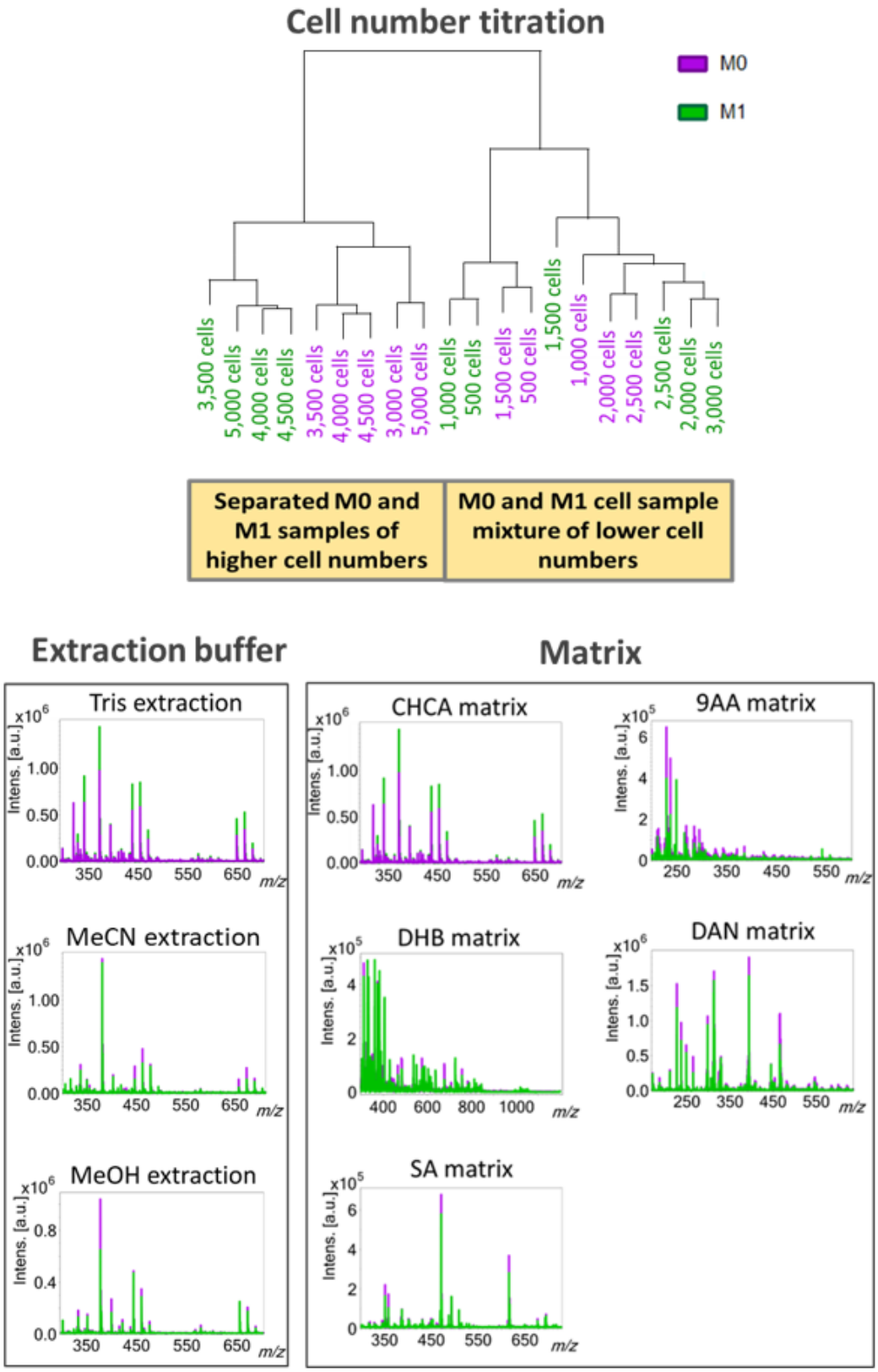

Figure 5.2. Exemplary results of the cellular MALDI-TOF MS assay workflow development. Dendrogram obtained from 500 - 5000 M0 and M1 (IFN-γ+LPS) macrophages. Spectra obtained from cell extracts in Tris-HCl, acetonitrile (MeCN) or methanol (MeOH) buffer in CHCA matrix. Spectra obtained from Tris-HCl cell extracts and spotting with different matrices: CHCA = α-cyano-4-hydroxycinnamic acid, DHB = 2,5-dihyroxybenzoic acid, SA = sinapinic acid, 9-AA = 9-aminoacridine, DAN = 1,5-diaminonaphthalene.

In summary, my final optimised workflow used ~4,500 iPSC-derived macrophages that were lysed through freeze-thawing cycles and the addition of the Tris-HCl+FA buffer. The lysates were spotted onto the MALDI-TOF MS target plate and dried prior to addition of 22.22mg/mL DHB matrix (70% MeCN, 0.1% FA). Samples were acquired in the mass range of *m/z* 400 - 1,000. With this method, I observed the most *m/z* features, which gave me the best chance to distinguish between the resting and pro-inflammatory macrophage phenotypes and to identify polarisation unique "biomarkers".

5.2 Data analysis workflows for MALDI-TOF MS cellular assays were assessed

I introduced miniaturisation and automation into the optimised workflow to generate a higher number of data points for the implementation of robustness and statistical analysis, including PCA and "biomarker" identification. Cells were lysed in 96-well format and then transferred into 384-well plates, enabling the use of the Mosquito liquid handling robot for cell sample and matrix spotting onto the MALDI-TOF MS target plate. I utilised an automated acquisition method in MS, and an R script previously adapted by Maria Emilia Dueñas and Ruth Walker in the Trost laboratory, following Gibb *et al.* 2012, which I further refined by adjusting the data processing parameters, implementing data analysis and visualisation tools, as well as establishing data filtering criteria.[316]

5.2.1 Separation between macrophage M0 and M1 phenotypes was observed in unsupervised clustering

First, unsupervised clustering was performed by PCA to examine global trends. Without further data processing, nearly complete separation between the M0 and M1 macrophage phenotypes was observed (Figure 5.3A).

To improve the clustering, I decided to reduce the complexity of the dataset, and hence filtered the peak list. First, I removed peaks that were classified as noise, characterised by low signal intensity and poor signal reproducibility, summarised by the CV. Secondly, I excluded peaks that showed minimal or no changes between the two treatments, indicating they were not indicative of a pro-inflammatory response. After testing multiple cut-offs, I decided to exclude peaks with a CV >75% in at least one of the two conditions and peaks with a log2 fold change

between -0.2 and 0.2 in the M1 when compared to the M0. The filtering resulted in a 67% reduction in peak numbers, from 326 to 108. Following this refinement, a clear and reproducible separation between the M0 and M1 macrophage phenotypes from three different human donors was observed (Figure 5.3B).

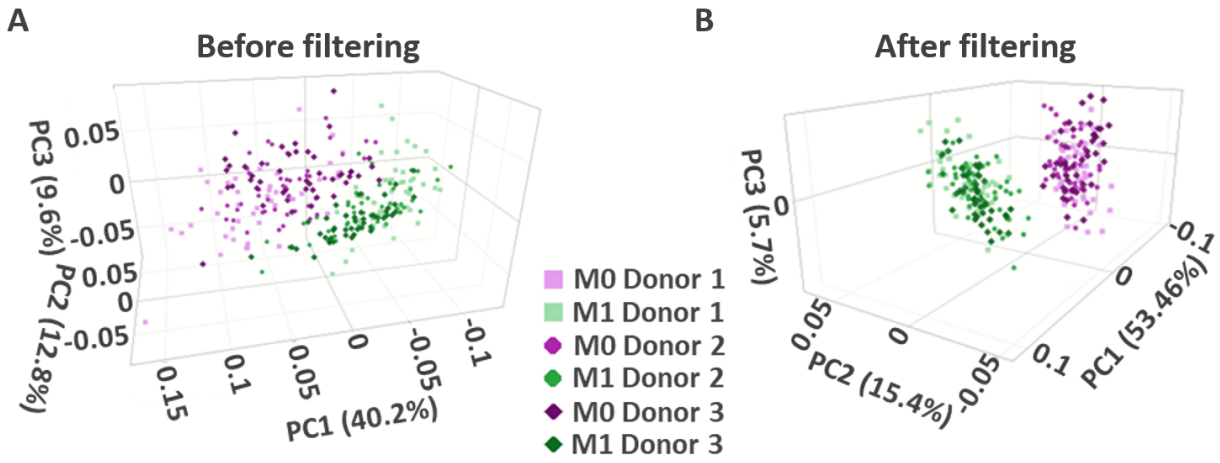

Figure 5.3. Clustering of M0 and M1 macrophages based on *m/z* features observed by MALDI-TOF MS.
PCA analysis of macrophage phenotypes from three human donors, (a) before peak list filtering and (b) after peak list filtering (excluding peaks with a CV >75% in at least one of the two polarisation conditions and peaks with a log2 fold change from the unpolarised to the polarised controls between -0.2 and 0.2); $n_{technical}$ = 92 per donor.

Previously it was demonstrated that PCA can be used in drug discovery efforts to distinguish between desired and undesired phenotypes, such as cytotoxicity by including compounds with known MoA within the screen.[44,229] However, the need for peak filtering to achieve clear phenotype separation as described here, may indicate potential challenges when analysing multiple compound-driven cell phenotypes with this method.

5.2.2 Mass features were identified as "biomarkers" for resting and pro-inflammatory macrophage phenotypes

The aim was to identify "biomarkers" in the MALDI-TOF MS assay that could be used to distinguish between resting and pro-inflammatory macrophages rapidly and reproducibly. I investigated "biomarker" expression upon IFN-γ+LPS dual stimulation, as well as individual stimulations with either IFN-γ or LPS alone, to see if I can distinguish between the different inflammation stimuli. Previous studies suggested that MALDI-TOF MS fingerprints of THP1 cells in the high mass region were primarily associated with TLR signalling.[229]

To assess biomarker suitability, I used the peak list pre-filtering and calculated the log2-fold change between all stimulants and the M0 control, and between the IFN-γ and LPS stimulations. Peaks that showed a log2-fold change >0.5 or <-0.5 in at least one condition were included in the analysis. The normalised peak intensities (z-scoring per row) of these *m/z* features were plotted in a heatmap for biomarker identification (Figure 5.4A).

While some of the selected 74 peaks showed no visible difference in intensity between groups, others exhibited high signal intensity within a single group, making them potential "biomarkers". Multiple high-intensity features (z-score ≥0.6) were detected for the resting M0 (n = 13), IFN-γ (n = 6), LPS (n = 14) and IFN-γ+LPS (n = 4) stimulated macrophages. Consistent with previous reports from MALDI-TOF MS acquisitions in the high mass range, signal intensities across the *m/z* features showed high similarity between the LPS and IFN-γ+LPS stimulations.[229]

Statistical analysis of four samples per macrophage stimulation from each of the three donors, acquired in analytical triplicate, resulted in the identification of three IFN-γ+LPS/LPS "biomarkers", one IFN-γ "biomarker," and three M0 "biomarkers" (Figure 5.4B). The IFN-γ+LPS/LPS "biomarkers" *m/z* 642.06, 707.05 and 626.08 showed the highest intensity in the LPS treatment, closely followed by the IFN-γ+LPS treatment, and a significant reduction in the IFN-γ and M0 condition. This difference was visually exemplified for *m/z* 626.08 (Figure 5.4B). Here, signal intensity in the IFN-γ+LPS stimulated cells was in the low to mid 10^5 range and approximately four times less in the M0s.

Conversely, the *m/z* 564.06 peak, a M0 marker along with *m/z* 664.25 and 450.07, had high signal intensity in the M0 condition (10^4 to low 10^5 region) and was nearly absent in the IFN-γ+LPS stimulated cells (Figure 5.4B). While *m/z* 564.06 and 664.25 features were mainly detected in the M0 condition, higher baseline levels in the pro-inflammatory cell treatments were reported for the *m/z* 450.07 marker.

Lastly, the *m/z* 697.59 peak was selected as IFN-γ marker. Although the signal intensity difference between the IFN-γ stimulation and the other three treatments was significant, the magnitude of the intensity change was low, indicating that "biomarker" robustness needed to be monitored closely in subsequent experiments.

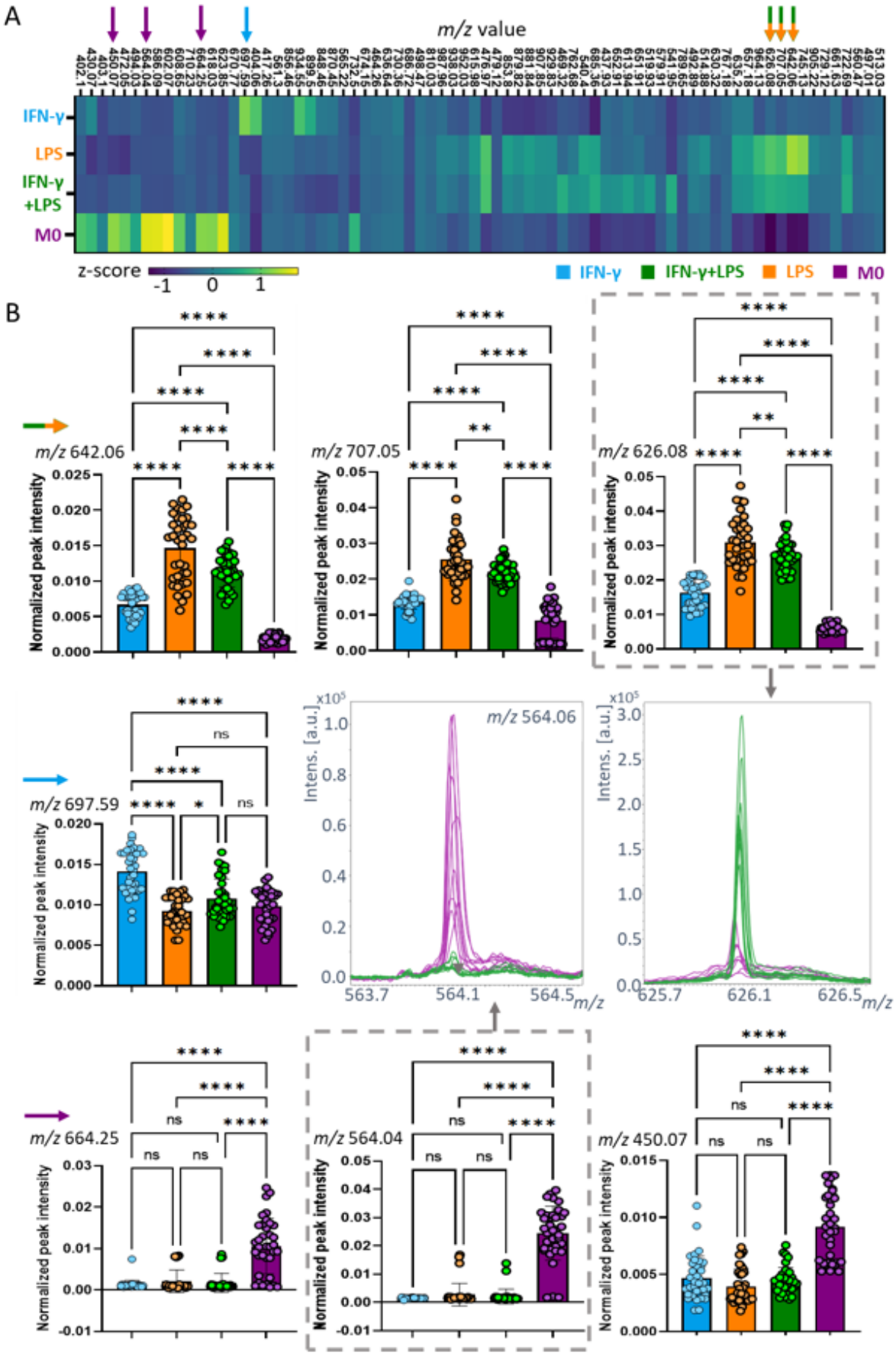

Figure 5.4. Identification of MALDI-TOF MS "biomarkers" for different macrophage phenotypes.

(A) Heatmap displaying the normalised peak intensities (z-scoring per row) of 74 potential "biomarker" *m/z* features for M0 (purple) and pro-inflammatory macrophage phenotypes: IFN-γ (cyan), LPS (orange), or IFN-γ+LPS (green) stimulation. (B) Identification of significantly altered peak intensity levels for selected "biomarkers" (IFN-γ+LPS/LPS: *m/z* 642.06, 707.05, 626.08; IFN-γ: *m/z* 697.59; M0: *m/z* 450.07, 564.04, 664.25). Statistical analysis was performed using one-way ANOVA, Tukey multiple comparison post-hoc test (n = 36; 4 samples from each of the three donors acquired in triplicate). Significance levels are indicated as follows: ns = p-value ≥0.05, * = p-value 0.01 - 0.05, ** = p-value 0.001 - 0.01, *** = p-value 0.0001 - 0.001, **** = p-value >0.0001. Exemplary mass spectra showing peak intensity levels at *m/z* 564.06 and 626.08 for M0 (purple) and IFN-γ+LPS (green) stimulated cells.

5.3 Phenotypic screening with a broad mechanism of action compound set – JUMP

To assess the performance of the developed MALDI-TOF MS workflow, including the subsequent data analysis pipeline, I screened the IFN-γ+LPS stimulated macrophages against 87 well-annotated compounds of the Joint Undertaking of Morphological Profiling (JUMP) set (1 µM final assay concentration). This set was originally assembled for image-based profiling drug discovery efforts and possesses a large reference database to allow matching of compound MoA (https://jump-cellpainting.broadinstitute.org/). The compound set was slightly modified by my industrial collaborator GSK to encompass a total of 52 different MoAs (38 duplicate and 14 single MoA, chapter 2.2). The set included several compounds known to induce broad phenotypic changes and others with annotated targets in fundamental cell processes such as epigenetics, cytoskeleton, mitochondria, metabolism and cAMP, making them potential frequent hitters in phenotypic screens.[358] It also contained compounds that had annotated targets in the IFN-γ and LPS signalling pathways.

5.3.1 Unsupervised clustering did not identify hit compounds from the JUMP set

After peak list filtering according to the previously established CV and fold change cut-offs based on the M0 and M1 controls, distinct M0 and M1 phenotype clusters were observed by PCA (four M0 and four M1 controls from each of the three donors acquired in triplicate, Figure 5.5). However, no clearly distinct compound clusters were identified across the 87 JUMP compounds (tested in each donor once and acquired in triplicate). This could be due to the selected mass feature filtering approach or the large number of data points, impeding visual identification of clusters.

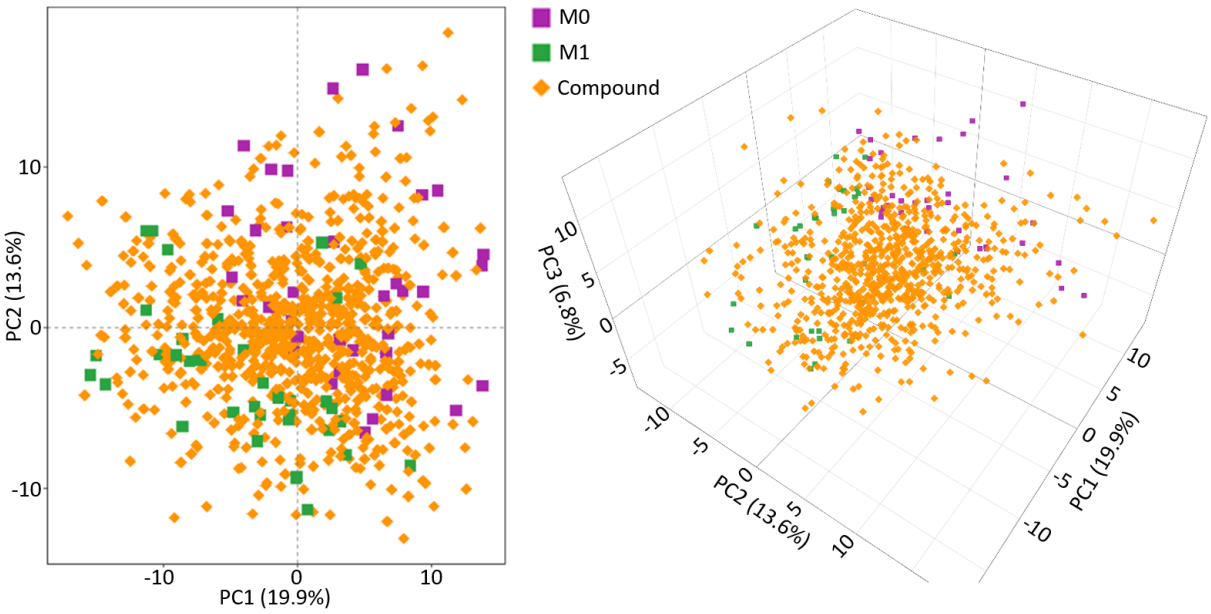

Figure 5.5. Clustering of control and JUMP compound set treated macrophages.
PCA analysis of M1 activated macrophages after treatment with 87 JUMP compounds (orange) with untreated M1 (green) and unstimulated M0 (purple) macrophage controls derived from three human donors. Data were filtered according to the previously established CV and fold change methods for the M0 and M1 controls; n_{M0} = 4 per donor, n_{M1} = 4 per donor, all acquisitions conducted in triplicate.

As an alternative approach to reduce the complexity of the large data set and to facilitate identification of hit compounds, I applied scalar projection analysis, a vector projection-based technique. This method determines two scores that characterise each compound within the space. First, a projection vector was drawn from the M1 to the M0 cluster to score the compound treatment's likeness to cell polarisation. Next, the rejection from this vector was calculated to indicate how far a compound treatment pushed the cell phenotype away from the controls.

The results showed that the M1 macrophages were clustered around a projection and rejection of 0 while the M0 macrophages were clustered around a projection of 1 and rejection of 0 (Figure 5.6A), demonstrating successful implementation of the workflow. However, there was considerable data spread within the controls, with $M1_{projection}$ of -0.5 to 0.6, and $M0_{projection}$ of 0.6 to 1.3. limiting the assay window. I conducted statistical testing with the z-scored projection and rejection values, comparing the compound treatments against the M1 macrophage control. A high z-score indicated a large difference between the compound treatment and the M1 control in both the projection and rejection vector dimensions respectively.

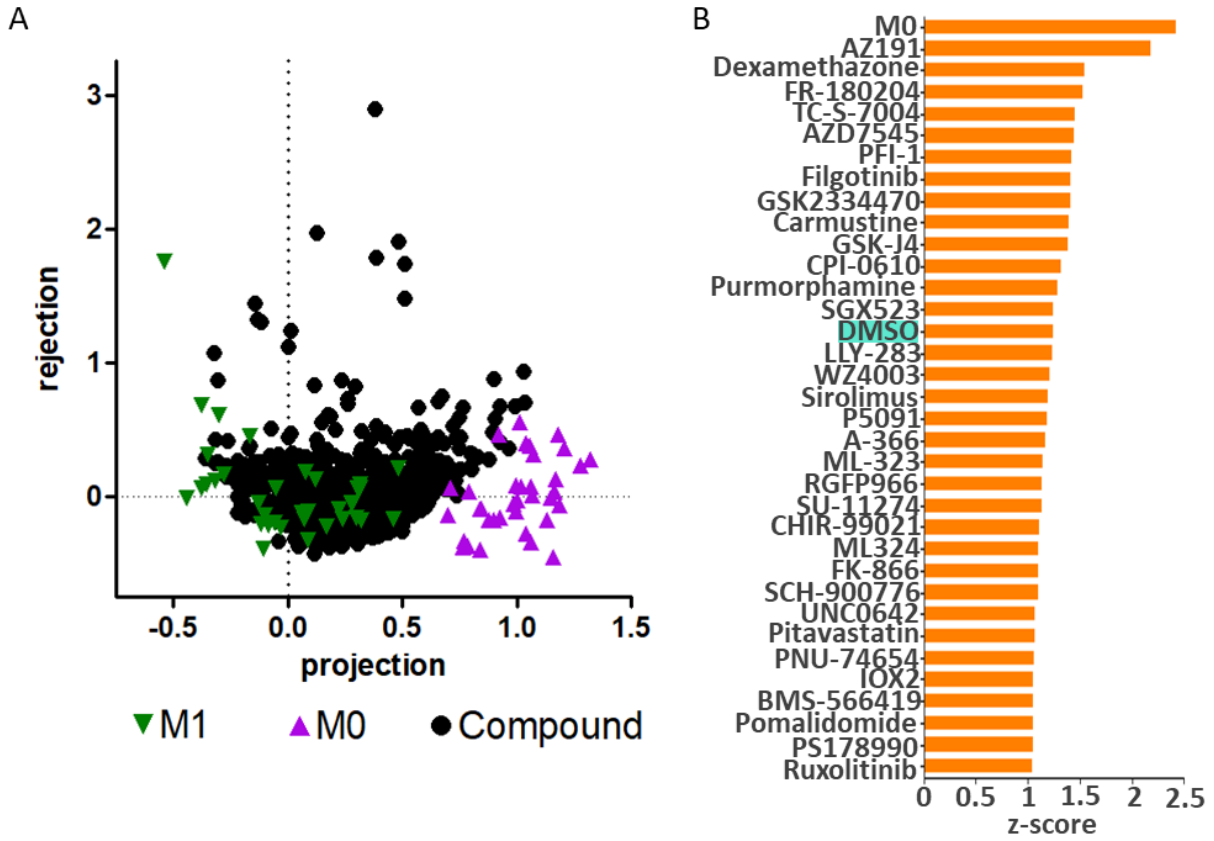

Figure 5.6. Scalar projection analysis of control and JUMP compound set treated macrophages.
(A) Scatter plot of rejection values plotted against projection values determined by scalar projection based on M1 (green) and M0 (purple) controls, n_{M0} = 4 per donor, n_{M1} = 4 per donor, acquisitions conducted in triplicate. (B) List of statistically significant compound projection z-scores in comparison to the M1 controls; t-test (Bonferroni Holm).

A comprehensive table of statistically significant hit compounds, along their projection and rejection scores, can be found in the supplementary materials (Supplementary Table S.1). Apart from a single compound (UNC0642, z-score$_{rejection}$ = 6.99) (Supplementary Table S.1), no significant rejection was observed. For hit compound identification, the focus was on the projection z-score. The highest score was observed for the M0 macrophages (z-score$_{projection}$ = 2.4), followed by 34 additional hit compounds (z-score$_{projection}$ between 0.38 and 2.2) (Figure 5.6B). Notably, the DMSO-only control treatment appeared in 14th place on the hit list with a projection z-score of 1.2. This control was expected to align closely with the M1 macrophage phenotype and should not have been identified as hit compound, suggesting this could be an outlier or a result of the earlier observed data variability. Further analysis revealed that the M0 control was only 2.4 standard deviations away from the M1 cells, indicating suboptimal population separation and a limited signal window for hit calling. These findings highlighted

that scalar projection was not the most suitable tool for cellular MALDI-TOF MS data analysis, possibly due to the data input, prompting a shift to the analysis of the previously identified "biomarkers", a more traditional approach to identify hits.

5.3.2 "Biomarker" analysis identified phenotypic screen frequent hits and inflammation modulators from the JUMP compound set

Initially, I examined the M0 "biomarker" features, *m/z* 450.07, 564.04 and 664.25. No mean intensity difference was observed between the M0 and M1 macrophages for the *m/z* 450 marker (Supplementary Figure S.2). While different mean intensities were noted for the *m/z* 564 and 664 features, a high data spread was observed (Supplementary Figure S.2). No hit compounds were identified which could be due to the compound treatment generating multiple phenotypes rather than just the goal M0 inflammatory phenotype. Consequently, the focus shifted to the pro-inflammatory stimuli *m/z* features, where signal reduction indicated M1 phenotype dissimilarity.

The IFN-γ "biomarker" *m/z* 697, which required careful evaluation for signal robustness, failed to show a mean intensity difference between the M0 and M1 macrophages (mean normalised peak intensity = 1.5 and 1, respectively, Figure 5.7). As a result, this marker was excluded from the analysis.

The remaining three IFN-γ+LPS and LPS-only stimulation markers, *m/z* 626.08, 642.06 and 707.05, demonstrated a difference in mean intensity between the macrophage phenotypes (M0 = ~0.2 normalised peak intensity, M1 = 1 normalised peak intensity, Figure 5.7), proving them suitable for compound screen analysis. Notably, a high CV (%CV M_0 = 95%, %CV M_1 = 52%) was observed for the *m/z* 642 marker, indicating reduced robustness and reproducibility. This variation could originate from outliers due to technical or experimental errors as stable signal intensities were previously reported.

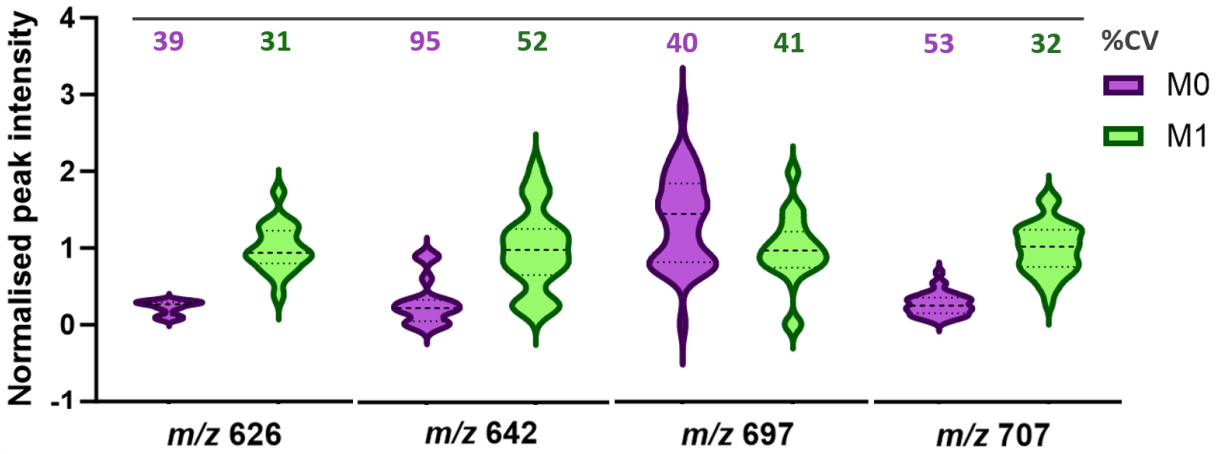

Figure 5.7. Stability and reproducibility of M1 "biomarkers" across the controls in the JUMP compound set screen.
Violin plots of the normalised peak intensities at *m/z* 626, 642, 697 and 707 from the resting (M0, purple) or pro-inflammatory (M1, green) iPSC-derived macrophage controls within the JUMP compound set screen. The %CV for each sample is indicated; n_{M0} = 4 per donor, n_{M1} = 4 per donor, acquisitions conducted in triplicate.

Upon evaluation of the 87 JUMP set compounds with the M1-specific "biomarkers", the intensity of the *m/z* 642 peak decreased for a total of 44 compounds, indicating their less M1-like phenotype or M1 dissimilarity (Figure 5.8). Given the earlier finding that this marker was less robust, I set a criterion that two markers had to show M1 dissimilarity (normalised peak intensity <0.6) for a compound to be considered a hit. This led to the identification of 17 hit compounds (Figure 5.8; indicated by the black box). The next step was to examine the MoA and target annotations for these hit compounds to narrow down hits and identify which phenotypes were detected with this assay.

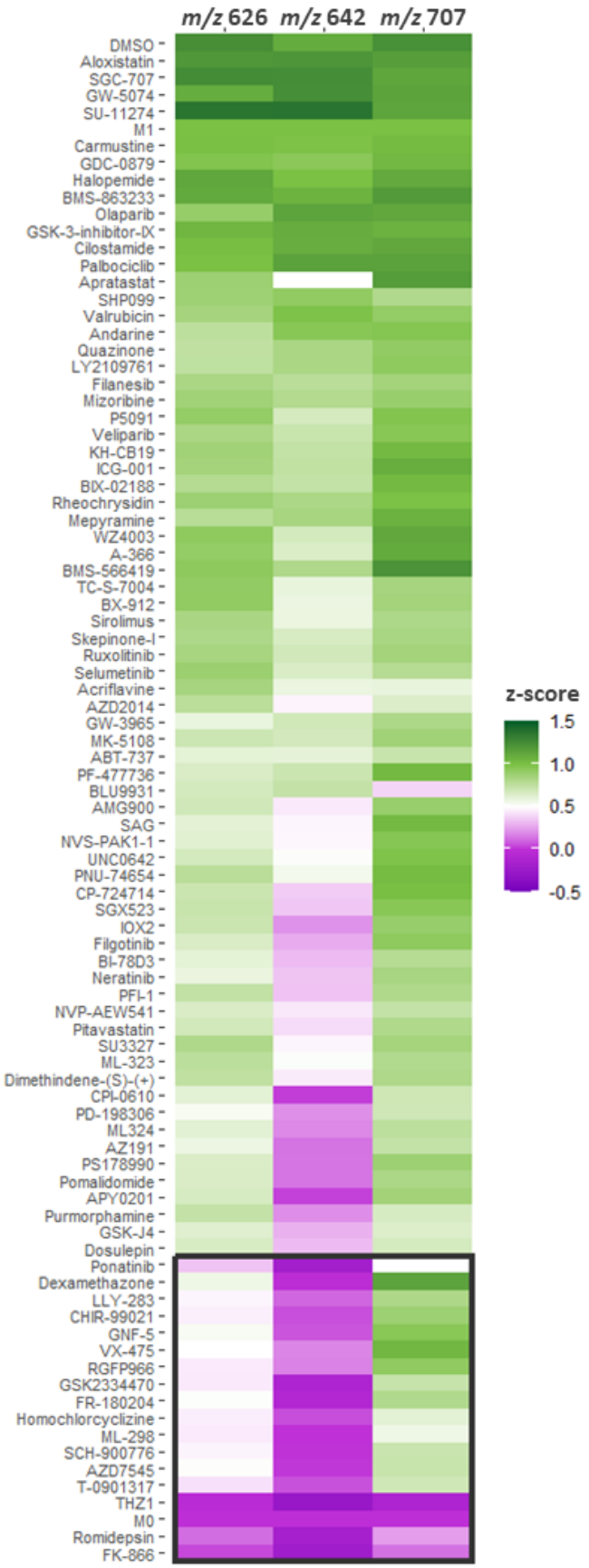

Figure 5.8. "Biomarker" evaluation in the JUMP compound set screen.
Heatmap of the averaged, normalised (based on M0 and M1) *m/z* 626, 642 and 707 signal intensities for 87 JUMP compounds and the M0 and M1 controls. The hit compound cut-off is

indicated by a black box (normalised peak intensity <0.6 for two markers); n_{M0} = 4 per donor, n_{M1} = 4 per donor, acquisitions conducted in triplicate.

Based on their biological target annotation (Table 5.2), nine hit compounds can be categorised into different frequent hitter groups, namely metabolism, cell cycle and transcription modulators, as they are commonly detected by phenotypic screens due to the fact that they effect key cellular processes.[358] FK-866 and AZD7545, were grouped as metabolism modulators.[366,367] FK-866 targets nicotinamide phosphoribosyltransferase (NAMPT) and NAMPT inhibition can also reduce macrophage inflammation through NAD+/PARP1 pathway and hence hit detection might be cross-linked to inhibitory inflammation activity.[368] Romidepsin was grouped with RGFP966, LLY-283, T-0901317, and Dexamethazone as transcription modulator.[369-372] Romidepsin targets histone deacetylases (HDAC) and HDAC inhibitors are known to have anti-inflammatory properties, again providing a cross-link to inflammation.[373] Further, LLY-283 targets PRMT-5, a methyltransferase, which was linked to NF-κB activity and hence hit calling might be inflammation associated.[374] THZ1, targeting CDK7, a member of the cyclin-dependent protein kinase family involved in cell cycle progression, was grouped with SCH-900776 in the cell cycle modulators category.[375,376] In inflammatory responses, CDKs regulate the activity of prominent transcription factors like NF-κB and STAT3, providing another cross-link.[377]

FK-866 and Dexamethazone, detected within this screen, were recommended by the JUMP consortium as positive controls for image-based drug discovery efforts due to their highly diverse phenotypes.

In addition to these potential frequent hitters, another subset of compounds encompassed the remaining eight hit compounds (Table 5.2). All eight compounds were associated with the immune system. CHIR-99021, FR-180204 and VX-475 target mitogen-activated protein kinases (MAPK), which are implicated in the inflammatory signalling cascade.[378,379] ML-298 targets PLD2, which regulates macrophage polarisation in inflammation.[380] Homochlorcyclizine, an antihistamine, affects LPS-induced signalling in macrophages.[381] BCR-Abl, targeted by GNF-5 and Ponatinib, activates cytokine signal transduction pathways in hematopoietic cells[382], and Ponatinib has been demonstrated to target the p38 MAPK in the LPS signalling pathway[229]. Lastly, GSK2334470 targets AURKA, known to affect PLD-1, demonstrating beneficial effects in tumour-targeted therapy and immunotherapy.[383]

Table 5.2. JUMP set hit compounds from the MALDI-TOF MS assay biomarker analysis. Indicated are also their categorisation, mechanism of action, target annotation, and if they are recommended as screen positive controls by the JUMP consortium.

Compound	Categorisation	Mechanism of action (MoA)	Protein target	Positive control
Romidepsin	Transcription	HDAC inhibitor	HDAC1, HDAC2, HDAC3, HDAC4, HDAC5, HDAC6, HDAC7, HDAC8, HDAC9	No
RGFP966	Transcription	HDAC inhibitor	HDAC3	No
LLY-283	Transcription	Protein arginine N-methyltransferase inhibitor	PRMT-5	No
T-0901317	Transcription	LXR agonist	NCOA1, NCOA2, NR1H2, NR1H3, NR1I2, RXRB	No
Dexamethazone	Transcription	Glucocorticoid receptor agonist	ANXA1	Yes
THZ1	Cell cycle	CDK inhibitor	CDK7	No
SCH-900776	Cell cycle	CHK inhibitor	CDK2, CHEK1	No
FK-866	Metabolism	Niacinamide phosphoribosyltrans-ferase inhibitor	NAMPT	Yes
AZD7545	Metabolism	Pyruvate dehydrogenase kinase inhibitor	PDK1	No
CHIR-99021	Inflammatory pathway	Glycogen synthase kinase inhibitor	CDK1, GSK3A, GSK3B, MAPK1	No
FR-180204	Inflammatory pathway	MAP kinase inhibitor	MAPK1, MAPK3	No
VX-475	Inflammatory pathway	p38 MAPK inhibitor	MAPK11, MAPK12, MAPK14	No
GNF-5	Inflammatory pathway	Bcr-Abl kinase inhibitor	ABL1, BCR	No
Ponatinib	Inflammatory pathway	Bcr-Abl kinase inhibitor, FLT3 inhibitor, PDGFR tyrosine kinase receptor inhibitor	ABL1, BCR, FGFR1, FGFR2, FGFR3, FGFR4, FLT3, KDR, KIT, LCK, LYN, PDGFRA, RET, SRC, TEK	No
GSK2334470	Inflammatory pathway	Phosphoinositide dependent kinase inhibitor	AURKA, AURKB, PDPK1	No
ML-298	Inflammatory pathway	Phospholipase inhibitor	PLD2	No

Homochlor-cyclizine	Inflammatory pathway	Antihistamine	HRH1	No

Together, these results indicated that the MALDI-TOF MS workflow with subsequent biomarker analysis, was able to identify metabolism, cell cycle and transcription modulators, as well as inflammation-associated compounds. However, these proposed mechanisms of action were ambiguous, and did not exclude the possibility that compound activity could also be elicited via off-target effects such as cytotoxicity, that can lead to M1 "biomarker" decrease (loss-of-function assay). As current data analysis workflows were insufficient to identify compound effects, for instance, an MTT assay could be conducted to test for cytotoxicity as follow up experiment. Further, cytotoxicity "biomarkers" could be determined and simultaneously measured by MALDI-TOF MS to filter out those compounds. However, I decided to proceed to screen a more targeted inflammation-specific compound set as I expected decrease in M1 "biomarkers" alongside an increase in M0 "biomarkers" for inflammation signalling cascade hits which might enable me to distinguish between on- and off-target effects.

5.4 Phenotypic screening with an inflammation-specific compound set

I curated an inflammation-specific compound set, consisting of 86 compounds which were tested at a final assay concentration of 10 µM. These compounds were obtained from my industrial collaborator, GSK, and are part of their chemogenomics library. Chemogenomic libraries typically contain between 3,000 and 5,000 annotated compounds with significant biological diversity, providing insight into the biology captured by a phenotypic screen.[384] The selected compounds in my inflammation-specific subset were annotated with various proteins involved in the inflammation signalling cascade, including ADAM17, BRD4, CREBBP, IKK, IRAK, JAK, MAPK, MTOR, MyD88, NF-κB, PIK, PLK, RIPK, STAT, and TLR4. The set also included compounds identified as hits in a proprietary anti-inflammatory screen conducted by GSK. Further modulators of glucose metabolism, which is altered in M1 macrophages were contained in the compound selection.

5.4.1 "Biomarker" analysis identified hits in the inflammation compound set and showed major hit alignment with an established cytokine profiling workflow

I employed the "biomarker" analysis workflow to analyse the MALDI-TOF MS-based inflammation compound set data as scalar projection analysis was again unsuitable due to large variability within the controls (Supplementary Figure S.3). The M0 "biomarkers" *m/z* 450.07, 564.04 and 664.25 exhibited again large signal variations and were therefor not used in the subsequent "biomarker" analysis (Supplementary Figure S.4). Similarly, the *m/z* 697 IFN-γ "biomarker" was excluded because no difference in mean signal intensity was observed between the M0 and M1 macrophages (Supplementary Figure S.5).

The remaining pro-inflammatory markers, *m/z* 626.08, 642.06 and 707.05, all showed stable %CV in the M1 polarised cells (20%, 15% and 21%, respectively) (Supplementary Figure S.5). The reduction in the *m/z* 642 CV from 52% in the previous JUMP screen to 15% in this screen resulted in an improved compound scoring alignment of this marker with the other two *m/z* features. Applying the previously established hit-calling criteria (two markers with normalised peak intensity <0.6), 24 hit compounds were identified (Figure 5.9A, black box). Within these hits, two subsets were distinguished based on the strength of the "biomarker" response, indicating either strong (10 compounds) or weak (14 compounds) M1 dissimilarity.

To validate the identified MALDI-TOF MS hits, instead of using target annotation, results were compared to an established fluorescence-based cytokine profiling assay that was conducted by GSK employee Lee Booty. This label-based assay measured the secreted levels of pro-inflammatory cytokines (IL-6, TNF-α, CXCL8 and GM-CSF) in the cell culture media.[346,385] TNF-α concentration was found to decrease first in response to compound treatment, indicating M1 dissimilarity for approximately one third of the tested compounds (Figure 5.9B). This response could be attributed to the lower overall concentration of TNF-α (chapter 4.4), which reduced the assay signal window and robustness. Therefore, consistent with the MALDI-TOF MS workflow, it was established that three cytokines had to show a normalised concentration <0.6 for hit calling. This criterion led to the identification of 20 hit compounds (Figure 5.9B, black box), further categorised into 12 compounds with strong M1 dissimilarity and 8 compounds with weak M1 dissimilarity (Figure 5.9B).

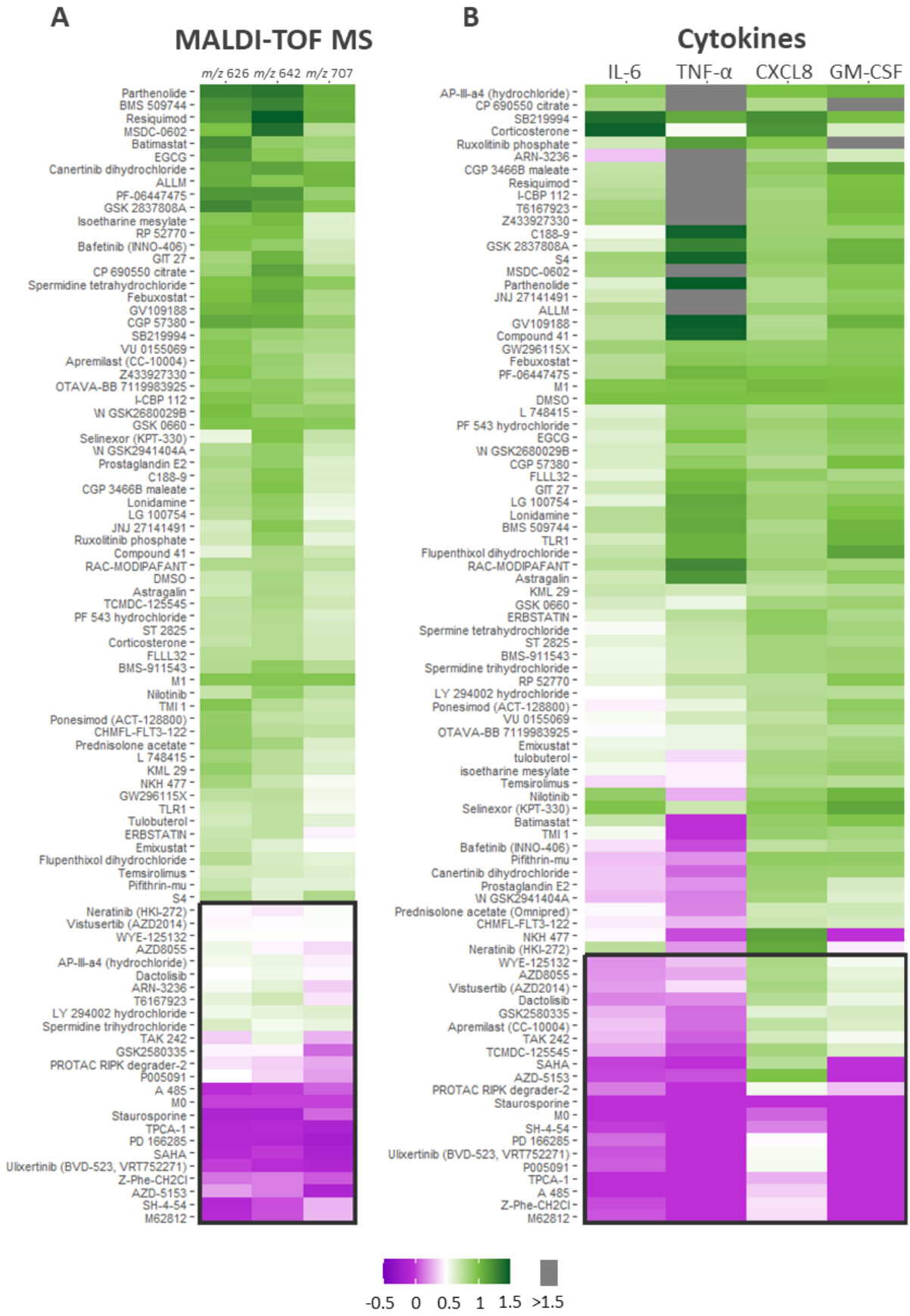

Figure 5.9. MALDI-TOF MS "biomarker" and pro-inflammatory cytokine evaluation in the inflammation compound set screen.

Heatmap of the averaged, normalised (based on M0 and M1) (A) MALDI-TOF MS "biomarker" signal intensities at *m/z* 626, 642 and 707, and (B) IL-6, TNF-α, CXCL8, and GM-CSF cytokine concentrations after treatment with 86 inflammation-specific compounds. Hit compounds are indicated by a black box, with the hit threshold defined as a normalised peak intensity <0.6 (A) for two markers, and (B) four cytokines; n_{M0} = 4 per donor, n_{M1} = 4 per donor, acquisitions conducted in triplicate for MALDI-TOF MS only.

Finally, a comparison of the hit compounds from the MALDI-TOF MS and cytokine profiling screen revealed a significant overlap: 18 hits (70%) were common between the two methods, 6 hits (23%) were unique to MALDI-TOF MS, and 2 hits (3%) were unique to cytokine profiling (Figure 5.10A). The technology-unique compounds (MALDI-TOF MS: AP-III-a4, Spermidine trihydrochloride, LY294002 hydrochloride, T6167932, ARN-3236, Neratinib; Cytokines: Apremilast, TCMDC-125545) showed weak M1 dissimilarity within their respective screens. All compounds that showed strong M1 dissimilarity overlapped between the two screens. Further, the compound scoring between the two technologies showed a degree of correlation as demonstrated for the *m/z* 626 MALDI-TOF MS "biomarker" and the IL-6 cytokine (R^2 = 0.41, Figure 5.10B).

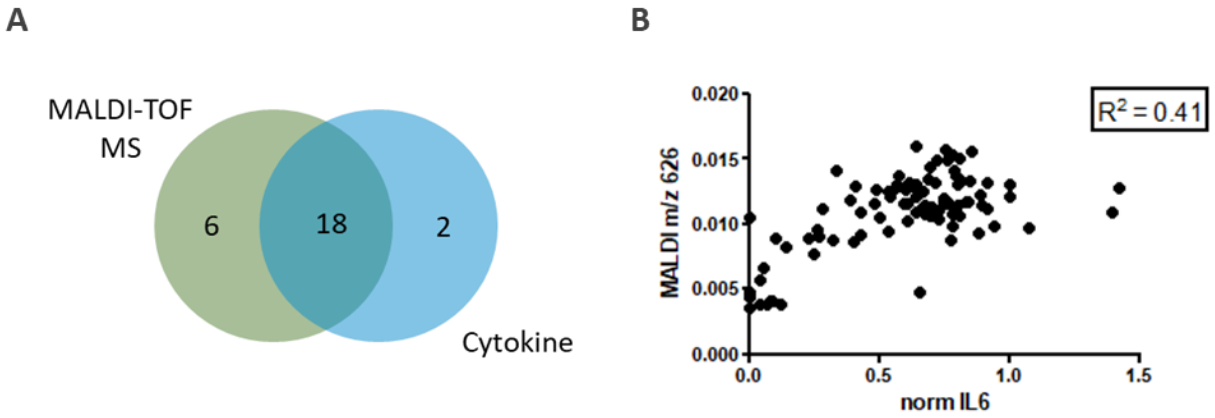

Figure 5.10. Comparison of inflammation compound set hits between the MALDI-TOF MS and cytokine screen.
(A) Venn diagram of hits identified between the two different assays. (B) Correlation plot of the *m/z* 626 MALDI "biomarker" signal intensity and the IL-6 cytokine concentration; averaged and normalised data, linear regression fit.

This large hit overlap between the MALDI-TOF MS method and the established cytokine screen indicated further successful hit calling by MALDI-TOF MS. However, I could not use the M0 "biomarkers" as I anticipated to distinguish between on- and off-target hits within this MALDI-TOF MS-based screen which was likely due to large signal variability. Further, the established cytokine screen also exclusively focussed on the reduction of pro-inflammatory cytokines and

hence also this approach cannot be used to profile false positive hits. Looking into the compound scoring within the inflammation-specific compound set, I noticed two compound subsets that either strongly or moderately reduced the inflammation marker. The group with the strongly decreased markers clustered together with the M0 control and could contain either highly effective or cytotoxic compounds that elicited signal loss. This hypothesis could be tested by including known cytotoxic compounds as controls into the screen or by performing different subsequent experiments that allow me to uncover compound MoA.

5.5 Discussion

I successfully developed a novel MALDI-TOF MS phenotyping workflow for resting and pro-inflammatory iPSC-derived macrophages from three human donors based on *m/z* features of the lipid and metabolite region of the mass spectrum. I was able to cluster polarised cell phenotypes via PCA and identify phenotype-specific "biomarkers". I used these "biomarkers" in conjunction with the target annotations of the JUMP compounds to hypothesise broad phenotypic changes induced by frequent phenotypic screen hits and inflammation-specific modulators. However, final MoA elucidation remained ambiguous. Instead, MALDI-TOF MS assay performance was validated by screening a customised inflammation-specific compound set. Multiple hits were robustly identified across three M1 "biomarkers" and a substantial overlap with results from an established cytokine profiling assay of the same compound set was observed. Notably, neither the MALDI-TOF MS assay nor the cytokine screen were able to distinguish between on- and off-target effects, such as cytotoxic as both approaches were loss of function assays, relying solely on a reduction in pro-inflammatory features for hit identification.

5.5.1 MALDI-TOF MS cellular assays

MALDI-TOF MS demonstrated promise as a novel tool for hit triaging in macrophage-centred phenotypic drug discovery screens. I systematically optimised the cellular MALDI-TOF MS workflow to achieve macrophage phenotype separation, featuring the importance of precise workflow optimisation as highlighted by Heap *et al.* 2019.[208] Although PCA did not identify hit compounds from the full mass spectrum data, limiting its ability to cluster known compounds and potentially predict cytotoxicity effects[44,229], further implementation of machine learning

algorithms could enhance spectral reference fingerprinting for better phenotype identification[195,196,386,387]. A novel software, M^{2}ara, has recently been released for data evaluation of whole cell MALDI-TOF MS assays.[388] It can be used to perform feature scoring and robustness evaluation to perform subsequently guided peak filtering which might result in improved clustering.

Nevertheless, the robustly and reproducibly identified "biomarkers" effectively guided hit identification. A future directive could be the confirmation of the "biomarker" identity. As metabolites and lipids are detected in a mass range up to 1500 Da, confirming the identity of these "biomarkers" would require additional experiments, such as LC-MS/MS or Fourier-transform ion cyclotron resonance MS.[389,390] While identifying these "biomarkers" was beyond the scope for this thesis, it could be a particularly valuable approach when analysing disease-specific cell phenotypes by MALDI-TOF MS.

While MALDI-TOF MS is extensively developed for bacterial phenotyping, its use for eukaryotic cells is still emerging. Standardised protocols for bacterial species have led to large spectral libraries for reliable species identification.[189,193,360] While ribosomal protein signatures are used to distinguish bacterial phenotypes, the workflow developed in this chapter focussed on lipids and metabolites (*m/z* 400 - 1,000). Overall, there is significant potential for translating MALDI-TOF MS cell phenotyping workflows to a broad range of cell phenotypes without the need to develop entirely new assays. For instance, a standardised MALDI-TOF MS workflow has already been used to rapidly characterise 66 different cell lines and a great methodological overlap between the here developed workflow and the already published lipid signature MALDI-TOF MS screens was observed.[206,209] Given the success of MALDI-TOF MS imaging in tracking metabolites and lipids for various applications, it is likely that these approaches can be adapted for HTS in various cell types.

5.5.2 Phenotypic screening

Cellular phenotypic screens, in contrast to biochemical assays, focus on detecting the overall phenotype, providing the possibility to capture both on- and off-target effects, such as cytotoxicity. However, the directionality of the assay needs to be carefully selected as toxic compounds are often detected among hits in loss-of-function assays but are not typically

identified in gain-of-function assays.[35,358] In this study, loss-of-signal assays were employed as reduction in pro-inflammatory MALDI-TOF MS "biomarkers" or cytokines was monitored.

Further, the selection of compound sets for phenotypic screening assay validation is crucial. Unlike target-based screens, which use large, chemically diverse sets (~10,000 compounds), phenotypic screens utilise biologically diverse and well-annotated libraries, such as the JUMP compound set or chemogenomic libraries, to inform on the biology captured by the phenotypic assay.[384] Customised libraries can be assembled for hypothesis-driven validation, reducing the scale of the initial screening efforts.

Lastly, the assay readout is a critical factor in assay performance. Different readouts capture various biological endpoints, from gene expression to protein activity.[37] While the gene expression is closely associated with the stimulus, protein activity would yield more information about the disease phenotype.[37] The MALDI-TOF MS and cytokine release assays used here are aimed to capture disease relevant phenotypes, which was supported by the observed overlap in hit compounds between the two methods. However, these loss-of-function assays require subsequent experiments to differentiate between on-and off-target effects.

Other phenotypic screening assays exist that are used for evaluation of macrophage polarisation including T cell activation assays[263], real-time phagocytosis activity assays[264] and cell surface marker detection via flow cytometry[40,265,266] but all are also unable to elucidate the MoA or intracellular targets of identified hits. These assays are mainly image-based or label-based methods that can suffer further from drawbacks outlined earlier for label-based assays. Still, they are frequently used for hit-triaging.

Assays which offer more complex information have gained interest in the phenotypic screening community as they promise to provide further compound information. Cell painting which uses multiplexed fluorescence dyes for image-based profiling, and bulk RNA sequencing methods to study transcriptomic effects are examples of more complex screening approaches. Although not yet extensively implemented, a new wave of higher throughput proteomics approaches holds potential to provide more data depth for phenotypic screening in the future.

Chapter 6. Proteomics as a tool to deconvolute mechanisms of action for phenotypic screen hit compounds

Interpreting the outputs of phenotypic screens can be complex and might require follow up experiments to distinguish if hits are acting by a desired or undesired MoA such as cytotoxicity. Various strategies for target identification and MoA profiling during and after phenotypic screening have been reported. First, compound-protein interactions can be identified subsequently to screening through methods such as affinity enrichment followed by chemoproteomics or thermal shift assays.[15] A second strategy involves introducing genetic perturbations in conjunction with compound treatments, allowing MoA elucidation simultaneously to screening.[391-393] Lastly, a common strategy involves comparing experimentally determined phenotype signatures against large libraries that already contain gene expression, cell morphology and biomarker information in response to chemical or genetic perturbations.[41,394-396] One key advantage of this library-based approach is the feasibility of screening numerous compounds compared to legacy slow-throughput proteomics efforts, but this library-based approach relies on the similarity of phenotypes to known compounds and, consequently, known MoAs.[35] In contrast, proteomics holds promise for discovering novel MoAs and with rapidly improving workflow capabilities is increasingly utilised.

In this chapter, I aimed to investigate if an increased throughput, label-free DIA proteomics workflow was suitable as a phenotypic screening tool, and additionally determined if the workflow could be used to elucidate the MoA of hits. I assessed iPSC-derived macrophages from three human donors which were differentiated with 100 ng/mL M-CSF, treated with the 86 curated inflammation compounds, and stimulated for 24-hours with IFN-γ+LPS. Initially, I determined hit compounds via scalar projection analysis and compared the results to the previously described phenotypic MALDI-TOF MS and cytokine profiling HTS approaches (chapter 5). Then, I attempted hit MoA elucidation by evaluating the global proteome and M1 protein biomarker expression.

6.1 Global proteome analysis revealed six compounds with a large number of missing values

IFN-γ+LPS polarised iPSC-derived macrophages (~27,000 cells) treated with the inflammation compound set (10 µM) were lysed, and subsequently the S-Trap method used for efficient peptide preparation. A peptide pool composed of equal amounts from all 288 samples was fractionated into 24 fractions (offline fractionation, chapter 2.6.3) and the resulting samples used for spectral library generation in FragPipe. Searching against this spectral library later in the analysis of the 288 samples (86 compounds, four M0 and four M1 polarised macrophage samples per donor) increased data analysis search speeds while maintaining data depth. The unfractionated peptide pool was acquired in DDA to design a 16 variable window dia-PASEF acquisition method (details chapter 2.6.2) that increased sample coverage. All 288 samples were acquired on the timsTOF HT MS, coupled to an Evosep LC system operated with the 60 sample per day method (21 min gradient) to reduce the total run time to five days (~24 days with 2-hour gradient legacy method). Data were searched in DIA-NN (detailed search parameters chapter 2.7.3) and mean normalisation, as well as batch correction on a donor level conducted. Post-filtering was applied to remove known contaminants and single peptide-protein matches.

In total, 5505 proteins remained after filtering and 5477 of these proteins were quantified within 75% or more samples. An average of 46,747 peptides and 5,153 proteins (standard deviation = ±372) was observed per sample which aligned with previous macrophage time course experiment results, indicating sufficient data depth to evaluate macrophage polarisation. Further, workflow robustness across the three different donors was observed as highly similar average protein numbers per sample were detected between the donors (donor 1 = 5141 ±306 proteins, donor 2 = 5169 ±421 proteins, donor 3 = 5148 ±382 proteins). The mean %CV of all protein intensities as an example investigated for the M0 and M1 macrophage controls indicated workflow robustness across technical replicates (donor 1: M0 = 13.72%, M1 = 12.42%; donor 2: M0 = 11.28%, M1 = 10.22%; donor 3: M0 = 12.53%, M1 = 13.79%) and between different donors (M0 = 12.30%, M1 = 12.90%).

The log2 signal intensity of the proteins was plotted for each compound treatment (Figure 6.1). In unsupervised hierarchical clustering, most compounds, as well as the resting and M1 macrophages, clustered together. Within this cluster, high and low abundant proteins were detected, but little differential expression within a protein across different treatments was

observed. This aligns with previous findings of a 5% expression change in the overall proteome in response to macrophage polarisation.[346,397] However, I observed a distinct cluster of six compounds, PD 166285, Ulixertinib, SH-4-54, A-485, TPCA-1 and Staurosporine (Figure 6.1; indicated by the black box), characterised by a higher number of missing values (six compound set: 1468 ±617 NAs, remaining compounds: 277 ±185 NAs), primarily in the lower intensity proteins. These missing identifications could indicate that these compounds induced significant cellular changes, affecting cellular protein content as seen in cell death, suggesting compound cytotoxicity.[398] The next step was to identify hit compounds and evaluate their MoA alongside the proposed cytotoxic compounds.

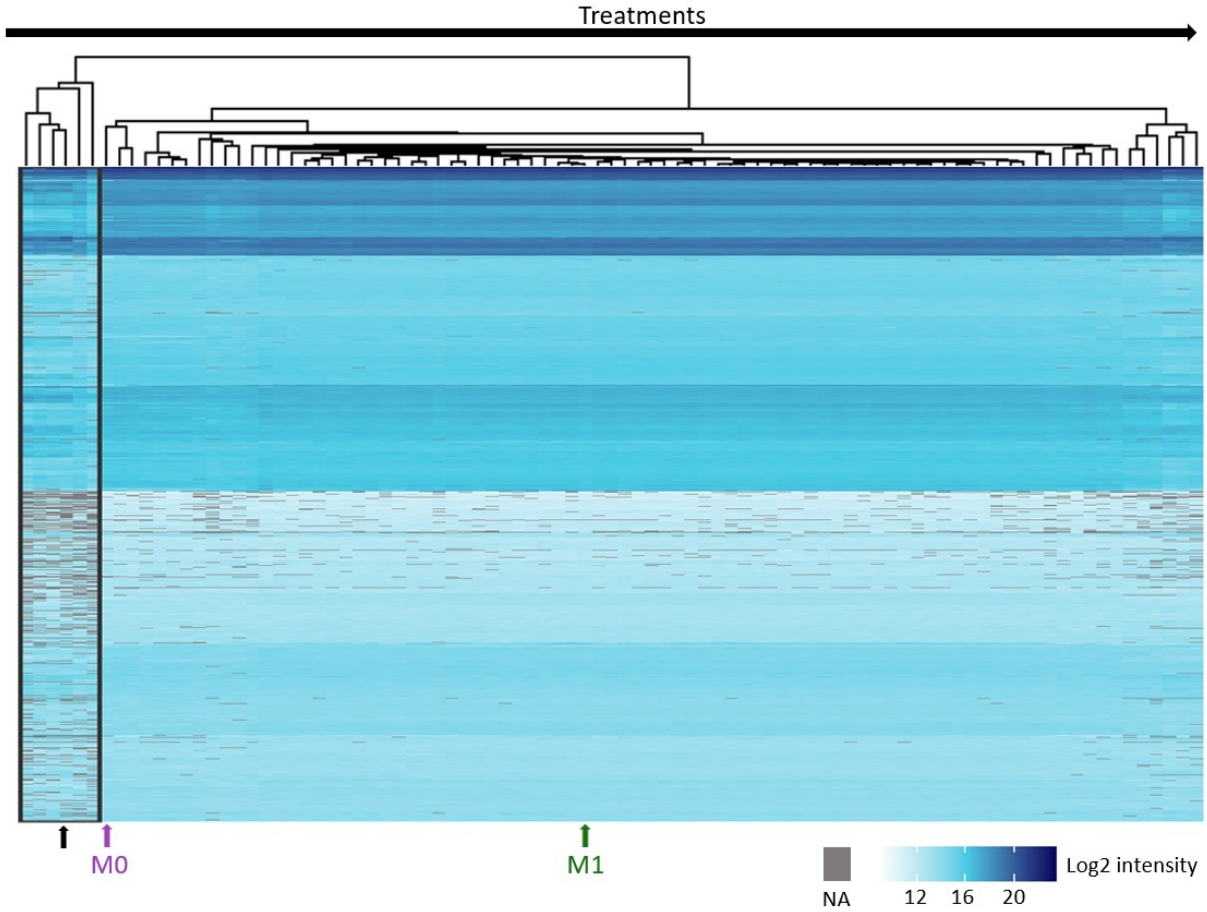

Figure 6.1. Macrophage compound treatment clustering on a global protein level.
Heatmap with unsupervised hierarchical clustering of log2 intensity of all proteins maintained after filtering, normalisation and batch correction. Median normalisation and batch correction at donor level was performed. Filtering was performed for known contaminants and proteins with a single unique peptide match. Analysis was performed for M1 activated macrophages after treatment with 86 inflammation-specific compounds with untreated M1 (green) and unstimulated M0 (purple) macrophage controls derived from three human donors; n_{M0} = 4 per donor, n_{M1} = 4 per donor.

6.2 Scalar projection analysis revealed 17 hits from the inflammation compound set by proteomics, showing a large overlap with HTS screen hit calling

I decided to test the previously described scalar projection analysis for hit compound identification from proteomics data. In the MALDI-TOF MS screen, scalar projection analysis suffered from high variability within the controls and further only ~150 features were used in the analysis. In contrast, with the proteomics dataset, >5000 proteins were detected and a tight clustering of the M1 (projection = -0.02 - 0.04, and rejection = -0.09 - 0.29) and M0 controls (projection = 0.89 - 1.09, and rejection = -0.10 - 0.21) observed (Figure 6.2A). This, along with a high projection z-score for the M0 control (M0 z-score$_{projection}$ = 4.1) (Figure 6.2B), confirmed that scalar projection was a suitable tool for hit calling from proteomics data.

In total, 17 hit compounds were identified by t-testing against the M1 control, yielding an overall hit rate of 20%. Comparing these proteomics hits with the MALDI-TOF MS "biomarker" and cytokine screen hits showed a large overlap between all technologies, with 15 common compounds (Figure 6.2C). This large overlap further validated the assay's suitability and the hit identification in the previously developed MALDI-TOF MS assay.

Among the 15 common hits were six compounds that previously showed a higher number of missing values. These compounds were characterised by high projection scores (z-score$_{projection}$ = 2.06 - 3.63), indicating high M1 dissimilarity, and some of the highest rejection scores (z-score$_{rejection}$ = 1.29 - 4.90), indicating high M1 and M0 dissimilarity (Figure 6.2B). This strengthened my hypothesis that these compounds induced off-target effects.

The remaining common compounds were AZD-5153, AZD8055, Dactolisib, M62812, P005091, SAHA, Vistusertib, WYE-125132, and Z-Phe-CH2Cl, that exhibited lower projection and rejection scores (z-score$_{projection}$ = 1.03 – 2.58, z-score$_{rejection}$ = 0.48 – 2.34) (Figure 6.2B) than the first group.

In addition to the 15 common hits, two compounds were identified uniquely by proteomics. These compounds showed a projection z-score of 2.00 and 1.03, and low rejection z-score of 0.49, and 0.39, for Ruxolitinib phosphate and CP 690550 citrate, respectively (Figure 6.2B).

Lastly, 11 compounds were identified as hits by either the MALDI-TOF MS or the cytokine screen (or both) but not by proteomics; three proteins were common to both methods, six

were unique to the MALDI-TOF MS screen, and two were unique to the cytokine screen (Figure 6.2C).

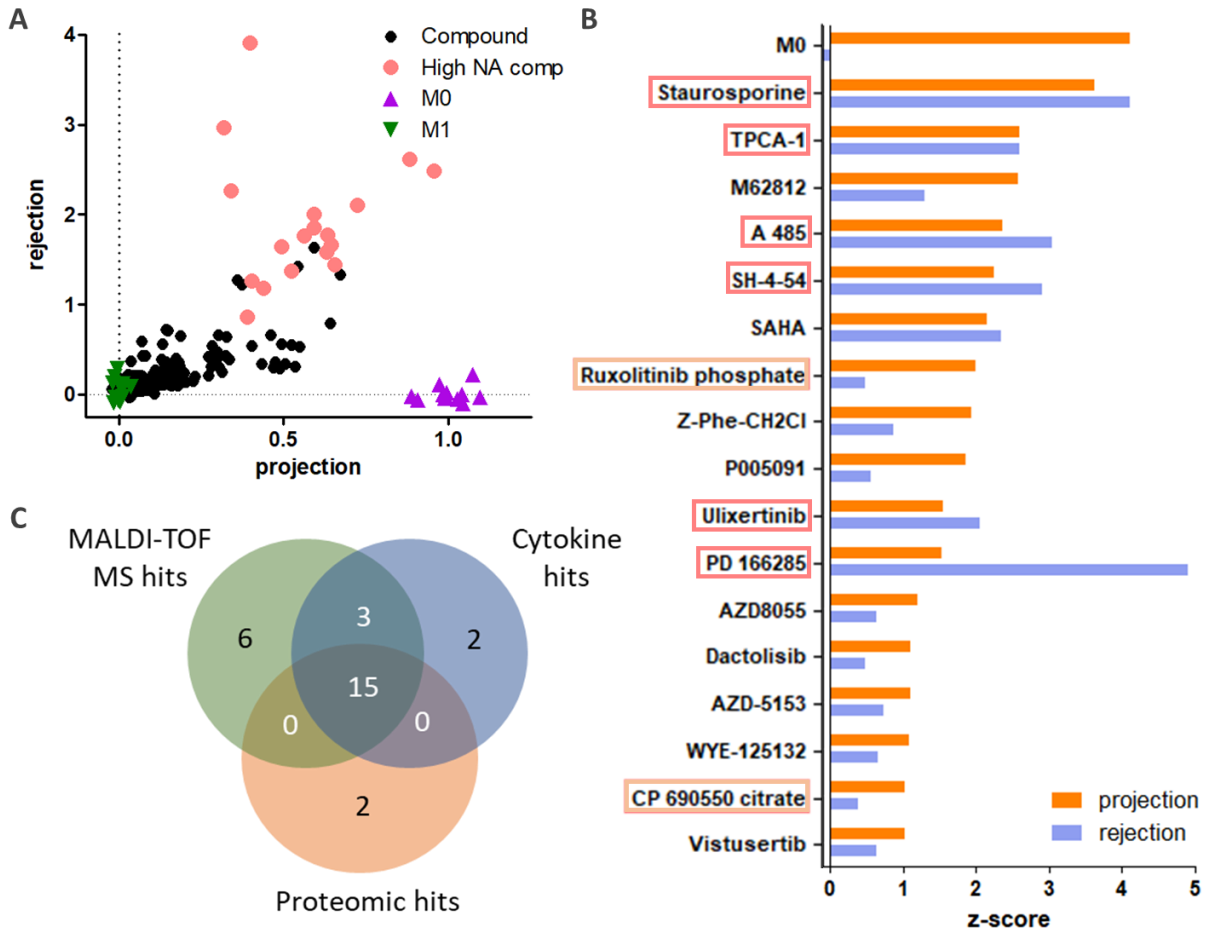

Figure 6.2. Scalar projection analysis of macrophage compound treatment induced proteome changes.
(A) Scatter plot of rejection values plotted against projection values determined by scalar projection analysis of M1 activated macrophages after treatment with 86 inflammation-specific compounds with untreated M1 (green) and unstimulated M0 (purple) macrophage controls derived from three human donors; n_{M0} = 4 per donor, n_{M1} = 4 per donor and highlighted high NA compounds identified earlier in global proteome analysis. (B) List of statistically significant compound projection z-scores in comparison to the M1 controls; t-test (Bonferroni Holm) and rejection z-scores. Highlighted on the y-axis are high NA compounds (pink) and proteomics screen unique hits (orange). (C) Venn diagram of hits identified with the proteomics (orange), MALDI-TOF MS (green) and cytokine (blue) screening assays.

Further proteomics analysis of both, non-proteomics and proteomics hits, was conducted to identify true hits from these screens and elucidate their MoA.

6.3 Global M1 biomarker analysis indicated grouping of proteomics hit compounds into two subsets

All compound treatments that led to an M1-deviating phenotype should show a reduction in M1 protein markers, including cell surface markers like CD44, interferon stimulated genes (ISGs) and interferon induced genes (IFITs), as well as proteins of the antigen presenting machinery (HLAs) extensively discussed in chapter 4.3.1. Following this loss of function approach, I assessed the fold change of the M1 protein markers (significantly upregulated proteins in the M1 polarisation compared to the M0, Supplementary Figure S.6) in the compound treatments relative to the M1 macrophage controls. The majority of compounds showed a low fold change in M1 protein markers, indicating that the compound treatment still resulted in an M1 macrophage phenotype (Figure 6.3A). However, 18 compounds exhibited a negative fold change, indicating an M1-deviating phenotype. Except for the PROTAC RIPK degrader-2, all 17 compounds had been previously identified as hits by scalar projection analysis of the proteomics data.

Unsupervised hierarchical clustering separated the hit compounds into two distinct subsets based on the magnitude of the fold change (Figure 6.3A). The first subset showed a strongly reduced fold change in M1 markers across eight compounds. Six of these compounds were earlier characterised by an increased number of NAs, as well as high projection and rejection scores. Further, these compounds were associated with strongly reduced inflammation markers in the MALDI-TOF MS and cytokine screen.

The second subset was characterised by a moderate fold change reduction in M1 protein markers and included ten compounds: AZD-5153, AZD8055, CP 690550 citrate, Dactolisib, P005091, PROTAC RIPK degrader-2, Ruxolitinib phosphate, Vistusertib (AZD2014), WYE-125132, and Z-Phe-CH2Cl. These compounds had lower projection ($z\text{-score}_{projection}$ = 1.03 - 2.00) and rejection ($z\text{-score}_{rejection}$ = 0.39 - 0.88) z-scores compared to set one (Figure 6.3B).

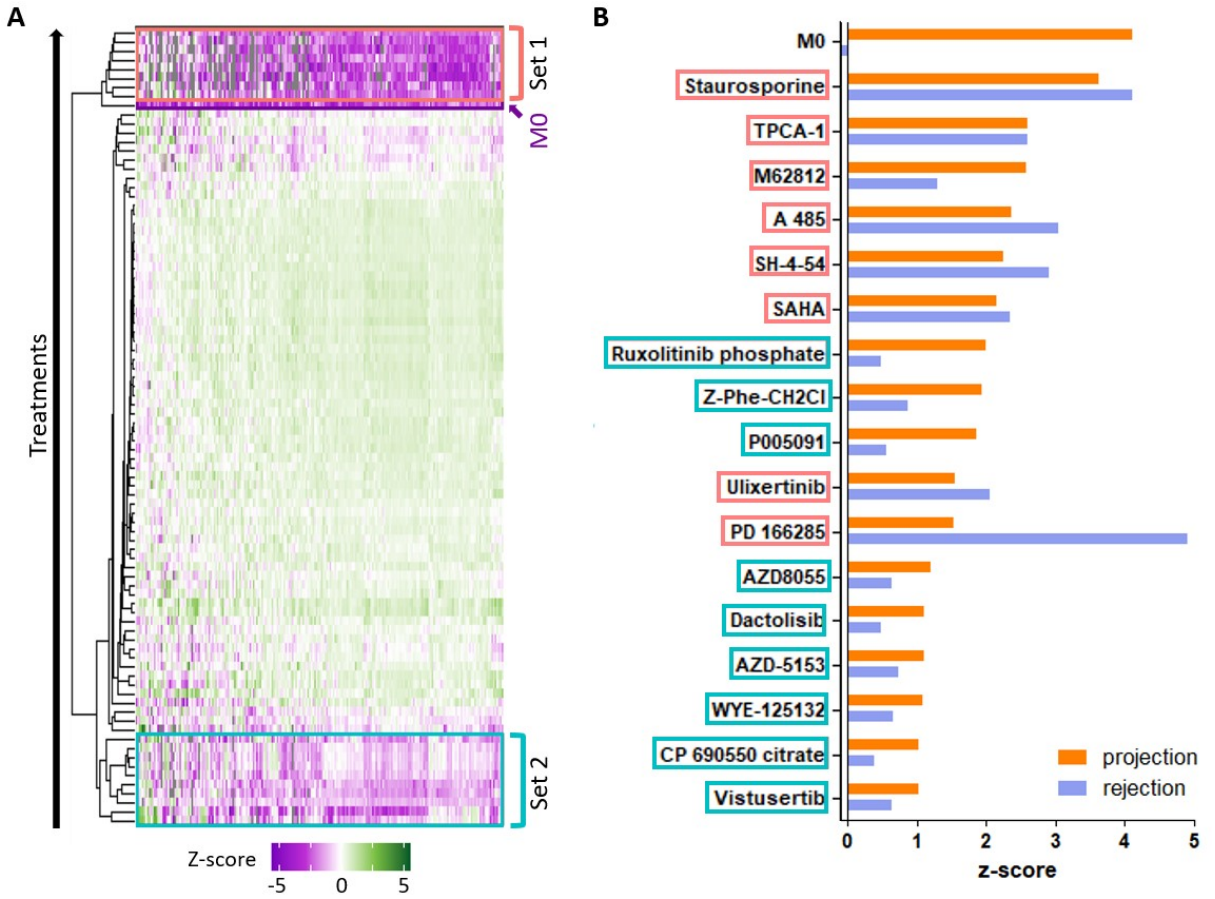

Figure 6.3. Macrophage compound treatment clustering based on selected pro-inflammatory protein levels.
Heatmap with unsupervised hierarchical clustering of z-scored log2 fold change intensities obtained by t-testing (Benjamin-Hochberg correction) the compound treated macrophages against the M1 controls. (A) Displayed M1 marker proteins were selected based on significant changes in comparison to the M0 control (log2 protein fold change cut-off = -2 or 2, -log10 adjusted p-value cut-off = 0.01); n_{M0} = 4 per donor, n_{M1} = 4 per donor. (B) List of statistically significant compound projection z-scores in comparison to the M1 controls; t-test (Bonferroni Holm) and rejection z-scores. Highlighted on the y-axis are set 1 (pink) and set 2 compounds (cyan) determined in (A).

The high overlap in grouping based on clustering and scalar projection approaches suggested that these initial analysis methods might distinguish between off-target/cytotoxic (set one) and on-target/inflammation-specific cell phenotypes (set two). However, the hypothesised biological effects leading to this clustering still needed to be confirmed.

6.3.1 Distinguishing cytotoxic compounds and on-pathway hits by proteomics

To classify the biological effects of the compounds, I analysed the Kyoto Encyclopaedia of Genes and Genomes (KEGG) pathway, as well as the Gene Ontology (GO) terms for biological processes (GO Bio), cellular components (GO Cell), and molecular functions (GO Molecular)

associated with the significantly downregulated proteins from each compound treatment in the two clusters.

First, I noted a higher number of associated pathways for the set one compounds compared to set two (set one: 262-802 pathways, set two: 76-167 pathways, Figure 6.4A). This was due to a higher number of significantly downregulated proteins in set one compounds compared to set two compounds (set one: 260-1278 downregulated proteins, set two: 93-139 downregulated proteins, Supplementary Figure S.7). I selected 22 GO Bio terms based on their adjusted p-value and fold enrichment to display inflammation/macrophage-specific pathways (12 terms, including inflammatory response, pattern recognition receptor signalling pathway, and response to cytokine) and cytotoxicity-associated pathways (10 terms, including autophagy, regulation of apoptotic signalling pathway, and response to reactive oxygen species) to determine the compound-induced biological effects.

The set one compounds showed significant association with all terms, supporting the hypothesis that cytotoxicity was induced instead of inflammation, explaining the absence/reduction in inflammation markers (Figure 6.4B). Literature research and GSK target annotation evaluation (Supplementary Table S.2) revealed that most compounds are well-known cell death inducers. Further, these compounds can be divided into three subsets.

<u>First subset: Kinase inhibitors</u>

Kinases targeted by Staurosporine, PD 166285, and Ulixertinib are key cell cycle checkpoint proteins, and their dysregulation can induce cell death.[399] Ulixertinib is a potent ERK1/2 inhibitor tested in the clinic for the treatment of solid tumours[400,401], while Staurosporine is a broad-spectrum kinase inhibitor that demonstrated cytotoxicity in several human cancers via dysregulation of the PI3K/Akt pathway, which is also part of the LPS signalling cascade[402].

<u>Second subset: Histone modulator inhibitors</u>

A-485 and SAHA, induced cell death via histone modulator inhibition. A-485 targets the histone acetyltransferase coactivator, which regulates transcription of genes for tumour progression, and its treatment has shown to induce cell death in murine hematopoietic cells.[403] Reduction in cell viability was also observed after treatment with low micromolar concentrations of the

histone deacetylase inhibitor SAHA.[404] Blank *et al.* 2022 have used SAHA to confirm the performance of their lipid-based MALDI-TOF MS screen for LPS-induced microglial activation as HDAC inhibitors showed next to cytotoxicity also beneficial effects in inflammation-related diseases.[373,405] The authors reported a reduction in M1 characteristic lipid markers and cytokines, indicating inflammation reduction at 1 µM SAHA. However, their cell viability assessment with an average of 80% showed a large standard deviation (>±20%), highlighting the benefit of proteomics for subsequent analysis of loss-of-function screen hits to provide reliable off-target effect identification.[139]

Third subset: Inflammation signalling cascade inhibitors

SH-4-54, TPCA-1, and M62812 target proteins in the inflammation signalling cascade. SH-4-54 and TPCA-1 are small molecule inhibitors of STAT3, a key protein in IFN-γ signalling, and M62812 is a TLR4 inhibitor. The experiments were conducted at 10 µM compound concentration, although all three compounds are reported to induce biological activity in cells at low nanomolar levels. Since compound toxicity is concentration-dependent, this explained the observed cytotoxicity.[406-410]

In contrast to the compounds of this set one (including all three subsets), the ten proteomics hit compounds from set two were not associated with the off-target GO Bio terms (Figure 6.4B). Furthermore, they showed a higher fold enrichment in the inflammation-associated terms compared to set one, supporting the hypothesis that they elicited inflammation pathway-specific effects.

To summarise, proteomics allowed me to distinguish between cytotoxic compounds and potential inflammation pathway hits, which was not possible with the MALDI-TOF MS or cytokine HT screening efforts.

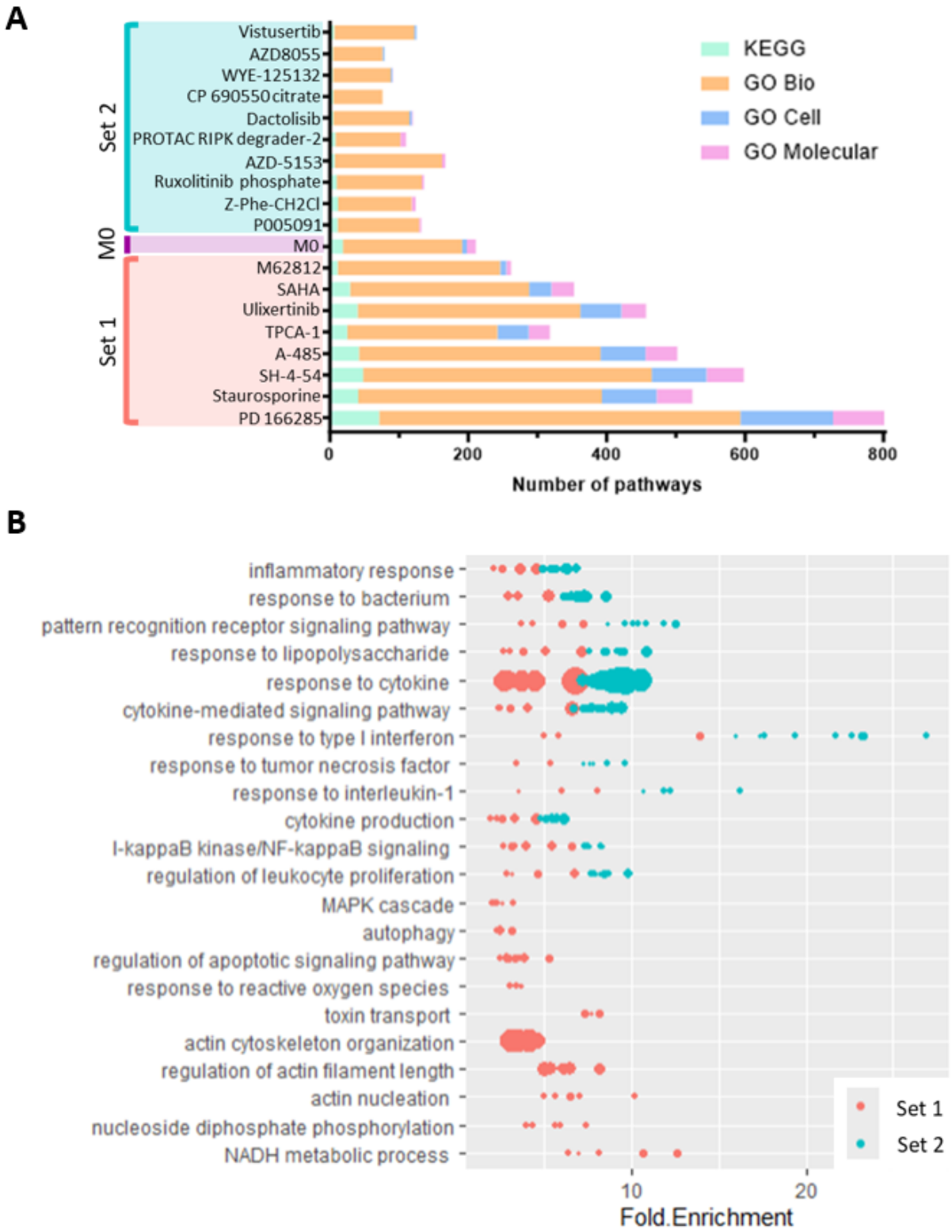

Figure 6.4. KEGG and GO term association of proteomics hit compounds.
Utilised were the significantly upregulated proteins to generate (A) Bar charts representing the number of significantly changing KEGG (green), GO Bio (orange), GO Cell (blue), and GO Molecular (pink) terms for the set 1 and set 2 associated hit compounds, as well as the M0 control. (B) Display of inflammation (top 12) and off-target/cytotoxicity (bottom 10) associated GO Bio terms for the set 1 (cyan) and set 2 (red) compounds. Fold enrichment from

significantly enriched terms (p-value $<10^{-5}$) are plotted as small (lower significance) and large (higher significance) dots.

6.4 Mechanism of action deconvolution of non-toxic proteomics hits revealed inflammation targets

The next step was to evaluate whether proteomics could also be used to deconvolute the MoA for the ten proposed inflammation pathway hits. First, clustering on a global proteome level was performed with only these compounds, including M0 and M1 controls. Three distinct compound clusters were revealed (Figure 6.5A). The first cluster contained WYE-125132, AZD8055, Vistusertib (AZD2014) and Dactolisib which cluster together with the M1 control. The next cluster included AZD-5153, PROTAC RIPK degrader-2, P005091, and Z-Phe-CH2Cl and was located between the M0 and M1 controls but with a higher rejection compared to the last cluster. This last cluster contained CP 690550 citrate, and Ruxolitinib phosphate which were clustered closest towards the M0 control.

This compound grouping was confirmed in a heatmap of the global proteome where only significantly changing proteins between the groups were analysed (Figure 6.5B).

Next, a more detailed investigation of all previously established M1 protein markers (significantly upregulated proteins in the M1 polarisation compared to the M0, Supplementary Figure S.6) was performed and revealed the same grouping into the three compound subsets. All subsets showed a strong reduction across the M1 markers (Figure 6.5C).

Together, this could indicate that differences between the subgroups were driven by the compounds ability to modulate the inflammatory response to the IFN-γ+LPS stimulus.

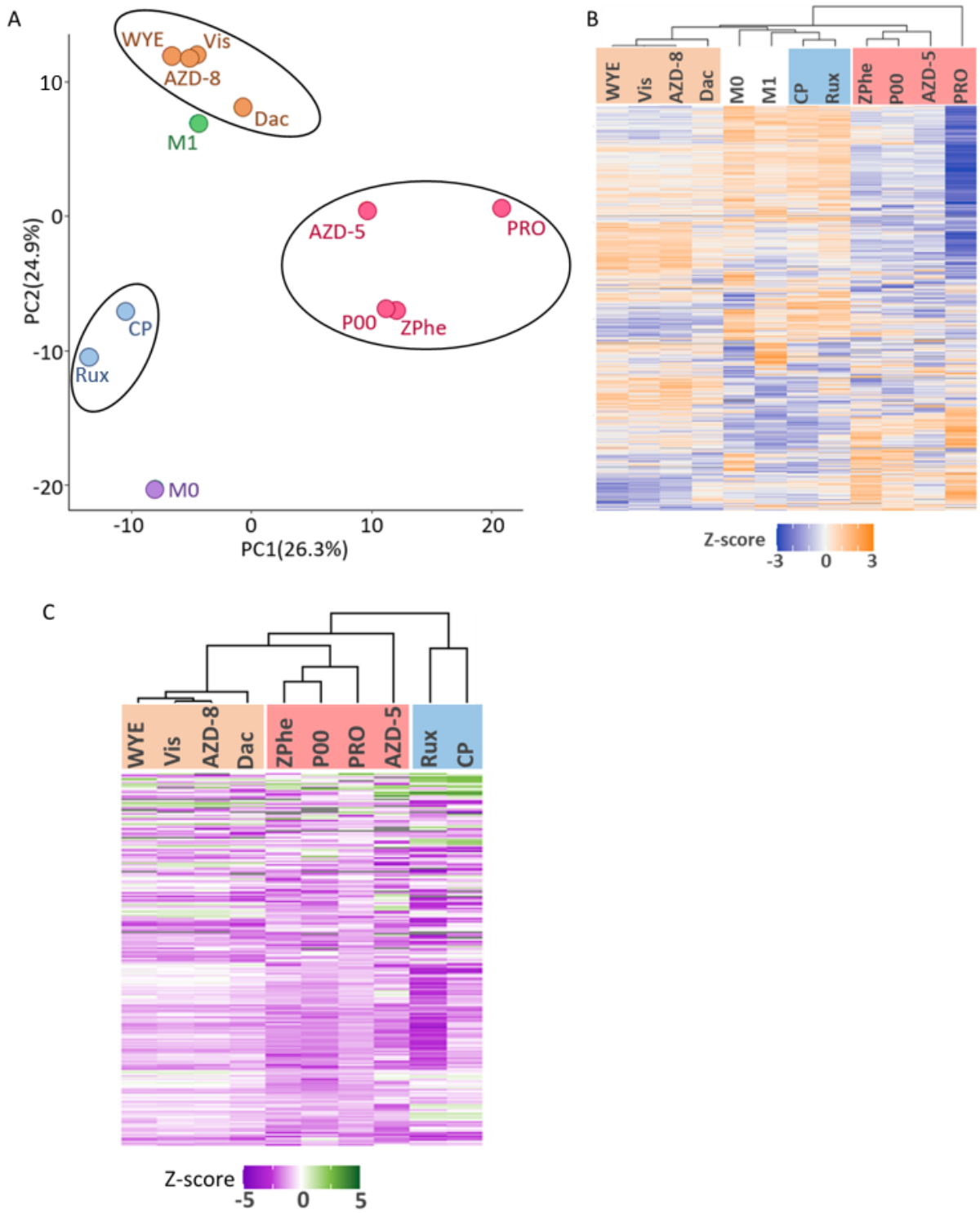

Figure 6.5. Clustering of proposed inflammation pathway hits based on the global proteome and inflammation specific proteins.

(A) PCA based on global proteome changes, (B) Heatmap based on significantly changing proteins in the whole proteome between all groups, and (C) Heatmap based on M1 protein marker expression (marker selection based on differential M0/M1 expression). RPO = PROTAC RIPK degrader-2, AZD-5 = AZD-5153, P00 = P005091, ZPhe = Z-Phe-CH2Cl, Dac = Dactolisib, AZD-8 = AZD8055, Vis = Vistusertib, WYE = WYE-125132, Rux = Ruxolitinib phosphate, CP = CP 690550 citrate.

Subsequently, I assessed the M0 likeness of the different compound treatments by evaluating the reduction of selected M1 protein markers that were associated with different inflammation signalling pathways to see if these markers can be used to evaluate the compound MoA. Based on the LPS and IFN-γ signalling-specific markers as well as cell surface proteins, I was able to distinguish the same three compound subsets previously described.

First subset: Core inflammatory pathway targeting compounds

The first subset contained four compounds: PROTAC RIPK degrader-2, AZD-5153, P005091 and Z-Phe-CH2Cl. These compounds were characterised by high M0 likeness across IFN-γ and LPS signalling as well as cell surface markers, suggesting they target core inflammatory pathway proteins like transcription factors, leading to complete suppression of M1 macrophage polarisation (Figure 6.6).

- PROTAC RIPK degrader-2 targets RIPK2, a kinase downstream of pattern recognition receptors NOD1 and NOD2.[411] NOD2 signalling can augment LPS-induced TLR4 signalling by increasing MyD88 expression and IKKγ activation.[412] High RIPK2 expression is also associated with innate immunotherapy resistance through the JAK/STAT3 IFN-γ signalling pathway.[413]
- AZD-5153 directly targets BRD4, which activates transcription of various immune and inflammatory genes.[414]
- P005091 targets USP7, which can deubiquitinate NF-κB, a transcription factor activated both by MyD88-dependant and independent cascades in LPS signalling, and which interacts with STAT1 in IFN-γ signalling.[415]
- Z-Phe-CH2Cl targets CREBBP (Supplementary Table S.3), a coactivator for transcription factors NF-κB and AP-1.[416]

Second subset: LPS pathway targeting compounds

The second subset included four compounds: Dactolisib, AZD8055, Vistusertib, and WYE-125132. These compounds showed high M0 likeness in the chemo- and cytokines and in the LPS signalling protein targets upstream of the transcription factors (Figure 6.6), indicating possible activity in the LPS signalling cascade. Looking into the GSK target annotations revealed that all these compounds targeted mTOR, and Dactolisib also targeted PIK3 (Supplementary

Table S.3). While mTOR is a metabolism-associated target that according to Vincent *et al.* 2020 is also targeted by frequent phenotypic screen hit compounds, mTOR activation is also described downstream of PI3K signalling in response to LPS stimulation.[417] Typical M1 metabolism markers were investigated, but no M0 likeness was observed in tryptophan catabolism or glycolysis (Supplementary Figure S.8). Although M0 likeness in chemo- and cytokines was observed, indicating the desired phenotype, the exact MoA remained unknown, highlighting a limitation of the proteomics workflow.

Third subset: IFN-γ pathway targeting compounds

The last subset contained two compounds: Ruxolitinib phosphate and CP 690550 citrate, detected only by proteomics and not in the MALDI-TOF MS or cytokine HT screens.

- Ruxolitinib phosphate showed M0 likeness across most IFN-γ signalling and antigen presentation markers but only slight M0 likeness in the chemo- and cytokines (Figure 6.6).
- CP 690550 citrate showed similar response in chemo-and cytokines but only M0 likeness in one-third of the IFN-γ signalling markers.

Both compounds are annotated JAK inhibitors (Supplementary Table S.3). JAK1 and JAK2 are recruited by the IFN-γR to phosphorylate STAT1 in response to IFN-γ stimulation. This explains why Ruxolitinib phosphate, a selective and potent inhibitor of JAK1 and JAK2, exhibited more dominant effects compared to CP 690550 citrate, which is most potent for JAK3.[418,419]

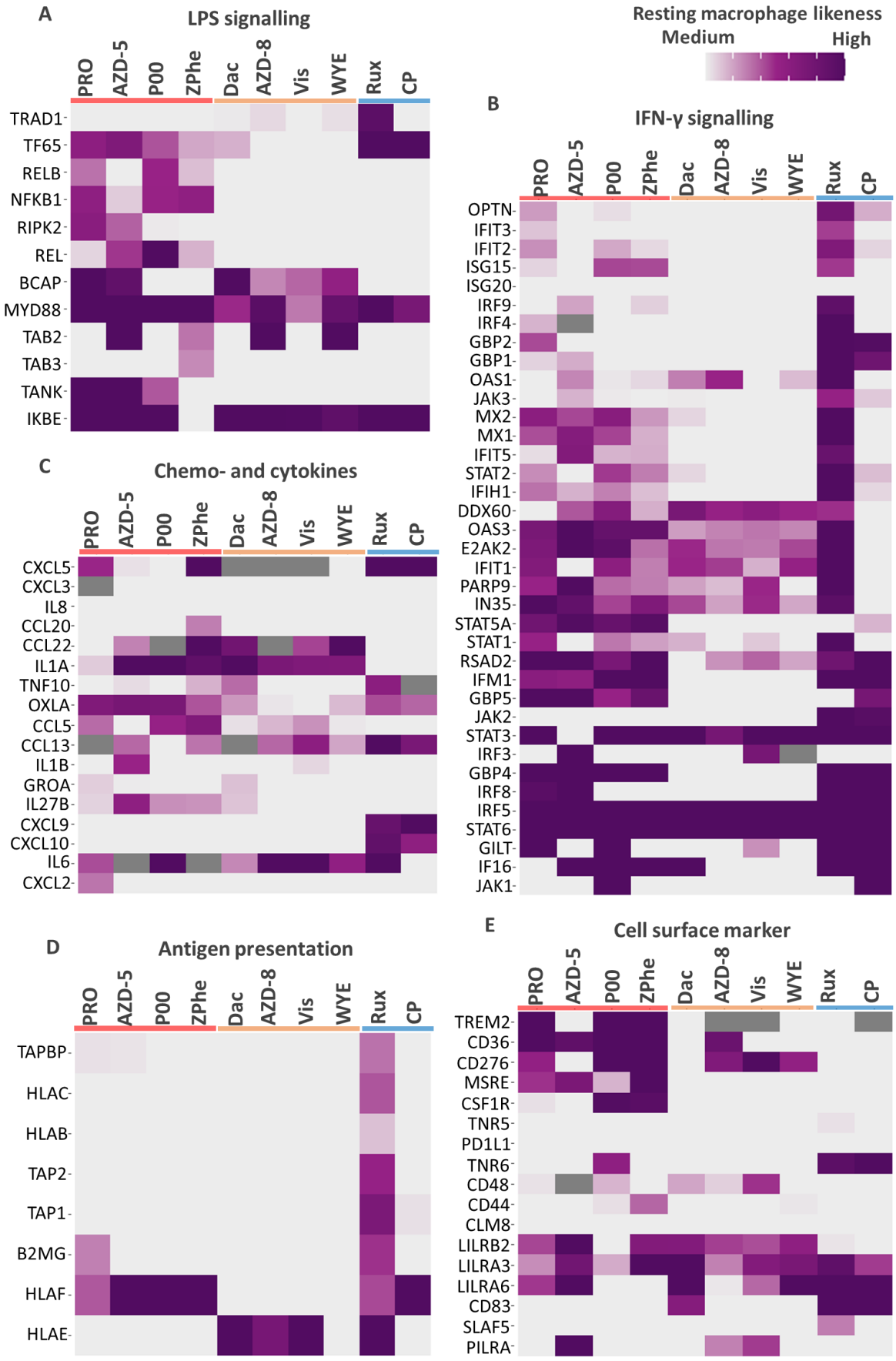

Figure 6.6. M0 macrophage likeness scoring of set 2 proteomics hit compounds across different signalling pathways.

Log2 protein intensity recorded for each compound treatment was normalised against intensity levels in the M0 and M1 controls for proteins associated to (A) LPS signalling, (B) IFN-γ, (C) chemo- and cytokine, (D) antigen presentation and (E) cell surface marker; RPO = PROTAC RIPK degrader-2, AZD-5 = AZD-5153, P00 = P005091, ZPhe = Z-Phe-CH2Cl, Dac = Dactolisib, AZD-8 = AZD8055, Vis = Vistusertib, WYE = WYE-125132, Rux = Ruxolitinib phosphate, CP = CP 690550 citrate

I was able to confirm the hits as inflammation modulators and proposed the MoA for some compounds but to evaluate the pathway engagement on the whole proteome level, I evaluated inflammation protein expression changes against the M0 control. Overall, I observed that the compounds reduced inflammation pathway activity, indicated by a decrease in inflammation pathway proteins detected after treatment compared to M1 macrophages but residual inflammation activity was still observed (Figure 6.7).

The mTOR inhibitors showed the largest proportion of remaining upregulated inflammation associated proteins (Figure 6.7C). As they were proposed to act in the LPS signalling cascade which showed protein expression changes overall in fewer proteins compared to IFN-γ signalling pathways this could explain the observation. Further analysis of the significantly changing proteins for these compounds revealed association with inflammation pathways but not glycolysis, strengthening the hypothesis that inflammation inhibition was exhibited through the LPS signalling cascade and not by changes in the metabolism. Subsequent metabolomic analysis would provide a more comprehensive picture.

The core inflammatory pathway targeting compounds showed reduced inflammatory protein levels (Figure 6.7A). An interesting compound within this group was the PROTAC RIPK degrader-2 which showed the largest proportion of downregulated proteins across all compounds. Analysis of the differentially regulated proteins revealed significant association with the G1/S-specific transcription (p-value = 0.01, fold enrichment = 18.5), and integrin cell surface interactions (p-value = 0.01, fold enrichment = 6) of the curated reactome pathways. This potentially indicated off-target effects associated to the PROTACs kinase degrading function. All kinases such as cyclin-dependent kinases that regulate the cell cycle and RIPK2 which modulates inflammatory responses share a conserved catalytic domain, a potential source for compound binding that could result in off-target effects.[420]

Finally, I was able to determine effectiveness between the two JAK inhibitors. CP 690550 citrate showed higher residual inflammation protein levels compared to Ruxolitinib phosphate (Figure 6.7B). Further, Ruxolitinib phosphate seemed to be the most potent inflammation inhibitor in this analysis. This inhibitor also clustered closest to the M0 control in PCA (Figure 6.5A) and showed the highest M0 projection z-score in scalar projection analysis after the cytotoxic compounds (Figure 6.3B). This highlighted that proteomics was also able to distinguish effectiveness of on-target compounds.

To summarise, I utilised global proteomics to derive clustering based on the compound MoA. Subsequent analysis with biomarkers allowed for association of MoAs to the different compound clusters. Further, compound effectiveness and potential off-target effects were derived from global proteome pathway engagement analysis.

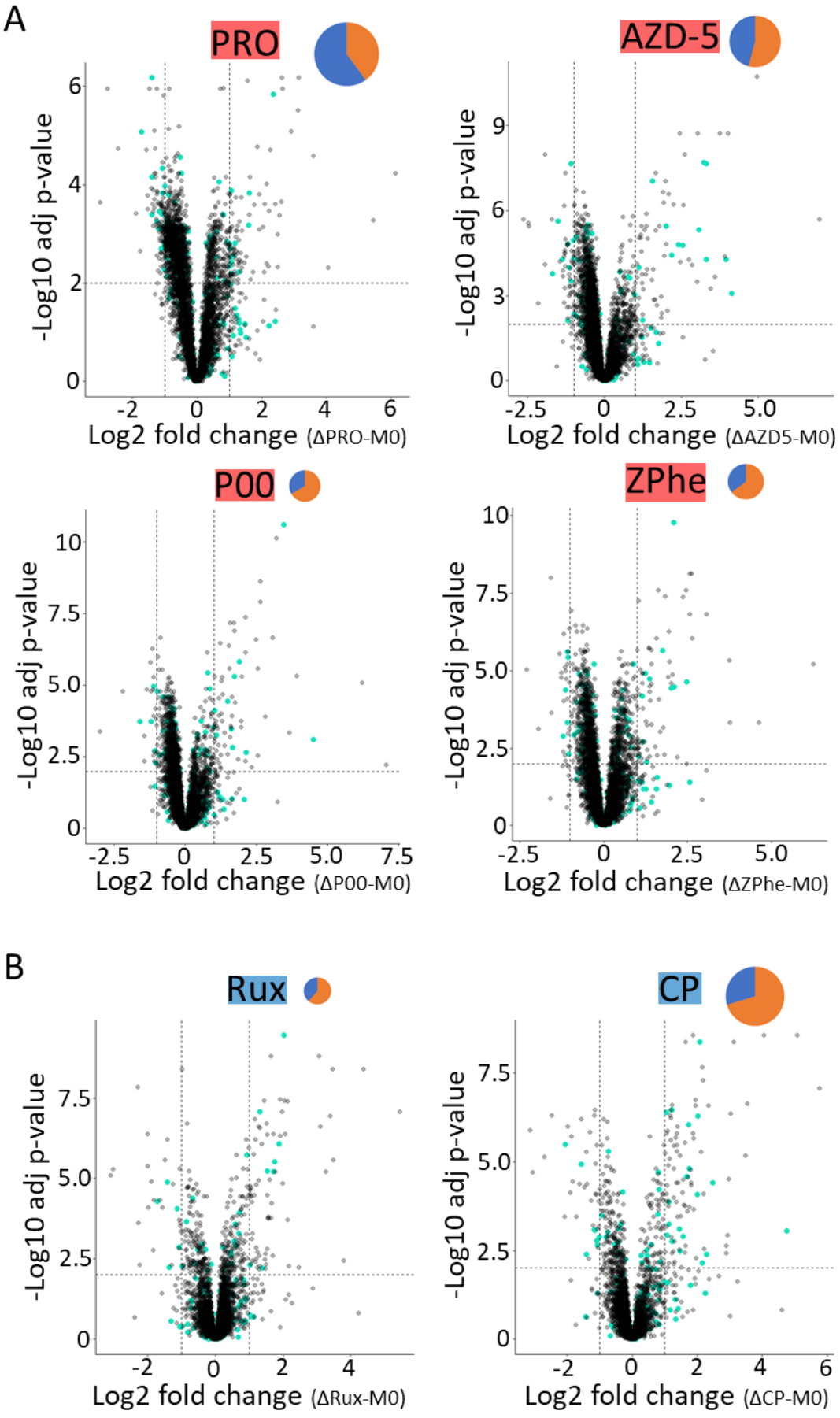
A
PRO
AZD-5
P00
ZPhe
B
Rux
CP
-Log10 adj p-value
Log2 fold change (ΔPRO-M0)
Log2 fold change (ΔAZD5-M0)
Log2 fold change (ΔP00-M0)
Log2 fold change (ΔZPhe-M0)
Log2 fold change (ΔRux-M0)
Log2 fold change (ΔCP-M0)

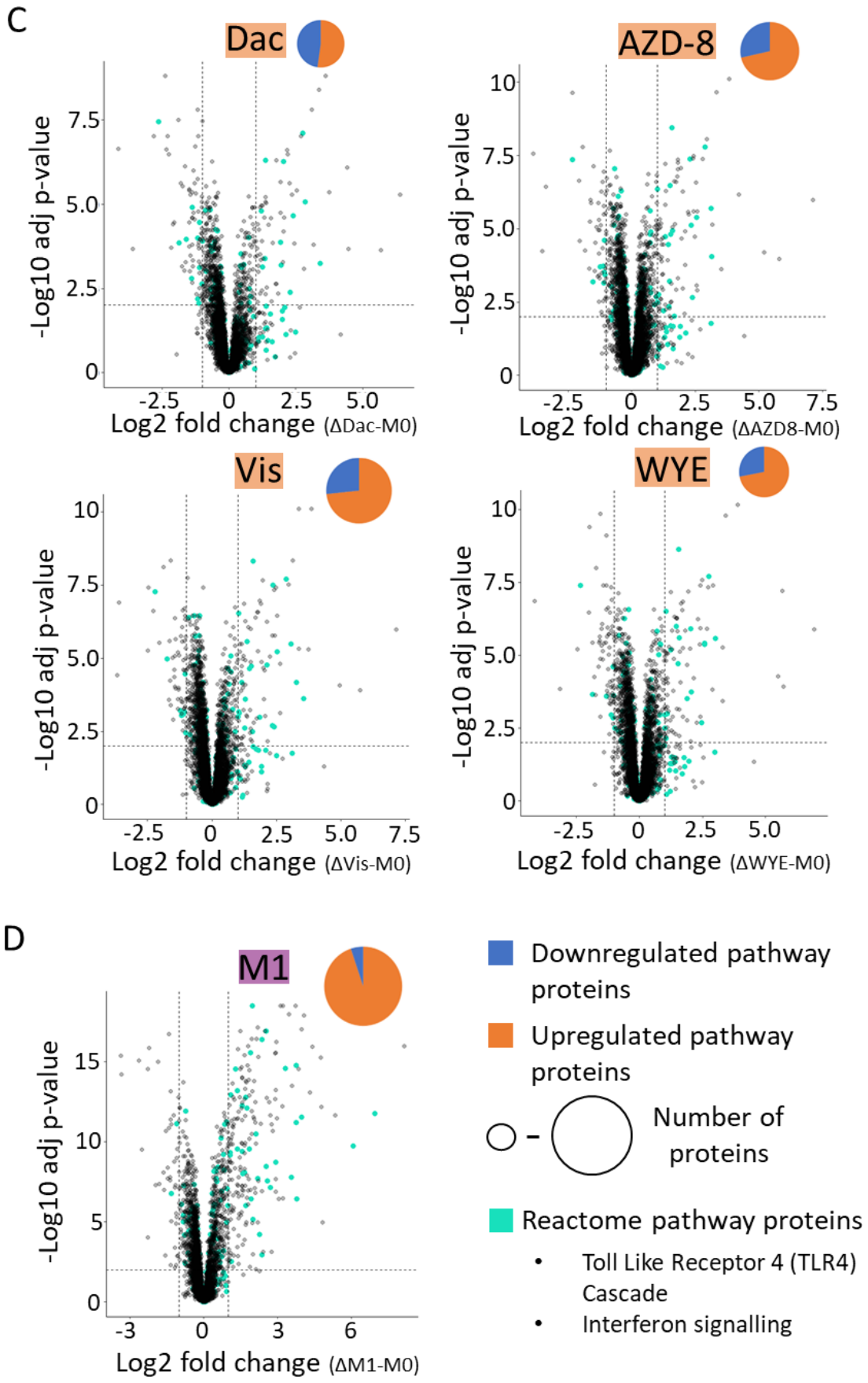

Figure 6.7. Protein expression changes of the set 2 proteomics hit compounds and the M1 control in comparison to the M0 control.

Inflammatory proteins based on their reactome pathway association are labelled and then displayed separated into down- and upregulated proteins in a pie chart (chart size corresponds to number of proteins). Comparison against M0 control for (A) Core inflammatory pathway targeting compounds: RPO = PROTAC RIPK degrader-2, AZD-5 = AZD-5153, P00 = P005091, ZPhe = Z-Phe-CH2Cl; (B) IFN-γ pathway targeting compounds: Rux = Ruxolitinib phosphate, CP = CP 690550 citrate; (C) LPS pathway targeting compounds: Dac = Dactolisib, AZD-8 = AZD8055, Vis = Vistusertib, WYE = WYE-125132; (D) M1 control

6.5 Mechanism of action analysis of HTS inflammation set hits revealed inflammation targets and potential false positive hits

Finally, I assessed whether the six compounds unique to the MALDI-TOF MS screen, the two unique to the cytokine screen , and the two overlapping hit compounds that were all not detected by proteomics were true hits. For these compounds, no cytotoxic or off-target associated GO Bio terms were observed (Figure 6.8).

In the broader inflammation-associated terms such as “inflammatory response” and “response to lipopolysaccharide” or “response to cytokine,” significant fold changes were observed. However, these changes were not highly significant, likely due to the low number of significantly downregulated proteins (2 - 58 proteins per treatment, Supplementary Figure S.7), potentially also explaining why these compounds were not initially identified as hits by proteomics.

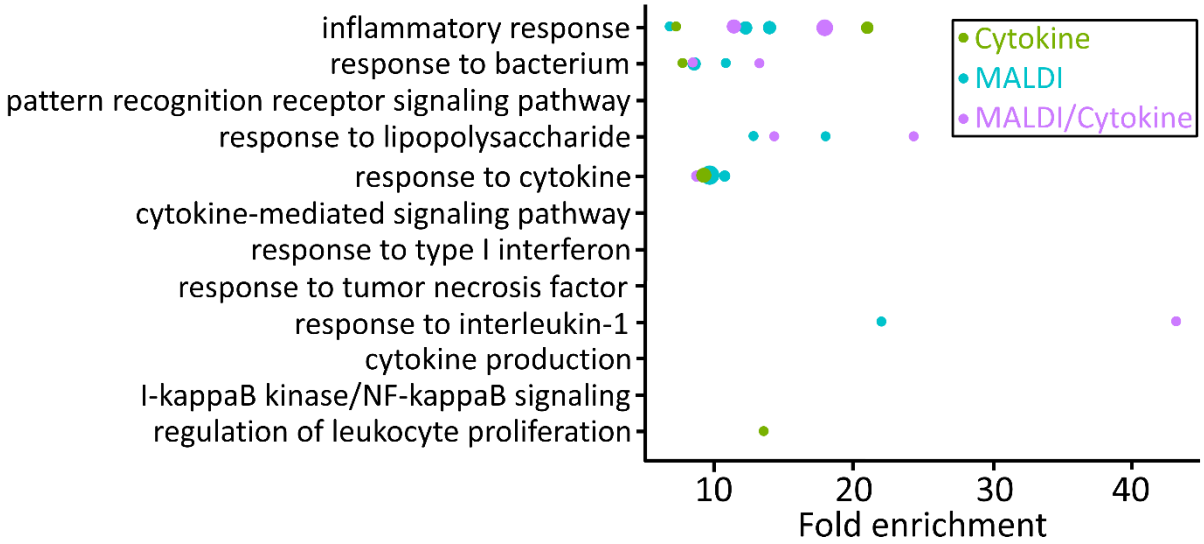

Figure 6.8. GO term association of MALDI-TOF MS and cytokine hit compounds.
Analysis of significantly upregulated proteins after treatment with compounds not identified as proteomics hits but identified as hits in the cytokine (green), MALDI-TOF MS (blue) or both (purple) HTS screens. Fold enrichment from significantly enriched terms (p-value <1E-5) are plotted as small (lower significance) and large (higher significance) dots.

Similarly to the GO term determination, the overall M0-like phenotype scoring across all markers and pathways was much lower for these compounds compared to the previously identified proteomics hit compounds. This was likely due to the reduced number of significantly changing proteins. Despite this, I was able to assign MoAs to some compounds based on the LPS and IFN-γ signalling markers, as well as chemo-and cytokines.

Core inflammatory pathway targeting compounds

I identified two compounds that showed M0 likeness within the IFN-γ and LPS signalling, suggesting core inflammatory pathway targets as eluded to earlier (Figure 6.9). The two hit compounds, ARN-3236 and Neratinib, target kinases which not only induce cell death but also drive inflammation.[421] ARN-3236 targets SIK2, which modulates the transcription factor coactivator CREBBP, regulating inflammation.[422,423] Both compounds were only identified in the MALDI-TOF MS-based screen. Previously, Heap *et al.* 2017 demonstrated that a biochemical MALDI-TOF MS-based screen was well-suited for identifying kinase inhibitors and Weigt *et al.* 2018 have introduced lipid biomarkers that can be used to monitor kinase inhibitor activity in a cellular-based MALDI-TOF MS screen.[122,225]

LPS pathway targeting compounds

The highest M0 likeness in the chemo- and cytokine intensities determined by proteomics was observed for TAK-242 (Figure 6.9), a TLR4 inhibitor detected by both the MALDI-TOF MS and cytokine screens.[424] The non-detection in the initial proteomics screen might be due to the low number of significantly changing proteins and the bias towards IFN-γ signalling detection by proteomics. Furthermore, TCMDC-125545 showed M0 likeness in LPS signalling and uniquely in two chemo- and cytokines (OXLA and GROA), indicating that it might target the LPS signalling pathway too (Figure 6.9). This compound is a PDE inhibitor, and PDE regulates cAMP levels known to inhibit LPS-elicited inflammatory responses.[425] For instance, cAMP antagonists increase pro-inflammatory cytokine levels, which may explain why this compound was identified only by the cytokine and not the MALDI-TOF MS screen.[425] Apremilast, another PDE inhibitor and hit in the cytokine screen, was expected to act via the same pathway, but this could not be confirmed by proteomics.[426]

Overall, half of the hit compounds not identified initially by proteomics were associated with an inflammation-relevant MoA, confirming them as true hits. Re-evaluation of these compounds showed that they were just on the edge of the hit selection via scalar projection (projection score = 0.15 - 0.22). Further, selecting a less stringent p-value (from 0.01 to 0.05) and fold change cut-off (from 2 to 1.5) to determine significantly changing proteins would still align with best practice in proteomics but allow to increase the number of changed proteins. Together, this would have resulted in the compound detection as hits by the proteomics workflow. This highlights the importance of carefully selecting cut-off values to balance missing identifications against false positive detections.

Non-associated compounds

The MALDI-TOF MS and cytokine HT screen hit GSK2580335 was excluded from further analysis as its target annotation was GSK proprietary. The remaining four MALDI-TOF MS screen hit compounds showed even lower M1 biomarker activity, and only 19 differentially expressed proteins on average, preventing confident MoA association (Figure 6.9). Hence, they were not confirmed as true hits by proteomics, indicating that they were potentially false positive hits.

- Ap-III-a4 targets ENO1 which is active in the glucose metabolism which is altered in macrophage inflammation.[427] This hit compound might have been detected by MALDI-TOF MS as shifts in the metabolite and lipid region were observed with this technology. Moving the proteomics analysis towards a focus on metabolism or conducting metabolomics might help to evaluate compound activity.
- LY294002 hydrochloride targets PI3K and may elicit downstream effects in LPS signalling, however cellular changes in a published macrophage-based assay were induced at 25 µM compound concentration, whereas I used only 10 µM.[428]
- T6167923's target annotation was MyD88, but only two proteins were significantly downregulated in response to the compound treatment, and to date, little validation work has been undertaken to confirm the proposed compound target.
- Spermidine trihydrochloride targets eIF5A, EP300, MTP, hCA, NMDAR, which are not associated with inflammation biology (Supplementary Table S.4).

Instead of utilising proteomics, dose-response curves could be recorded to identify false positive hits from the MALDI-TOF MS screen. Dose-response curve screens are commonly performed in HTS efforts to eliminate commonly observed false positives and confirm true hits.

To summarise, proteomics confirmed that some true hits were solely identified in the HTS efforts due to the stringent identification cut-offs values selected in proteomics, highlighting balance between missing identifications and false positive detections. Secondly, proteomics was also able to identify false positive hits form the MALDI-TOF MS screen. These hits were weak identifications in the MALDI-TOF MS screen and hence cut-off modification should also be evaluated in this case as it might prove beneficial to reduce the false positive observations.

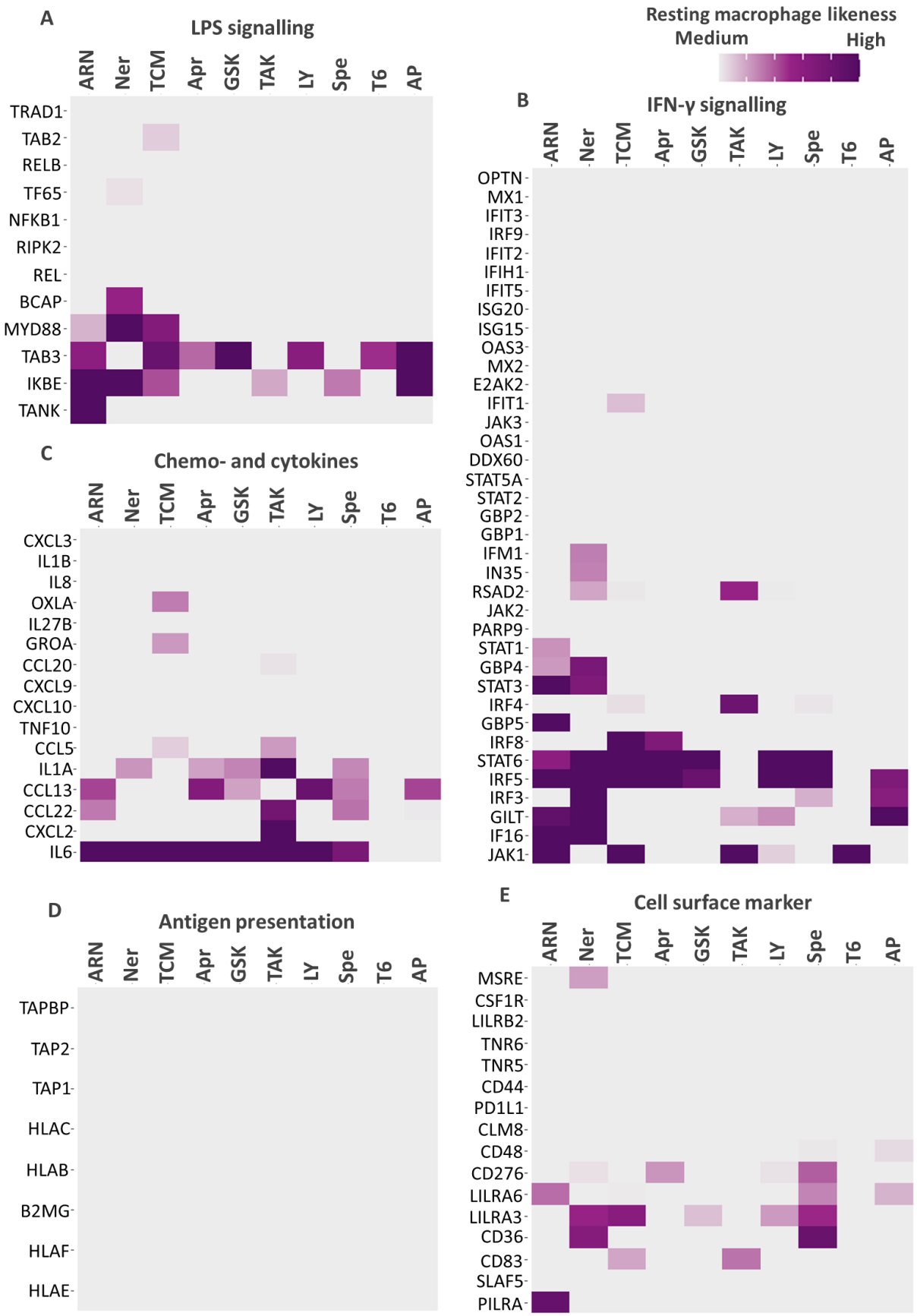

Figure 6.9. M0 macrophage likeness scoring of MALDI-TOF MS and cytokine hit compounds across different signalling pathways.

Log2 protein intensity recorded for each compound treatment was normalised against intensity levels in the M0 and M1 controls for proteins associated to (A) LPS signalling, (B) IFN-γ, (C) chemo- and cytokine, (D) antigen presentation and (E) cell surface marker; $n_{compound} = 3$, ARN = ARN-3236, Ner = Neratinib, TCM = TCMDC-125545, APR = Apremilast, GSK = GSK2580335, TAK = TAK-242, LY = LY294002 hydrochloride, Spe = Spermidine trihydrochloride, T6 = T6167923, AP = Ap-III-a4

6.6 Discussion

The substantial overlap between phenotypic screen hits identified by proteomics, MALDI-TOF MS and cytokine screens demonstrated robust hit calling and assay suitability. Proteomics analysis offered the advantage of deep data depth, enabling early identification of cytotoxic hit compounds. Further, clustering of hit compounds on a global protein level, MoA identification for compounds, determination of compound efficacy and potential identification of off-target effects was achieved by proteomics in a complex multimodal assay that uses multiple cellular stimuli. Proteomics was also able to identify false positive hits from the MALDI-TOF MS screen while failing identification of some true hits due to the stringent cut-off selection.

6.6.1 MoA and target deconvolution tools

MoA and target elucidation using proteomics is a rapidly evolving field. I decided to focus on inflammation protein markers, associating them to different inflammation signalling pathways to aid MoA elucidation of hit compounds. Alternatively to pathway-specific biomarker selection, I could have conducted subsequent screens in the presence of single IFN-γ or LPS stimulation, though this would limit biological complexity as both stimuli act synergistically *in vivo* for robust macrophage activation.

Some researchers have employed full proteome expression atlases to deduce MoAs and off-target effects using a fingerprinting approach.[310] Different data analysis strategies for MoA identification from large proteomics datasets have emerged. For example, a study on lung cancer cell lines subjected to more than 50 compounds improved MoA identification by excluding ubiquitously responding proteins, revealing mitochondrial function inhibition as an off-target effect of PD184352.[429] Mitchel *et al.* 2023 conducted the largest study to date, documenting proteome-level changes induced by 875 compounds in HCT116 cells to link compound structure and MoA.[311] While most approaches use single compound

concentrations to maintain scalability, Eckert *et al.* 2024 demonstrated the advantages of systematic dose-response evaluation, showing that histone deacetylase inhibitors impaired human T cell activation.[397]

Phosphoproteomics has been used to assess the activity of kinase inhibitors on a global phosphopeptide level, with recent work by Zecha *et al.* 2023 highlighting the time- and dose-response characteristics of drug-induced PTMs, revealing kinase inhibitor-specific PTM signatures.[430-432] This indicates an interesting starting point for further experiments to confirm the MoA of the LPS signalling cascade hits that were proposed within this thesis. LPS pathway activation is often associated with PTMs rather than changes in protein levels.[349] Although these approaches shed light on broad proteome changes and MoAs, they are not sufficient to elucidate the drug target.

Chemoproteomics, a field combining chemical biology and MS, has developed to determine drug-target interactions. Approaches can be classified into modification-based and modification-free workflows. Modification-based approaches involve enriching targets by immobilising, tagging, or labelling with probes, followed by affinity- or activity-based profiling.[308] For example, kinobeads coated with kinase inhibitors successfully identified JAK inhibitors in human primary cells.[433] In contrast, modification-free approaches rely on stabilising proteins against thermal, chemical, or enzymatic denaturation upon small molecule binding, thus avoiding perturbation of the probed biology.[15] For instance, thermal proteome profiling has been used to identify the target of losmapimod in acute leukaemia cells.[309] In contrast, the PISA approach uses ligand-induced alterations in protein solubility, offering reduced analysis time and sample consumption in comparison to other modification-free approaches.[434-437] Despite the potential of proteomics to uncover novel MoAs and targets, its throughput remains limited, and sample costs are high compared to non-LC-MS/MS-based tools used for MoA and target deconvolution.

HT, cost-effective cheminformatics tools can predict target interactions based on chemical similarity and protein-target interaction scoring that is derived from large libraries.[42] Biochemical screens expose a hit compound to prospective protein targets for rapid binder screening, although this can reduce biological relevance.[43] Cell Painting, a morphology profiling technology using fluorescence dyes, captures features like cell size, shape, including cellular organelles, allowing the comparison of morphological phenotypes to a reference

library for MoA elucidation.[41] Conversely, DrugSeq involves bulk RNA sequencing of disease-relevant cell models or cells with directed mutations to reveal compound responses such as resistance or sensitivity.[42] Gene signatures generated by this low-cost, HT screen are compared to control compounds or a gene signature library like the Connectivity Map for target and MoA deconvolution.[43]

In summary, each deconvolution tool has its strength and limitations, and therefore they are often simultaneously used. Although knowledge of molecular targets and MoAs is not required for clinical trials or FDA approval, identifying these aspects in early drug discovery stages significantly enhances drug efficacy and safety by uncovering opportunities for therapeutic expansion and anticipating off-target effects like cytotoxicity.[438,439] I presented a proteomics screen that was conducted subsequently of a MALDI-TOF MS and cytokine profiling HTS approach to identify cytotoxic compounds and MoAs related to the IFN-γ+LPS signalling cascades. With continued technological advancements in workflow speed and sensitivity, proteomics is expected to become a more widely used tool for MoA and target identification in earlier stages of drug discovery efforts.

7. **Conclusion and outlook**

Throughout this thesis, I showcased the application of MS-based workflows in early drug discovery efforts, highlighting their advantages and limitations. I demonstrated applications within the immunology field, a cornerstone in drug discovery due to its links to oncology, infectious diseases, and auto-immune disorders amongst others.

I developed a MALDI-TOF MS biochemical drug discovery assay for the high-profile immunology target ERAP1, building upon an established RapidFire MS assay. The development process included optimising buffer composition, analyte ionisation, as well as substrate and enzyme concentrations. Workflow automation enabled robust and reproducible screening of ~10,000 compounds. Activity profiling of pre-determined ERAP1 binders was reproducible by MALDI-TOF MS and showed strong correlation with the established RapidFire MS platform. Hits were validated through dose-response screening, demonstrating the complementary value of these approaches. Both MS-based techniques outperformed label-based assays, which suffered from disrupted physiology and a limited dynamic range.[55] While analyte and buffer optimisations were necessary for the MALDI-TOF MS assay due to the lack of a sample cleanup stage, the optimised assay showed increased throughput, miniaturisation, and reduced costs compared to the RapidFire MS assay.

Further expansion of this MALDI-TOF MS assay format would allow evaluation of hit compound efficacy across different ERAP1 allotypes. Moreover, screening other highly homologous zinc metalloaminopeptidases, may provide insights into off-target effects, aiding lead selection. To increase biological relevance of findings, compound-modulated ERAP1 activity could be analysed by monitoring MHC associated cell surface peptides through immunopeptidomics. Findings could benefit the development of novel drugs in auto-immune and auto-inflammatory diseases, as well as in immune-oncology. In summary, I highlighted the benefits of MS techniques for enzymatic screening approaches in early drug discovery. This leads the way to leverage higher-throughput compatible MS techniques, such as MALDI-TOF MS, in other early drug discovery target-based screens, including affinity binding, and fragment screening, which are still largely dominated by label-based and LC-MS techniques.

Higher-throughput MS tools also hold significant potential for early drug discovery phenotypic screens which promise to deliver more translatable findings. To demonstrate the effectiveness

of MS in phenotypic screening approaches, I selected, optimised, and benchmarked an immunologically relevant phenotypic screening model using iPSC derived macrophages from three human donors. Macrophages are frequently targeted in early drug screening efforts, given their role in many auto-immune and auto-inflammatory diseases, as well as in immune-oncology. I optimised iPSC-derived macrophage cell culture and demonstrated that increased M-CSF exposure heightened macrophage responsiveness to activating stimuli. I examined macrophage response to a dual stimulation with IFN-γ and LPS, synergistic stimulants *in vivo* that robustly activate macrophages during infection. Conversely, I also stimulated macrophages with IL-4, a cytokine involved in tissue repair signalling. Morphological examination confirmed polarisation into classically activated macrophages (M1) with IFN-γ+LPS, and alternatively activated macrophages (M2) with IL-4. Proteomics analysis further characterised the cell phenotypes but revealed little differential protein expression in M2 macrophages, likely due to metabolic shifts that drive M2 polarisation and a shortened stimulation time. However, the workflow effectively detected protein expression changes after M1 macrophage polarisation, identifying pro-inflammatory biomarkers, including cell surface, LPS signalling, IFN-γ signalling, and antigen presentation proteins, as well as chemokines and cytokines.

Building on these findings, I used the adjusted M-CSF concentration and IFN-γ+LPS dual stimulation to develop a MALDI-TOF MS-based, HT compatible phenotypic screen. I optimised various parameters for the MALDI-TOF MS assay such as cell number, extraction buffer, matrix choice, matrix concentration, matrix-sample-ratio, matrix spotting technique and acquisition mass range. This resulted in a novel metabolite/lipid profile-based MALDI-TOF MS screen that robustly clustered resting (M0) and pro-inflammatory (M1) iPSC-derived macrophages across different donors. While it was hypothesised that this clustering approach allows for hit identification and inference of drug MoA, I was unable to achieve compound clustering, possibly due to a mixture of phenotype descriptive and non-descriptive mass features within the analysis. Implementation of machine learning algorithms to refine the data promises improvements. I identified robust “biomarker” mass features that drove the pro-inflammatory cell phenotype. First, I tracked these “biomarkers” in a screen with compounds exhibiting broad mechanism of action, establishing assay robustness. This informed detection of compounds frequently selected as hits in phenotypic screens and indicated activity of

inflammation associated compounds, however MoA association remained ambiguous. An inflammation-specific compound set was used to further profile inflammation signalling pathway engagement, resulting in the detection of 21 hit compounds that overlapped with hit calling from an established cytokine screen, confirming assay performance.

To reduce false-positive hits and determine compound effectiveness, the screening should be extended towards dose-response measurements. Further, interrogating “biomarker” identity could be especially valuable when evaluating disease models by MALDI-TOF MS. A MALDI-TOF MS phenotypic screen analysing high mass range features has already shown utility to identify an anti-inflammatory drug that translated to activity in human monocytes derived from acute myeloid leukaemia.[229] A standardised screening approach based on the low or high mass range of the spectrum should allow transfer across different cell and disease phenotypes without extensive method development that often precedes highly individualised phenotypic screens. While the presented workflow was suitable for hit triaging in drug discovery, it did not elucidate the MoA, and therefore could not distinguish between desired and undesired compound effects such as cytotoxicity. MoA could be explored by conducting screens with a single pro-inflammatory stimulus to deconvolute target engagement, however this would reduce the physiological relevance of the model. Cell viability assays could be used to evaluate compound cytotoxicity but would reduce workflow throughput and increase workflow cost.

Instead, to distinguish desired and undesired compound effects, I employed proteomics which is traditionally used for biological target identification, and drug-target interaction elucidation in the drug discovery pipeline via historically low throughput methods. Here, I presented a medium-throughput proteomics workflow, which showed a large overlap in hit calling with the MALDI-TOF MS and chemokine screens for inflammation-specific compounds. Despite being lower throughput, the proteomics workflow had a major advantage in informing the compound’s MoA. I identified known cell death inducers, including inhibitors of kinases and histone modulators, as well as inflammation-specific compounds that induced cell death at higher concentrations. I revealed non-toxic hit compound clustering based on global protein expression and analysed the expression of pro-inflammatory M1 protein markers to propose a MoA for these compounds. Proteomics uniquely identified inhibitors acting only within the IFN-γ signalling cascade when compared to the MALDI-TOF MS and cytokine screen. By protein level comparison of the non-toxic hits against the resting macrophages, compound efficacy

and non-toxic off-target effects were determined. The proteomics workflow further identified false positive hits from the MALDI-TOF MS screen yet showed some false negative hits due to the stringent cut-off selection, highlighting the need to carefully balance cut-off values. Leveraging a new wave of higher-throughput proteomics technologies, I highlighted the power of proteomics in an initial step to profile drug MoA of HTS hits, particularly in complex multimodal assays that use multiple stimuli. With further advancements in sample preparation and MS technology, proteomics could become a standard tool in phenotypic screening, similar to the adoption of transcriptomics. A next step is to conduct more target-focussed analyses such as chemoproteomics to elucidate drug-target interactions.

In conclusion, I demonstrated that MALDI-TOF MS is a valuable tool for hit-triaging in target-based enzymatic and phenotypic screens in the lead generation stage of the drug discovery pipeline. Furthermore, I showed that a proteomics workflow with moderate throughput can significantly improve lead compound selection by elucidating off-target effects, such as toxicity and pathway-specific mechanisms of action. To develop this work further, additional inflammation-associated stimuli, such as bacteria could be employed, thereby expanding the application to a wider range of research questions while further assessing workflow performance and versatility. Efforts to improve pipeline efficiency in early drug discovery calls for utilisation of more biologically relevant models, and here my work contributes to advancing the application of MS technologies alongside iPSC derived models to meet these needs. Different cell models outside of immunology should be subjected to the developed workflows to establish transferability. Given the growing number of publications and technological developments in the MS field, I believe that MS will continue to gain further importance in early-stage drug discovery.

References

1. Osuchowski MF, Winkler MS, Skirecki T, et al. The COVID-19 puzzle: deciphering pathophysiology and phenotypes of a new disease entity. *Lancet Respir Med*. Jun 2021;9(6):622-642. doi:10.1016/S2213-2600(21)00218-6
2. Aslam B, Wang W, Arshad MI, et al. Antibiotic resistance: a rundown of a global crisis. *Infect Drug Resist*. 2018;11:1645-1658. doi:10.2147/IDR.S173867
3. Liu Z, Hu M, Yang Y, et al. An overview of PROTACs: a promising drug discovery paradigm. *Mol Biomed*. Dec 20 2022;3(1):46. doi:10.1186/s43556-022-00112-0
4. de Smet MD, Meenken CJ, van den Horn GJ. Fomivirsen - a phosphorothioate oligonucleotide for the treatment of CMV retinitis. *Ocul Immunol Inflamm*. Dec 1999;7(3-4):189-98. doi:10.1076/ocii.7.3.189.4007
5. Her M, Kavanaugh A. Alterations in immune function with biologic therapies for autoimmune disease. *J Allergy Clin Immunol*. Jan 2016;137(1):19-27. doi:10.1016/j.jaci.2015.10.023
6. Macy E. Immune-Related Adverse Drug Reactions and Immunologically Mediated Drug Hypersensitivity. *Immunol Allergy Clin North Am*. Nov 2020;40(4):635-647. doi:10.1016/j.iac.2020.06.003
7. Sun D, Gao W, Hu H, Zhou S. Why 90% of clinical drug development fails and how to improve it? *Acta Pharm Sin B*. Jul 2022;12(7):3049-3062. doi:10.1016/j.apsb.2022.02.002
8. Mohs RC, Greig NH. Drug discovery and development: Role of basic biological research. *Alzheimers Dement (N Y)*. Nov 2017;3(4):651-657. doi:10.1016/j.trci.2017.10.005
9. Wildey MJ, Haunso A, Tudor M, Webb M, Connick JH. Chapter Five - High-Throughput Screening. In: Goodnow RA, ed. *Annual Reports in Medicinal Chemistry*. Academic Press; 2017:149-195.
10. Hughes JP, Rees S, Kalindjian SB, Philpott KL. Principles of early drug discovery. *Br J Pharmacol*. Mar 2011;162(6):1239-49. doi:10.1111/j.1476-5381.2010.01127.x
11. Hefti FF. Requirements for a lead compound to become a clinical candidate. *BMC Neurosci*. Dec 10 2008;9 Suppl 3(Suppl 3):S7. doi:10.1186/1471-2202-9-S3-S7
12. Urban PL. Quantitative mass spectrometry: an overview. *Philos Trans A Math Phys Eng Sci*. Oct 28 2016;374(2079)doi:10.1098/rsta.2015.0382
13. Liu M, Van Voorhis WC, Quinn RJ. Development of a target identification approach using native mass spectrometry. *Sci Rep*. Jan 27 2021;11(1):2387. doi:10.1038/s41598-021-81859-4
14. Meissner F, Geddes-McAlister J, Mann M, Bantscheff M. The emerging role of mass spectrometry-based proteomics in drug discovery. *Nat Rev Drug Discov*. Sep 2022;21(9):637-654. doi:10.1038/s41573-022-00409-3
15. George AL, Dueñas ME, Marín-Rubio JL, Trost M. Stability-based approaches in chemoproteomics. *Expert Rev Mol Med*. Apr 12 2024;26:e6. doi:10.1017/erm.2024.6
16. Chen G, Pramanik BN, Liu YH, Mirza UA. Applications of LC/MS in structure identifications of small molecules and proteins in drug discovery. *J Mass Spectrom*. Mar 2007;42(3):279-87. doi:10.1002/jms.1184
17. Cuyckens F. Mass spectrometry in drug metabolism and pharmacokinetics: Current trends and future perspectives. *Rapid Commun Mass Spectrom*. Jul 2019;33 Suppl 3:90-95. doi:10.1002/rcm.8235

18. Castellino S, Lareau NM, Groseclose MR. The emergence of imaging mass spectrometry in drug discovery and development: Making a difference by driving decision making. *J Mass Spectrom*. Aug 2021;56(8):e4717. doi:10.1002/jms.4717
19. Cornett DS, Frappier SL, Caprioli RM. MALDI-FTICR imaging mass spectrometry of drugs and metabolites in tissue. *Anal Chem*. Jul 15 2008;80(14):5648-53. doi:10.1021/ac800617s
20. Naithani U, Guleria V. Integrative computational approaches for discovery and evaluation of lead compound for drug design. Review. *Frontiers in Drug Discovery*. 2024;4
21. Prudent R, Annis DA, Dandliker PJ, Ortholand JY, Roche D. Exploring new targets and chemical space with affinity selection-mass spectrometry. *Nat Rev Chem*. Jan 2021;5(1):62-71. doi:10.1038/s41570-020-00229-2
22. Kairys V, Baranauskiene L, Kazlauskiene M, Matulis D, Kazlauskas E. Binding affinity in drug design: experimental and computational techniques. *Expert Opin Drug Discov*. Aug 2019;14(8):755-768. doi:10.1080/17460441.2019.1623202
23. Peterson AA, Liu DR. Small-molecule discovery through DNA-encoded libraries. *Nat Rev Drug Discov*. Sep 2023;22(9):699-722. doi:10.1038/s41573-023-00713-6
24. Erlanson DA, Fesik SW, Hubbard RE, Jahnke W, Jhoti H. Twenty years on: the impact of fragments on drug discovery. *Nat Rev Drug Discov*. Sep 2016;15(9):605-619. doi:10.1038/nrd.2016.109
25. Kirsch P, Hartman AM, Hirsch AKH, Empting M. Concepts and Core Principles of Fragment-Based Drug Design. *Molecules*. Nov 26 2019;24(23)doi:10.3390/molecules24234309
26. Kuljanin M, Mitchell DC, Schweppe DK, et al. Reimagining high-throughput profiling of reactive cysteines for cell-based screening of large electrophile libraries. *Nat Biotechnol*. May 2021;39(5):630-641. doi:10.1038/s41587-020-00778-3
27. Biggs GS, Cawood EE, Vuorinen A, et al. Robust proteome profiling of cysteine-reactive fragments using label-free chemoproteomics. *bioRxiv*. 2024:2024.07.25.605137. doi:10.1101/2024.07.25.605137
28. Keeley A, Petri L, Ábrányi-Balogh P, Keserű GM. Covalent fragment libraries in drug discovery. *Drug Discov Today*. Jun 2020;25(6):983-996. doi:10.1016/j.drudis.2020.03.016
29. Holdgate GA, Meek TD, Grimley RL. Mechanistic enzymology in drug discovery: a fresh perspective. *Nat Rev Drug Discov*. Jan 2018;17(1):78. doi:10.1038/nrd.2017.257
30. Leveridge MV, Bardera AI, LaMarr W, et al. Lead discovery for microsomal prostaglandin E synthase using a combination of high-throughput fluorescent-based assays and RapidFire mass spectrometry. *J Biomol Screen*. Jun 2012;17(5):641-50. doi:10.1177/1087057111435700
31. Meng J, Lai MT, Munshi V, et al. Screening of HIV-1 Protease Using a Combination of an Ultra-High-Throughput Fluorescent-Based Assay and RapidFire Mass Spectrometry. *J Biomol Screen*. Jun 2015;20(5):606-15. doi:10.1177/1087057115570838
32. Takamiya M, Sakurai M, Teranishi F, Ikeda T, Kamiyama T, Asai A. Lead discovery for mammalian elongation of long chain fatty acids family 6 using a combination of high-throughput fluorescent-based assay and RapidFire mass spectrometry assay. *Biochem Biophys Res Commun*. Nov 25 2016;480(4):721-726. doi:10.1016/j.bbrc.2016.10.103

33. Adam GC, Meng J, Rizzo JM, et al. Use of high-throughput mass spectrometry to reduce false positives in protease uHTS screens. *J Biomol Screen*. Feb 2015;20(2):212-22. doi:10.1177/1087057114555832
34. Liu C, Li T, Chen J. Role of High-Throughput Electrophysiology in Drug Discovery. *Curr Protoc Pharmacol*. Dec 2019;87(1):e69. doi:10.1002/cpph.69
35. Vincent F, Nueda A, Lee J, Schenone M, Prunotto M, Mercola M. Phenotypic drug discovery: recent successes, lessons learned and new directions. *Nat Rev Drug Discov*. Dec 2022;21(12):899-914. doi:10.1038/s41573-022-00472-w
36. Moffat JG, Vincent F, Lee JA, Eder J, Prunotto M. Opportunities and challenges in phenotypic drug discovery: an industry perspective. *Nat Rev Drug Discov*. Aug 2017;16(8):531-543. doi:10.1038/nrd.2017.111
37. Vincent F, Loria P, Pregel M, et al. Developing predictive assays: the phenotypic screening "rule of 3". *Sci Transl Med*. Jun 24 2015;7(293):293ps15. doi:10.1126/scitranslmed.aab1201
38. Berg A, Hallowell S, Tibbetts M, et al. High-Throughput Surface Liquid Absorption and Secretion Assays to Identify F508del CFTR Correctors Using Patient Primary Airway Epithelial Cultures. *SLAS Discov*. Aug 2019;24(7):724-737. doi:10.1177/2472555219849375
39. Platchek M, Lu Q, Tran H, Xie W. Comparative Analysis of Multiple Immunoassays for Cytokine Profiling in Drug Discovery. *SLAS Discov*. Dec 2020;25(10):1197-1213. doi:10.1177/2472555220954389
40. Ullas S, Sinclair C. Applications of Flow Cytometry in Drug Discovery and Translational Research. *Int J Mol Sci*. Mar 29 2024;25(7)doi:10.3390/ijms25073851
41. Bray MA, Singh S, Han H, et al. Cell Painting, a high-content image-based assay for morphological profiling using multiplexed fluorescent dyes. *Nat Protoc*. Sep 2016;11(9):1757-74. doi:10.1038/nprot.2016.105
42. Hughes RE, Elliott RJR, Dawson JC, Carragher NO. High-content phenotypic and pathway profiling to advance drug discovery in diseases of unmet need. *Cell Chem Biol*. Mar 18 2021;28(3):338-355. doi:10.1016/j.chembiol.2021.02.015
43. Wilkinson IVL, Terstappen GC, Russell AJ. Combining experimental strategies for successful target deconvolution. *Drug Discov Today*. Sep 21 2020;doi:10.1016/j.drudis.2020.09.016
44. Dueñas ME, Peltier-Heap RE, Leveridge M, Annan RS, Büttner FH, Trost M. Advances in high-throughput mass spectrometry in drug discovery. *EMBO Mol Med*. Jan 11 2023;15(1):e14850. doi:10.15252/emmm.202114850
45. Challen B, Cramer R. Advances in ionisation techniques for mass spectrometry-based omics research. *Proteomics*. Aug 2022;22(15-16):e2100394. doi:10.1002/pmic.202100394
46. El-Aneed A, Cohen A, Banoub J. Mass Spectrometry, Review of the Basics: Electrospray, MALDI, and Commonly Used Mass Analyzers. *Applied Spectroscopy Reviews*. 2009/04/01 2009;44(3):210-230. doi:10.1080/05704920902717872
47. Taflin DC, Ward TL, Davis EJ. Electrified droplet fission and the Rayleigh limit. *Langmuir*. 1989/03/01 1989;5(2):376-384. doi:10.1021/la00086a016
48. Banerjee S, Mazumdar S. Electrospray ionization mass spectrometry: a technique to access the information beyond the molecular weight of the analyte. *Int J Anal Chem*. 2012;2012:282574. doi:10.1155/2012/282574

49. Bretschneider T, Ozbal C, Holstein M, et al. RapidFire BLAZE-Mode Is Boosting ESI-MS Toward High-Throughput-Screening. *SLAS Technol*. Aug 2019;24(4):386-393. doi:10.1177/2472630318822449
50. Leveridge M, Buxton R, Argyrou A, et al. Demonstrating enhanced throughput of RapidFire mass spectrometry through multiplexing using the JmjD2d demethylase as a model system. *J Biomol Screen*. Feb 2014;19(2):278-86. doi:10.1177/1087057113496276
51. McManus J, He T, Gavigan JA, et al. A Robust Multiplex Mass Spectrometric Assay for Screening Small-Molecule Inhibitors of CD73 with Diverse Inhibition Modalities. *SLAS Discov*. Mar 2018;23(3):264-273. doi:10.1177/2472555217750386
52. Resnick E, Bradley A, Gan J, et al. Rapid Covalent-Probe Discovery by Electrophile-Fragment Screening. *J Am Chem Soc*. Jun 05 2019;141(22):8951-8968. doi:10.1021/jacs.9b02822
53. Thomas RP, Heap RE, Zappacosta F, et al. A direct-to-biology high-throughput chemistry approach to reactive fragment screening. *Chem Sci*. Sep 22 2021;12(36):12098-12106. doi:10.1039/d1sc03551g
54. Hutchinson SE, Leveridge MV, Heathcote ML, et al. Enabling lead discovery for histone lysine demethylases by high-throughput RapidFire mass spectrometry. *J Biomol Screen*. Jan 2012;17(1):39-48. doi:10.1177/1087057111416660
55. Liddle J, Hutchinson JP, Kitchen S, et al. Targeting the Regulatory Site of ER Aminopeptidase 1 Leads to the Discovery of a Natural Product Modulator of Antigen Presentation. *J Med Chem*. Mar 26 2020;63(6):3348-3358. doi:10.1021/acs.jmedchem.9b02123
56. Soulard P, McLaughlin M, Stevens J, et al. Development of a high-throughput screening assay for stearoyl-CoA desaturase using rat liver microsomes, deuterium labeled stearoyl-CoA and mass spectrometry. *Anal Chim Acta*. Oct 03 2008;627(1):105-11. doi:10.1016/j.aca.2008.04.017
57. Jonas M, LaMarr WA, Ozbal C. Mass spectrometry in high-throughput screening: a case study on acetyl-coenzyme a carboxylase using RapidFire--mass spectrometry (RF-MS). *Comb Chem High Throughput Screen*. Sep 2009;12(8):752-9. doi:10.2174/138620709789104924
58. Leveridge M, Collier L, Edge C, et al. A High-Throughput Screen to Identify LRRK2 Kinase Inhibitors for the Treatment of Parkinson's Disease Using RapidFire Mass Spectrometry. *J Biomol Screen*. Feb 2016;21(2):145-55. doi:10.1177/1087057115606707
59. Uchiyama N, Dougan DR, Lawson JD, et al. Identification of AHCY inhibitors using novel high-throughput mass spectrometry. *Biochem Biophys Res Commun*. Sep 09 2017;491(1):1-7. doi:10.1016/j.bbrc.2017.05.107
60. Yoneyama-Hirozane M, Matsumoto SI, Toyoda Y, et al. Identification of PARP14 inhibitors using novel methods for detecting auto-ribosylation. *Biochem Biophys Res Commun*. May 06 2017;486(3):626-631. doi:10.1016/j.bbrc.2017.03.052
61. Bretschneider T, Luippold AH, Romig H, et al. Ultrafast and Predictive Mass Spectrometry-Based Autotaxin Assays for Label-Free Potency Screening. *SLAS Discov*. Apr 2017;22(4):425-432. doi:10.1177/2472555217690484
62. Dittakavi S, Mahadevan L, Chandrashekar DV, et al. High-throughput screening assay for the quantification of Cer d18:1/16:0, d18:1/24:0, d18:1/24:1, d18:1/18:0, d18:1/14:0, d18:1/20:0, and d18:1/22:0 in HepG2 cells using RapidFire mass spectrometry. *Biomed Chromatogr*. May 2020;34(5):e4790. doi:10.1002/bmc.4790

63. Gordon LJ, Allen M, Artursson P, et al. Direct Measurement of Intracellular Compound Concentration by RapidFire Mass Spectrometry Offers Insights into Cell Permeability. *J Biomol Screen*. Feb 2016;21(2):156-64. doi:10.1177/1087057115604141
64. Highkin MK, Yates MP, Nemirovskiy OV, et al. High-throughput screening assay for sphingosine kinase inhibitors in whole blood using RapidFire® mass spectrometry. *J Biomol Screen*. Feb 2011;16(2):272-7. doi:10.1177/1087057110391656
65. Häbe TT, Liu C, Covey TR, et al. Ultrahigh-Throughput ESI-MS: Sampling Pushed to Six Samples per Second by Acoustic Ejection Mass Spectrometry. *Anal Chem*. Sep 15 2020;92(18):12242-12249. doi:10.1021/acs.analchem.0c01632
66. Zhang H. Acoustic dispensing-mass spectrometry: the next high throughput bioanalytical platform for early drug discovery. *Bioanalysis*. Nov 2017;9(21):1619-1621. doi:10.4155/bio-2017-4980
67. Wen X, Liu C, Ghislain L, et al. Direct Analysis from Phase-Separated Liquid Samples using ADE-OPI-MS: Applicability to High-Throughput Screening for Inhibitors of Diacylglycerol Acyltransferase 2. *Anal Chem*. Apr 20 2021;93(15):6071-6079. doi:10.1021/acs.analchem.0c04312
68. Winter M, Simon RP, Häbe TT, et al. Label-free high-throughput screening via acoustic ejection mass spectrometry put into practice. *SLAS Discov*. Jul 2023;28(5):240-246. doi:10.1016/j.slasd.2023.04.001
69. Simon RP, Häbe TT, Ries R, et al. Acoustic Ejection Mass Spectrometry: A Fully Automatable Technology for High-Throughput Screening in Drug Discovery. *SLAS Discov*. Sep 2021;26(8):961-973. doi:10.1177/24725552211028135
70. Speckmeier E, Pommereau A, Grosser KC, et al. A high-throughput screening assay for mutant isocitrate dehydrogenase 1 using acoustic droplet ejection mass spectrometry. *SLAS Discov*. Jul 2022;27(5):298-305. doi:10.1016/j.slasd.2022.04.002
71. Zacharias AO, Liu C, VanAernum ZL, et al. Ultrahigh-Throughput Intact Protein Analysis with Acoustic Ejection Mass Spectrometry. *J Am Soc Mass Spectrom*. Jan 04 2023;34(1):4-9. doi:10.1021/jasms.2c00276
72. Sinclair I, Davies G, Semple H. Acoustic mist ionization mass spectrometry (AMI-MS) as a drug discovery platform. *Expert Opin Drug Discov*. Jul 2019;14(7):609-617. doi:10.1080/17460441.2019.1613369
73. Morato NM, Cooks RG. Desorption Electrospray Ionization Mass Spectrometry: 20 Years. *Acc Chem Res*. Sep 19 2023;56(18):2526-2536. doi:10.1021/acs.accounts.3c00382
74. Morato NM, Holden DT, Cooks RG. High-Throughput Label-Free Enzymatic Assays Using Desorption Electrospray-Ionization Mass Spectrometry. *Angew Chem Int Ed Engl*. Nov 09 2020;59(46):20459-20464. doi:10.1002/anie.202009598
75. Morato NM, Le MT, Holden DT, Graham Cooks R. Automated High-Throughput System Combining Small-Scale Synthesis with Bioassays and Reaction Screening. *SLAS Technol*. Dec 2021;26(6):555-571. doi:10.1177/24726303211047839
76. Kulathunga SC, Morato NM, Zhou Q, Cooks RG, Mesecar AD. Desorption Electrospray Ionization Mass Spectrometry Assay for Label-Free Characterization of SULT2B1b Enzyme Kinetics. *ChemMedChem*. May 04 2022;17(9):e202200043. doi:10.1002/cmdc.202200043
77. Szalwinski LJ, Gonzalez LE, Morato NM, Marsh BM, Cooks RG. Bacterial growth monitored by two-dimensional tandem mass spectrometry. *Analyst*. Feb 28 2022;147(5):940-946. doi:10.1039/d1an01901e

78. Mrksich M. Mass spectrometry of self-assembled monolayers: a new tool for molecular surface science. *ACS Nano*. Jan 2008;2(1):7-18. doi:10.1021/nn7004156
79. VanderPorten EC, Scholle MD, Sherrill J, Tran JC, Liu Y. Identification of Small-Molecule Noncovalent Binders Utilizing SAMDI Technology. *SLAS Discov*. Dec 2017;22(10):1211-1217. doi:10.1177/2472555217712761
80. Scholle MD, McLaughlin D, Gurard-Levin ZA. High-Throughput Affinity Selection Mass Spectrometry Using SAMDI-MS to Identify Small-Molecule Binders of the Human Rhinovirus 3C Protease. *SLAS Discov*. Sep 2021;26(8):974-983. doi:10.1177/24725552211023211
81. Gurard-Levin ZA, Kilian KA, Kim J, Bähr K, Mrksich M. Peptide arrays identify isoform-selective substrates for profiling endogenous lysine deacetylase activity. *ACS Chem Biol*. Sep 17 2010;5(9):863-73. doi:10.1021/cb100088g
82. Gurard-Levin ZA, Scholle MD, Eisenberg AH, Mrksich M. High-throughput screening of small molecule libraries using SAMDI mass spectrometry. *ACS Comb Sci*. Jul 11 2011;13(4):347-50. doi:10.1021/co2000373
83. Ban L, Pettit N, Li L, et al. Discovery of glycosyltransferases using carbohydrate arrays and mass spectrometry. *Nat Chem Biol*. Sep 2012;8(9):769-73. doi:10.1038/nchembio.1022
84. Swalm BM, Hallenbeck KK, Majer CR, et al. Convergent evolution of chromatin modification by structurally distinct enzymes: comparative enzymology of histone H3 Lys^{27} methylation by human polycomb repressive complex 2 and vSET. *Biochem J*. Jul 15 2013;453(2):241-7. doi:10.1042/BJ20130439
85. Patel K, Sherrill J, Mrksich M, Scholle MD. Discovery of SIRT3 Inhibitors Using SAMDI Mass Spectrometry. *J Biomol Screen*. Aug 2015;20(7):842-8. doi:10.1177/1087057115588512
86. Anderson SE, Fahey NS, Park J, O'Kane PT, Mirkin CA, Mrksich M. A high-throughput SAMDI-mass spectrometry assay for isocitrate dehydrogenase 1. *Analyst*. Jun 07 2020;145(11):3899-3908. doi:10.1039/d0an00174k
87. Scholle MD, Liu C, Deval J, Gurard-Levin ZA. Label-Free Screening of SARS-CoV-2 NSP14 Exonuclease Activity Using SAMDI Mass Spectrometry. *SLAS Discov*. Jul 2021;26(6):766-774. doi:10.1177/24725552211008854
88. Scholle MD, O'Kane PT, Dib S, Gurard-Levin ZA. Label-free duplex SAMDI-MS screen reveals novel SARS-CoV-2 3CLpro inhibitors. *Antiviral Res*. Apr 2022;200:105279. doi:10.1016/j.antiviral.2022.105279
89. Simon RP, Winter M, Kleiner C, et al. MALDI-TOF-Based Affinity Selection Mass Spectrometry for Automated Screening of Protein-Ligand Interactions at High Throughput. *SLAS Discov*. Jan 2021;26(1):44-57. doi:10.1177/2472555220959266
90. Karas M, Bachmann D, Hillenkamp F. Influence of the wavelength in high-irradiance ultraviolet laser desorption mass spectrometry of organic molecules. *Analytical Chemistry*. 1985/12/01 1985;57(14):2935-2939. doi:10.1021/ac00291a042
91. Tanaka K, Waki H, Ido Y, et al. Protein and polymer analyses up to m/z 100 000 by laser ionization time-of-flight mass spectrometry. *Rapid Communications in Mass Spectrometry*. 1988/08/01 1988;2(8):151-153. doi:https://doi.org/10.1002/rcm.1290020802
92. Edwards JR, Ruparel H, Ju J. Mass-spectrometry DNA sequencing. *Mutat Res*. Jun 03 2005;573(1-2):3-12. doi:10.1016/j.mrfmmm.2004.07.021

93. Harvey DJ. Analysis of carbohydrates and glycoconjugates by matrix-assisted laser desorption/ionization mass spectrometry: An update for 2013-2014. *Mass Spectrom Rev*. Jul 2018;37(4):353-491. doi:10.1002/mas.21530
94. Leopold J, Popkova Y, Engel KM, Schiller J. Recent Developments of Useful MALDI Matrices for the Mass Spectrometric Characterization of Lipids. *Biomolecules*. Dec 13 2018;8(4)doi:10.3390/biom8040173
95. Dreisewerd K. The desorption process in MALDI. *Chem Rev*. Feb 2003;103(2):395-426. doi:10.1021/cr010375i
96. Kafka AP, Kleffmann T, Rades T, McDowell A. The application of MALDI TOF MS in biopharmaceutical research. *Int J Pharm*. Sep 30 2011;417(1-2):70-82. doi:10.1016/j.ijpharm.2010.12.010
97. Vestal ML, Juhasz P, Martin SA. Delayed extraction matrix-assisted laser desorption time-of-flight mass spectrometry. *Rapid Communications in Mass Spectrometry*. 2024/11/27 1995;9(11):1044-1050. doi:https://doi.org/10.1002/rcm.1290091115
98. Bahr U, Stahl-Zeng J, Gleitsmann E, Karas M. Delayed extraction time-of-flight MALDI mass spectrometry of proteins above 25,000 Da. *J Mass Spectrom*. Oct 1997;32(10):1111-6. doi:10.1002/(sici)1096-9888(199711)32:10<1111::aid-jms567>3.0.co;2-y
99. Nakayama K, Li X, Shimizu K, et al. qShot MALDI analysis: A rapid, simple, convenient, and reliable quantitative phospholipidomics approach using MALDI-TOF/MS. *Talanta*. Mar 01 2023;254:124099. doi:10.1016/j.talanta.2022.124099
100. Heijs B, Potthoff A, Soltwisch J, Dreisewerd K. MALDI-2 for the Enhanced Analysis of N-Linked Glycans by Mass Spectrometry Imaging. *Analytical Chemistry*. 2020/10/20 2020;92(20):13904-13911. doi:10.1021/acs.analchem.0c02732
101. Laiko VV, Taranenko NI, Berkout VD, et al. Desorption/ionization of biomolecules from aqueous solutions at atmospheric pressure using an infrared laser at 3 microm. *J Am Soc Mass Spectrom*. Apr 2002;13(4):354-61. doi:10.1016/s1044-0305(02)00341-0
102. Cramer R, Pirkl A, Hillenkamp F, Dreisewerd K. Liquid AP-UV-MALDI enables stable ion yields of multiply charged peptide and protein ions for sensitive analysis by mass spectrometry. *Angew Chem Int Ed Engl*. Feb 18 2013;52(8):2364-7. doi:10.1002/anie.201208628
103. Ryumin P, Brown J, Morris M, Cramer R. Investigation and optimization of parameters affecting the multiply charged ion yield in AP-MALDI MS. *Methods*. Jul 15 2016;104:11-20. doi:10.1016/j.ymeth.2016.01.015
104. Ryumin P, Cramer R. The composition of liquid atmospheric pressure matrix-assisted laser desorption/ionization matrices and its effect on ionization in mass spectrometry. *Anal Chim Acta*. Jul 12 2018;1013:43-53. doi:10.1016/j.aca.2018.01.070
105. Krenkel H, Brown J, Richardson K, Hoyes E, Morris M, Cramer R. Ultrahigh-Throughput Sample Analysis Using Liquid Atmospheric Pressure Matrix-Assisted Laser Desorption/Ionization Mass Spectrometry. *Anal Chem*. Mar 15 2022;94(10):4141-4145. doi:10.1021/acs.analchem.1c05614
106. Krenkel H, Hartmane E, Piras C, Brown J, Morris M, Cramer R. Advancing Liquid Atmospheric Pressure Matrix-Assisted Laser Desorption/Ionization Mass Spectrometry Toward Ultrahigh-Throughput Analysis. *Anal Chem*. Feb 18 2020;92(4):2931-2936. doi:10.1021/acs.analchem.9b05202
107. Hale OJ, Cramer R. Collision-induced dissociation of doubly-charged barium-cationized lipids generated from liquid samples by atmospheric pressure matrix-assisted laser

desorption/ionization provides structurally diagnostic product ions. *Anal Bioanal Chem*. Feb 2018;410(5):1435-1444. doi:10.1007/s00216-017-0788-6
108. Piras C, Ceniti C, Hartmane E, et al. Rapid Liquid AP-MALDI MS Profiling of Lipids and Proteins from Goat and Sheep Milk for Speciation and Colostrum Analysis. *Proteomes*. Aug 21 2020;8(3)doi:10.3390/proteomes8030020
109. Hale OJ, Morris M, Jones B, Reynolds CK, Cramer R. Liquid Atmospheric Pressure Matrix-Assisted Laser Desorption/Ionization Mass Spectrometry Adds Enhanced Functionalities to MALDI MS Profiling for Disease Diagnostics. *ACS Omega*. Jul 31 2019;4(7):12759-12765. doi:10.1021/acsomega.9b01476
110. Piras C, Hale OJ, Reynolds CK, et al. LAP-MALDI MS coupled with machine learning: an ambient mass spectrometry approach for high-throughput diagnostics. *Chem Sci*. Feb 09 2022;13(6):1746-1758. doi:10.1039/d1sc05171g
111. Lellman SE, Reynolds CK, Jones AKB, Taylor N, Cramer R. LAP-MALDI MS Profiling and Identification of Potential Biomarkers for the Detection of Bovine Tuberculosis. *J Agric Food Chem*. Sep 20 2023;71(37):13899-13905. doi:10.1021/acs.jafc.3c01879
112. Lellman SE, Cramer R. Bacterial identification by lipid profiling using liquid atmospheric pressure matrix-assisted laser desorption/ionization mass spectrometry. *Clin Chem Lab Med*. Jun 25 2020;58(6):930-938. doi:10.1515/cclm-2019-0908
113. Barry JA, Muddiman DC. Global optimization of the infrared matrix-assisted laser desorption electrospray ionization (IR MALDESI) source for mass spectrometry using statistical design of experiments. *Rapid Commun Mass Spectrom*. Dec 15 2011;25(23):3527-36. doi:10.1002/rcm.5262
114. Bokhart MT, Muddiman DC. Infrared matrix-assisted laser desorption electrospray ionization mass spectrometry imaging analysis of biospecimens. *Analyst*. Sep 21 2016;141(18):5236-45. doi:10.1039/c6an01189f
115. Bagley MC, Pace CL, Ekelöf M, Muddiman DC. Infrared matrix-assisted laser desorption electrospray ionization (IR-MALDESI) mass spectrometry imaging analysis of endogenous metabolites in cherry tomatoes. *Analyst*. Aug 10 2020;145(16):5516-5523. doi:10.1039/d0an00818d
116. Bagley MC, Stepanova AN, Ekelöf M, Alonso JM, Muddiman DC. Development of a relative quantification method for infrared matrix-assisted laser desorption electrospray ionization mass spectrometry imaging of Arabidopsis seedlings. *Rapid Communications in Mass Spectrometry*. 2020/03/30 2020;34(6):e8616. doi:https://doi.org/10.1002/rcm.8616
117. Knizner KT, Guymon JP, Garrard KP, et al. Next-Generation Infrared Matrix-Assisted Laser Desorption Electrospray Ionization Source for Mass Spectrometry Imaging and High-Throughput Screening. *J Am Soc Mass Spectrom*. Nov 02 2022;33(11):2070-2077. doi:10.1021/jasms.2c00178
118. Radosevich AA-O, Pu F, Chang-Yen D, et al. Ultra-High-Throughput Ambient MS: Direct Analysis at 22 Samples per Second by Infrared Matrix-Assisted Laser Desorption Electrospray Ionization Mass Spectrometry. (1520-6882 (Electronic))
119. Shanley J, Pu F, Williams JD, et al. Collaborative robotics to enable ultra-high-throughput IR-MALDESI. *SLAS Technol*. Jul 23 2024:100163. doi:10.1016/j.slast.2024.100163
120. Knizner KT, Bagley MC, Pu F, Elsen NL, Williams JD, Muddiman DC. Normalization techniques for high-throughput screening by infrared matrix-assisted laser desorption

electrospray ionization mass spectrometry. *J Mass Spectrom*. Jun 2022;57(6):e4869. doi:10.1002/jms.4869
121. Pu F, Ugrin SA, Radosevich AJ, et al. High-Throughput Intact Protein Analysis for Drug Discovery Using Infrared Matrix-Assisted Laser Desorption Electrospray Ionization Mass Spectrometry. *Anal Chem*. Oct 04 2022;94(39):13566-13574. doi:10.1021/acs.analchem.2c03211
122. Heap RE, Hope AG, Pearson LA, et al. Identifying Inhibitors of Inflammation: A Novel High-Throughput MALDI-TOF Screening Assay for Salt-Inducible Kinases (SIKs). *SLAS Discov*. Dec 2017;22(10):1193-1202. doi:10.1177/2472555217717473
123. Winter M, Bretschneider T, Kleiner C, et al. Establishing MALDI-TOF as Versatile Drug Discovery Readout to Dissect the PTP1B Enzymatic Reaction. *SLAS Discov*. Jul 2018;23(6):561-573. doi:10.1177/2472555218759267
124. De Cesare V, Moran J, Traynor R, et al. High-throughput matrix-assisted laser desorption/ionization time-of-flight (MALDI-TOF) mass spectrometry-based deubiquitylating enzyme assay for drug discovery. *Nat Protoc*. Dec 2020;15(12):4034-4057. doi:10.1038/s41596-020-00405-0
125. Haslam C, Hellicar J, Dunn A, et al. The Evolution of MALDI-TOF Mass Spectrometry toward Ultra-High-Throughput Screening: 1536-Well Format and Beyond. *J Biomol Screen*. Feb 2016;21(2):176-86. doi:10.1177/1087057115608605
126. Chandler J, Haslam C, Hardy N, Leveridge M, Marshall P. A Systematic Investigation of the Best Buffers for Use in Screening by MALDI-Mass Spectrometry. *SLAS Discov*. Dec 2017;22(10):1262-1269. doi:10.1177/1087057116681726
127. Leite JF, Hajivandi MR, Diller T, Pope RM. Removal of sodium and potassium adducts using a matrix additive during matrix-associated laser desorption/ionization time-of-flight mass spectrometric analysis of peptides. *Rapid Commun Mass Spectrom*. 2004;18(23):2953-9. doi:10.1002/rcm.1711
128. Wang CC, Lai YH, Ou YM, Chang HT, Wang YS. Critical factors determining the quantification capability of matrix-assisted laser desorption/ionization- time-of-flight mass spectrometry. *Philos Trans A Math Phys Eng Sci*. Oct 28 2016;374(2079)doi:10.1098/rsta.2015.0371
129. Choi H, Lee D, Kim Y, Nguyen H-Q, Han S, Kim J. Effects of Matrices and Additives on Multiple Charge Formation of Proteins in MALDI–MS Analysis. *Journal of the American Society for Mass Spectrometry*. 2019/07/01 2019;30(7):1174-1178. doi:10.1007/s13361-019-02213-7
130. Leszyk JD. Evaluation of the new MALDI matrix 4-chloro-alpha-cyanocinnamic acid. *J Biomol Tech*. Jul 2010;21(2):81-91.
131. Perry WJ, Patterson NH, Prentice BM, Neumann EK, Caprioli RM, Spraggins JM. Uncovering matrix effects on lipid analyses in MALDI imaging mass spectrometry experiments. *J Mass Spectrom*. Apr 2020;55(4):e4491. doi:10.1002/jms.4491
132. Fagerer SR, Nielsen S, Ibáñez A, Zenobi R. Matrix-assisted laser desorption/ionization matrices for negative mode metabolomics. *Eur J Mass Spectrom (Chichester)*. 2013;19(1):39-47. doi:10.1255/ejms.1209
133. Herkt M, Foinquinos A, Batkai S, Thum T, Pich A. Pharmacokinetic Studies of Antisense Oligonucleotides Using MALDI-TOF Mass Spectrometry. *Front Pharmacol*. 2020;11:220. doi:10.3389/fphar.2020.00220

134. Smirnov IP, Zhu X, Taylor T, et al. Suppression of α-Cyano-4-hydroxycinnamic Acid Matrix Clusters and Reduction of Chemical Noise in MALDI-TOF Mass Spectrometry. *Analytical Chemistry*. 2004;76(10):2958-2965. doi:10.1021/ac035331j
135. Patil AA, Descanzo MJN, Dhisale VB, Peng W-P. MALDI sample preparation methods: A mini review. *International Journal of Mass Spectrometry*. 2024;498:117219. doi:https://doi.org/10.1016/j.ijms.2024.117219
136. Shi CY, Deng CH. Recent advances in inorganic materials for LDI-MS analysis of small molecules. *Analyst*. 2016;141(10):2816-2826. doi:10.1039/C6AN00220J
137. Cohen SL, Chait BT. Influence of matrix solution conditions on the MALDI-MS analysis of peptides and proteins. *Anal Chem*. Jan 01 1996;68(1):31-7. doi:10.1021/ac9507956
138. Weigt D, Sammour DA, Ulrich T, Munteanu B, Hopf C. Automated analysis of lipid drug-response markers by combined fast and high-resolution whole cell MALDI mass spectrometry biotyping. *Sci Rep*. Jul 26 2018;8(1):11260. doi:10.1038/s41598-018-29677-z
139. Blank M, Enzlein T, Hopf C. LPS-induced lipid alterations in microglia revealed by MALDI mass spectrometry-based cell fingerprinting in neuroinflammation studies. *Sci Rep*. Feb 21 2022;12(1):2908. doi:10.1038/s41598-022-06894-1
140. Schmidt S, Geisel A, Enzlein T, et al. Label-free Assessment of Complement-Dependent Cytotoxicity of Therapeutic Antibodies via a Whole-Cell MALDI Mass Spectrometry Bioassay. *bioRxiv*. 2024:2024.05.03.592336. doi:10.1101/2024.05.03.592336
141. Jaskolla TW, Karas M, Roth U, Steinert K, Menzel C, Reihs K. Comparison Between Vacuum Sublimed Matrices and Conventional Dried Droplet Preparation in MALDI-TOF Mass Spectrometry. *Journal of the American Society for Mass Spectrometry*. 2009;20(6):1104-1114. doi:https://doi.org/10.1016/j.jasms.2009.02.010
142. Acker MG, Auld DS. Considerations for the design and reporting of enzyme assays in high-throughput screening applications. *Perspectives in Science*. 2014/05/01/ 2014;1(1):56-73. doi:https://doi.org/10.1016/j.pisc.2013.12.001
143. Wu G, Yuan Y, Hodge CN. Determining appropriate substrate conversion for enzymatic assays in high-throughput screening. *J Biomol Screen*. Dec 2003;8(6):694-700. doi:10.1177/1087057103260050
144. Greis KD, Zhou S, Burt TM, et al. MALDI-TOF MS as a label-free approach to rapid inhibitor screening. *J Am Soc Mass Spectrom*. Jun 2006;17(6):815-822. doi:10.1016/j.jasms.2006.02.019
145. Wang P, Giese RW. Recommendations for quantitative analysis of small molecules by matrix-assisted laser desorption ionization mass spectrometry. *J Chromatogr A*. Feb 24 2017;1486:35-41. doi:10.1016/j.chroma.2017.01.040
146. Zhang JH, Chung TD, Oldenburg KR. A Simple Statistical Parameter for Use in Evaluation and Validation of High Throughput Screening Assays. *J Biomol Screen*. 1999;4(2):67-73. doi:10.1177/108705719900400206
147. Murray D, Wigglesworth M. HTS Methods: Assay Design and Optimisation. In: Bittker JA, Ross NT, eds. *High Throughput Screening Methods: Evolution and Refinement*. The Royal Society of Chemistry; 2016:0.
148. Atmaramani R, Pancrazio JJ, Black BJ. Adaptation of robust Z' factor for assay quality assessment in microelectrode array based screening using adult dorsal root ganglion neurons. *J Neurosci Methods*. Jun 01 2020;339:108699. doi:10.1016/j.jneumeth.2020.108699

149. Beeman K, Baumgärtner J, Laubenheimer M, et al. Integration of an In Situ MALDI-Based High-Throughput Screening Process: A Case Study with Receptor Tyrosine Kinase c-MET. *SLAS Discov*. Dec 2017;22(10):1203-1210. doi:10.1177/2472555217727701
150. Guitot K, Drujon T, Burlina F, et al. A direct label-free MALDI-TOF mass spectrometry based assay for the characterization of inhibitors of protein lysine methyltransferases. *Anal Bioanal Chem*. Jun 2017;409(15):3767-3777. doi:10.1007/s00216-017-0319-5
151. De Cesare V, Johnson C, Barlow V, Hastie J, Knebel A, Trost M. The MALDI-TOF E2/E3 Ligase Assay as Universal Tool for Drug Discovery in the Ubiquitin Pathway. *Cell Chem Biol*. Sep 20 2018;25(9):1117-1127.e4. doi:10.1016/j.chembiol.2018.06.004
152. Ritorto MS, Ewan R, Perez-Oliva AB, et al. Screening of DUB activity and specificity by MALDI-TOF mass spectrometry. *Nat Commun*. Aug 27 2014;5:4763. doi:10.1038/ncomms5763
153. Munteanu B, Meyer B, von Reitzenstein C, et al. Label-free in situ monitoring of histone deacetylase drug target engagement by matrix-assisted laser desorption ionization-mass spectrometry biotyping and imaging. *Anal Chem*. May 20 2014;86(10):4642-7. doi:10.1021/ac500038j
154. Unger MS, Blank M, Enzlein T, Hopf C. Label-free cell assays to determine compound uptake or drug action using MALDI-TOF mass spectrometry. *Nature Protocols*. 2021/12/01 2021;16(12):5533-5558. doi:10.1038/s41596-021-00624-z
155. Unger MS, Schumacher L, Enzlein T, et al. Direct Automated MALDI Mass Spectrometry Analysis of Cellular Transporter Function: Inhibition of OATP2B1 Uptake by 294 Drugs. *Anal Chem*. Sep 01 2020;92(17):11851-11859. doi:10.1021/acs.analchem.0c02186
156. Winter M, Bretschneider T, Thamm S, et al. Chemical Derivatization Enables MALDI-TOF-Based High-Throughput Screening for Microbial Trimethylamine (TMA)-Lyase Inhibitors. *SLAS Discov*. Aug 2019;24(7):766-777. doi:10.1177/2472555219838216
157. Simon RP, Winter M, Kleiner C, et al. MALDI-TOF Mass Spectrometry-Based High-Throughput Screening for Inhibitors of the Cytosolic DNA Sensor cGAS. *SLAS Discov*. Apr 2020;25(4):372-383. doi:10.1177/2472555219880185
158. Winter M, Simon RP, Wang Y, et al. Differential analyte derivatization enables unbiased MALDI-TOF-based high-throughput screening: A proof-of-concept study for the discovery of catechol-o-methyltransferase inhibitors. *SLAS Discov*. Jul 2022;27(5):287-297. doi:10.1016/j.slasd.2022.05.002
159. Marshall JS, Warrington R, Watson W, Kim HL. An introduction to immunology and immunopathology. *Allergy Asthma Clin Immunol*. 2018;14(Suppl 2):49. doi:10.1186/s13223-018-0278-1
160. Medzhitov R. Recognition of microorganisms and activation of the immune response. *Nature*. Oct 18 2007;449(7164):819-26. doi:10.1038/nature06246
161. Lantz O, Teyton L. Identification of T cell antigens in the 21st century, as difficult as ever. *Semin Immunol*. Mar 2022;60:101659. doi:10.1016/j.smim.2022.101659
162. Koumantou D, Barnea E, Martin-Esteban A, et al. Editing the immunopeptidome of melanoma cells using a potent inhibitor of endoplasmic reticulum aminopeptidase 1 (ERAP1). *Cancer Immunol Immunother*. Aug 2019;68(8):1245-1261. doi:10.1007/s00262-019-02358-0
163. Raskov H, Orhan A, Christensen JP, Gögenur I. Cytotoxic CD8(+) T cells in cancer and cancer immunotherapy. *Br J Cancer*. Jan 2021;124(2):359-367. doi:10.1038/s41416-020-01048-4

164. Chaplin DD. Overview of the immune response. *J Allergy Clin Immunol*. Feb 2010;125(2 Suppl 2):S3-23. doi:10.1016/j.jaci.2009.12.980
165. de Verteuil D, Muratore-Schroeder TL, Granados DP, et al. Deletion of immunoproteasome subunits imprints on the transcriptome and has a broad impact on peptides presented by major histocompatibility complex I molecules. *Mol Cell Proteomics*. Sep 2010;9(9):2034-47. doi:10.1074/mcp.M900566-MCP200
166. Lázaro S, Gamarra D, Del Val M. Proteolytic enzymes involved in MHC class I antigen processing: A guerrilla army that partners with the proteasome. *Mol Immunol*. Dec 2015;68(2 Pt A):72-6. doi:10.1016/j.molimm.2015.04.014
167. Leone P, Shin EC, Perosa F, Vacca A, Dammacco F, Racanelli V. MHC class I antigen processing and presenting machinery: organization, function, and defects in tumor cells. *J Natl Cancer Inst*. Aug 21 2013;105(16):1172-87. doi:10.1093/jnci/djt184
168. Stratikos E, Stern LJ. Antigenic peptide trimming by ER aminopeptidases--insights from structural studies. *Mol Immunol*. Oct 2013;55(3-4):212-9. doi:10.1016/j.molimm.2013.03.002
169. Serwold T, Gaw S, Shastri N. ER aminopeptidases generate a unique pool of peptides for MHC class I molecules. *Nat Immunol*. Jul 2001;2(7):644-51. doi:10.1038/89800
170. Birtley JR, Saridakis E, Stratikos E, Mavridis IM. The crystal structure of human endoplasmic reticulum aminopeptidase 2 reveals the atomic basis for distinct roles in antigen processing. *Biochemistry*. Jan 10 2012;51(1):286-95. doi:10.1021/bi201230p
171. Nguyen TT, Chang SC, Evnouchidou I, et al. Structural basis for antigenic peptide precursor processing by the endoplasmic reticulum aminopeptidase ERAP1. *Nat Struct Mol Biol*. May 2011;18(5):604-13. doi:10.1038/nsmb.2021
172. Sui L, Gandhi A, Guo HC. Crystal structure of a polypeptide's C-terminus in complex with the regulatory domain of ER aminopeptidase 1. *Mol Immunol*. Dec 2016;80:41-49. doi:10.1016/j.molimm.2016.10.012
173. Kochan G, Krojer T, Harvey D, et al. Crystal structures of the endoplasmic reticulum aminopeptidase-1 (ERAP1) reveal the molecular basis for N-terminal peptide trimming. *Proc Natl Acad Sci U S A*. May 10 2011;108(19):7745-50. doi:10.1073/pnas.1101262108
174. Giastas P, Mpakali A, Papakyriakou A, et al. Mechanism for antigenic peptide selection by endoplasmic reticulum aminopeptidase 1. *Proc Natl Acad Sci U S A*. Dec 26 2019;116(52):26709-26716. doi:10.1073/pnas.1912070116
175. Chang SC, Momburg F, Bhutani N, Goldberg AL. The ER aminopeptidase, ERAP1, trims precursors to lengths of MHC class I peptides by a "molecular ruler" mechanism. *Proc Natl Acad Sci U S A*. Nov 22 2005;102(47):17107-12. doi:10.1073/pnas.0500721102
176. Evnouchidou I, Momburg F, Papakyriakou A, et al. The internal sequence of the peptide-substrate determines its N-terminus trimming by ERAP1. *PLoS One*. 2008;3(11):e3658. doi:10.1371/journal.pone.0003658
177. Li L, Batliwala M, Bouvier M. ERAP1 enzyme-mediated trimming and structural analyses of MHC I-bound precursor peptides yield novel insights into antigen processing and presentation. *J Biol Chem*. Dec 06 2019;294(49):18534-18544. doi:10.1074/jbc.RA119.010102
178. Mpakali A, Maben Z, Stern LJ, Stratikos E. Molecular pathways for antigenic peptide generation by ER aminopeptidase 1. *Mol Immunol*. Sep 2019;113:50-57. doi:10.1016/j.molimm.2018.03.026

179. Agrawal N, Brown MA. Genetic associations and functional characterization of M1 aminopeptidases and immune-mediated diseases. *Genes Immun*. Dec 2014;15(8):521-7. doi:10.1038/gene.2014.46
180. Pepelyayeva Y, Amalfitano A. The role of ERAP1 in autoinflammation and autoimmunity. *Hum Immunol*. May 2019;80(5):302-309. doi:10.1016/j.humimm.2019.02.013
181. López de Castro JA. How ERAP1 and ERAP2 Shape the Peptidomes of Disease-Associated MHC-I Proteins. *Front Immunol*. 2018;9:2463. doi:10.3389/fimmu.2018.02463
182. Reeves E, Islam Y, James E. ERAP1: a potential therapeutic target for a myriad of diseases. *Expert Opin Ther Targets*. Jun 2020;24(6):535-544. doi:10.1080/14728222.2020.1751821
183. Compagnone M, Cifaldi L, Fruci D. Regulation of ERAP1 and ERAP2 genes and their disfunction in human cancer. *Hum Immunol*. May 2019;80(5):318-324. doi:10.1016/j.humimm.2019.02.014
184. Stratikos E, Stamogiannos A, Zervoudi E, Fruci D. A role for naturally occurring alleles of endoplasmic reticulum aminopeptidases in tumor immunity and cancer pre-disposition. *Front Oncol*. 2014;4:363. doi:10.3389/fonc.2014.00363
185. James E, Bailey I, Sugiyarto G, Elliott T. Induction of protective antitumor immunity through attenuation of ERAAP function. *J Immunol*. Jun 01 2013;190(11):5839-46. doi:10.4049/jimmunol.1300220
186. Joyce P, Leishman A, Braun A, et al. 1131 GRWD5769: A first-in-class inhibitor of ERAP1, generating novel cancer antigens to drive de novo anti-tumor T cell responses. *Journal for ImmunoTherapy of Cancer*. 2022;10(Suppl 2):A1175. doi:10.1136/jitc-2022-SITC2022.1131
187. Chen L, Ridley A, Hammitzsch A, et al. Silencing or inhibition of endoplasmic reticulum aminopeptidase 1 (ERAP1) suppresses free heavy chain expression and Th17 responses in ankylosing spondylitis. *Ann Rheum Dis*. May 2016;75(5):916-23. doi:10.1136/annrheumdis-2014-206996
188. Zervoudi E, Saridakis E, Birtley JR, et al. Rationally designed inhibitor targeting antigen-trimming aminopeptidases enhances antigen presentation and cytotoxic T-cell responses. *Proc Natl Acad Sci U S A*. Dec 03 2013;110(49):19890-5. doi:10.1073/pnas.1309781110
189. Freiwald A, Sauer S. Phylogenetic classification and identification of bacteria by mass spectrometry. *Nat Protoc*. 2009;4(5):732-42. doi:10.1038/nprot.2009.37
190. Sauer S, Kliem M. Mass spectrometry tools for the classification and identification of bacteria. *Nat Rev Microbiol*. Jan 2010;8(1):74-82. doi:10.1038/nrmicro2243
191. Hou TY, Chiang-Ni C, Teng SH. Current status of MALDI-TOF mass spectrometry in clinical microbiology. *J Food Drug Anal*. Apr 2019;27(2):404-414. doi:10.1016/j.jfda.2019.01.001
192. Calderaro A, Chezzi C. MALDI-TOF MS: A Reliable Tool in the Real Life of the Clinical Microbiology Laboratory. *Microorganisms*. Feb 03 2024;12(2)doi:10.3390/microorganisms12020322
193. Holland RD, Wilkes JG, Rafii F, et al. Rapid identification of intact whole bacteria based on spectral patterns using matrix-assisted laser desorption/ionization with time-of-flight mass spectrometry. *Rapid Commun Mass Spectrom*. 1996;10(10):1227-32. doi:10.1002/(SICI)1097-0231(19960731)10:10<1227::AID-RCM659>3.0.CO;2-6

194. Claydon MA, Davey SN, Edwards-Jones V, Gordon DB. The rapid identification of intact microorganisms using mass spectrometry. *Nat Biotechnol*. Nov 1996;14(11):1584-6. doi:10.1038/nbt1196-1584
195. Keys CJ, Dare DJ, Sutton H, et al. Compilation of a MALDI-TOF mass spectral database for the rapid screening and characterisation of bacteria implicated in human infectious diseases. *Infect Genet Evol*. Sep 2004;4(3):221-42. doi:10.1016/j.meegid.2004.02.004
196. Bright JJ, Claydon MA, Soufian M, Gordon DB. Rapid typing of bacteria using matrix-assisted laser desorption ionisation time-of-flight mass spectrometry and pattern recognition software. *J Microbiol Methods*. Feb 2002;48(2-3):127-38. doi:10.1016/s0167-7012(01)00317-7
197. Mortier T, Wieme AD, Vandamme P, Waegeman W. Bacterial species identification using MALDI-TOF mass spectrometry and machine learning techniques: A large-scale benchmarking study. *Comput Struct Biotechnol J*. 2021;19:6157-6168. doi:10.1016/j.csbj.2021.11.004
198. Urakami S, Hinou H. Direct MALDI Glycotyping of Glycoproteins toward Practical Subtyping of Biological Samples. *ACS Omega*. Nov 01 2022;7(43):39280-39286. doi:10.1021/acsomega.2c05429
199. Urakami S, Hinou H. MALDI glycotyping of O-antigens from a single colony of gram-negative bacteria. *Sci Rep*. Jun 03 2024;14(1):12719. doi:10.1038/s41598-024-62729-1
200. Patel R. MALDI-TOF MS for the diagnosis of infectious diseases. *Clin Chem*. Jan 2015;61(1):100-11. doi:10.1373/clinchem.2014.221770
201. Mutters NT, Hodiamont CJ, de Jong MD, Overmeijer HP, van den Boogaard M, Visser CE. Performance of Kiestra total laboratory automation combined with MS in clinical microbiology practice. *Ann Lab Med*. Mar 2014;34(2):111-7. doi:10.3343/alm.2014.34.2.111
202. Asukabe H, Akahori S, Ueno E, et al. Cyanobacterial Classification with the Toxicity Using MALDI Biotyper. *J Am Soc Mass Spectrom*. Jul 01 2020;31(7):1572-1578. doi:10.1021/jasms.0c00148
203. Ashfaq MY, Da'na DA, Al-Ghouti MA. Application of MALDI-TOF MS for identification of environmental bacteria: A review. *J Environ Manage*. Mar 01 2022;305:114359. doi:10.1016/j.jenvman.2021.114359
204. Singhal N, Kumar M, Kanaujia PK, Virdi JS. MALDI-TOF mass spectrometry: an emerging technology for microbial identification and diagnosis. *Front Microbiol*. 2015;6:791. doi:10.3389/fmicb.2015.00791
205. Urwyler SK, Glaubitz J. Advantage of MALDI-TOF-MS over biochemical-based phenotyping for microbial identification illustrated on industrial applications. *Lett Appl Microbiol*. Feb 2016;62(2):130-7. doi:10.1111/lam.12526
206. Zhang X, Scalf M, Berggren TW, Westphall MS, Smith LM. Identification of mammalian cell lines using MALDI-TOF and LC-ESI-MS/MS mass spectrometry. *J Am Soc Mass Spectrom*. Apr 2006;17(4):490-499. doi:10.1016/j.jasms.2005.12.007
207. Serafim V, Shah A, Puiu M, et al. Classification of cancer cell lines using matrix-assisted laser desorption/ionization time-of-flight mass spectrometry and statistical analysis. *Int J Mol Med*. Oct 2017;40(4):1096-1104. doi:10.3892/ijmm.2017.3083
208. Heap RE, Segarra-Fas A, Blain AP, Findlay GM, Trost M. Profiling embryonic stem cell differentiation by MALDI TOF mass spectrometry: development of a reproducible and robust sample preparation workflow. *Analyst*. Oct 22 2019;144(21):6371-6381. doi:10.1039/c9an00771g

209. Karger A, Bettin B, Lenk M, Mettenleiter TC. Rapid characterisation of cell cultures by matrix-assisted laser desorption/ionisation mass spectrometric typing. *J Virol Methods*. Mar 2010;164(1-2):116-21. doi:10.1016/j.jviromet.2009.11.022
210. Povey JF, Saintas E, Aderemi AV, et al. Intact-Cell MALDI-ToF Mass Spectrometry for the Authentication of Drug-Adapted Cancer Cell Lines. *Cells*. Oct 02 2019;8(10)doi:10.3390/cells8101194
211. Petre G, Durand H, Pelletier L, et al. Rapid Proteomic Profiling by MALDI-TOF Mass Spectrometry for Better Brain Tumor Classification. *Proteomics Clin Appl*. Sep 2020;14(5):e1900116. doi:10.1002/prca.201900116
212. Hanrieder J, Wicher G, Bergquist J, Andersson M, Fex-Svenningsen A. MALDI mass spectrometry based molecular phenotyping of CNS glial cells for prediction in mammalian brain tissue. *Anal Bioanal Chem*. Jul 2011;401(1):135-47. doi:10.1007/s00216-011-5043-y
213. Petukhova VZ, Young AN, Wang J, et al. Whole Cell MALDI Fingerprinting Is a Robust Tool for Differential Profiling of Two-Component Mammalian Cell Mixtures. *J Am Soc Mass Spectrom*. Feb 2019;30(2):344-354. doi:10.1007/s13361-018-2088-6
214. Dong H, Shen W, Cheung MT, et al. Rapid detection of apoptosis in mammalian cells by using intact cell MALDI mass spectrometry. *Analyst*. Dec 21 2011;136(24):5181-9. doi:10.1039/c1an15750g
215. Schwamb S, Munteanu B, Meyer B, Hopf C, Hafner M, Wiedemann P. Intact cell MALDI mass spectrometry biotyping for "at-line" monitoring of apoptosis progression in CHO cell cultures. *BMC Proc*. Copyright © 2013 Schwamb et al.; licensee BioMed Central Ltd.; 2013:P8. vol. Suppl 6.
216. Munteanu B, von Reitzenstein C, Hänsch GM, Meyer B, Hopf C. Sensitive, robust and automated protein analysis of cell differentiation and of primary human blood cells by intact cell MALDI mass spectrometry biotyping. *Anal Bioanal Chem*. Nov 2012;404(8):2277-86. doi:10.1007/s00216-012-6357-0
217. Reddy JK, Rao MS. Lipid metabolism and liver inflammation. II. Fatty liver disease and fatty acid oxidation. *Am J Physiol Gastrointest Liver Physiol*. May 2006;290(5):G852-8. doi:10.1152/ajpgi.00521.2005
218. Fuchs B, Schiller J. MALDI-TOF MS analysis of lipids from cells, tissues and body fluids. *Subcell Biochem*. 2008;49:541-65. doi:10.1007/978-1-4020-8831-5_21
219. Goldberg IJ, Trent CM, Schulze PC. Lipid metabolism and toxicity in the heart. *Cell Metab*. Jun 06 2012;15(6):805-12. doi:10.1016/j.cmet.2012.04.006
220. Holčapek M, Červená B, Cífková E, et al. Lipidomic analysis of plasma, erythrocytes and lipoprotein fractions of cardiovascular disease patients using UHPLC/MS, MALDI-MS and multivariate data analysis. *J Chromatogr B Analyt Technol Biomed Life Sci*. May 15 2015;990:52-63. doi:10.1016/j.jchromb.2015.03.010
221. Neumann EK, Comi TJ, Rubakhin SS, Sweedler JV. Lipid Heterogeneity between Astrocytes and Neurons Revealed by Single-Cell MALDI-MS Combined with Immunocytochemical Classification. *Angew Chem Int Ed Engl*. Apr 23 2019;58(18):5910-5914. doi:10.1002/anie.201812892
222. Neumann EK, Ellis JF, Triplett AE, Rubakhin SS, Sweedler JV. Lipid Analysis of 30 000 Individual Rodent Cerebellar Cells Using High-Resolution Mass Spectrometry. *Anal Chem*. Jun 18 2019;91(12):7871-7878. doi:10.1021/acs.analchem.9b01689

223. Schulz S, Becker M, Groseclose MR, Schadt S, Hopf C. Advanced MALDI mass spectrometry imaging in pharmaceutical research and drug development. *Curr Opin Biotechnol*. Feb 2019;55:51-59. doi:10.1016/j.copbio.2018.08.003
224. Karlsson O, Hanrieder J. Imaging mass spectrometry in drug development and toxicology. *Arch Toxicol*. Jun 2017;91(6):2283-2294. doi:10.1007/s00204-016-1905-6
225. Weigt D, Parrish CA, Krueger JA, Oleykowski CA, Rendina AR, Hopf C. Mechanistic MALDI-TOF Cell-Based Assay for the Discovery of Potent and Specific Fatty Acid Synthase Inhibitors. *Cell Chem Biol*. Sep 19 2019;26(9):1322-1331.e4. doi:10.1016/j.chembiol.2019.06.004
226. Ouedraogo R, Flaudrops C, Ben Amara A, Capo C, Raoult D, Mege JL. Global analysis of circulating immune cells by matrix-assisted laser desorption ionization time-of-flight mass spectrometry. *PLoS One*. Oct 27 2010;5(10):e13691. doi:10.1371/journal.pone.0013691
227. Ouedraogo R, Daumas A, Ghigo E, Capo C, Mege JL, Textoris J. Whole-cell MALDI-TOF MS: a new tool to assess the multifaceted activation of macrophages. *J Proteomics*. Oct 22 2012;75(18):5523-32. doi:10.1016/j.jprot.2012.07.046
228. Portevin D, Pflüger V, Otieno P, Brunisholz R, Vogel G, Daubenberger C. Quantitative whole-cell MALDI-TOF MS fingerprints distinguishes human monocyte sub-populations activated by distinct microbial ligands. *BMC Biotechnol*. Apr 11 2015;15:24. doi:10.1186/s12896-015-0140-1
229. Marín-Rubio JL, Peltier-Heap RE, Dueñas ME, et al. A Matrix-Assisted Laser Desorption/Ionization Time-of-Flight Assay Identifies Nilotinib as an Inhibitor of Inflammation in Acute Myeloid Leukemia. *J Med Chem*. Sep 22 2022;65(18):12014-12030. doi:10.1021/acs.jmedchem.2c00671
230. Mass E, Nimmerjahn F, Kierdorf K, Schlitzer A. Tissue-specific macrophages: how they develop and choreograph tissue biology. *Nat Rev Immunol*. Sep 2023;23(9):563-579. doi:10.1038/s41577-023-00848-y
231. Epelman S, Lavine KJ, Randolph GJ. Origin and functions of tissue macrophages. *Immunity*. Jul 17 2014;41(1):21-35. doi:10.1016/j.immuni.2014.06.013
232. Gordon S, Plüddemann A. Tissue macrophages: heterogeneity and functions. *BMC Biol*. Jun 29 2017;15(1):53. doi:10.1186/s12915-017-0392-4
233. Hirayama D, Iida T, Nakase H. The Phagocytic Function of Macrophage-Enforcing Innate Immunity and Tissue Homeostasis. *Int J Mol Sci*. Dec 29 2017;19(1)doi:10.3390/ijms19010092
234. Mosser DM, Edwards JP. Exploring the full spectrum of macrophage activation. *Nat Rev Immunol*. Dec 2008;8(12):958-69. doi:10.1038/nri2448
235. Kotwal GJ, Chien S. Macrophage Differentiation in Normal and Accelerated Wound Healing. *Results Probl Cell Differ*. 2017;62:353-364. doi:10.1007/978-3-319-54090-0_14
236. Stein M, Keshav S, Harris N, Gordon S. Interleukin 4 potently enhances murine macrophage mannose receptor activity: a marker of alternative immunologic macrophage activation. *J Exp Med*. Jul 01 1992;176(1):287-92. doi:10.1084/jem.176.1.287
237. Takeda K, Tanaka T, Shi W, et al. Essential role of Stat6 in IL-4 signalling. *Nature*. Apr 18 1996;380(6575):627-30. doi:10.1038/380627a0
238. Ciesielska A, Matyjek M, Kwiatkowska K. TLR4 and CD14 trafficking and its influence on LPS-induced pro-inflammatory signaling. *Cell Mol Life Sci*. Feb 2021;78(4):1233-1261. doi:10.1007/s00018-020-03656-y

239. Dai X, Sayama K, Tohyama M, et al. The NF-kappaB, p38 MAPK and STAT1 pathways differentially regulate the dsRNA-mediated innate immune responses of epidermal keratinocytes. *Int Immunol*. Jul 2008;20(7):901-9. doi:10.1093/intimm/dxn048
240. Israël A. The IKK complex, a central regulator of NF-kappaB activation. *Cold Spring Harb Perspect Biol*. Mar 2010;2(3):a000158. doi:10.1101/cshperspect.a000158
241. Holloway AF, Rao S, Shannon MF. Regulation of cytokine gene transcription in the immune system. *Mol Immunol*. Jan 2002;38(8):567-80. doi:10.1016/s0161-5890(01)00094-3
242. Arango Duque G, Descoteaux A. Macrophage cytokines: involvement in immunity and infectious diseases. *Front Immunol*. 2014;5:491. doi:10.3389/fimmu.2014.00491
243. Gorbacheva V, Fan R, Wang X, Baldwin WM, 3rd, Fairchild RL, Valujskikh A. IFN-γ production by memory helper T cells is required for CD40-independent alloantibody responses. *J Immunol*. Feb 1 2015;194(3):1347-56. doi:10.4049/jimmunol.1401573
244. Krause CD, Mei E, Xie J, et al. Seeing the light: preassembly and ligand-induced changes of the interferon gamma receptor complex in cells. *Mol Cell Proteomics*. Oct 2002;1(10):805-15. doi:10.1074/mcp.m200065-mcp200
245. Morris R, Kershaw NJ, Babon JJ. The molecular details of cytokine signaling via the JAK/STAT pathway. *Protein Sci*. Dec 2018;27(12):1984-2009. doi:10.1002/pro.3519
246. Bach EA, Tanner JW, Marsters S, et al. Ligand-induced assembly and activation of the gamma interferon receptor in intact cells. *Mol Cell Biol*. Jun 1996;16(6):3214-21. doi:10.1128/MCB.16.6.3214
247. Shuai K, Horvath CM, Huang LH, Qureshi SA, Cowburn D, Darnell JE. Interferon activation of the transcription factor Stat91 involves dimerization through SH2-phosphotyrosyl peptide interactions. *Cell*. Mar 11 1994;76(5):821-8. doi:10.1016/0092-8674(94)90357-3
248. Meshkani R, Vakili S. Tissue resident macrophages: Key players in the pathogenesis of type 2 diabetes and its complications. *Clin Chim Acta*. Nov 01 2016;462:77-89. doi:10.1016/j.cca.2016.08.015
249. Zhang K, Guo J, Yan W, Xu L. Macrophage polarization in inflammatory bowel disease. *Cell Commun Signal*. Dec 21 2023;21(1):367. doi:10.1186/s12964-023-01386-9
250. Silvin A, Qian J, Ginhoux F. Brain macrophage development, diversity and dysregulation in health and disease. *Cell Mol Immunol*. Nov 2023;20(11):1277-1289. doi:10.1038/s41423-023-01053-6
251. Moskalik A, Niderla-Bielińska J, Ratajska A. Multiple roles of cardiac macrophages in heart homeostasis and failure. *Heart Fail Rev*. Jul 2022;27(4):1413-1430. doi:10.1007/s10741-021-10156-z
252. Wen Y, Lambrecht J, Ju C, Tacke F. Hepatic macrophages in liver homeostasis and diseases-diversity, plasticity and therapeutic opportunities. *Cell Mol Immunol*. Jan 2021;18(1):45-56. doi:10.1038/s41423-020-00558-8
253. Bied M, Ho WW, Ginhoux F, Blériot C. Roles of macrophages in tumor development: a spatiotemporal perspective. *Cell Mol Immunol*. Sep 2023;20(9):983-992. doi:10.1038/s41423-023-01061-6
254. Brodin P, Davis MM. Human immune system variation. *Nat Rev Immunol*. Jan 2017;17(1):21-29. doi:10.1038/nri.2016.125
255. Varadé J, Magadán S, González-Fernández Á. Human immunology and immunotherapy: main achievements and challenges. *Cell Mol Immunol*. Apr 2021;18(4):805-828. doi:10.1038/s41423-020-00530-6

256. Reynolds G, Haniffa M. Human and Mouse Mononuclear Phagocyte Networks: A Tale of Two Species? *Front Immunol*. 2015;6:330. doi:10.3389/fimmu.2015.00330
257. Vijayan V, Pradhan P, Braud L, et al. Human and murine macrophages exhibit differential metabolic responses to lipopolysaccharide - A divergent role for glycolysis. *Redox Biol*. Apr 2019;22:101147. doi:10.1016/j.redox.2019.101147
258. Gudgeon J, Marin Rubio JL, Sidgwick F, Trost M. Mass spectrometry-based proteomic exploration of diverse murine macrophage cellular models. *bioRxiv*. 2024:2024.04.09.588684. doi:10.1101/2024.04.09.588684
259. Bosshart H, Heinzelmann M. THP-1 cells as a model for human monocytes. *Ann Transl Med*. Nov 2016;4(21):438. doi:10.21037/atm.2016.08.53
260. Bitzer S, Harati MD, El Kasmi KC, et al. Application of human iPSC-derived macrophages in a miniaturized high-content-imaging-based efferocytosis assay. *SLAS Discov*. Jun 2023;28(4):149-162. doi:10.1016/j.slasd.2023.04.002
261. van Harten RM, Veldhuizen EJA, Haagsman HP, Scheenstra MR. The cathelicidin CATH-2 efficiently neutralizes LPS- and E. coli-induced activation of porcine bone marrow derived macrophages. *Vet Immunol Immunopathol*. Feb 2022;244:110369. doi:10.1016/j.vetimm.2021.110369
262. Moore KJ, Andersson LP, Ingalls RR, et al. Divergent response to LPS and bacteria in CD14-deficient murine macrophages. *J Immunol*. Oct 15 2000;165(8):4272-80. doi:10.4049/jimmunol.165.8.4272
263. Zhu J, Cao J, Liesz A, Roth S. A macrophage-T cell coculture model for severe tissue injury-induced T cell death. *STAR Protoc*. Dec 17 2021;2(4):100983. doi:10.1016/j.xpro.2021.100983
264. Kapellos TS, Taylor L, Lee H, et al. A novel real time imaging platform to quantify macrophage phagocytosis. *Biochem Pharmacol*. Sep 15 2016;116:107-19. doi:10.1016/j.bcp.2016.07.011
265. Liu L, Stokes JV, Tan W, Pruett SB. An optimized flow cytometry panel for classifying macrophage polarization. *J Immunol Methods*. Dec 2022;511:113378. doi:10.1016/j.jim.2022.113378
266. Willmann K, Dunne JF. A flow cytometric immune function assay for human peripheral blood dendritic cells. *J Leukoc Biol*. Apr 2000;67(4):536-44.
267. Abdelkader Y, Perez-Davalos L, LeDuc R, Zahedi RP, Labouta HI. Omics approaches for the assessment of biological responses to nanoparticles. *Adv Drug Deliv Rev*. Sep 2023;200:114992. doi:10.1016/j.addr.2023.114992
268. Al-Amrani S, Al-Jabri Z, Al-Zaabi A, Alshekaili J, Al-Khabori M. Proteomics: Concepts and applications in human medicine. *World J Biol Chem*. Sep 27 2021;12(5):57-69. doi:10.4331/wjbc.v12.i5.57
269. Walgren JL, Thompson DC. Application of proteomic technologies in the drug development process. *Toxicol Lett*. Apr 01 2004;149(1-3):377-85. doi:10.1016/j.toxlet.2003.12.047
270. Cassidy L, Kaulich PT, Maaß S, Bartel J, Becher D, Tholey A. Bottom-up and top-down proteomic approaches for the identification, characterization, and quantification of the low molecular weight proteome with focus on short open reading frame-encoded peptides. *Proteomics*. Dec 2021;21(23-24):e2100008. doi:10.1002/pmic.202100008
271. Dupree EJ, Jayathirtha M, Yorkey H, Mihasan M, Petre BA, Darie CC. A Critical Review of Bottom-Up Proteomics: The Good, the Bad, and the Future of this Field. *Proteomes*. Jul 06 2020;8(3)doi:10.3390/proteomes8030014

272. Varnavides G, Madern M, Anrather D, Hartl N, Reiter W, Hartl M. In Search of a Universal Method: A Comparative Survey of Bottom-Up Proteomics Sample Preparation Methods. *J Proteome Res*. Oct 07 2022;21(10):2397-2411. doi:10.1021/acs.jproteome.2c00265
273. Zougman A, Selby PJ, Banks RE. Suspension trapping (STrap) sample preparation method for bottom-up proteomics analysis. *Proteomics*. May 2014;14(9):1006-0. doi:10.1002/pmic.201300553
274. Wang F, Veth T, Kuipers M, Altelaar M, Stecker KE. Optimized Suspension Trapping Method for Phosphoproteomics Sample Preparation. *Anal Chem*. Jun 27 2023;95(25):9471-9479. doi:10.1021/acs.analchem.3c00324
275. Gershon PD. Cleaved and missed sites for trypsin, lys-C, and lys-N can be predicted with high confidence on the basis of sequence context. *J Proteome Res*. Feb 07 2014;13(2):702-9. doi:10.1021/pr400802z
276. Kota U, Stolowitz ML. Improving Proteome Coverage by Reducing Sample Complexity via Chromatography. *Adv Exp Med Biol*. 2016;919:83-143. doi:10.1007/978-3-319-41448-5_5
277. Alvarez-Segura T, Torres-Lapasió JR, Ortiz-Bolsico C, García-Alvarez-Coque MC. Stationary phase modulation in liquid chromatography through the serial coupling of columns: A review. *Anal Chim Acta*. Jun 07 2016;923:1-23. doi:10.1016/j.aca.2016.03.040
278. Karpievitch YV, Polpitiya AD, Anderson GA, Smith RD, Dabney AR. Liquid Chromatography Mass Spectrometry-Based Proteomics: Biological and Technological Aspects. *Ann Appl Stat*. 2010;4(4):1797-1823. doi:10.1214/10-AOAS341
279. Bache N, Geyer PE, Bekker-Jensen DB, et al. A Novel LC System Embeds Analytes in Pre-formed Gradients for Rapid, Ultra-robust Proteomics. *Mol Cell Proteomics*. Nov 2018;17(11):2284-2296. doi:10.1074/mcp.TIR118.000853
280. Nadler WM, Waidelich D, Kerner A, et al. MALDI versus ESI: The Impact of the Ion Source on Peptide Identification. *J Proteome Res*. Mar 03 2017;16(3):1207-1215. doi:10.1021/acs.jproteome.6b00805
281. Penanes PA, Gorshkov V, Ivanov MV, Gorshkov MV, Kjeldsen F. Potential of Negative-Ion-Mode Proteomics: An MS1-Only Approach. *J Proteome Res*. Aug 04 2023;22(8):2734-2742. doi:10.1021/acs.jproteome.3c00307
282. Antoniewicz MR. Tandem mass spectrometry for measuring stable-isotope labeling. *Curr Opin Biotechnol*. Feb 2013;24(1):48-53. doi:10.1016/j.copbio.2012.10.011
283. Hecht ES, Scigelova M, Eliuk S, Makarov A. Fundamentals and Advances of Orbitrap Mass Spectrometry. *Encyclopedia of Analytical Chemistry*. 2019:1-40.
284. Zubarev RA, Makarov A. Orbitrap mass spectrometry. *Anal Chem*. Jun 04 2013;85(11):5288-96. doi:10.1021/ac4001223
285. Heil LR, Damoc E, Arrey TN, et al. Evaluating the Performance of the Astral Mass Analyzer for Quantitative Proteomics Using Data-Independent Acquisition. *J Proteome Res*. Oct 06 2023;22(10):3290-3300. doi:10.1021/acs.jproteome.3c00357
286. Meier F, Brunner AD, Koch S, et al. Online Parallel Accumulation-Serial Fragmentation (PASEF) with a Novel Trapped Ion Mobility Mass Spectrometer. *Mol Cell Proteomics*. Dec 2018;17(12):2534-2545. doi:10.1074/mcp.TIR118.000900
287. Eliuk S, Makarov A. Evolution of Orbitrap Mass Spectrometry Instrumentation. *Annu Rev Anal Chem (Palo Alto Calif)*. 2015;8:61-80. doi:10.1146/annurev-anchem-071114-040325

288. Skowronek P, Thielert M, Voytik E, et al. Rapid and In-Depth Coverage of the (Phospho-)Proteome With Deep Libraries and Optimal Window Design for dia-PASEF. *Mol Cell Proteomics*. Sep 2022;21(9):100279. doi:10.1016/j.mcpro.2022.100279
289. Krasny L, Huang PH. Data-independent acquisition mass spectrometry (DIA-MS) for proteomic applications in oncology. *Mol Omics*. Feb 01 2021;17(1):29-42. doi:10.1039/d0mo00072h
290. Bruderer R, Bernhardt OM, Gandhi T, et al. Extending the limits of quantitative proteome profiling with data-independent acquisition and application to acetaminophen-treated three-dimensional liver microtissues. *Mol Cell Proteomics*. May 2015;14(5):1400-10. doi:10.1074/mcp.M114.044305
291. Kitata RB, Yang JC, Chen YJ. Advances in data-independent acquisition mass spectrometry towards comprehensive digital proteome landscape. *Mass Spectrom Rev*. 2023;42(6):2324-2348. doi:10.1002/mas.21781
292. Johnson RS, Martin SA, Biemann K. Collision-induced fragmentation of (M + H)+ ions of peptides. Side chain specific sequence ions. *International Journal of Mass Spectrometry and Ion Processes*. 1988/12/29/ 1988;86:137-154. doi:https://doi.org/10.1016/0168-1176(88)80060-0
293. Xiao Y, Vecchi MM, Wen D. Distinguishing between Leucine and Isoleucine by Integrated LC–MS Analysis Using an Orbitrap Fusion Mass Spectrometer. *Analytical Chemistry*. 2016/11/01 2016;88(21):10757-10766. doi:10.1021/acs.analchem.6b03409
294. Cox J, Mann M. MaxQuant enables high peptide identification rates, individualized p.p.b.-range mass accuracies and proteome-wide protein quantification. *Nat Biotechnol*. Dec 2008;26(12):1367-72. doi:10.1038/nbt.1511
295. Demichev V, Messner CB, Vernardis SI, Lilley KS, Ralser M. DIA-NN: neural networks and interference correction enable deep proteome coverage in high throughput. *Nat Methods*. Jan 2020;17(1):41-44. doi:10.1038/s41592-019-0638-x
296. Chen C, Hou J, Tanner JJ, Cheng J. Bioinformatics Methods for Mass Spectrometry-Based Proteomics Data Analysis. *Int J Mol Sci*. Apr 20 2020;21(8)doi:10.3390/ijms21082873
297. Mallick P, Schirle M, Chen SS, et al. Computational prediction of proteotypic peptides for quantitative proteomics. *Nat Biotechnol*. Jan 2007;25(1):125-31. doi:10.1038/nbt1275
298. Ignjatovic V, Geyer PE, Palaniappan KK, et al. Mass Spectrometry-Based Plasma Proteomics: Considerations from Sample Collection to Achieving Translational Data. *J Proteome Res*. Dec 06 2019;18(12):4085-4097. doi:10.1021/acs.jproteome.9b00503
299. Olsen JV, Mann M. Status of large-scale analysis of post-translational modifications by mass spectrometry. *Mol Cell Proteomics*. Dec 2013;12(12):3444-52. doi:10.1074/mcp.O113.034181
300. Bekker-Jensen DB, Bernhardt OM, Hogrebe A, et al. Rapid and site-specific deep phosphoproteome profiling by data-independent acquisition without the need for spectral libraries. *Nat Commun*. Feb 07 2020;11(1):787. doi:10.1038/s41467-020-14609-1
301. Bortel P, Piga I, Koenig C, Gerner C, Martinez-Val A, Olsen JV. Systematic Optimization of Automated Phosphopeptide Enrichment for High-Sensitivity Phosphoproteomics. *Mol Cell Proteomics*. May 2024;23(5):100754. doi:10.1016/j.mcpro.2024.100754

302. Heunis T, Lamoliatte F, Marín-Rubio JL, Dannoura A, Trost M. Technical report: Targeted proteomic analysis reveals enrichment of atypical ubiquitin chains in contractile murine tissues. *J Proteomics*. Oct 30 2020;229:103963. doi:10.1016/j.jprot.2020.103963
303. Heap RE, Gant MS, Lamoliatte F, Peltier J, Trost M. Mass spectrometry techniques for studying the ubiquitin system. *Biochem Soc Trans*. Oct 15 2017;45(5):1137-1148. doi:10.1042/BST20170091
304. Steger M, Demichev V, Backman M, et al. Time-resolved in vivo ubiquitinome profiling by DIA-MS reveals USP7 targets on a proteome-wide scale. *Nat Commun*. Sep 13 2021;12(1):5399. doi:10.1038/s41467-021-25454-1
305. Malaker SA. Glycoproteomics: Charting new territory in mass spectrometry and glycobiology. *J Mass Spectrom*. Jun 2024;59(6):e5034. doi:10.1002/jms.5034
306. Gatto L, Aebersold R, Cox J, et al. Initial recommendations for performing, benchmarking and reporting single-cell proteomics experiments. *Nat Methods*. Mar 2023;20(3):375-386. doi:10.1038/s41592-023-01785-3
307. Gao Y, Ma M, Li W, Lei X. Chemoproteomics, A Broad Avenue to Target Deconvolution. *Adv Sci (Weinh)*. Feb 2024;11(8):e2305608. doi:10.1002/advs.202305608
308. Ziegler S, Pries V, Hedberg C, Waldmann H. Target identification for small bioactive molecules: finding the needle in the haystack. *Angew Chem Int Ed Engl*. Mar 04 2013;52(10):2744-92. doi:10.1002/anie.201208749
309. George AL, Sidgwick FR, Watt JE, et al. Comparison of Quantitative Mass Spectrometric Methods for Drug Target Identification by Thermal Proteome Profiling. *J Proteome Res*. Aug 04 2023;22(8):2629-2640. doi:10.1021/acs.jproteome.3c00111
310. Saei AA, Beusch CM, Chernobrovkin A, et al. ProTargetMiner as a proteome signature library of anticancer molecules for functional discovery. *Nat Commun*. Dec 16 2019;10(1):5715. doi:10.1038/s41467-019-13582-8
311. Mitchell DC, Kuljanin M, Li J, et al. A proteome-wide atlas of drug mechanism of action. *Nat Biotechnol*. Jun 2023;41(6):845-857. doi:10.1038/s41587-022-01539-0
312. Hutchinson JP, Temponeras I, Kuiper J, et al. Common allotypes of ER aminopeptidase 1 have substrate-dependent and highly variable enzymatic properties. *J Biol Chem*. 2021;296:100443. doi:10.1016/j.jbc.2021.100443
313. van Wilgenburg B, Browne C, Vowles J, Cowley SA. Efficient, long term production of monocyte-derived macrophages from human pluripotent stem cells under partly-defined and fully-defined conditions. *PLoS One*. 2013;8(8):e71098. doi:10.1371/journal.pone.0071098
314. Bernard EM, Fearns A, Bussi C, et al. infection of human iPSC-derived macrophages reveals complex membrane dynamics during xenophagy evasion. *J Cell Sci*. Nov 25 2020;134(5)doi:10.1242/jcs.252973
315. Penny J, Arefian M, Schroeder GN, Bengoechea JA, Collins BC. A gas phase fractionation acquisition scheme integrating ion mobility for rapid diaPASEF library generation. *Proteomics*. Apr 2023;23(7-8):e2200038. doi:10.1002/pmic.202200038
316. Gibb S, Strimmer K. MALDIquant: a versatile R package for the analysis of mass spectrometry data. *Bioinformatics*. Sep 01 2012;28(17):2270-1. doi:10.1093/bioinformatics/bts447
317. Frankenfield AM, Ni J, Ahmed M, Hao L. Protein Contaminants Matter: Building Universal Protein Contaminant Libraries for DDA and DIA Proteomics. *J Proteome Res*. Sep 2 2022;21(9):2104-2113. doi:10.1021/acs.jproteome.2c00145

318. Kong AT, Leprevost FV, Avtonomov DM, Mellacheruvu D, Nesvizhskii AI. MSFragger: ultrafast and comprehensive peptide identification in mass spectrometry–based proteomics. *Nature Methods*. 2017/05/01 2017;14(5):513-520. doi:10.1038/nmeth.4256
319. Hall MD, Yasgar A, Peryea T, et al. Fluorescence polarization assays in high-throughput screening and drug discovery: a review. *Methods Appl Fluoresc*. Apr 28 2016;4(2):022001. doi:10.1088/2050-6120/4/2/022001
320. Winter M, Ries R, Kleiner C, et al. Automated MALDI Target Preparation Concept: Providing Ultra-High-Throughput Mass Spectrometry-Based Screening for Drug Discovery. *SLAS Technol*. Apr 2019;24(2):209-221. doi:10.1177/2472630318791981
321. Müller L, Burton AK, Tayler CL, et al. A high-throughput MALDI-TOF MS biochemical screen for small molecule inhibitors of the antigen aminopeptidase ERAP1. *SLAS Discov*. Jan 2023;28(1):3-11. doi:10.1016/j.slasd.2022.11.002
322. Borges AC, Jayakrishnan A, Bourban P-E, Plummer CJG, Pioletti DP, Månson J-AE. Synthesis and Photopolymerization of Tween 20 Methacrylate/N-vinyl-2-Pyrrolidone Blends. *Materials Science and Engineering: C*. 2012/12/01/ 2012;32(8):2235-2241. doi:https://doi.org/10.1016/j.msec.2012.06.009
323. Jakop U, Fuchs B, Süss R, et al. The solubilisation of boar sperm membranes by different detergents - a microscopic, MALDI-TOF MS, (31)P NMR and PAGE study on membrane lysis, extraction efficiency, lipid and protein composition. *Lipids Health Dis*. Nov 11 2009;8:49. doi:10.1186/1476-511x-8-49
324. Krause E, Wenschuh H, Jungblut PR. The dominance of arginine-containing peptides in MALDI-derived tryptic mass fingerprints of proteins. *Anal Chem*. Oct 01 1999;71(19):4160-5. doi:10.1021/ac990298f
325. Brancia FL, Oliver SG, Gaskell SJ. Improved matrix-assisted laser desorption/ionization mass spectrometric analysis of tryptic hydrolysates of proteins following guanidination of lysine-containing peptides. *Rapid Commun Mass Spectrom*. 2000;14(21):2070-3. doi:10.1002/1097-0231(20001115)14:21<2070::AID-RCM133>3.0.CO;2-G
326. Cifaldi L, Romania P, Falco M, et al. ERAP1 regulates natural killer cell function by controlling the engagement of inhibitory receptors. *Cancer Res*. Mar 01 2015;75(5):824-34. doi:10.1158/0008-5472.CAN-14-1643
327. Bufalieri F, Infante P, Bernardi F, et al. ERAP1 promotes Hedgehog-dependent tumorigenesis by controlling USP47-mediated degradation of βTrCP. *Nat Commun*. Jul 24 2019;10(1):3304. doi:10.1038/s41467-019-11093-0
328. Maben Z, Arya R, Rane D, et al. Discovery of Selective Inhibitors of Endoplasmic Reticulum Aminopeptidase 1. *J Med Chem*. Jan 09 2020;63(1):103-121. doi:10.1021/acs.jmedchem.9b00293
329. Honarnejad S, van Boeckel S, van den Hurk H, van Helden S. Hit Discovery for Public Target Programs in the European Lead Factory: Experiences and Output from Assay Development and Ultra-High-Throughput Screening. *SLAS Discov*. Feb 2021;26(2):192-204. doi:10.1177/2472555220942765
330. Yu F, Haynes SE, Teo GC, Avtonomov DM, Polasky DA, Nesvizhskii AI. Fast Quantitative Analysis of timsTOF PASEF Data with MSFragger and IonQuant. *Mol Cell Proteomics*. Sep 2020;19(9):1575-1585. doi:10.1074/mcp.TIR120.002048
331. Wysocki VH, Tsaprailis G, Smith LL, Breci LA. Mobile and localized protons: a framework for understanding peptide dissociation. *J Mass Spectrom*. Dec 2000;35(12):1399-406. doi:10.1002/1096-9888(200012)35:12<1399::aid-jms86>3.0.co;2-r

332. von Ahsen O, Schmidt A, Klotz M, Parczyk K. Assay concordance between SPA and TR-FRET in high-throughput screening. *J Biomol Screen*. Sep 2006;11(6):606-16. doi:10.1177/1087057106288183
333. Lowe DM, Gee M, Haslam C, et al. Lead discovery for human kynurenine 3-monooxygenase by high-throughput RapidFire mass spectrometry. *J Biomol Screen*. Apr 2014;19(4):508-15. doi:10.1177/1087057113518069
334. Izquierdo M, Lin D, O'Neill S, et al. Development of a High-Throughput Screening Assay to Identify Inhibitors of the Major M17-Leucyl Aminopeptidase from. *SLAS Discov*. Oct 2020;25(9):1064-1071. doi:10.1177/2472555220923367
335. O'Connell L, Winter DC, Aherne CM. The Role of Organoids as a Novel Platform for Modeling of Inflammatory Bowel Disease. *Front Pediatr*. 2021;9:624045. doi:10.3389/fped.2021.624045
336. Odero MD, Zeleznik-Le NJ, Chinwalla V, Rowley JD. Cytogenetic and molecular analysis of the acute monocytic leukemia cell line THP-1 with an MLL-AF9 translocation. *Genes Chromosomes Cancer*. Dec 2000;29(4):333-8.
337. Heap RE, Marín-Rubio JL, Peltier J, et al. Proteomics characterisation of the L929 cell supernatant and its role in BMDM differentiation. *Life Sci Alliance*. Jun 2021;4(6)doi:10.26508/lsa.202000957
338. Murray PJ. Macrophage Polarization. *Annu Rev Physiol*. Feb 10 2017;79:541-566. doi:10.1146/annurev-physiol-022516-034339
339. McWhorter FY, Wang T, Nguyen P, Chung T, Liu WF. Modulation of macrophage phenotype by cell shape. *Proc Natl Acad Sci U S A*. Oct 22 2013;110(43):17253-8. doi:10.1073/pnas.1308887110
340. Thanou E, Koopmans F, Pita-Illobre D, et al. Suspension TRAPping Filter (sTRAP) Sample Preparation for Quantitative Proteomics in the Low µg Input Range Using a Plasmid DNA Micro-Spin Column: Analysis of the Hippocampus from the 5xFAD Alzheimer's Disease Mouse Model. *Cells*. 2023;12(9). doi:10.3390/cells12091242
341. Demichev V, Szyrwiel L, Yu F, et al. dia-PASEF data analysis using FragPipe and DIA-NN for deep proteomics of low sample amounts. *Nat Commun*. Jul 08 2022;13(1):3944. doi:10.1038/s41467-022-31492-0
342. Viode A, van Zalm P, Smolen KK, et al. A simple, time- and cost-effective, high-throughput depletion strategy for deep plasma proteomics. *Science Advances*. 2024/12/03 9(13):eadf9717. doi:10.1126/sciadv.adf9717
343. Vitko D, Chou WF, Nouri Golmaei S, et al. timsTOF HT Improves Protein Identification and Quantitative Reproducibility for Deep Unbiased Plasma Protein Biomarker Discovery. *J Proteome Res*. Mar 01 2024;23(3):929-938. doi:10.1021/acs.jproteome.3c00646
344. Jeong K, Kim S, Bandeira N. False discovery rates in spectral identification. *BMC Bioinformatics*. 2012;13 Suppl 16(Suppl 16):S2. doi:10.1186/1471-2105-13-S16-S2
345. Dubois E, Galindo AN, Dayon L, Cominetti O. Assessing normalization methods in mass spectrometry-based proteome profiling of clinical samples. *Biosystems*. Jun 2022;215-216:104661. doi:10.1016/j.biosystems.2022.104661
346. Murugesan G, Davidson L, Jannetti L, Crocker PR, Weigle B. Quantitative Proteomics of Polarised Macrophages Derived from Induced Pluripotent Stem Cells. *Biomedicines*. Jan 23 2022;10(2)doi:10.3390/biomedicines10020239

347. Jolliffe IT, Cadima J. Principal component analysis: a review and recent developments. *Philos Trans A Math Phys Eng Sci*. Apr 13 2016;374(2065):20150202. doi:10.1098/rsta.2015.0202
348. Guo M, Härtlova A, Gierliński M, et al. Triggering MSR1 promotes JNK-mediated inflammation in IL-4-activated macrophages. *Embo j*. Jun 3 2019;38(11)doi:10.15252/embj.2018100299
349. Dunne A, O'Neill L. New insights into the post-translational modification of Toll-like receptor signaling molecules. *J Endotoxin Res*. 2005;11(6):325-32. doi:10.1179/096805105X58742
350. Zamyatina A, Heine H. Lipopolysaccharide Recognition in the Crossroads of TLR4 and Caspase-4/11 Mediated Inflammatory Pathways. *Front Immunol*. 2020;11:585146. doi:10.3389/fimmu.2020.585146
351. You K, Gu H, Yuan Z, Xu X. Tumor Necrosis Factor Alpha Signaling and Organogenesis. *Front Cell Dev Biol*. 2021;9:727075. doi:10.3389/fcell.2021.727075
352. Hu WH, Mo XM, Walters WM, Brambilla R, Bethea JR. TNAP, a novel repressor of NF-kappaB-inducing kinase, suppresses NF-kappaB activation. *J Biol Chem*. Aug 20 2004;279(34):35975-83. doi:10.1074/jbc.M405699200
353. Harris KG, Coyne CB. Unc93b Induces Apoptotic Cell Death and Is Cleaved by Host and Enteroviral Proteases. *PLoS One*. 2015;10(10):e0141383. doi:10.1371/journal.pone.0141383
354. Tanaka T, Narazaki M, Kishimoto T. IL-6 in inflammation, immunity, and disease. *Cold Spring Harb Perspect Biol*. Sep 4 2014;6(10):a016295. doi:10.1101/cshperspect.a016295
355. Jiang Y, Rex DAB, Schuster D, et al. Comprehensive Overview of Bottom-Up Proteomics using Mass Spectrometry. *ArXiv*. Nov 13 2023;
356. Searle BC, Swearingen KE, Barnes CA, et al. Generating high quality libraries for DIA MS with empirically corrected peptide predictions. *Nat Commun*. Mar 25 2020;11(1):1548. doi:10.1038/s41467-020-15346-1
357. Guzman UH, Martinez-Val A, Ye Z, et al. Ultra-fast label-free quantification and comprehensive proteome coverage with narrow-window data-independent acquisition. *Nat Biotechnol*. Feb 01 2024;doi:10.1038/s41587-023-02099-7
358. Vincent F, Loria PM, Weston AD, et al. Hit Triage and Validation in Phenotypic Screening: Considerations and Strategies. *Cell Chem Biol*. Nov 19 2020;27(11):1332-1346. doi:10.1016/j.chembiol.2020.08.009
359. Subramanian N, Torabi-Parizi P, Gottschalk RA, Germain RN, Dutta B. Network representations of immune system complexity. *Wiley Interdiscip Rev Syst Biol Med*. 2015;7(1):13-38. doi:10.1002/wsbm.1288
360. Conway GC, Smole SC, Sarracino DA, Arbeit RD, Leopold PE. Phyloproteomics: species identification of Enterobacteriaceae using matrix-assisted laser desorption/ionization time-of-flight mass spectrometry. *J Mol Microbiol Biotechnol*. Jan 2001;3(1):103-12.
361. Munteanu B, Hopf C. Emergence of whole-cell MALDI-MS biotyping for high-throughput bioanalysis of mammalian cells? *Bioanalysis*. Apr 2013;5(8):885-93. doi:10.4155/bio.13.47
362. Povey JF, O'Malley CJ, Root T, et al. Rapid high-throughput characterisation, classification and selection of recombinant mammalian cell line phenotypes using intact cell MALDI-ToF mass spectrometry fingerprinting and PLS-DA modelling. *J Biotechnol*. Aug 20 2014;184:84-93. doi:10.1016/j.jbiotec.2014.04.028

363. Schwamb S, Munteanu B, Meyer B, Hopf C, Hafner M, Wiedemann P. Monitoring CHO cell cultures: cell stress and early apoptosis assessment by mass spectrometry. *J Biotechnol*. Dec 2013;168(4):452-61. doi:10.1016/j.jbiotec.2013.10.014
364. Feenstra AD, Hansen RL, Lee YJ. Multi-matrix, dual polarity, tandem mass spectrometry imaging strategy applied to a germinated maize seed: toward mass spectrometry imaging of an untargeted metabolome. 10.1039/C5AN01079A. *Analyst*. 2015;140(21):7293-7304. doi:10.1039/C5AN01079A
365. Holzlechner M, Strasser K, Zareva E, et al. In Situ Characterization of Tissue-Resident Immune Cells by MALDI Mass Spectrometry Imaging. *J Proteome Res*. Jan 6 2017;16(1):65-76. doi:10.1021/acs.jproteome.6b00610
366. Patel MS, Nemeria NS, Furey W, Jordan F. The pyruvate dehydrogenase complexes: structure-based function and regulation. *J Biol Chem*. Jun 13 2014;289(24):16615-23. doi:10.1074/jbc.R114.563148
367. Hasmann M, Schemainda I. FK866, a highly specific noncompetitive inhibitor of nicotinamide phosphoribosyltransferase, represents a novel mechanism for induction of tumor cell apoptosis. *Cancer Res*. Nov 1 2003;63(21):7436-42.
368. Lu J, Wang M, Chen Y, et al. NAMPT inhibition reduces macrophage inflammation through the NAD+/PARP1 pathway to attenuate liver ischemia-reperfusion injury. *Chem Biol Interact*. Jan 05 2023;369:110294. doi:10.1016/j.cbi.2022.110294
369. Bonday ZQ, Cortez GS, Grogan MJ, et al. LLY-283, a Potent and Selective Inhibitor of Arginine Methyltransferase 5, PRMT5, with Antitumor Activity. *ACS Med Chem Lett*. Jul 12 2018;9(7):612-617. doi:10.1021/acsmedchemlett.8b00014
370. Zhang R, Wang Y, Li R, Chen G. Transcriptional Factors Mediating Retinoic Acid Signals in the Control of Energy Metabolism. *Int J Mol Sci*. Jun 23 2015;16(6):14210-44. doi:10.3390/ijms160614210
371. Xiao D, Zeng T, Zhu W, et al. ANXA1 Promotes Tumor Immune Evasion by Binding PARP1 and Upregulating Stat3-Induced Expression of PD-L1 in Multiple Cancers. *Cancer Immunol Res*. Oct 04 2023;11(10):1367-1383. doi:10.1158/2326-6066.CIR-22-0896
372. Petrich A, Nabhan C. Use of class I histone deacetylase inhibitor romidepsin in combination regimens. *Leuk Lymphoma*. Aug 2016;57(8):1755-65. doi:10.3109/10428194.2016.1160082
373. Hull EE, Montgomery MR, Leyva KJ. HDAC Inhibitors as Epigenetic Regulators of the Immune System: Impacts on Cancer Therapy and Inflammatory Diseases. *Biomed Res Int*. 2016;2016:8797206. doi:10.1155/2016/8797206
374. Hartley AV, Wang B, Jiang G, et al. Regulation of a PRMT5/NF-κB Axis by Phosphorylation of PRMT5 at Serine 15 in Colorectal Cancer. *Int J Mol Sci*. May 23 2020;21(10)doi:10.3390/ijms21103684
375. Herůdková J, Paruch K, Khirsariya P, et al. Chk1 Inhibitor SCH900776 Effectively Potentiates the Cytotoxic Effects of Platinum-Based Chemotherapeutic Drugs in Human Colon Cancer Cells. *Neoplasia*. Oct 2017;19(10):830-841. doi:10.1016/j.neo.2017.08.002
376. Malumbres M. Cyclin-dependent kinases. *Genome Biol*. 2014;15(6):122. doi:10.1186/gb4184
377. Sundar V, Vimal S, Sai Mithlesh MS, Dutta A, Tamizhselvi R, Manickam V. Transcriptional cyclin-dependent kinases as the mediators of inflammation-a review. *Gene*. Feb 15 2021;769:145200. doi:10.1016/j.gene.2020.145200

378. Moens U, Kostenko S, Sveinbjørnsson B. The Role of Mitogen-Activated Protein Kinase-Activated Protein Kinases (MAPKAPKs) in Inflammation. *Genes (Basel)*. Mar 26 2013;4(2):101-33. doi:10.3390/genes4020101
379. Broom OJ, Widjaya B, Troelsen J, Olsen J, Nielsen OH. Mitogen activated protein kinases: a role in inflammatory bowel disease? *Clin Exp Immunol*. Dec 2009;158(3):272-80. doi:10.1111/j.1365-2249.2009.04033.x
380. Hwang WC, Seo SH, Kang M, et al. PLD1 and PLD2 differentially regulate the balance of macrophage polarization in inflammation and tissue injury. *J Cell Physiol*. Jul 2021;236(7):5193-5211. doi:10.1002/jcp.30224
381. Shi Z, Fultz RS, Engevik MA, et al. Distinct roles of histamine H1- and H2-receptor signaling pathways in inflammation-associated colonic tumorigenesis. *Am J Physiol Gastrointest Liver Physiol*. Jan 01 2019;316(1):G205-G216. doi:10.1152/ajpgi.00212.2018
382. Neshat MS, Raitano AB, Wang HG, Reed JC, Sawyers CL. The survival function of the Bcr-Abl oncogene is mediated by Bad-dependent and -independent pathways: roles for phosphatidylinositol 3-kinase and Raf. *Mol Cell Biol*. Feb 2000;20(4):1179-86. doi:10.1128/MCB.20.4.1179-1186.2000
383. Meng B, Zhao X, Jiang S, et al. AURKA inhibitor-induced PD-L1 upregulation impairs antitumor immune responses. *Front Immunol*. 2023;14:1182601. doi:10.3389/fimmu.2023.1182601
384. Canham SM, Wang Y, Cornett A, et al. Systematic Chemogenetic Library Assembly. *Cell Chem Biol*. Sep 17 2020;27(9):1124-1129. doi:10.1016/j.chembiol.2020.07.004
385. Bhattacharya P, Budnick I, Singh M, et al. Dual Role of GM-CSF as a Pro-Inflammatory and a Regulatory Cytokine: Implications for Immune Therapy. *J Interferon Cytokine Res*. Aug 2015;35(8):585-99. doi:10.1089/jir.2014.0149
386. Demirev PA, Feldman AB, Kowalski P, Lin JS. Top-down proteomics for rapid identification of intact microorganisms. *Anal Chem*. Nov 15 2005;77(22):7455-61. doi:10.1021/ac051419g
387. Sogawa K, Watanabe M, Sato K, et al. Use of the MALDI BioTyper system with MALDI-TOF mass spectrometry for rapid identification of microorganisms. *Anal Bioanal Chem*. Jun 2011;400(7):1905-11. doi:10.1007/s00216-011-4877-7
388. Enzlein T, Geisel A, Hopf C, S S. M2ara: unraveling metabolomic drug responses in whole-cell MALDI mass spectrometry bioassays. ChemRxiv2024.
389. Adamski J. Key elements of metabolomics in the study of biomarkers of diabetes. *Diabetologia*. Dec 2016;59(12):2497-2502. doi:10.1007/s00125-016-4044-y
390. Berry KA, Hankin JA, Barkley RM, Spraggins JM, Caprioli RM, Murphy RC. MALDI imaging of lipid biochemistry in tissues by mass spectrometry. *Chem Rev*. Oct 12 2011;111(10):6491-512. doi:10.1021/cr200280p
391. Neggers JE, Kwanten B, Dierckx T, et al. Target identification of small molecules using large-scale CRISPR-Cas mutagenesis scanning of essential genes. *Nat Commun*. Feb 5 2018;9(1):502. doi:10.1038/s41467-017-02349-8
392. Deans RM, Morgens DW, Ökesli A, et al. Parallel shRNA and CRISPR-Cas9 screens enable antiviral drug target identification. *Nat Chem Biol*. May 2016;12(5):361-6. doi:10.1038/nchembio.2050
393. Matheny CJ, Wei MC, Bassik MC, et al. Next-generation NAMPT inhibitors identified by sequential high-throughput phenotypic chemical and functional genomic screens. *Chem Biol*. Nov 21 2013;20(11):1352-63. doi:10.1016/j.chembiol.2013.09.014

394. Lamb J, Crawford ED, Peck D, et al. The Connectivity Map: using gene-expression signatures to connect small molecules, genes, and disease. *Science*. Sep 29 2006;313(5795):1929-35. doi:10.1126/science.1132939
395. Pahl A, Sievers S. The Cell Painting Assay as a Screening Tool for the Discovery of Bioactivities in New Chemical Matter. *Methods Mol Biol*. 2019;1888:115-126. doi:10.1007/978-1-4939-8891-4_6
396. Kunkel EJ, Plavec I, Nguyen D, et al. Rapid structure-activity and selectivity analysis of kinase inhibitors by BioMAP analysis in complex human primary cell-based models. *Assay Drug Dev Technol*. Aug 2004;2(4):431-41. doi:10.1089/adt.2004.2.431
397. Eckert S, Berner N, Kramer K, et al. Decrypting the molecular basis of cellular drug phenotypes by dose-resolved expression proteomics. *Nat Biotechnol*. May 07 2024;doi:10.1038/s41587-024-02218-y
398. Elmore S. Apoptosis: a review of programmed cell death. *Toxicol Pathol*. Jun 2007;35(4):495-516. doi:10.1080/01926230701320337
399. Sokhi S, Lewis CW, Bukhari AB, et al. Myt1 overexpression mediates resistance to cell cycle and DNA damage checkpoint kinase inhibitors. *Front Cell Dev Biol*. 2023;11:1270542. doi:10.3389/fcell.2023.1270542
400. Ji N, Yang Y, Lei ZN, et al. Ulixertinib (BVD-523) antagonizes ABCB1- and ABCG2-mediated chemotherapeutic drug resistance. *Biochem Pharmacol*. Dec 2018;158:274-285. doi:10.1016/j.bcp.2018.10.028
401. Yu Y, Zhao Y, Choi J, et al. ERK Inhibitor Ulixertinib Inhibits High-Risk Neuroblastoma Growth In Vitro and In Vivo. *Cancers (Basel)*. Nov 10 2022;14(22)doi:10.3390/cancers14225534
402. Ding Y, Wang B, Chen X, Zhou Y, Ge J. Staurosporine suppresses survival of HepG2 cancer cells through Omi/HtrA2-mediated inhibition of PI3K/Akt signaling pathway. *Tumour Biol*. Mar 2017;39(3):1010428317694317. doi:10.1177/1010428317694317
403. Huo S, Liu X, Zhang S, et al. p300/CBP inhibitor A-485 inhibits the differentiation of osteoclasts and protects against osteoporotic bone loss. *Int Immunopharmacol*. May 2021;94:107458. doi:10.1016/j.intimp.2021.107458
404. Natarajan U, Venkatesan T, Radhakrishnan V, Samuel S, Rasappan P, Rathinavelu A. Cell Cycle Arrest and Cytotoxic Effects of SAHA and RG7388 Mediated through p21(WAF1/CIP1) and p27(KIP1) in Cancer Cells. *Medicina (Kaunas)*. Jan 29 2019;55(2)doi:10.3390/medicina55020030
405. Zierfuss B, Weinhofer I, Buda A, et al. Targeting foam cell formation in inflammatory brain diseases by the histone modifier MS-275. *Ann Clin Transl Neurol*. Nov 2020;7(11):2161-2177. doi:10.1002/acn3.51200
406. Yin L, Xu J, Wu W, et al. Dual inhibition of STAT3 and STAT5 may overcome imatinib resistance in chronic myeloid leukemia. *Hematology*. Dec 2023;28(1):2224625. doi:10.1080/16078454.2023.2224625
407. Haftchenary S, Luchman HA, Jouk AO, et al. Potent Targeting of the STAT3 Protein in Brain Cancer Stem Cells: A Promising Route for Treating Glioblastoma. *ACS Med Chem Lett*. Nov 14 2013;4(11):1102-7. doi:10.1021/ml4003138
408. Tagoug I, Sauty De Chalon A, Dumontet C. Inhibition of IGF-1 signalling enhances the apoptotic effect of AS602868, an IKK2 inhibitor, in multiple myeloma cell lines. *PLoS One*. 2011;6(7):e22641. doi:10.1371/journal.pone.0022641

409. Nan J, Du Y, Chen X, et al. TPCA-1 is a direct dual inhibitor of STAT3 and NF-κB and regresses mutant EGFR-associated human non-small cell lung cancers. *Mol Cancer Ther*. Mar 2014;13(3):617-29. doi:10.1158/1535-7163.mct-13-0464
410. Nakamura M, Shimizu Y, Sato Y, et al. Toll-like receptor 4 signal transduction inhibitor, M62812, suppresses endothelial cell and leukocyte activation and prevents lethal septic shock in mice. *Eur J Pharmacol*. Aug 27 2007;569(3):237-43. doi:10.1016/j.ejphar.2007.05.013
411. Mares A, Miah AH, Smith IED, et al. Extended pharmacodynamic responses observed upon PROTAC-mediated degradation of RIPK2. *Commun Biol*. Mar 20 2020;3(1):140. doi:10.1038/s42003-020-0868-6
412. Strober W, Murray PJ, Kitani A, Watanabe T. Signalling pathways and molecular interactions of NOD1 and NOD2. *Nat Rev Immunol*. Jan 2006;6(1):9-20. doi:10.1038/nri1747
413. Song J, Yang R, Wei R, Du Y, He P, Liu X. Pan-cancer analysis reveals RIPK2 predicts prognosis and promotes immune therapy resistance via triggering cytotoxic T lymphocytes dysfunction. *Mol Med*. May 04 2022;28(1):47. doi:10.1186/s10020-022-00475-8
414. Wang N, Wu R, Tang D, Kang R. The BET family in immunity and disease. *Signal Transduct Target Ther*. Jan 19 2021;6(1):23. doi:10.1038/s41392-020-00384-4
415. Guo Q, Jin Y, Chen X, et al. NF-κB in biology and targeted therapy: new insights and translational implications. *Signal Transduct Target Ther*. Mar 4 2024;9(1):53. doi:10.1038/s41392-024-01757-9
416. Matt T. Transcriptional control of the inflammatory response: a role for the CREB-binding protein (CBP). *Acta Med Austriaca*. 2002;29(3):77-9. doi:10.1046/j.1563-2571.2002.02010.x
417. Katholnig K, Linke M, Pham H, Hengstschläger M, Weichhart T. Immune responses of macrophages and dendritic cells regulated by mTOR signalling. *Biochem Soc Trans*. Aug 2013;41(4):927-33. doi:10.1042/BST20130032
418. Manshouri T, Quintás-Cardama A, Nussenzveig RH, et al. The JAK kinase inhibitor CP-690,550 suppresses the growth of human polycythemia vera cells carrying the JAK2V617F mutation. *Cancer Sci*. Jun 2008;99(6):1265-73. doi:10.1111/j.1349-7006.2008.00817.x
419. Quintás-Cardama A, Vaddi K, Liu P, et al. Preclinical characterization of the selective JAK1/2 inhibitor INCB018424: therapeutic implications for the treatment of myeloproliferative neoplasms. *Blood*. Apr 15 2010;115(15):3109-17. doi:10.1182/blood-2009-04-214957
420. McClendon CL, Kornev AP, Gilson MK, Taylor SS. Dynamic architecture of a protein kinase. *Proc Natl Acad Sci U S A*. Oct 28 2014;111(43):E4623-31. doi:10.1073/pnas.1418402111
421. Zarrin AA, Bao K, Lupardus P, Vucic D. Kinase inhibition in autoimmunity and inflammation. *Nat Rev Drug Discov*. Jan 2021;20(1):39-63. doi:10.1038/s41573-020-0082-8
422. Lombardi MS, Gilliéron C, Dietrich D, Gabay C. SIK inhibition in human myeloid cells modulates TLR and IL-1R signaling and induces an anti-inflammatory phenotype. *J Leukoc Biol*. May 2016;99(5):711-21. doi:10.1189/jlb.2A0715-307R
423. Cohen P. Protein kinases--the major drug targets of the twenty-first century? *Nat Rev Drug Discov*. Apr 2002;1(4):309-15. doi:10.1038/nrd773

424. Takashima K, Matsunaga N, Yoshimatsu M, et al. Analysis of binding site for the novel small-molecule TLR4 signal transduction inhibitor TAK-242 and its therapeutic effect on mouse sepsis model. *Br J Pharmacol*. Aug 2009;157(7):1250-62. doi:10.1111/j.1476-5381.2009.00297.x
425. Hertz AL, Bender AT, Smith KC, et al. Elevated cyclic AMP and PDE4 inhibition induce chemokine expression in human monocyte-derived macrophages. *Proc Natl Acad Sci U S A*. Dec 22 2009;106(51):21978-83. doi:10.1073/pnas.0911684106
426. Schett G, Sloan VS, Stevens RM, Schafer P. Apremilast: a novel PDE4 inhibitor in the treatment of autoimmune and inflammatory diseases. *Ther Adv Musculoskelet Dis*. Oct 2010;2(5):271-8. doi:10.1177/1759720X10381432
427. Jung DW, Kim WH, Park SH, et al. A unique small molecule inhibitor of enolase clarifies its role in fundamental biological processes. *ACS Chem Biol*. 2013;8(6):1271-82. doi:10.1021/cb300687k
428. Zhao W, Qi J, Wang L, Zhang M, Wang P, Gao C. LY294002 inhibits TLR3/4-mediated IFN-β production via inhibition of IRF3 activation with a PI3K-independent mechanism. *FEBS Lett*. Mar 23 2012;586(6):705-10. doi:10.1016/j.febslet.2012.01.016
429. Ruprecht B, Di Bernardo J, Wang Z, et al. A mass spectrometry-based proteome map of drug action in lung cancer cell lines. *Nat Chem Biol*. Oct 2020;16(10):1111-1119. doi:10.1038/s41589-020-0572-3
430. Pan C, Olsen JV, Daub H, Mann M. Global effects of kinase inhibitors on signaling networks revealed by quantitative phosphoproteomics. *Mol Cell Proteomics*. Dec 2009;8(12):2796-808. doi:10.1074/mcp.M900285-MCP200
431. Franciosa G, Locard-Paulet M, Jensen LJ, Olsen JV. Recent advances in kinase signaling network profiling by mass spectrometry. *Curr Opin Chem Biol*. Apr 2023;73:102260. doi:10.1016/j.cbpa.2022.102260
432. Zecha J, Bayer FP, Wiechmann S, et al. Decrypting drug actions and protein modifications by dose- and time-resolved proteomics. *Science*. Apr 07 2023;380(6640):93-101. doi:10.1126/science.ade3925
433. Eberl HC, Werner T, Reinhard FB, et al. Chemical proteomics reveals target selectivity of clinical Jak inhibitors in human primary cells. *Sci Rep*. Oct 02 2019;9(1):14159. doi:10.1038/s41598-019-50335-5
434. Gaetani M, Sabatier P, Saei AA, et al. Proteome Integral Solubility Alteration: A High-Throughput Proteomics Assay for Target Deconvolution. *J Proteome Res*. Nov 01 2019;18(11):4027-4037. doi:10.1021/acs.jproteome.9b00500
435. Gaetani M, Zubarev RA. Proteome Integral Solubility Alteration (PISA) for High-Throughput Ligand Target Deconvolution with Increased Statistical Significance and Reduced Sample Amount. *Methods Mol Biol*. 2023;2554:91-106. doi:10.1007/978-1-0716-2624-5_7
436. Zhang X, Lytovchenko O, Lundström SL, Zubarev RA, Gaetani M. Proteome Integral Solubility Alteration (PISA) Assay in Mammalian Cells for Deep, High-Confidence, and High-Throughput Target Deconvolution. *Bio Protoc*. Nov 20 2022;12(22)doi:10.21769/BioProtoc.4556
437. Sabatier P, Beusch CM, Saei AA, et al. An integrative proteomics method identifies a regulator of translation during stem cell maintenance and differentiation. *Nat Commun*. Nov 12 2021;12(1):6558. doi:10.1038/s41467-021-26879-4

438. Becher I, Werner T, Doce C, et al. Thermal profiling reveals phenylalanine hydroxylase as an off-target of panobinostat. *Nat Chem Biol*. Nov 2016;12(11):908-910. doi:10.1038/nchembio.2185
439. Klaeger S, Gohlke B, Perrin J, et al. Chemical Proteomics Reveals Ferrochelatase as a Common Off-target of Kinase Inhibitors. *ACS Chem Biol*. May 20 2016;11(5):1245-54. doi:10.1021/acschembio.5b01063

Appendix A. Supplementary figures

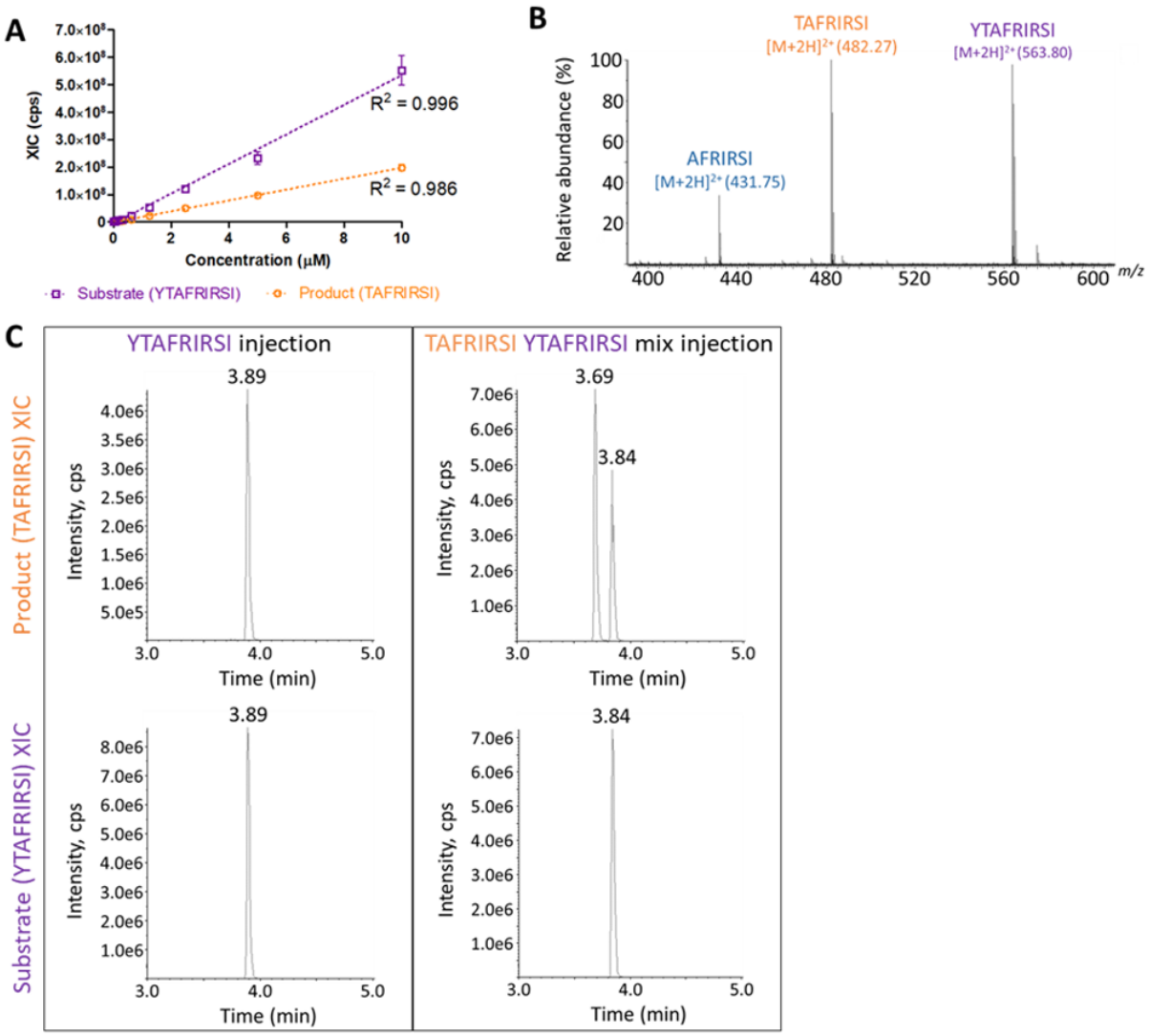

Supplementary Figure S.1: Fragmentation of basic peptides (BP) upon measurement by RapidFire MS. (A) Standard curve from substrate only wells obtained by plotting extracted ion chromatogram (XIC) counts per second (cps) for the doubly charged, protonated substrate (YTAFRIRSI, purple) and product (TAFRIRSI, orange); $n_{technical}$ = 6, mean ± standard deviation. (B) MS1 from 1 µM substrate injection into a Xevo G2-XS TOF system (QTOF, Waters) indicating relative abundance for the doubly charged, protonated 9mer substrate (YTAFRIRSI, purple, *m/z* 563.80), 8mer product (TAFRIRSI, orange, *m/z* 482.27) and 7mer (AFRIRSI, cyan, *m/z* 431.75). (C) LC-MS analysis (Exion LC (Sciex), Sciex 6500⁺ triple quadrupole (QqQ) setup) of substrate (YTAFRIRSI), and 1:1 product:substrate (TAFRIRSI:YTAFRIRSI); product signal intensity (top panel, orange) and substrate signal intensity (bottom panel, purple) plotted against the retention time.

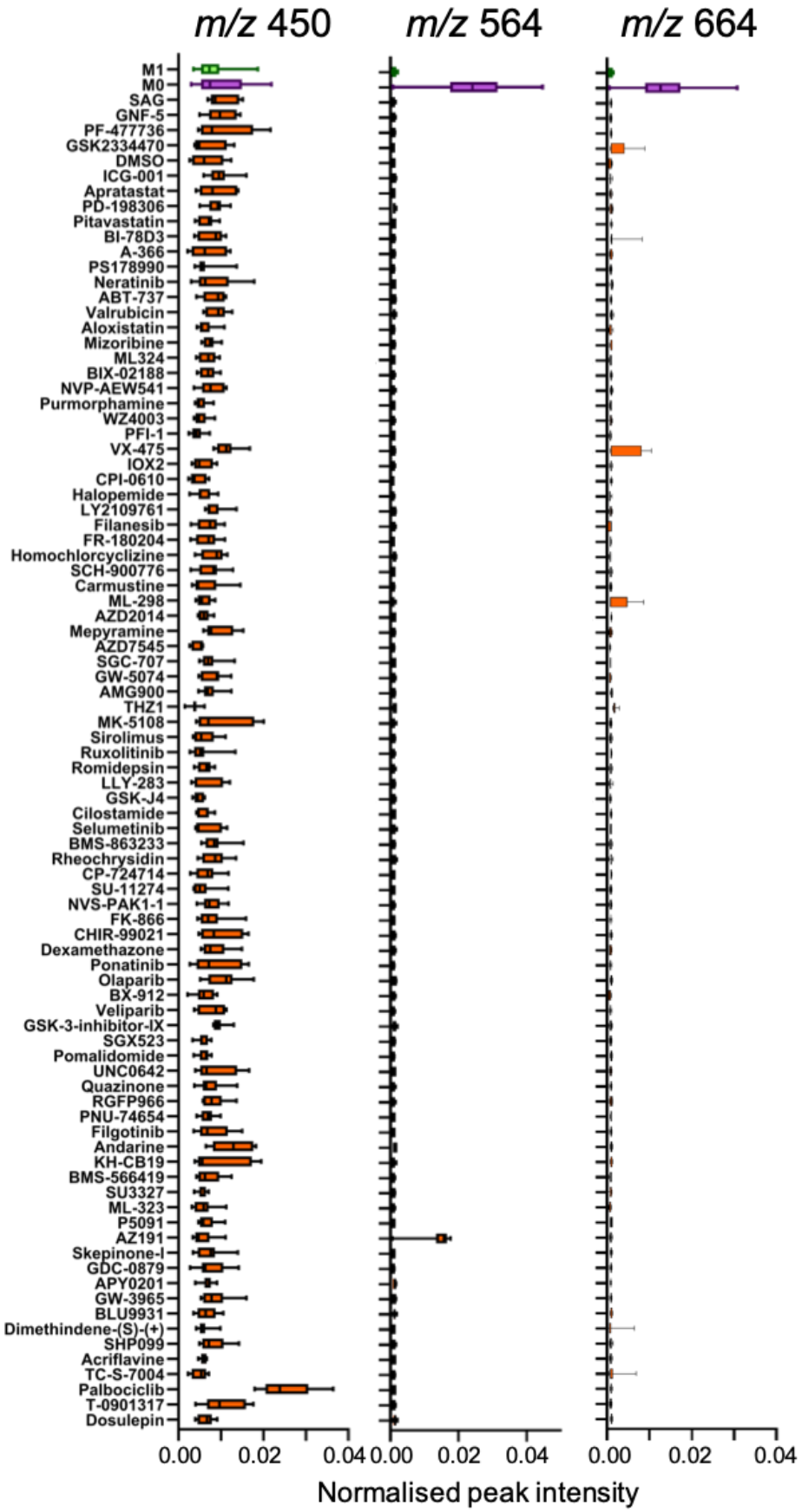

Supplementary Figure S.2: Boxplot of the normalised *m/z* 450, 564 and 664 M0 "biomarker" signal intensities for 87 different JUMP set compounds and the M0 (purple) and M1 (green) controls. n_{M0} = 4 per donor, n_{M1} = 4 per donor, acquisitions conducted in triplicate.

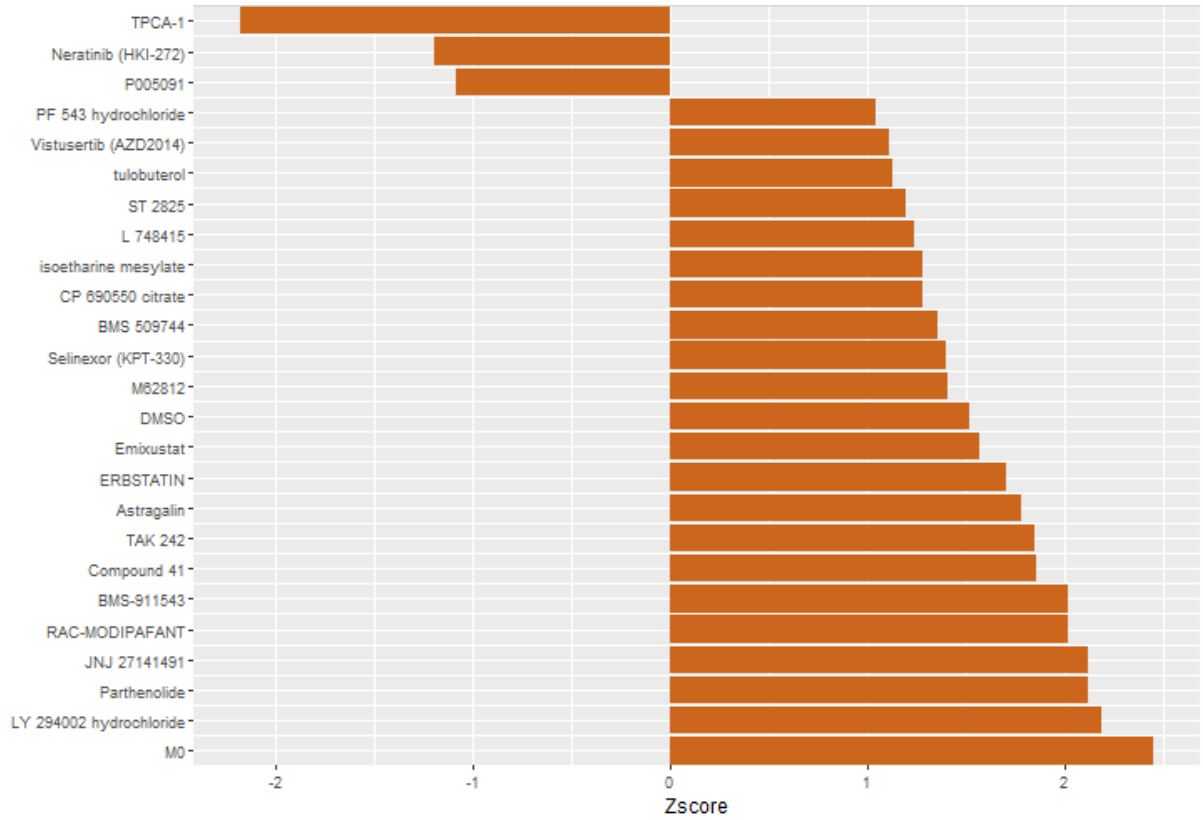

Supplementary Figure S.3: Scalar projection analysis of M1 polarised macrophages that were treated with the inflammation compound set. Bar chart of statistically significant compound projection z-scores in comparison to the M1 controls; t-test (Bonferroni Holm).

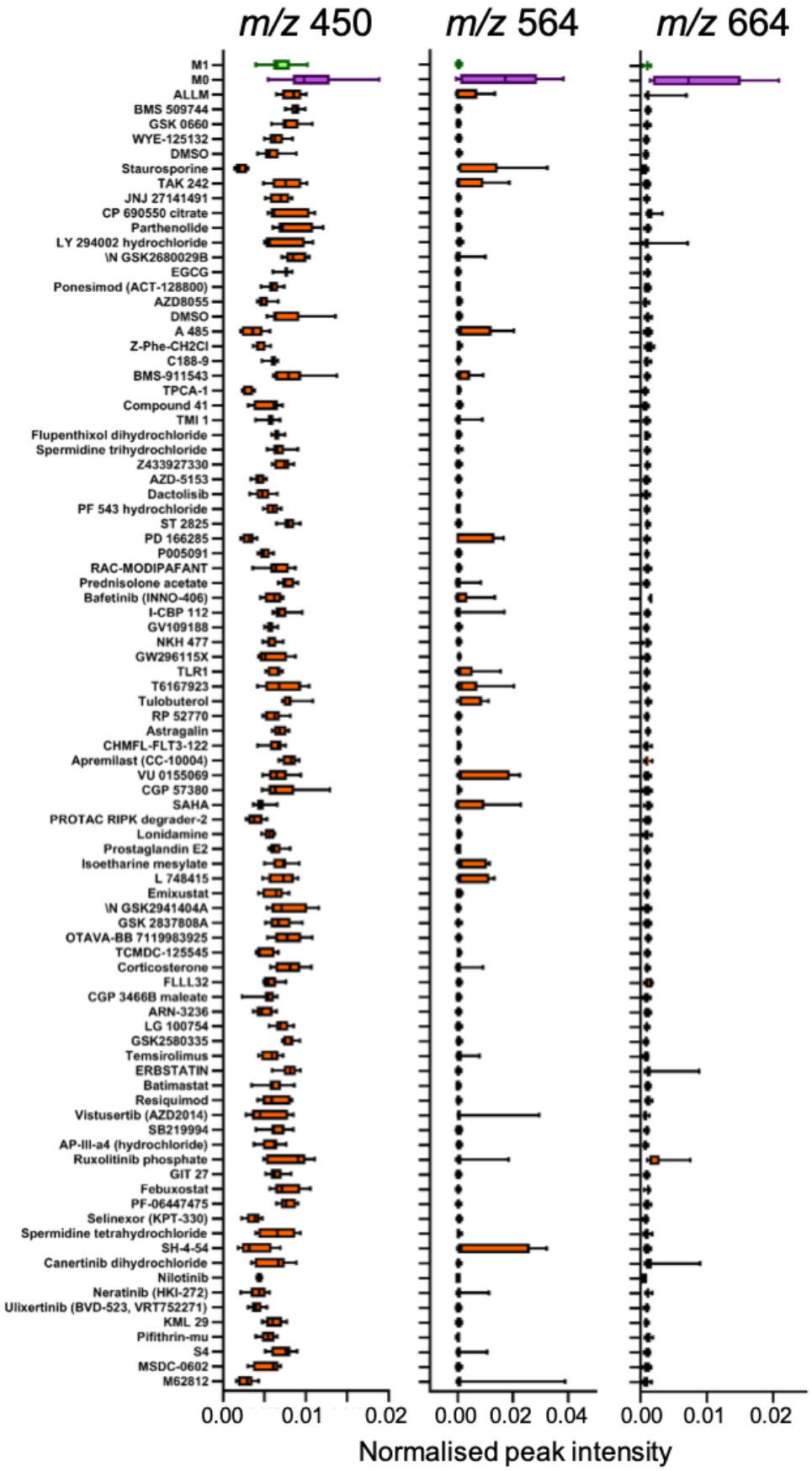

Supplementary Figure S.4: Boxplot of the normalised *m/z* 450, 564 and 664 M0 "biomarker" signal intensities for 86 different inflammation set compounds and the M0 (purple) and M1 (green) controls. n_{M0} = 4 per donor, n_{M1} = 4 per donor, acquisitions conducted in triplicate.

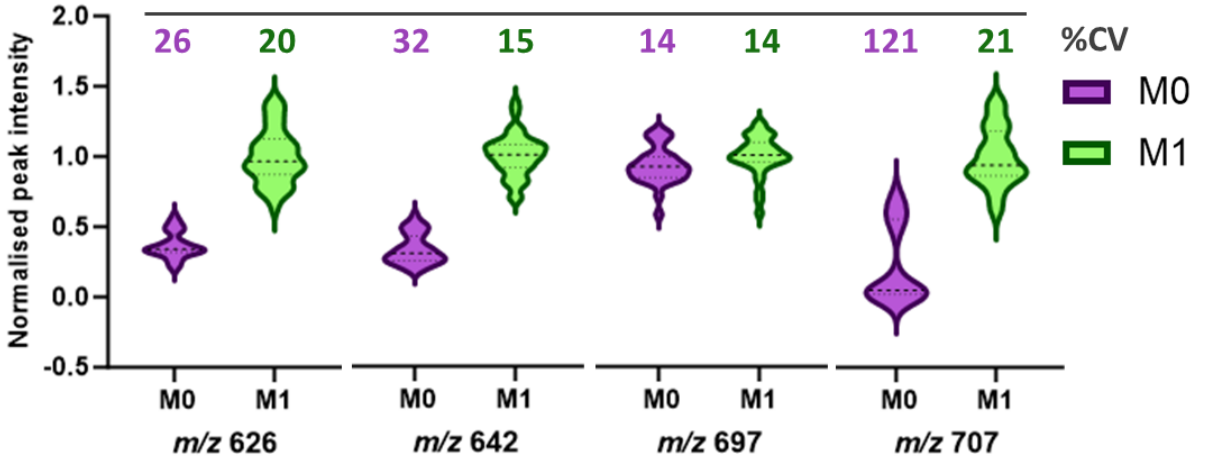

Supplementary Figure S.5: Violin plots of the normalised peak intensities at *m/z* 626, 642, 697 and 707 from the resting (M0, purple) or pro-inflammatory (M1, green) iPSC-derived macrophage controls contained within the inflammation compound set screen. Indicated is the %CV for each of the samples; n_{M0} = 4 per donor, n_{M1} = 4 per donor, acquisitions conducted in triplicate.

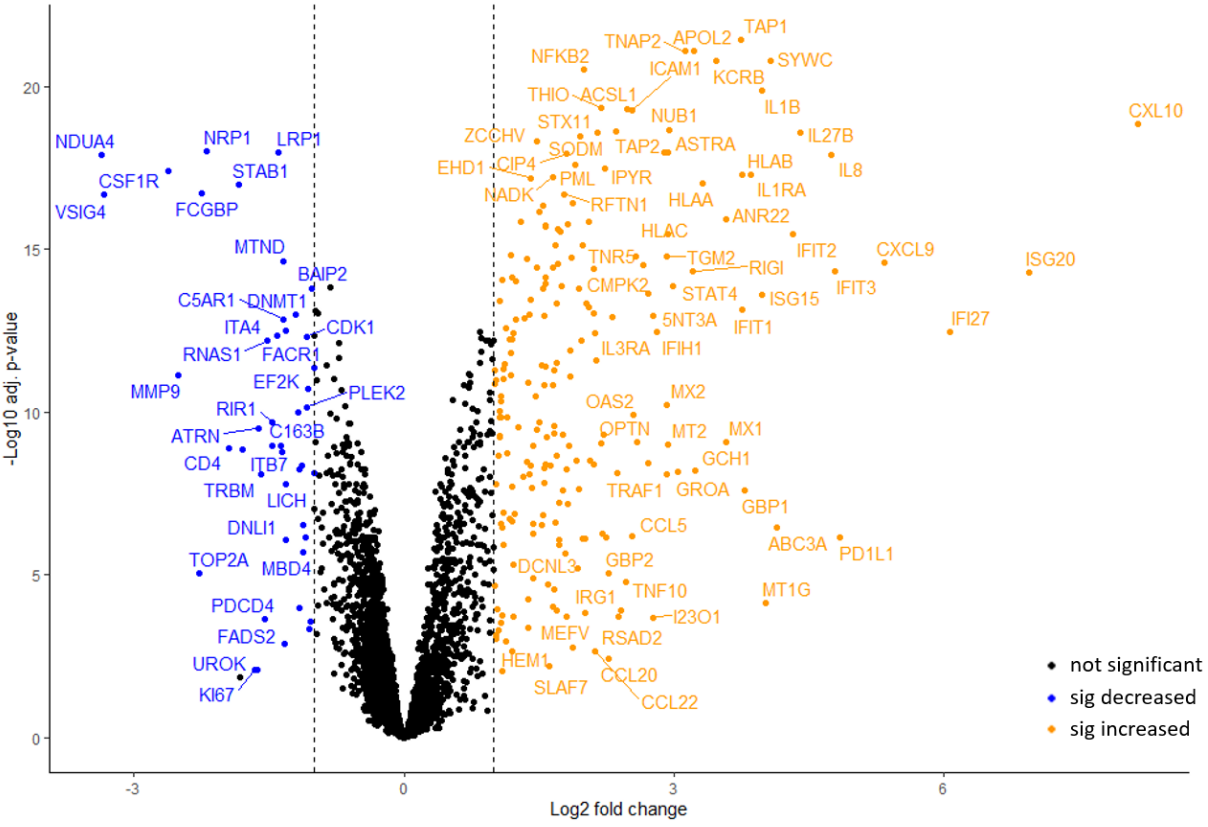

Figure S.6: Volcano plot indicating the significantly up and downregulated proteins of the M1 macrophage stimulation in comparison to the resting macrophage. Both samples were taken from the inflammation compound set proteomics experiment. Log2 protein fold change (cut-off = -2 or 2) against -log10 adjusted p-value (cut-off = 0.01) after t-testing (Benjamin-Hochberg correction) with highlighted significantly down (blue) and upregulated (orange) proteins.

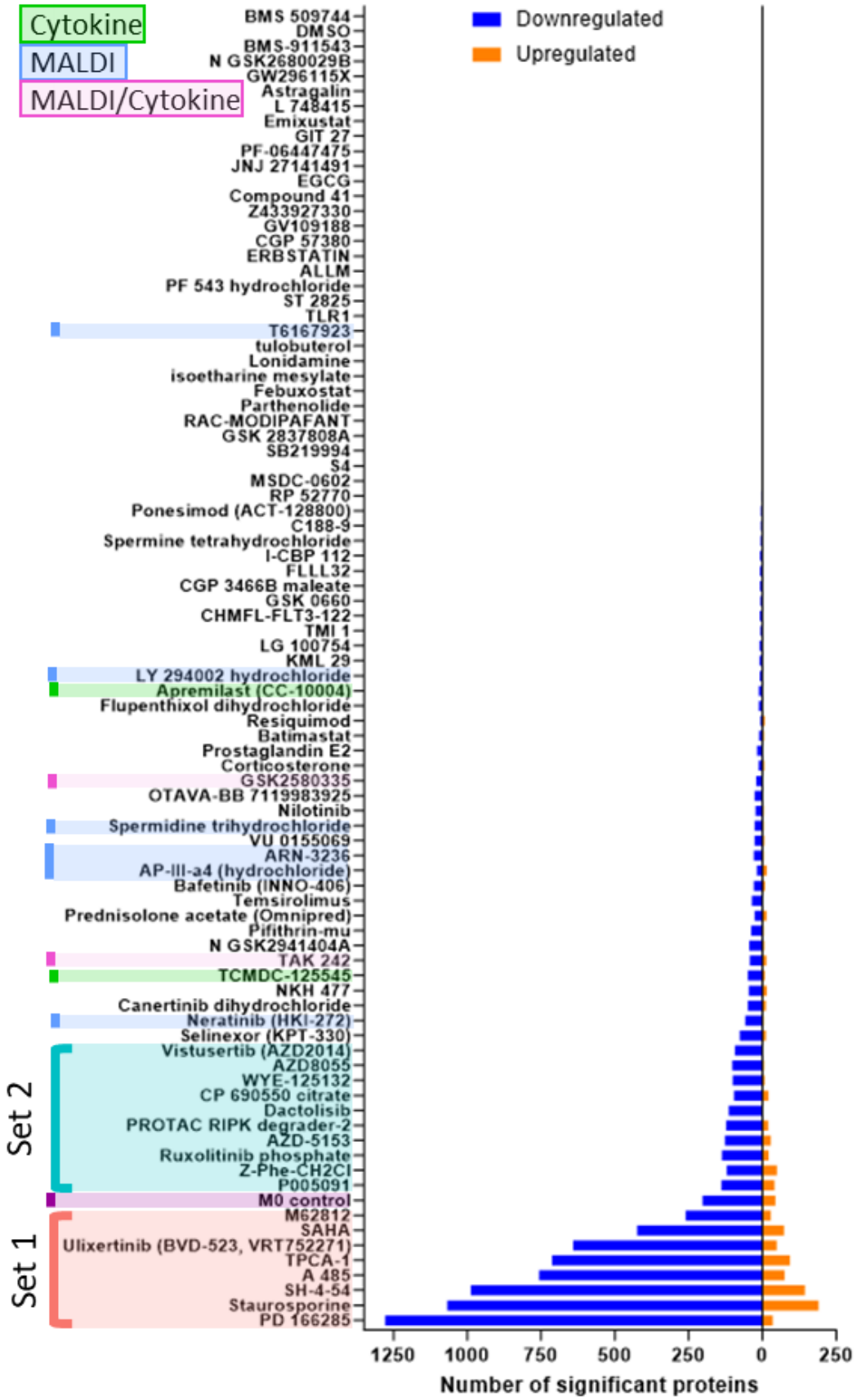

Figure S.7: Number of significantly changing proteins in the inflammation compound set treatments in comparison to the M1 macrophage control (t-testing, Benjamin-Hochberg correction).

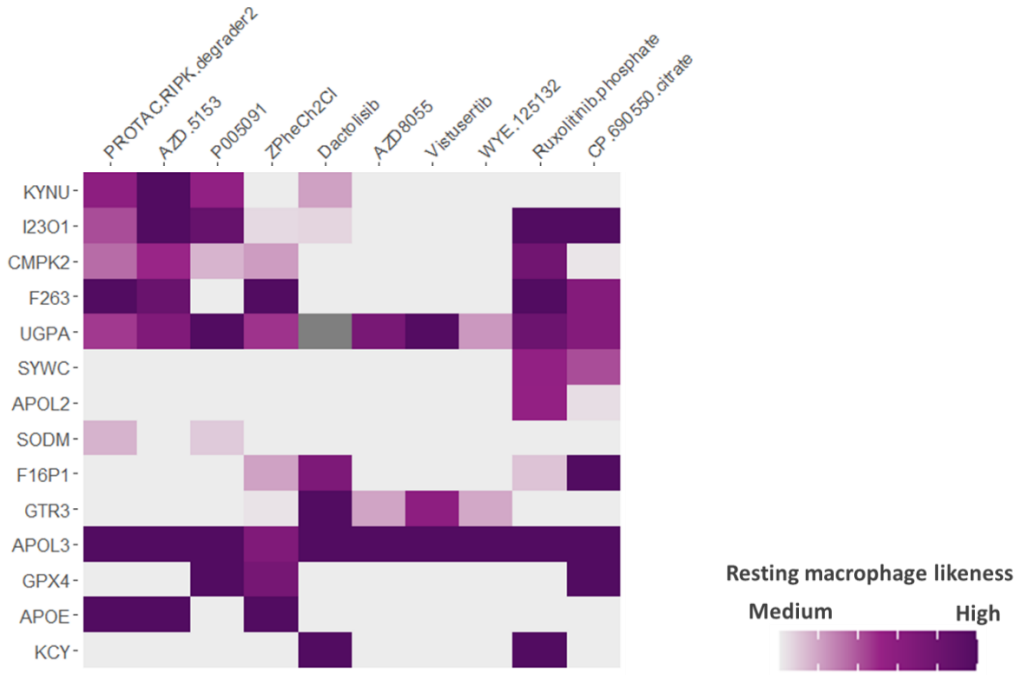

Figure S.8: M0 macrophage likeness scoring across different metabolic protein marker for compounds identified within the second set of proteomics hits. Log2 protein intensity recorded for each compound treatment was normalised against intensity levels in the M0 and M1 controls.

Appendix B. Supplementary tables

Supplementary Table S.1: List of all significant hits according to the scalar projection analysis from the JUMP compound treatments when compared to the M1 macrophage phenotype. Listed are the mean, z-score and adjusted p-value for the compound projection and rejection; n_{M0} = 4 per donor, n_{M1} = 4 per donor, acquisitions conducted in triplicate, t-test (Bonferroni Holm).

Compound	Projection			Rejection		
	Mean	z	adj p-value	Mean	z	adj p-value
M1	0.00	0.30	1.00E+00	0.05	-0.43	1.00E+00
Ruxolitinib phosphate	0.38	1.04	8.71E-04	-0.09	-0.75	3.97E-01
PS178990	0.41	1.05	2.69E-07	-0.11	-0.71	2.75E-01
Pomalidomide	0.38	1.05	4.81E-04	-0.14	-1.12	1.99E-01
BMS-566419	0.39	1.05	5.73E-04	-0.03	-0.36	7.63E-01
IOX2	0.37	1.05	1.78E-04	-0.11	-0.53	2.41E-01
PNU-74654	0.36	1.06	1.57E-07	-0.12	-0.97	1.67E-01
Pitavastatin	0.38	1.07	1.42E-06	-0.02	-0.73	8.17E-01
UNC0642	0.29	1.07	4.67E-03	1.66	6.99	8.48E-04
SCH-900776	0.36	1.10	1.42E-06	-0.09	-0.65	2.04E-01
FK-866	0.34	1.10	2.39E-05	-0.12	-0.84	1.85E-01
ML324	0.27	1.10	4.69E-02	0.06	-0.23	9.41E-01
CHIR-99021	0.34	1.11	4.58E-03	-0.05	-0.43	5.33E-01
SU-11274	0.43	1.13	1.94E-06	-0.02	-0.29	7.63E-01
RGFP966	0.35	1.13	1.75E-04	-0.08	-0.83	3.97E-01
ML-323	0.45	1.14	6.90E-06	-0.03	-0.41	7.41E-01
A-366	0.42	1.17	7.11E-05	0.15	0.24	6.24E-01
P5091	0.38	1.18	4.21E-07	-0.10	-0.53	2.04E-01
Sirolimus	0.34	1.19	3.08E-03	-0.18	-1.07	4.79E-02
WZ4003	0.44	1.21	7.73E-07	0.19	0.47	5.20E-01
LLY-283	0.46	1.23	1.37E-04	0.04	-0.19	9.67E-01
DMSO	0.47	1.24	9.07E-07	0.06	0.16	9.86E-01
SGX523	0.42	1.24	1.26E-06	-0.05	-0.54	5.82E-01
Purmorphamine	0.47	1.28	2.33E-04	0.00	-0.29	8.51E-01
CPI-0610	0.49	1.32	4.04E-06	0.08	-0.51	9.19E-01
GSK-J4	0.46	1.38	2.95E-07	0.05	-0.21	1.00E+00
Carmustine	0.47	1.39	8.69E-07	0.01	-0.15	8.59E-01
GSK2334470	0.52	1.41	3.77E-06	0.13	0.17	7.41E-01
Filgotinib	0.39	1.41	3.75E-03	-0.06	-0.41	5.86E-01
PFI-1	0.56	1.42	1.57E-07	0.01	-0.37	8.59E-01
AZD7545	0.55	1.44	3.61E-08	0.02	-0.14	8.64E-01
TC-S-7004	0.52	1.45	2.27E-05	0.06	-0.08	9.86E-01
FR-180204	0.57	1.53	1.31E-09	0.17	0.45	4.98E-01
Dexamethazone	0.58	1.54	6.26E-05	0.15	0.58	8.17E-01
AZ191	0.85	2.18	1.31E-09	0.67	2.52	1.81E-08
M0	1.00	2.42	5.03E-24	0.00	-0.31	8.49E-01

Table S.2: List of compounds identified within the first set of proteomics hits together with their annotated targets obtained from the GSK chemogenomic library.

Compound	Target annotation
M62812	TLR4
SAHA	NCOR1, HDAC3, KDM1A, KDM4E, HDAC9, HDAC11, HDAC7, HDAC5, HDAC10, HDAC4, HDAC2, HDAC8, HDAC6, HDAC1, ESR1, BRD4, KCNH2, NCOR2, EGFR, ERBB2
Ulixertinib	MAPK1, MAPK3, TAOK1
TPCA-1	JAK2, IKBKB
A-485	EP300, CREBBP
SH-4-54	STAT3, STAT5A
Staurosporine	AAK1, ABL1, ABL2, AKT1, AKT2, AKT3, ALK, ANKK1, AURKA, AURKB, AURKC, AXL, BCL2L1, BLK, BMP2K, BMX, BRAF, BRSK1, BRSK2, BTK, C8orf44-SGK3, CAMK1, CAMK1D, CAMK1G, CAMK2A, CAMK2B, CAMK2D, CAMK2G, CAMKK1, CAMKK2, CASK, CCNA1, CCNA2, CCNB1, CCNB2, CCNB3, CCNC, CCND1, CCND3, CCNE1, CCNE2, CCNH, CCNK, CCNO, CCNT1, CCNY, CDC42BPA, CDC42BPB, CDC42BPG, CDC7, CDK1, CDK12, CDK16, CDK18, CDK2, CDK3, CDK4, CDK5, CDK5R1, CDK6, CDK7, CDK8, CDK9, CHEK1, CHEK2, CHUK, CILK1, CLK1, CLK2, CLK4, CSF1R, CSK, CSNK2A2, CYP11B2, DAPK1, DAPK2, DAPK3, DBF4, DCLK3, DDR1, DDR2, DMPK, DSTYK, DYRK1A, DYRK1B, DYRK3, EGFR, EIF2AK4, EPHA3, EPHA4, EPHA5, EPHA6, EPHB1, EPHB3, ERBB2, ERBB4, ERN1, ERN2, FER, FES, FGFR1, FGFR2, FGFR3, FGR, FLT1, FLT3, FLT4, FPGT-TNNI3K, FRK, FYN, GAK, GCK, GRK1, GRK2, GRK3, GRK5, GRK7, GSK3A, GSK3B, HCK, IGF1R, IKBKB, IKBKE, INSR, INSRR, IRAK1, IRAK3, IRAK4, ITK, JAK1, JAK2, JAK3, KDR, KIT, LATS1, LATS2, LCK, LIMK1, LIMK2, LMTK3, LRRK2, LTK, LYN, MAK, MAP2K1, MAP2K2, MAP2K3, MAP2K4, MAP2K5, MAP2K6, MAP3K10, MAP3K11, MAP3K12, MAP3K15, MAP3K19, MAP3K2, MAP3K21, MAP3K3, MAP3K5, MAP3K7, MAP3K9, MAP4K1, MAP4K2, MAP4K3, MAP4K4, MAP4K5, MAPK1, MAPK12, MAPK14, MAPK15, MARK1, MARK2, MARK3, MARK4, MELK, MERTK, MINK1, MKNK2, MNAT1, MST1R, MUSK, MYLK, MYLK2, MYLK4, MYO3B, NEK1, NEK11, NEK4, NEK8, NEK9, NIM1K, NTRK1, NTRK2, NTRK3, NUAK1, NUAK2, OSR1, PAK1, PAK2, PAK3, PAK4, PAK5, PAK6, PASK, PBK, PDGFRA, PDGFRB, PDK1, PDPK1, PEAK1, PHKG1, PHKG2, PIM1, PIM2, PIM3, PKN1, PKN2, PKN3, PLK4, PNCK, PREP, PRKAA1, PRKAA2, PRKACA, PRKACB, PRKACG, PRKCA, PRKCB, PRKCD, PRKCE, PRKCG, PRKCH, PRKCI, PRKCQ, PRKCZ, PRKD1, PRKD2, PRKD3, PRKG1, PRKG2, PRKX, PTK2, PTK2B, RAF1, RB1, RET, RIPK2, ROCK1, ROCK2, ROS1, RPS6KA1, RPS6KA2, RPS6KA3, RPS6KA4, RPS6KA5, RPS6KA6, RPS6KB1, RPS6KB2, SBK1, SBK3, SGK1, SGK2, SGK3, SIK1, SIK2, SIK3, SLK, SNRK, SRC, SRPK1, STK10, STK17A, STK17B, STK24, STK25, STK26, STK3, STK32A, STK32B, STK33, STK38, STK38L, STK39, STK4, SYK, TAB1, TAOK1, TAOK2, TAOK3, TBK1, TEC, TLK1,

	TLK2, TNIK, TNK1, TNK2, TSSK1B, TSSK2, TSSK3, TSSK6, TTK, TXK, TYK2, TYRO3, ULK1, ULK2, ULK3, YES1, ZAP70
PD 166285	WEE2, MYT1, PKMYT1, ACVR1, TNK2, ABL1, CSF1R, WEE1, PDGFRA, RET, LCK, SRC, BTK, FYN, MAPK14, EGFR, KDR

Table S.3: List of compounds identified within the second set of proteomics hits together with their annotated targets obtained from the GSK chemogenomic library.

Compound	Target annotation
PROTAC RIPK degrader-2	VHL
AZD-5153	BDR4, BRD3, BRD2, BRDT
P005091	USP7
Z-Phe-Ch2Cl	ATG4B, CMA1, EP300, CREBBP
Dactolisib	ATM, PIK3C3, PIK3CB, MTOR, PIK3CA, PIK3CG, AKT1, PIK3CD, PIK3R1, PIK3R5
AZD8055	MTOR
Vistusertib (AZD2014)	MTOR, PFKP
WYE-125132	MTOR
Ruxolitinib phosphate	JAK1, JAK2
CP 690550 citrate	DCLK3, JAK3, JAK1, JAK2, TYK2

Table S.4: List of compounds not identified as proteomics hits but obtained from the MALDI-TOF MS and cytokine HTS screens together with their annotated targets obtained from the GSK chemogenomic library.

Compound	Target annotation
MALDI and Cytokine hits	
GSK2580335	Proprietary
TAK-242	TLR4
MALDI hits	
ARN-3236	SIK2
AP-III-a4 (hydrochloride)	ENO1

LY294002 hydrochloride	PI3K
Neratinib (HKI-272)	STK24, STK26, ERBB3, STK25, MAP4K5, MAP3K19, MAP4K3, MAP3K8, ERBB4, TPTEP2-CSNK1E, ERBB2, EGFR
Spermidine trihydrochloride	eIF5A, EP300, MTP, hCA, NMDAR
T6167932	MyD88
Cytokine hits	
Apremilast	PDE4
TCMDC-125545	PDE3

Appendix C. Publications

- **Müller L**, Burton AK, Tayler CL, Rowedder JE, Hutchinson JP, Peace S, Quayle JM, Leveridge MV, Annan RS, Trost M, Peltier Heap RE, Dueñas ME. A high throughput MALDI TOF MS biochemical screen for small molecule inhibitors of the antigen aminopeptidase ERAP1. SLAS Discov. 2023;28:3 11